Wave Propagation and Interaction in Mindlin-Type Microstructured Solids: Numerical Simulation

KERT TAMM

TALLIN UNIVERSITY OF TECHNOLOGY
Faculty of Science
Department of Mechanics
Institute of Cybernetics

The dissertation was accepted for the defense of the degree of Doctor of Philosophy in Natural and Exact Sciences on February 3rd 2011

Supervisor: Professor Andrus Salupere,
Department of Mechanics and Institute of Cybernetics,
Tallinn University of Technology, Estonia

Opponents:

Jiří Plešek, PhD, Deputy Director of the Institute of Thermomechanics AS CR, Prague, Czech Republic

Alexey V. Porubov, DSc, Leading Research Fellow, Institute of Problems in Mechanical Engineering, Russian Academy of Sciences, Saint-Petersburg, Russia

Defense of the thesis: April 27th 2011

Declaration:
Hereby I declare that this doctoral thesis, my original investigation and achievement, submitted for the doctoral degree at Tallinn University of Technology has not been submitted for any academic degree.

Kert Tamm

Lainelevi ja interaktsiooni numbriline modelleerimine Mindlini tüüpi mikrostruktuursetes tahkistes

KERT TAMM

TTÜ
KIRJASTUS

Contents

List of Figures

List of publications

Publication I: A. Salupere, K. Tamm, J. Engelbrecht, and P. Peterson. On the interaction of deformation waves in microstructured solids. *Proceedings of the Estonian Academy of Sciences, Physics, Mathematics*, 56(2):93–99, 2007

Publication II: A. Salupere, L. Ilison, and K. Tamm. On numerical simulation of propagation of solitons in microstructured media. In M. Todorov, editor, *Proceedings of the 34th Conference on Applications of Mathematics in Engineering and Economics*, pages 155–165, Melville, NY, 2008. vol. 1067 of AIP Conference Proceedings

Publication III: A. Salupere, K. Tamm, and J. Engelbrecht. Numerical simulation of interaction of solitary deformation waves in microstructured solids. *International Journal of Non-Linear Mechanics*, 43(3):201–208, 2008

Publication IV: T. Peets and K. Tamm. Dispersion analysis of wave motion in microstructured solids. In T.-T. Wu and C.-C. Ma, editors, *IUTAM Symposium on Recent Advances of Acoustic Waves in Solids: Proceedings, Taipei, Taiwan, May 25–28, 2009*, volume 26 of *IUTAM Bookseries*, pages 349–354, Dordrecht, 2010. Springer

Publication V: K. Tamm and A. Salupere. On the propagation of solitary waves in Mindlin-type microstructured solids. *Proceedings of the Estonian Academy of Sciences*, 59(2):118–125, 2010

Publication VI: K. Tamm and A. Salupere. On the propagation of 1D solitary waves in Mindlin-type microstructured solids. *Mathematics and Computers in Simulation*, (in press, doi: 10.1016/j.matcom.2010.06.022), 2011

Approbation:

A. Salupere, K. Tamm and J. Engelbrecht, 'Interaction of solitary deformation waves in microstructured solids', The Fifth International Conference on Nonlinear Evolution Equations and Wave Phenomena: Computation and Theory, The University of Georgia, Athens, USA, April 16–19, 2007.

A. Salupere, K. Tamm and J. Engelbrecht, 'Emergence and interaction of solitary waves in microstructured solids', XII International Workshop on Nonlinear Elasticity in Materials, Ajaccio, Corsica, France, June 3–9, 2007.

A. Salupere, K. Tamm and J. Engelbrecht, 'Numerical simulation of propagation of solitary deformation waves in microstructured solids', The ninth U.S. National Congress on Computational Mechanics (USNCCM IX), San Francisco, USA, July 23–26, 2007.

A. Salupere, M. Randrüüt and K. Tamm, 'Emergence of soliton trains in microstructured materials', XXII International Congress of Theoretical and Applied Mechanics ICTAM 2008, Adelaide, Australia, August 24–29 2008.

K. Tamm, 'Deformatsioonilained Mindlini tüüpi mikrostruktuuriga materjalides' ('Deformation waves in Mindlin-type microstructured materials'), XIII Estonian Days of Mechanics, Tallinn, Sept 15–16, 2008.

K. Tamm amd A. Salupere, 'On propagation of 1D solitary waves in Mindlin-type microstructured solids', The Sixth International Conference on Nonlinear Evolution Equations and Wave Phenomena: Computation and Theory, The University of Georgia, Athens, USA, March 23–26, 2009.

T. Peets and K. Tamm, 'Dispersion analysis on wave motion in microstructured solids', IUTAM Symposium on Recent Advances of Acoustic Waves in Solids, Taiwan, May 25–28, 2009.

K. Tamm and A. Salupere, 'Emergence of solitary waves in Mindlin-type microstructured solids', International Conference on Complexity of Nonlinear Waves, Tallinn, Estonia, October 5–7, 2009.

Introduction

Materials with microstructure have been in use throughout the history of human civilisation: wood and marble in earlier times, followed by alloys, crystallites, ceramics, composite and functionally graded materials later. It is possible to claim that in reality solid matter has always some sort of microstructure. Surely, the first humans who grabbed for sticks and rocks did not understand the character of microstructure of primitive instruments they used. As our technological applications become more sophisticated, the ideas of better usage of microstructure of materials are also growing thanks to better understanding of the behaviour of materials. Human civilisation has after all significantly advanced since sticks and rocks and many new materials are nowadays designed bearing in mind the microstructure in them.

The driving force for the present study is to understand better the wave propagation in nonlinear materials with microstructure. The Mindlin–Engelbrecht–Pastrone model, a nonlinear dispersive model with microstructure taken into account through microstructure-related parameters [12, 13, 14, 28, 29], is used where from the full system of equations (FSE) a hierarchical equation (HE) is derived by making use of the slaving principle. The main motivation for comparison of the FSE and HE solutions, which forms the core of the second half of the present work, is related to possible practical applications in the nondestructive testing of microstructured materials, although the present study is purely theoretical.

The results of the present thesis are presented in six scientific papers. In Publications I–III [46, 47, 48] the HE solutions are investigated. In Publications IV–VI [38, 49, 50] the HE and FSE solutions are investigated and compared.

Several papers by other authors must be highlighted as highly relevant in the context of the present work. In [13] the foundation of the Mindlin–Engelbrecht–Pastrone model is formulated. In [12] the detailed derivation process as well as dispersion analysis and discussion about the acceptable level of simplifications for the model are presented. In [28, 29] the inverse problem for the HE is investigated, the conditions necessary for the existence of the solitary wave solution are derived and the asymmetry of solitary waves as a result of nonlinearity in microstructure is described. This forms the main foundation for solving numerically the HE and FSE and for investigating the differences between the FSE and HE solutions. The study [37] must be mentioned as the main motivation for defining 'combined parameters' γ_A^2 and γ_1^2 in the same way as it is done for the dispersion analysis of the Mindlin–Engelbrecht–Pastrone model.

The thesis is organized as follows. Section 1 starts with the description of the history of solitons and solitary waves and ends with a short list of famous equations with terms needed for the formation of solitons. Section 2 describes microstructured material models in general and introduces the Mindlin–Engelbrecht–Pastrone

11

model. Section 3 contains the statement of the problem as well as the description of the numerical scheme. In Section 4 results are presented, followed by discussion. Conclusions can be found in Section 5.

Acknowledgements

1.   Solitary waves and solitons

The past few centuries can be seen as a triumph of linear physics. Starting with Maxwell's equations, quantum mechanics with its superposition principle and mathematical tools of physics like Fourier transform, perturbative expansions plus other intrinsically linear methods are the best known examples. On the other hand, it is clear that nonlinear phenomena cannot be discarded without losing description accuracy in many models, for example, in Navier–Stokes equations, gravitational theory and collective effects arising from the interaction between particles in solid state physics. In the past half-century significant progress has been made in the understanding of nonlinear phenomena. For example, concepts of the strange attractor and the soliton, both being properties of nonlinear systems, were introduced. The strange attractor is linked to the idea of chaos in a system which is described by deterministic equations, usually with a relatively low number of degrees of freedom. Solitons, on the other hand, tend to appear in systems a with relatively large number of degrees of freedom. So it is apparent that adding degrees of freedom to the system does not always make the behaviour of that system more complex. Collective effects can lead to spatially coherent structures, which result in self-organization. One of the remaining open questions is the coexistence of coherent structures and chaos in nonlinear systems [9].

1.1.   History

When writing about the history of solitons or solitary waves it is not possible to skip John Scott Russell's observations in 1834. John Scott Russell, a hydrodynamic engineer, was riding his horse along a canal near Edinburgh and saw 'the great solitary wave', which he followed for a few miles before losing it in the meanders of the canal. He dedicated 10 years of his life to studying this phenomenon. Theoretical understanding of John Scott Russell's observation emerged in 1895 with derivation of the Korteweg–de Vries (KdV) equation. It should be mentioned that this equation was in implicit form also described in the earlier study of Joseph Valentin de Boussinesq that was published in 1872. Because of its remarkable mathematical properties (the simplest model equation capable of solitonic solutions), the KdV equation can be considered as one of the prototype equations of soliton theory. Many nonlinear equations can have solitonic solutions like, for example the Boussinesq equation, the sine-Gordon equation and the nonlinear Schrödinger equation from the selection of more classical ones. The 'rediscovery' of solitary waves in modern physics was in 1965, when John Zabusky and Martin David Kruskal investigated the Fermi–Pasta–Ulam problem (proposed a decade earlier by the named persons) [9, 10]. The Fermi–Pasta–Ulam problem deals with the question of how a one-dimensional crystal evolves towards the thermal equilibrium. When the first computers became more

accessible this problem was studied numerically by using a relatively simple model of a chain of particles, linked by the quadratic interaction potential, but also by weak nonlinear interaction and with fixed ends. One of the consequences of the numerical experiment was the rediscovery of the KdV equation at the continuum limit, and Zabusky and Kruskal coined the term 'soliton'.

A significant amount of the studies on solitons or solitonic structures in non-integrable systems are nowadays numerical. A possibility of finding exact analytical solitonic solutions for corresponding equations remains a rarity even with modern mathematical methods.

1.2. Solitons

A soliton can be described as a stable particle-like state of a nonlinear system [10]. Another way of describing the phenomenon we call soliton is through its properties. A soliton is a wave in the nonlinear environment that (1) has a stable form, (2) is localized in space and (3) restores its speed and structure after interaction with another soliton [11]. Solitons emerge when there is a balance in the system between dispersive and nonlinear effects. In essence it can be said that solitons are nonlinear waves that behave between interactions like linear waves. A solitary wave is usually a wave in the nonlinear environment where all the key properties of solitons are not strictly fulfilled. For example, if the interaction between two waves is not entirely elastic (or it is not possible to observe the interaction) or if the form of the wave is not sufficiently stable in time, then the wave is often called a solitary wave to distinguish it from the soliton.

In the context of this work solitons (and solitary waves) are understood through the three observable properties mentioned before [11]. As the interactions between solitary waves are not fully elastic, in the present work the term 'solitary wave' is mostly preferred, although in many cases the distortions from the interactions over shorter integration intervals are small enough, so that the stronger term 'soliton' could be used.

1.3. Solitonic equations

The KdV equation

$$u_t + uu_x + u_{xxx} = 0 \tag{1}$$

is probably the best-known equation with solitonic solutions. It has the simplest terms needed for solitonic solution — a nonlinear term uu_x and a dispersion term u_{xxx}. The subscript x denotes the spatial partial derivative (often noted by ξ in the

moving frame of reference) and subscript t (often noted by τ in the moving frame of reference) — a partial derivative with respect to time. Here the usual coefficients have been discarded. There are many fields in physics where the KdV equation emerges in addition to the shallow water waves for which it was initially derived. For example, the atomic lattice model in the Fermi–Pasta–Ulam problem or acoustic solitons in plasmas. Some modifications of the KdV equation have mixed derivatives in the dispersive term like, for example, the Benjamin–Bona–Mahony equation [1] or higher-order derivatives in addition to usual ones like, for example, the modifications of the KdV equation presented in papers [7, 27, 40, 45].

The Boussinesq equation

$$u_{tt} - u_{xx} - u_{xx}^2 - u_{xxxx} = 0 \tag{2}$$

emerges, for example, in shallow water theory and when dealing with nonlinear lattices. The usual coefficients have here also been discarded. Equation (2) is one of the simplest model equations which can have solitonic solutions that travel in opposite directions. When dropping nonlinearity and dispersion from the Boussinesq equation, all that is left is the classical wave equation.

The sine-Gordon equation

$$u_{xx} - u_{tt} = \sin(u) \tag{3}$$

is the third of the classical models with solitonic solutions. It emerged from the field theory. This equation (or some of its modifications) is usually involved when topological solitons are present. The sine-Gordon equation emerges, for example, when dealing with Josephson junctions, moving of dislocations in crystals or behaviour of some of the elementary particles.

The nonlinear Schrödinger equation

$$u_{xx} + \mathrm{i}u_t + |u|^2 u = 0 \tag{4}$$

is the fourth of the classical model equations where solitonic solutions are possible. In equation (4) u is a complex function. It appears in many areas of physics, for example in nonlinear optics, heat transfer in solids, superconductivity and plasma physics, to name a few. The nonlinear Schrödinger equation usually gives rise to the envelope solitons [10].

In a nutshell, the nonlinearity tries to make the wave steeper, while the dispersion tries to smear the wave over a wider area. Thus it is possible that if the nonlinear and dispersive effects balance each other, then solitary waves and solitons can exist in such a system.

The KdV equation (1) is an evolution equation or a so-called one-wave equation, while the Boussinesq equation (2) is a two-wave equation like the classical wave equation, i.e., it describes waves moving to the right and left. The analysis of the

KdV equation has revealed many important features of solitons, but not all. The Boussinesq equation (2) permits us to analyse also the soliton emerging process, including trains moving to the right and to the left, 'head-on' collisions of solitons, etc. This is why in this thesis attention is devoted to two-wave models.

2. Mathematical models of microstructured materials

The microstructure in a material causes dispersive and dissipative effects. Microstructured materials can be characterized by existing space-scales in the matter like, for example the lattice period, the size of the grain or the distance between microcracks, which introduce a scale dependence into the governing equations (see, e.g., [12, 17, 34]). As mentioned earlier, when we have dispersive as well as nonlinear effects and if these two effects are in balance, solitons and solitary waves can exist in such media. Solitary wave type solutions are of special interest as under suitable material parameters they tend to maintain their shape relatively well and thus it might be possible to extract information about material parameters by examining the solitary wave after it has propagated for some distance through the material (see, for example, [28]).

2.1. Microstructured material models

Two ubiquitous ways can be used when dealing with material models: the discrete approach and the continuum approach.

In the discrete approach one starts usually from lattice theory (see, for example, [2, 34, 35]) and treats volume elements of matter as point masses with some distribution over the whole scale and some interaction laws between those point masses. The simplest model would be a 1D infinite chain of particles connected by springs (often known as the Born–Karman model).

In the continuum approach it is possible to distinguish between two approaches (see [35] and references therein). The first is to model each microstructural component separately through the classical continuum theory (i.e., microstructure is considered as inhomogeneous classical continuum). The second approach is to use homogeneous continuum and to take into account the influence of the microstructure as an averaged quantity. In the second case further segmentation is possible, depending on the way how the averaged influence of the microstructure is taken into account:

- A phenomenological approach where additional terms are added to the energy functional or to the constitutive relation.

- A statistical approach where from an inhomogeneous classical continuum average values of the state parameters are computed to give enhanced field equations.

- A continualization approach where starting from a discrete model a continuum model is retrieved.

17

In the classical continuum view one starts with some conservation laws and ends up with a solid composed of volume elements dV, with some physical properties in each material volume being defined [15, 16, 33, 36].

From the viewpoint of the microstructure the implementation of the discrete approach is relatively simple. It is usually sufficient to take two or more different 'particles' in the lattice model and microstructure-related effects emerge naturally in the governing equations. A straightforward way of dealing with the microstructure in continuum is assigning some additional degrees of freedom to each material volume dV. In the present work the separation of the macro- and microstructure is preferred, allowing either formulating conservation laws for both structures separately [15, 16, 36] or taking microstructural quantities into account in one set of conservation laws [33]. When separating the macro- and microstructure it is possible to consider both structures inertial (as done in [15, 16, 36]) or to suppose that microstructural quantities behave non-inertially, which, in turn, leads to the formalism of internal variables (as done in [33]). Even when separating the micro- and macrostructure there are many ways to choose the degrees of freedom. For example, allowing deformations of the microstructure results in the Mindlin model, while keeping the microstructure rigid but allowing rotational degree of freedom results in the Cosserat model [8, 23].

2.2. Mindlin–Engelbrecht–Pastrone model

In the present work a model derived by Engelbrecht and Pastrone [12, 13, 14, 28, 29] is applied to describe wave propagation in nonlinear dispersive media with microstructure. The model is based on Mindlin's and Eringen's earlier works [15, 16, 36]. In this model the microelement is taken as a deformable cell with an additional assumption that the deformation gradient is small, thus allowing one to express microdeformation in terms of macrodisplacement. Balance laws are formulated separately for the macro- and microscale. In order to clarify the principal essence and the role of the parameters of the model, we repeat here the basic steps of modelling.

In the 1D case the Lagrangian L is expressed as follows:

$$L = K - W, \qquad K = \frac{1}{2}\rho u_t^2 + \frac{1}{2}I\varphi_t^2, \quad W = W(u_x, \varphi, \varphi_x). \qquad (5)$$

Here K is the kinetic energy, W is the free (potential) energy, I is the microinertia, φ is the microdeformation, u is the macrodisplacement, ρ is the macroscale density, and partial derivatives are denoted by subscripts.

Equations of motion are derived by making use of Euler–Lagrange equations

$$\left(\frac{\partial L}{\partial u_t}\right)_t + \left(\frac{\partial L}{\partial u_x}\right)_x - \frac{\partial L}{\partial u} = 0, \qquad \left(\frac{\partial L}{\partial \varphi_t}\right)_t + \left(\frac{\partial L}{\partial \varphi_x}\right)_x - \frac{\partial L}{\partial \varphi} = 0, \qquad (6)$$

resulting in

$$\rho u_{tt} - \left(\frac{\partial W}{\partial u_x}\right)_x = 0, \qquad I\varphi_{tt} - \left(\frac{\partial W}{\partial \varphi_x}\right)_x + \frac{\partial W}{\partial \varphi} = 0, \tag{7}$$

where partial derivatives

$$\sigma = \frac{\partial W}{\partial u_x}, \qquad \eta = \frac{\partial W}{\partial \varphi_x}, \qquad \tau = \frac{\partial W}{\partial \varphi}, \tag{8}$$

can be interpreted as follows: σ as the macrostress, η as the microstress and τ as the interactive force. Equations of motion can be then presented in the familiar form

$$\rho u_{tt} = \sigma_x, \qquad I\varphi_{tt} = \eta_x - \tau. \tag{9}$$

In order to take into account the nonlinearity in the micro- and macroscale, one can write the free energy as

$$W = \frac{A}{2}u_x^2 + \frac{B}{2}\varphi^2 + \frac{C}{2}\varphi_x^2 + D\varphi u_x + \frac{N}{6}u_x^3 + \frac{M}{6}\varphi_x^3. \tag{10}$$

Here A, B, C, D are material parameters responsible for the linear part of the model and N, M are responsible for the nonlinearity in the macro- and microscale, respectively [28, 29]. Making use of the free energy function (10) and the governing equations derived through the Euler–Lagrange equations, one arrives at equations of motion

$$\begin{aligned}
\rho u_{tt} &= D\varphi_x + Au_{xx} + Nu_x u_{xx}, \\
I\varphi_{tt} &= C\varphi_{xx} + M\varphi_x \varphi_{xx} - B\varphi - Du_x.
\end{aligned} \tag{11}$$

For further analysis dimensionless variables and parameters

$$X = \frac{x}{L_o}, \quad T = \frac{\sqrt{A}t}{\sqrt{\rho}L_o}, \quad U = \frac{u}{U_o}, \quad \delta = \frac{l_o^2}{L_o^2}, \quad \varepsilon = \frac{U_o}{L_o} \tag{12}$$

are introduced [28, 29]. Here U_o and L_o are the amplitude and the wavelength of the initial excitation, and l_o is the characteristic scale of the microstructure. In the 1D case above we have 11 different parameters — 8 of them are material (6 free energy parameters, macroscale density and microinertia) and 3 are geometrical (the amplitude and the wavelength of the initial excitation and the scale of the microstructure). Making use of change of variables (12), one arrives at dimensionless equations of motion

$$\begin{aligned}
U_{TT} &= \frac{DL_o}{AU_o}\varphi_X + \frac{NU_o}{AL_o}U_X U_{XX} + U_{XX}, \\
\varphi_{TT} &= \frac{C\rho}{AI}\varphi_{XX} - \frac{B\rho L_o^2}{AI}\varphi - \frac{D\rho U_o L_o}{AI}U_X + \frac{M\rho}{AIL_o}\varphi_X \varphi_{XX}.
\end{aligned} \tag{13}$$

Equations (13) are referred to as the full fystem of equations (the FSE for short) below. Making use of the slaving principle (see [12] for details) allows one to derive a single equation in terms of macrodisplacement U from the FSE:

$$U_{TT} - bU_{XX} - \frac{\mu}{2}\left(U_X^2\right)_X = \delta\left(\beta U_{TT} - \gamma U_{XX} + \frac{\lambda\sqrt{\delta}}{2}U_{XX}^2\right)_{XX}. \tag{14}$$

Equation (14) is hierarchical in Whitham's sense [14, 51]. In terms of deformation $V = U_X$ equation (14) can be expressed as

$$V_{TT} - bV_{XX} - \frac{\mu}{2}\left(V^2\right)_{XX} = \delta\left(\beta V_{TT} - \gamma V_{XX} + \frac{\lambda\sqrt{\delta}}{2}(V_X)_X^2\right)_{XX}. \tag{15}$$

Constants in equations (14) and (15) in terms of material and geometrical parameters are

$$b = 1 - \frac{D^2}{AB}, \ \mu = \frac{NU_o}{AL_o}, \ \beta = \frac{ID^2}{\rho l_o^2 B^2}, \ \gamma = \frac{CD^2}{AB^2 l_o^2}, \ \lambda = \frac{D^3 MU_o}{AB^3 l_o^3 L_o}. \tag{16}$$

Equations (14) and (15) can be considered as an approximation of the FSE (13) and are referred to as the hierarchical equations (HE) below. The HE in deformation terms (15) is used in the part of the thesis dealing only with the HE, while the HE in displacement terms (14) is used in the part of the thesis where both the FSE and HE are solved under the same material and geometrical parameters. A characteristic feature of the investigated governing equations (equations (13), (14) and (15)) is that, unlike the evolution equations, these describe two waves instead of one. This gives us an opportunity to analyse also head-on collision of waves. Furthermore, according to [5], the HE (14) and (15) are of Boussinesq type and therefore one can expect solutions of soliton type.

In the present thesis equations (13), (14) and (15) are used for the numerical simulation of wave propagation in microstructured solids.

2.3. Combined parameters

Three combined parameters are used. Parameters γ_A^2 and γ_1^2 combine the linear parts of the material parameters [12, 37] describing macro- and microstructure and interaction between those

$$\gamma_A^2 = 1 - b = \frac{D^2}{AB}, \qquad \gamma_1^2 = \frac{\gamma}{\beta} = \frac{\rho C}{AI}, \tag{17}$$

while parameter γ_N is related to nonlinearity

$$\gamma_N = \frac{\lambda}{\mu} = \frac{D^3 M}{B^3 N l_o^3}. \tag{18}$$

Parameters b, γ, β, μ and λ are defined by expressions (16).

2.4. Dispersion

The dispersion type for the HE can be determined by the sign of quantity (see [12] for details):

$$\Gamma = 1 - \gamma_A^2 - \gamma_1^2 \qquad (19)$$

One can interpret γ_1 as dimensionless speed of short waves and $\sqrt{1 - \gamma_A^2}$ as the dimensionless speed of long waves. If Γ is positive, we have the normal dispersion case, if negative, we have the anomalous dispersion case and if it is equal to zero, we have the dispersionless case.
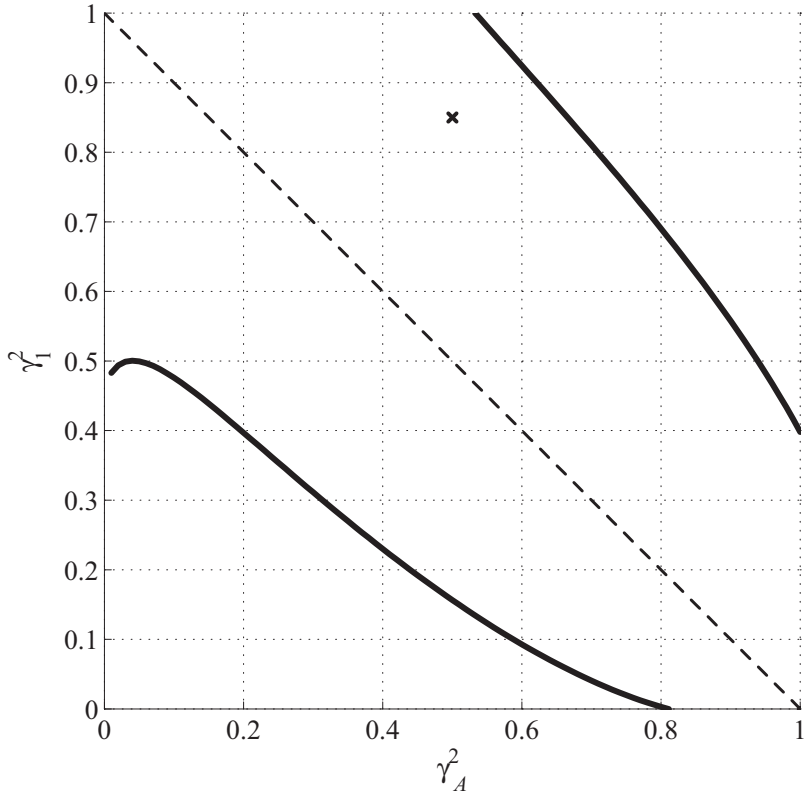
Figure 1: Domain in the $\gamma_A^2-\gamma_1^2$ plane where the difference between acoustic branches of dispersion curves for the HE and FSE is less than 5%.
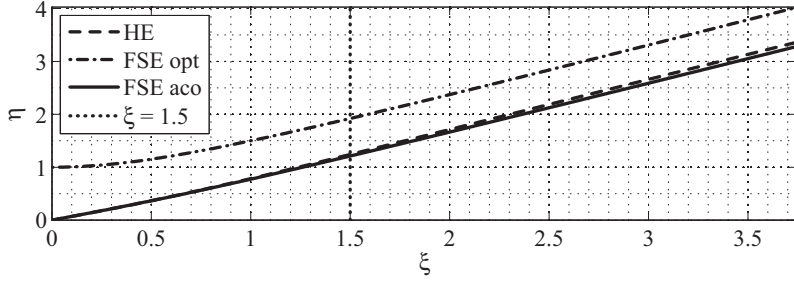
Figure 2: Dispersion curves, $\gamma_A^2 = 0.5$, $\gamma_1^2 = 0.85$.

According to the dispersion analysis carried out in [37], acoustic branches of the dispersion curves of the HE and FSE are close to each other in the domain between solid curves in Fig. 1, which corresponds to 5% difference between acoustic branches at the dimensionless wavenumber $\xi = 1.5$ ($\xi = k\sqrt{(AI)/(B\rho)}$ (Fig. 2), where k is the wavenumber). The dashed line in Fig. 1 corresponds to parameter combinations that result in the dispersionless case for acoustic branches of the FSE and HE. In Fig. 2 one can see an example of dispersion curves at $\gamma_A^2 = 0.5$ and $\gamma_1^2 = 0.85$ (the point is marked with 'x' in Fig. 1). The quantity η is the dimensionless frequency and the dotted vertical line represents $\xi = 1.5$ where difference between acoustic branches of the HE and FSE is calculated. One can see that the FSE also has a second, so-called 'optical' branch, while the HE has only the acoustic branch: in Fig. 2 the dashed line represents the acoustic branch of the HE, the solid line represents acoustic branch of the FSE and the dash-dotted line represents the optical branch of the FSE.

3. Statement of the problem and the numerical method

Below, the main motivation for problem selection is presented, followed by the statement of the problem. The description of the numerical method is given in subsection 3.2. The accuracy of the numerical scheme is discussed in Appendix A.

3.1. Statement of the problem

The underlying driving force for the present study is to understand better the wave propagation in nonlinear materials with a microstructure. Much research has been done in the field and there are already several theories capable of describing wave propagation within such materials (see, for example, [4] and [16] and references therein). However, the Mindlin–Engelbrecht–Pastrone model has certain advantages. For example, it starts from the energy function and arrives at equations of motion that satisfy balance laws and causality without the need of adding more terms into equations in ad-hoc style just to make things fit. Applications of the theory are possible in a relatively straightforward manner, although interpretation of the microstructure-related parameters will need some work. Possible practical application in the nondestructive testing of nonlinear materials with microstructure is another strong motivator for the present study. Comprehensive description for the HE and FSE in the linear case has been provided in [37] through dispersion analysis, with the main focus on finding domains in the parameter space where the HE is a good approximation of the FSE.

The goals of the present study are

- to simulate numerically the propagation and interaction of solitary waves in Mindlin-type microstructured solids modelled by the FSE (13) and HE (14), (15) for different values of parameters;

- to characterize and analyse the space-time behaviour of solutions;

- to analyse the character of interactions in terms of solitons, i.e., to understand whether solitary waves that emerge from initial pulses interact elastically or not;

- to estimate the influence of microlevel nonlinearity on the solutions of the HE (15);

- to estimate the influence of combined parameters γ_A and γ_1 on the character of solutions of the FSE (13) and HE (14) in the linear and nonlinear cases;

- to analyse the behaviour of the solutions against the results obtained from (linear) dispersion analysis [37]:

  - to clarify the different behaviour of solutions of nonlinear equations (13) and (14) in the anomalous and normal dispersion cases;
  - to estimate the concurrency between solutions of the FSE (13) and HE (14) in domains predicted in [37].

3.2. Numerical method

There are many numerical methods that can be used to solve nonlinear differential equations, for example the finite difference methods, the Galerkin method, the Hopscotch method, the Fourier expansion method, the split-step Fourier method and the spectral and pseudospectral methods. All the named methods have some advantages and disadvantages that should be taken into account when used. The pseudospectral method (PSM) is a well established method, used frequently to solve differential equations under localized as well as harmonic initial conditions. The advantages and disadvantages of the PSM have been examined in several papers (see [18, 19, 20, 22, 42, 43] and references therein) and the method has been found to be adequately accurate and stable at a relatively low number of grid points.

In the present thesis PSM based on the discrete Fourier transform (DFT)[18, 19, 20, 32, 43, 44] is applied. The version of the DFT used is:

$$\widehat{U}(k,T) = \mathrm{F}[U] = \sum_{j=0}^{n-1} U(j\Delta X, T) \exp\left(-\frac{2\pi \mathrm{i} jk}{n}\right), \qquad (20)$$

where n is the number of space-grid points, $\Delta X = 2\pi/n$ is the space step, i is the imaginary unit, $k = 0, \pm 1, \pm 2, \ldots, \pm(n/2 - 1), -n/2$, F denotes the DFT and F^{-1} denotes the inverse DFT. Basically, the idea of the PSM is to approximate space derivatives by making use of the DFT

$$\frac{\partial^m U}{\partial X^m} = \mathrm{F}^{-1}\left[(\mathrm{i}k)^m \mathrm{F}(U)\right], \qquad (21)$$

and then to use standard ordinary differential equation (ODE) solvers for integration with respect to time.

The regular PSM algorithm is derived for $u_t = \Phi(u, u_x, u_{2x}, \ldots, u_{mx})$ type equations. In our case, however, we have also a mixed partial derivative term $\delta\beta U_{TTXX}$ in the HE (14) and (15) and thus the standard PSM has to be modified [25, 26, 43]. Therefore we rewrite the HE (14) so that all partial derivatives with respect to time are in

the left-hand side of the HE

$$U_{TT} - \delta\beta U_{TTXX} = bU_{XX} + \frac{\mu}{2}\left(U_X^2\right)_X - \delta\left(\gamma U_{XX} - \frac{\lambda\sqrt{\delta}}{2}U_{XX}^2\right)_{XX}, \qquad (22)$$

and introduce a new variable $\Phi = U - \delta\beta U_{XX}$. After that, making use of properties of the DFT, one can express the variable U and its spatial derivatives in terms of the new variable Φ:

$$U = F^{-1}\left[\frac{F(\Phi)}{1 + \delta\beta k^2}\right], \qquad \frac{\partial^m U}{\partial X^m} = F^{-1}\left[\frac{(ik)^m F(\Phi)}{1 + \delta\beta k^2}\right]. \qquad (23)$$

Finally, equation (14) can be rewritten in terms of the variable Φ

$$\Phi_{TT} = bU_{XX} + \frac{\mu}{2}\left(U_X^2\right)_X - \delta\left(\gamma U_{XX} - \frac{\lambda\sqrt{\delta}}{2}U_{XX}^2\right)_{XX}. \qquad (24)$$

In equation (24) all partial derivatives of U with respect to X are calculated in terms of Φ by using expression (23) and therefore one can apply the PSM to numerical integration of equation (24). Equation (15) is solved in the same way as equation (14). The FSE (13) is reduced to the system of first-order differential equations which are solved by the standard PSM without any further modifications.

The calculations are carried out with the Python package SciPy [30], using the FFTW library [21] for the DFT and the F2PY [39] generated Python interface to the ODE-PACK Fortran code [24] for the ODE solver.

4. Results

Publications I–VI can roughly be divided into two groups: the first group where the main focus is on the HE in deformation terms and the second group where both the HE and FSE are studied.

The first group is composed of three papers. In Publication I the HE in deformation terms (15) is used. It is noted that if interacting waves have equal amplitudes, then a negligible phase shift can be detected, while if interacting waves have different amplitudes, then the interaction results in a more distinctive phase shift. Two cases are considered, one with nonlinearity present in the microstructure and the other with nonlinearity absent in the microstructure. In both cases, however, nonlinearity is present in the macrsoscale. The interactions are described as near-elastic. The main focus is on head-on collision and overtaking interaction is addressed in the discussion. In Publication II the HKdV (describing wave propagation in dilatant granular material) solutions are compared to the solutions of the HE. For the HE it is demonstrated how a single bell-shaped initial condition splits into two bell-shaped waves propagating in opposite directions and these, in turn, split further into soliton-like waves during evolution. In Publication III a detailed analysis is carried out for the head-on collision of the waves represented by the HE presented in deformation terms. Phase shifts, inelasticity of interactions, the depression zone after the passing compression wave and different amplitudes of the waves propagating in opposite directions are noted as effects related to near-solitonic behaviour and microstructure nonlinearity.

The second group contains three papers. In Publication IV the HE (14) and FSE (13) are compared from the standpoint of (linear) dispersion analysis. Additional oscillations in the solutions of the FSE are detected when compared to the solutions of the HE. A hypothesis is proposed in the discussion linking those additional oscillations to the presence of the optical branch in the FSE dispersion curves. In Publication V the solutions of the FSE and HE are compared under three dispersion cases (normal, anomalous, dispersionless) with emphasis placed on phase shifts between the main pulses of the propagating wave structures. The quality of the approximation (the HE) is discussed. In Publication VI solutions of the FSE and HE are compared along the fixed dispersion (weak normal) line in the combined parameter space. Both the linear and nonlinear cases are considered. Oscillations present in the solutions of the FSE but not in the HE are noted, as well as asymmetry between waves propagating in opposite directions. Nonlinear effects are discussed.

The present thesis is based on Publications I–VI mentioned above. In papers of the first group, dealing with the HE (15) in deformation terms, parameters (16) are inserted directly into model equations. In the second group, dealing with the HE (14) and FSE (13) in displacement terms, combined parameters are used. Combined parameters are defined by linking together geometrical and material parameters. Three
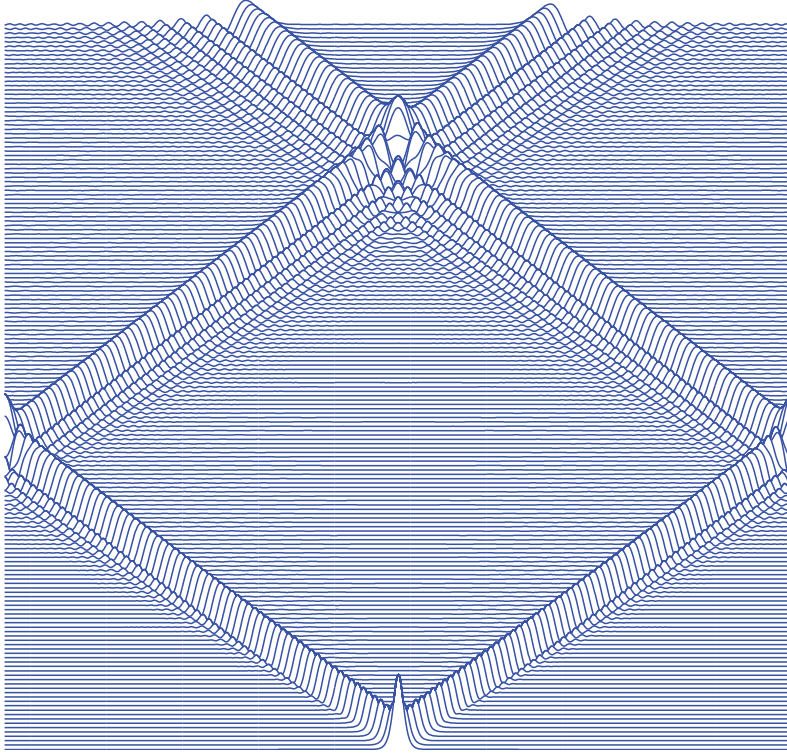
Figure 3: Example of the solution of the FSE in the nonlinear case ($\gamma_A^2 = 0.8$, $\gamma_I^2 = 0.5$ and $\gamma_N = 0.5$).

microstructure-related parameters are used for changing values of the combined parameters.

The main results are divided into two subsections. The first subsection deals with the HE in deformation terms and combines results from the papers of the first group. The second subsection contains comparison of the FSE and HE solutions under combined material parameters and combines results from the second group of publications.

Before moving on to results it stands to reason to provide a preliminary glance at a typical solution of the model equations under used initial conditions. A typical example of the solution of the FSE can be seen in Fig. 3, where on the horizontal axis there is spatial coordinate X and on the vertical axis time T. Solutions of the HE are visually similar to those presented in Fig. 3 with just small differences in the amplitudes and phases.

4.1. The HE in deformation terms

The present section is based on Publications I–III.

In theoretical applications it is often preferred to use model equations in terms of deformation, because deformation is dimensionless as opposed to displacement which, as a rule, is a quantity with dimension. In the present case, however, there is no significant difference between model equations in terms of deformation (15) and in terms of displacement (14), because as a result of change of variables (12) these are both in dimensionless form. Solutions of equations (15) and (13) are similar if initial conditions of the same type are used. However, a bell-shaped wave in deformation terms is a kink wave in terms of displacement.

4.1.1. The problem and conditions for the existence of single solitary wave solutions

In the present case it is more comfortable to use parameters (16) directly as opposed to going through the free energy parameters (10). Equation (15) is non-integrable but it is possible to find its travelling wave solution $V(X - cT)$ in the form of an asymmetric solitary wave, using numerical integration under asymptotic boundary conditions (i.e., $U, U_X, U_{XX}, \ldots \to 0$ if $X \to \pm\infty$). Janno and Engelbrecht [28, 29] have found analytic conditions for the existence of single solitary wave solutions:

$$
\frac{c^2 - b}{\beta c^2 - \gamma} > 0, \quad \left(\frac{\beta c^2 - \gamma}{c^2 - b} \right)^3 > \frac{4\lambda^2}{\mu^2},
$$
$$
\mu \neq 0, \quad \beta c^2 - \gamma \neq 0, \quad c^2 - b \neq 0,
$$

(25)

where parameters $b, \beta, \gamma, \lambda, \mu$ are given in (16) and c is a characteristic speed of the system. If $\lambda = 0$, then (15) admits analytical bell-like solitary wave solutions [28, 41]

$$
V(X - cT) = A \operatorname{sech}^2 \frac{\varkappa(X - cT)}{2},
$$
$$
A = \frac{3(c^2 - b)}{\mu}, \quad \varkappa = \sqrt{\frac{c^2 - b}{\delta(\beta c^2 - \gamma)}}.
$$

(26)

Three problems are of importance from the viewpoint of soliton dynamics: (i) the existence of solitary waves, (ii) the emergence of solitary waves and (iii) the interaction of solitary waves. The last one is important in order to prove the solitonic character of solitary waves, i.e., to understand if the solitary waves are able to propagate at a constant speed and shape and to restore these quantities after interactions. If yes, then we can call those solitary waves solitons. The last two problems are the key issues investigated in Publications I–III, while the first problem has been solved by Janno and Engelbrecht in [28, 29] for the HE (15). In addition to (ii) and (iii), the influence of microstructure on the character of solutions is investigated, in particular the influence of the microlevel nonlinear parameter λ.

4.1.2. Numerical scheme

For numerical integration the DFT based PSM is used (see Section 3.2. for details). As equation (15) is in terms of deformations, a new variable (used to circumvent the issue of mixed derivatives in the equation) is also introduced in terms of deformations

$$\Phi = V - \delta\beta V_{XX}, \tag{27}$$

and the variable V and its spatial derivatives are expressed in terms of the variable Φ as

$$V = F^{-1}\left[\frac{F(\Phi)}{1 + \delta\beta k^2}\right], \qquad \frac{\partial^m V}{\partial X^m} = F^{-1}\left[\frac{(ik)^m F(\Phi)}{1 + \delta\beta k^2}\right]. \tag{28}$$

Similar to the HE in displacement terms (24), equation (15) is rewritten in terms of the variable Φ

$$\Phi_{TT} = bV_{XX} + \frac{\mu}{2}\left[V^2\right]_{XX} - \delta\left(\gamma V_{XX} - \frac{\lambda\sqrt{\delta}}{2}\left[V_X^2\right]_X\right)_{XX}. \tag{29}$$

Equation (29) can be solved with the use of the PSM after reducing it to a system of two first-order differential equations.

4.1.3. Parameters and initial conditions

Equation (15) is integrated numerically under localized initial conditions. In the case of $\lambda = 0$ the analytical solution is known in the form of a single symmetric bell-like solitary wave (26). The analytical solution

$$V(X,0) = \sum_{i=1}^{2} A_i^0 \operatorname{sech}^2 \frac{\varkappa_i(X - \xi_i)}{2}, \quad 0 \le X < 2k\pi, \tag{30}$$

is used as the initial condition in the present numerical simulation in the case of $\lambda = 0$ as well as $\lambda \ne 0$. Initial amplitudes A_1^0, A_2^0 and widths $\varkappa_1$ and $\varkappa_2$ correspond to different initial speeds c_1, c_2; ξ_i are initial phase shifts and k is an integer. In the case of $c_1 c_2 < 0$ it is possible to observe head-on collision and in the case of $c_1 c_2 > 0$ overtaking interaction (under periodic boundary conditions this is true for both $c_1 > c_2$ and $c_1 < c_2$).

Several parameter sets, fulfilling conditions (25) for the existence of solitary wave type solution for (15), were considered. For example,

$$b = 0.719, \quad \mu = 2.083, \quad \delta = 0.25, \quad \beta = 45.04, \quad \gamma = 9.375,$$
$$\lambda = 2.083, \quad c = 0, \quad A = 1, \quad \varkappa = 0.05. \tag{31}$$

As can be seen in (31), the initial phase speed is equal to zero. This can be interpreted as starting from the peak of interaction and the initial condition will split into two waves with initially equal amplitudes propagating in opposite directions. Under this

parameter set solitary wave emergence and head-on interaction of solitary waves with equal amplitudes are investigated.

Under the second set both head-on and overtaking interactions are investigated. Parameters

$$b = 0.7683, \quad \mu = 0.125, \quad \delta = 9, \quad \beta = 7.6452, \quad \gamma = 6.1817,$$
$$c_1 = 0.9, \quad c_2 = -0.9, \quad A_1 = A_2 = 1, \quad \varkappa_1 = \varkappa_2 = 0.65 \tag{32}$$

are used to investigate the head-on collision of solitary waves with equal amplitudes.

For the head-on collision of solitary waves with different amplitudes equation parameters are the same as in (32), but initial speeds and widths of initial pulses are different:

$$c_1 = 0.9, \quad c_2 = -0.9115, \quad A_1 = 1, \quad A_2 = 1.5, \quad \varkappa_1 = 0.65, \quad \varkappa_2 = 0.202. \tag{33}$$

Parameter λ has three different values (0, 0.0025 and 0.005) in (32) and (33). In the case of overtaking interaction speeds c_1 and c_2 are both positive.

4.1.4. Results and discussion

In Publications I and III parameter set (32) and (33) is in use, while in Publication II parameter set (31) is used.

In Publication I head-on collision and overtaking interactions were studied over time intervals $0 \leq T \leq 500$. The length of the space interval was 24π for the equal initial amplitude case and 96π in the case of non-equal amplitudes. It was found that for $\lambda = 0$ (analytical solution known) and for relatively small values of λ the behaviour of solitary waves was very close to that of the solitons for the considered time and space intervals. It was possible to show that interaction between solitary waves with equal amplitudes has a very small phase shift, while phase shifts are larger in the case of interacting solitary waves with different amplitudes.

In Publication II the length of the space interval was 200π in combination with a relatively long time interval $0 \leq T \leq 5000$. It was demonstrated that the initial bell-like pulse splits into several bell-shaped waves with different amplitudes and propagation speeds (Fig. 4) and with nearly solitonic behaviour. Interactions were described as nearly elastic.

Findings of Publications I and II are expanded in Publication III where the time interval $0 \leq T \leq 3000$ is used and the space period is 60π, allowing observation of 29 interactions between the waves propagating in opposite directions.

For determining the influence of microstructure nonlinearity related parameter λ on the character of solutions, head-on collision of solitary waves was studied in the case of equal amplitudes as well as when the amplitudes were not equal.
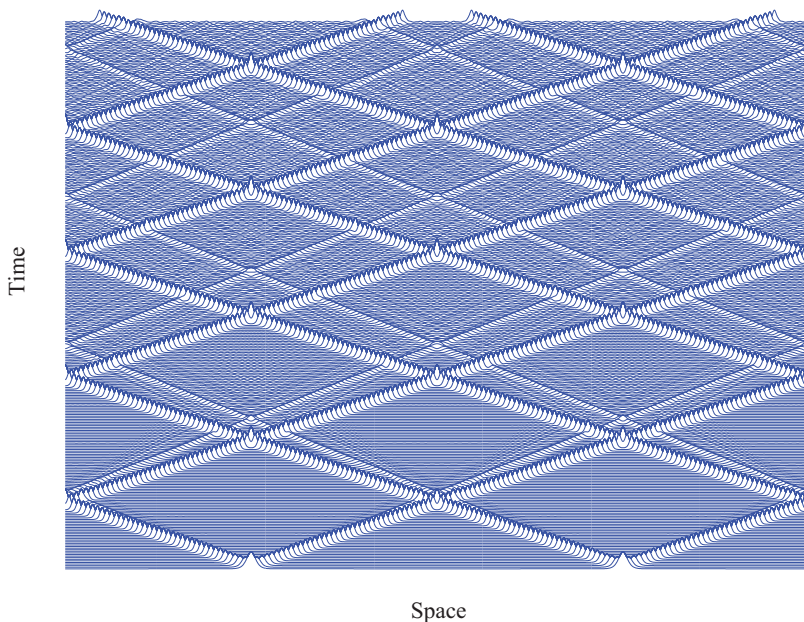
Figure 4: Emergence of trains of solitons in the case of model equation (15) — time-slice plot over two space periods.

Waveprofile minima and maxima against time can be observed in Fig. 5 in the case of $\lambda = 0$ and $\lambda = 0.005$ when interacting waves have equal initial amplitudes ($A_1^0 = A_2^0 = 1.0$) and in Fig. 6 when interacting waves have different initial amplitudes ($A_1^0 = 1.0$ and $A_2^0 = 1.5$). In the case of $\lambda = 0$ in Fig. 5 it can be seen that the waves propagating in opposite directions have equal amplitudes, however, in the case of $\lambda \neq 0$ amplitudes evolve to be different for waves propagating in opposite directions. It must be noted that the difference between the cases $\lambda = 0$ and $\lambda \neq 0$ is very small in Fig. 6 where initial amplitudes are different.

In Figs. 7 and 8 the cumulative phase shift of solitary waves propagating to the left and to the right can be observed when solitary waves have equal amplitudes as well as when they have different amplitudes. The cumulative phase shift is found by comparing actual trajectories of solitary waves with straight lines of $X_i = \xi_i \pm ct$, where c is the initial speed of the solitary wave ± 0.9 (when solitary waves have equal amplitudes and $c_1 = 0.9$, $c_2 = -0.9115$ when they have different amplitudes). It can be seen that in the case of $\lambda = 0$ phase shifts are equal for both solitary waves during interactions (Fig. 7). However, in the case of $\lambda \neq 0$ the phase shifts of solitary waves

31
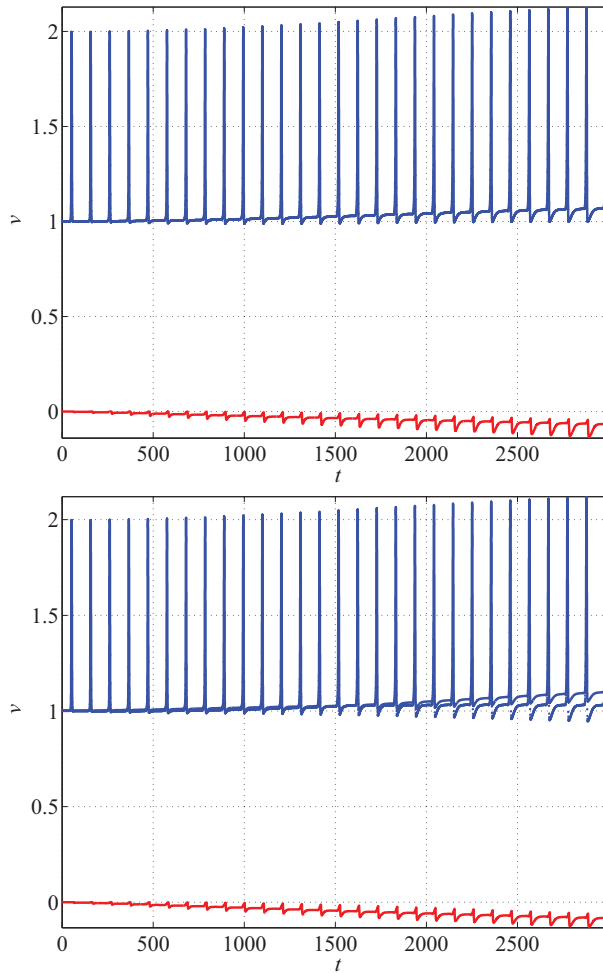
Figure 5: Waveprofile maxima and minima against time, $c_1 = -c_2 = 0.9$, $\lambda = 0$ (top) and $\lambda = 0.005$ (bottom).

propagating in opposite directions are not equal, as can be seen in Fig. 7. In the case of $\lambda = 0$ the cumulative phase shift is 0.43% of the length of the space period, while in the case of $\lambda \neq 0$ the cumulative phase shift is 0.64% for the left propagating pulse and 0.23% for the right propagating pulse. When interacting solitary waves have different initial amplitudes, different phase shifts can be observed even in the case of
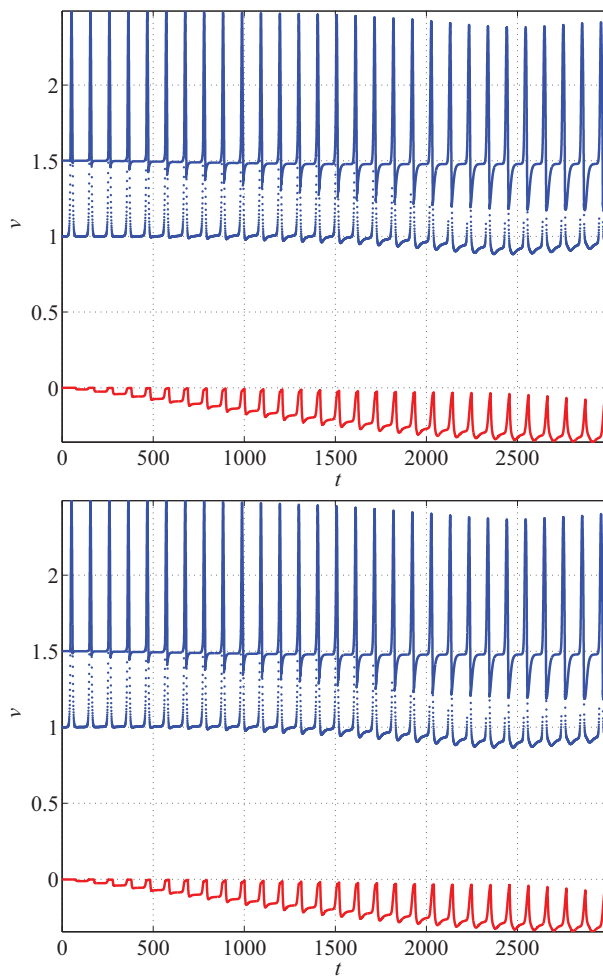
Figure 6: Waveprofile maxima and minima against time, $c_1 = 0.9$, $c_2 = -0.9115$, $\lambda = 0$ (top) and $\lambda = 0.005$ (bottom).

$\lambda = 0$. In the case of $\lambda \neq 0$ the phase shifts are slightly stronger, but overall, the influence of parameter λ on the character of interaction is small (Fig. 8). Cumulative phase shifts of the solitary waves are considerably stronger (4.78% for the right propagating pulse and 1.75% for the left propagating pulse) than in the case of equal amplitudes regardless of the parameter λ value.
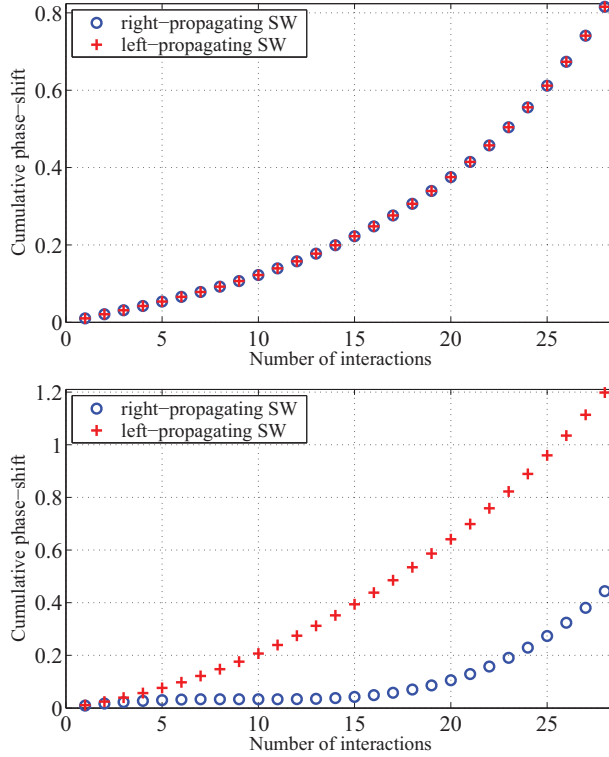
Figure 7: Cumulative phase shift of left and right propagating solitary waves, $c_1 = -c_2 = 0.9$, $\lambda = 0$ (top) and $\lambda = 0.005$ (bottom).

In summary, the numerical simulations showed that the initial bell-like pulse (26) is altered to that of asymmetric shape during propagation in the case of $\lambda > 0$. In the case of $\lambda = 0$ the initial pulse (26) propagated at a constant speed and shape until the first interaction. However, it was apparent that interactions were not fully elastic. Even in the case of $\lambda = 0$ the initial symmetric bell-like pulse was morphed into asymmetric one and some radiation was generated during interactions (Publication II). In the case of $\lambda = 0$ and $A_1^0 = A_2^0$ the asymmetry was very weak after the very first interactions. However, the higher the number of interactions, the more distinctive the asymmetry. In the case of $A_1^0 \neq A_2^0$ the shape of the higher wave had only minor distortions, while the shape of the lower amplitude wave was subject to stronger distortions. The asymmetry of the pulse was reflected in the altering of the shape of the compression region of the pulse as well as in the emergence of the depression
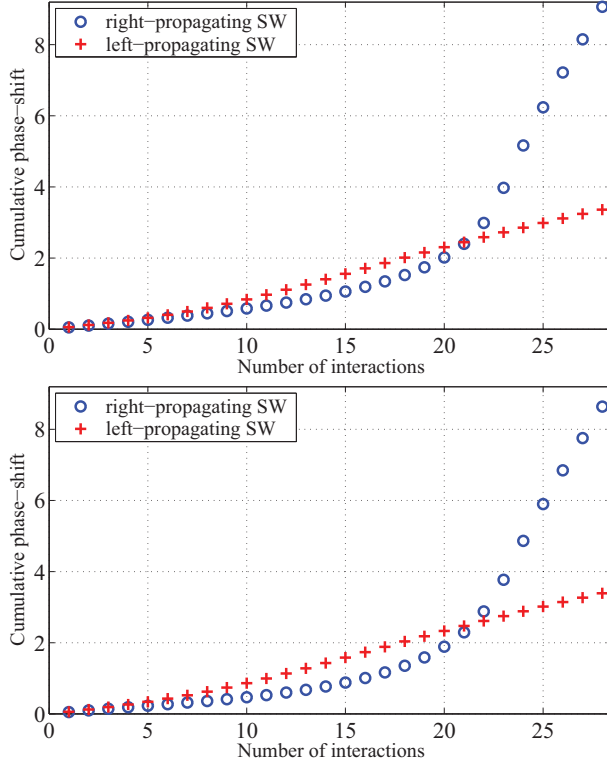
Figure 8: Cumulative phase shift of left and right propagating solitary waves, $c_1 = 0.9$, $c_2 = -0.9115$, $\lambda = 0$ (top) and $\lambda = 0.005$ (bottom).

zone beside the compression region (Publication III). Phase shifts, characteristic of soliton-type interactions, can be easily traced in the case of $A_0^1 \neq A_0^2$. In the case of $A_0^1 = A_0^2$ even the cumulative phase shifts over long time intervals were small compared to the considered space interval and/or distance travelled by interacting waves. If $\lambda = 0$ and $A_0^1 = A_0^2$, then the phase shifts during interactions were equal for both solitary waves. If $\lambda \neq 0$ or $A_0^1 \neq A_0^2$ then the phase-shifts during interactions were different. Parameter λ had stronger influence on the character of the solutions if $A_0^1 = A_0^2$. Over short time intervals and at a small number of interactions the behaviour of the solution was very close to the solitonic behaviour in all considered cases. The higher the number of interactions and the longer the time interval, the more the initial and the restored waveprofiles differed. Key results from the present subsection are listed in Conclusions.

35

4.2. The HE and FSE in displacement terms

From the theoretical point of view there is no difference between using the model equation either in deformation terms or displacement terms. Usually the model equation in deformation terms is preferred in theoretical works as a more convenient one, while in practical applications often model equations in the displacement terms are preferred. The main reason for using model equations in displacement terms in the present case is the more convenient shape of an initial condition, as a bell-shaped wave in deformation terms is a kink wave in terms of displacement, however, a kink wave is inconvenient to handle under periodic boundary conditions. A bell-shaped wave in displacement terms is straightforward to handle under periodic boundary conditions even when shifting into deformation. After all, it is a matter of preference. A bell shape is preferred in the present case for the ease of visualization and numerical analysis.

The present section is based on the second group of publications (Publications IV–VI). The structure of the section is the following: (i) initial and boundary conditions; (ii) material parameters; (iii) conserved quantities; (iv) analysis of results. Tables and figures (besides those presented in the text) can be found in Appendix B.

4.2.1. Initial and boundary conditions

In Section 4.2. the numerical simulation of propagation of solitary waves in Mindlin type microstructured solids is carried out by numerically integrating HE (14) and FSE (13) under sech^2-type localized initial conditions and periodic boundary conditions

$$U(X,0) = U_o \operatorname{sech}^2 B_o X, \quad U(X,T) = U(X + 2km\pi, T), \quad m = 1, 2, \ldots, \quad (34)$$

where $k = 6$, i.e., the total length of the spatial period is 12π. For the amplitude and the width of the initial pulse we use the values $U_o = 1$ and $B_o = \pi/2$. Initial phase speed is taken to be zero, which can be interpreted as starting from the peak of the interaction of two waves propagating in opposite directions. For the FSE two more initial conditions are needed for the microdeformation. We assume that at $T = 0$ the microdeformation and the corresponding velocity are zero, i.e., $\varphi(X,0) = 0$ and $\varphi_T(X,0) = 0$. The integration interval is from zero to $T_f = 100$. In all considered cases two solitary waves that propagate in opposite directions emerge from the initial pulse (34).

4.2.2. Material parameters

The nonlinear and linear cases are both considered. In the nonlinear case material parameters M and N are chosen so that $\gamma_N = 0.5$. Parameters

$$A = 12, \quad D = 5, \quad \rho = 10, \quad I = 8 \quad (35)$$
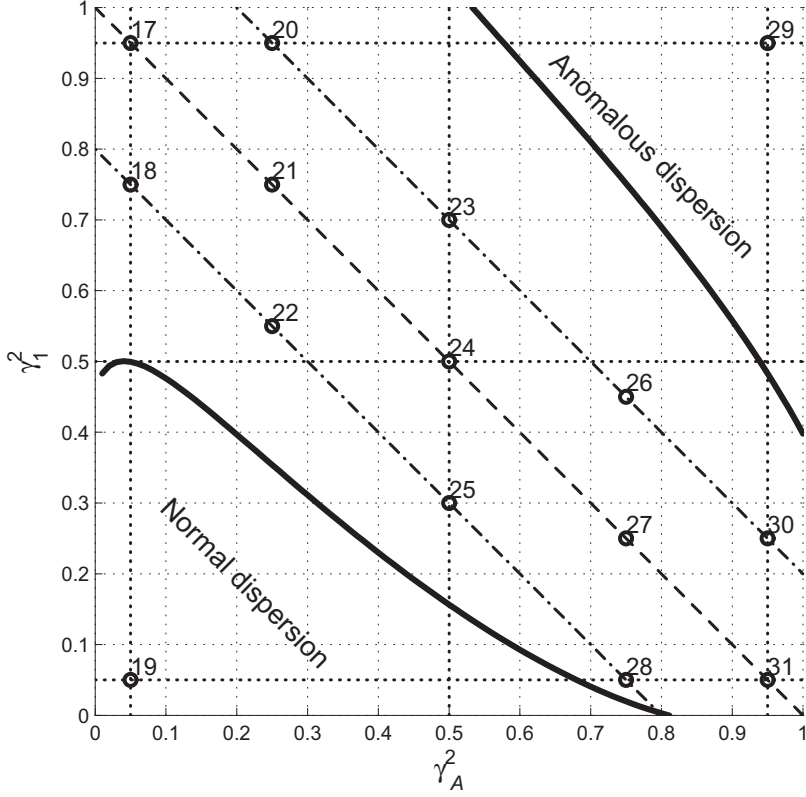
Figure 9: Points and sections under detailed view in the $\gamma_A^2 - \gamma_1^2$ plane.

are the same for all cases while non-constant material parameters have the values

$$B = \frac{25}{12\gamma_A}, \quad C = \frac{48\gamma_1}{5}, \quad N = 1 \text{ and } 0, \quad M = \frac{\gamma_N B^3}{125} \text{ and } 0, \tag{36}$$

where B is used to change the values of γ_A, C is used to change the values of γ_1 and M is used to change the values of λ so that $\gamma_N = 0.5$, i.e.,

$$\gamma_A = \frac{25}{12B}, \quad \gamma_1 = \frac{5C}{48}, \quad \gamma_N = \frac{125M}{B^3}. \tag{37}$$

Geometrical parameters $l_o = 1$, $L_o = 50$, $U_o = 1$ are taken the same for all cases. In the dimensionless model equations only material parameter ratios are important, so we have used 'dimensionless' parameters (16) giving convenient ratios.

Three combined parameters (γ_A^2, γ_1^2 and γ_N) collect 8 material and 3 geometrical parameters defined above. As mentioned before, most material and all geometrical parameters are kept constant and only three microstructure-related material parameters are used to change the values of the combined parameters. In the analysis parameters γ_A^2 and γ_1^2 are changed from 0.05 to 0.95 with a step of 0.05 (19 steps), resulting in 361 points in the $\gamma_A^2 - \gamma_1^2$ plane. Nonlinearity-related parameter γ_N is changed from zero value (nonlinearity only in macroscale) up to 0.95 with a step of 0.05 (20 steps) plus an additional 'undefined' value for the fully linear case. Altogether this provides 7581 points covering the combined parameter domain. Analysis of numerical results demonstrated that the influence of parameter γ_N on the character of the solution was relatively weak in the considered domain and therefore only the value $\gamma_N = 0.5$ is used in the present study. In all points energy conservation and pseudomomentum conservation was monitored.

Locations in parameter domain where examples are provided are marked by circles in Fig. 9. The corresponding set of figures can be found in Appendix B, whereas the numbers close to circles in Fig. 9 show the figure number where the example can be found. The dashed line represents the dispersionless case ($\Gamma = 0$), while dash-dotted lines represent the anomalous ($\Gamma = -0.2$) and normal ($\Gamma = +0.2$) dispersion cases investigated below (the quantity Γ is defined by equation (19)). Dotted lines represent fixed values of γ_A^2 and γ_1^2 where the difference between solutions of the FSE (13) and HE (14) is analysed in detail. In Fig. 9, in the domain between thick solid lines, the difference between acoustic branches of dispersion curves of the FSE and HE is less than 5% at a fixed dimensionless wavenumber of $\xi = 1.5$ (see Section 2.4.).

4.2.3. Conserved quantities

One of the conditions needed for solitonic solutions is that the system must be conservative. In the present case energy conservation and pseudomomentum conservation are checked. It is relatively straightforward to check energy conservation for the FSE by just adding up kinetic and free energy ($E = W + K$) and observing if this quantity is conserved over the integration interval. As our solutions are for the governing equations in dimensionless form, we have to express the free and kinetic energy in dimensionless form for the FSE as follows:

$$
\begin{aligned}
W &= \frac{AU_o^2}{2L_o^2}U_X^2 + \frac{B}{2}\varphi^2 + \frac{C}{2L_o^2}\varphi_X^2 + \frac{DU_o}{L_o}\varphi U_X + \frac{NU_o^3}{6L_o^3}U_X^3 + \frac{M}{6L_o^3}\varphi_X^3, \\
K &= \frac{AU_o^2}{2L_o^2}U_T^2 + \frac{AI}{2\rho L_o^2}\varphi_T^2.
\end{aligned}
\tag{38}
$$

The total energy density

$$
\overline{E}(T) = \frac{1}{n}\Sigma_{i=1}^n E(X_i, T)
\tag{39}
$$

is conserved (deviation from constant value is under allowed errors 10^{-7}, see Appendix A) over the observed $\gamma_1^2 - \gamma_A^2$ domain for all of the considered parameter com-
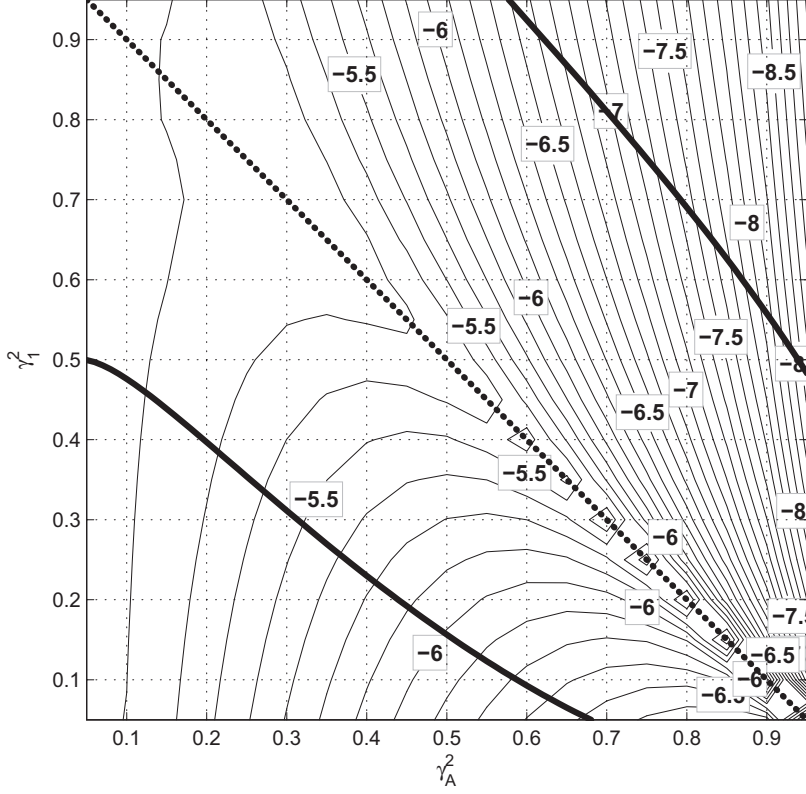
Figure 10: Conservation of pseudomomentum $\log_{10}(P_T - b_X)$ against γ_A^2 and γ_1^2. The FSE in the nonlinear case ($\gamma_N = 0.5$).

binations. In (39) n is the number of grid points and T is dimensionless time.

A second convenient quantity that should be conserved for the FSE is pseudomomentum [5, 6, 12, 14]. In dimensionless form conservation of pseudomomentum can be expressed as $P_T - b_X = 0$, where P_T is the time derivative of pseudomomentum in dimensionless form

$$P_T = -\left[\frac{AI}{\rho L_o^3}\varphi_T\varphi_{XT} + \frac{AI}{\rho L_o^3}\varphi_X\varphi_{TT} + \frac{AU_o^2}{L_o^3}U_TU_{XT} + \frac{AU_o^2}{L_o^3}U_XU_{TT}\right] \qquad (40)$$

39

and b_X is the spatial derivative of the Eshelby stress in dimensionless form

$$
\begin{aligned}
b_X &= \frac{B}{L_o}\varphi\varphi_X - \left(\frac{M}{L_o^4}\left(\varphi_X\right)^2 + \frac{C}{L_o^3}\varphi_X\right)\varphi_{XX} - \frac{AI}{\rho L_o^3}\varphi_T\varphi_{XT} \\
&\quad - \left(\frac{NU_o^3}{L_o^4}\left(U_X\right)^2 + \frac{AU_o^2}{L_o^3}U_X\right)U_{XX} - \frac{AU_o^2}{L_o^3}U_TU_{XT}.
\end{aligned}
\tag{41}
$$

As over the considered $\gamma_1^2 - \gamma_A^2$ domain the defined quantities are changed by several orders in magnitude, we visualize them in the logarithmic scale. Pseudomomentum conservation for the FSE is fulfilled for the linear case with deviation from zero value under allowed error margins. In the nonlinear case (Fig. 10) pseudomomentum conservation is not strictly fulfilled but deviation from zero value is small: $-8.5 < \log_{10}|P_T - b_X| < -5$.

4.2.4. Analysis of results

The behaviour of the quantities presented in Tables 1–12 (see Appendix B) is analysed first and then the examples are discussed afterwards.

Characteristics under investigation

Several characteristics of the pulses emerging from the initial condition and propagating in opposite directions are tracked. The observed effects can be roughly divided into two groups: the first group where it is easy to quantify some characteristics of the waves (amplitude loss, speeds, difference between solutions) and the second group where it is harder to attach a numerical characteristic to the observations (tails associated with the pulses, peakons [3, 31] (short for 'peaked soliton'), elasticity of interactions).

First, it is possible to calculate average speeds of the pulses. The average speed of the pulse can be compared to the characteristic speed of the system. The characteristic speed c_0 (denoted as c_R in [37]) and the average speed c_{avg} are calculated as

$$
c_0 = \sqrt{1 - \frac{D^2}{AB}}, \quad c_{avg} = \frac{\Delta X_s}{T},
\tag{42}
$$

where A, B, D are material parameters and ΔX_s is the distance the pulse peak has travelled during the considered time interval T. The characteristic speed c_0 can be interpreted as the speed of the very long waves in the system. Unless otherwise noted, we take $T = 100$. The results of the calculations are presented in Tables 1–6 (see Appendix B). Note that the calculated speed actually belongs to the peak of the wave. One might get different results by finding some other point to track in the waveprofile (for example, by tracking the wave front at a fixed amplitude value or by using some averaged value for the entire wave structure propagating in the same direction). Because there exist minor differences between the speeds of waves propagating in

opposite directions, separate tables are produced for the pulses propagating to the left and right in the nonlinear cases. For the nonlinear FSE Tables 1 and 2 show the average speed of the left and right propagating pulses, respectively. In the linear case there is no speed difference between the left and right propagating waves, so Table 3 presents average speeds for the linear FSE. For the nonlinear HE, speeds of left and right propagating pulses can be found in Tables 4 and 5, respectively. Linear HE speed is presented in Table 6.

A second quantity that can be easily quantified is the loss of the amplitude of the pulse by the end of integration. The amplitude loss of the pulse by the end of integration is calculated in per cent compared to the initial amplitude after the splitting of the initial single pulse into two pulses that have amplitudes $A_0 = 0.5$. Amplitude loss is calculated as

$$\Delta A = 100 - \frac{A_{end}}{A_0} \cdot 100, \tag{43}$$

where A_{end} is the amplitude of the pulse at the end of integration. Under some parameter combinations interaction of waveprofiles happens in close proximity of the end of integration. In these cases extrapolation is used to estimate the amplitude at the end of integration. In the nonlinear cases the quantity ΔA is different for pulses propagating in opposite directions. For the nonlinear FSE Table 7 presents amplitude losses for the pulse propagating to the left and Table 8 for the pulse propagating to the right. In the linear case pulses propagating in opposite directions have equal amplitudes. For the linear FSE amplitude loss by the end of integration is presented in Table 9. For the nonlinear HE Tables 10 and 11 show amplitude losses for the pulses propagating to the left and right, respectively, while Table 12 shows amplitude loss for the linear HE. The essence of the amplitude losses is exposed in the discussion.

In order to calculate the difference between the solutions of the HE and FSE the quantity Δ^S is introduced as

$$\Delta^S = \frac{1}{n} \sum_{i=1}^{n} \Delta_i, \qquad \Delta_i = \left| U^{HE}(X_i, T_f) - U^{FSE}(X_i, T_f) \right|, \tag{44}$$

where n is the number of grid points. In the dispersion analysis [37] the quantity calculated was the difference between acoustic branches of the dispersion curves at one specific dimensionless wavenumber, while quantity (44) calculates the average difference between the FSE and HE solutions at the end of integration. It should be noted that while (43) could be used to trace differences in the main pulse amplitudes, quantity (44) takes into account also differences in the tail parts of the waveprofiles. The quantity Δ^S against γ_A^2 and γ_1^2 is presented in Figs. 35 and 36 (Appendix B) for the linear and nonlinear cases, respectively. In Figs. 37–45 the difference between solutions of the FSE (13) and HE (14) is shown in 6 sections at fixed values of γ_A^2 and γ_1^2 and in 3 dispersion-related sections ($\Gamma = -0.2, 0, +0.2$) pointed out in Fig. 9.

Some of the effects are best exposed with the help of examples. For that end in Fig. 9 locations in the γ_A^2–γ_1^2 domain where examples (Figs. 20–34) are presented are marked by circles. The effects that are easiest to expose with the help of examples are, for example, observations about tails associated with the main pulses and emergence of peakons (short for 'peaked soliton').

Average speeds of waves

Average speeds (42) of the pulses are presented in Tables 1–6 in Appendix B. The accuracy of the calculation of the speeds is $\approx 10^{-5}$ (number of grid points for the speed calculations is 2^{16}, i.e., $\Delta X = 5.75 \times 10^{-4}$). In the tables the direction of the γ_1^2 axis has been reversed compared to Fig. 9, so the parameter combinations resulting in the dispersionless case are located on the diagonal from the lower left corner to the upper right corner in the tables and dispersion is of normal type above and of anomalous type under that diagonal.

It is possible to see that average speeds of the pulses decrease in the direction of increasing γ_A^2 and increase in the direction of increasing γ_1^2, however, the influence of γ_1^2 is weak. Taking a look at characteristic speed c_0 (42), one can note that the calculated average speeds are smaller than or equal to the characteristic speed in the case of normal dispersion, while in the anomalous dispersion case the calculated speeds are greater than or equal to the characteristic speed. In the dispersionless case the calculated speeds tend to be close (or in most cases equal) to the characteristic speeds.

In the nonlinear cases minor differences can be noted in the average speeds between pulses propagating to the right and to the left. The pulses propagating to the left tend to be faster than these propagating to the right (other than two small subdomains, see Figs. 18 and 19 in Appendix B). However, it must be noted that the speed differences are too small to show any noticeable effect over the considered integration interval in the presented examples. In the linear cases there is no speed difference between waves propagating in opposite directions.

Under some parameter combinations distortions from the oscillations associated with pulses are too strong or the interaction event is too close to the end of integration to get reliable measurements. For this reason a shorter time interval was used for measuring the average speed. The location of waveprofile peaks was found at $T = 95$ for $\gamma_A^2 = 0.5$; $T = 90$ for $\gamma_A^2 = 0.1$ and $\gamma_A^2 = 0.45$; $T = 85$ for $\gamma_A^2 = 0.4$, $\gamma_A^2 = 0.65$ and $\gamma_A^2 = 0.70$; $T = 50$ for $\gamma_A^2 = 0.75$ and $\gamma_A^2 = 0.8$; $T = 25$ for $\gamma_A^2 = 0.85\ldots0.95$.

Amplitude losses

In order to quantify the behaviour of the solutions over the considered parameter domain, we introduced the quantity ΔA (43), which describes the amplitude loss of the main pulses in per cent compared to the initial amplitude (after the splitting of the initial pulse). Amplitude losses are presented in Tables 7–12 in Appendix B. As mentioned, in the tables the direction of the γ_1^2 axis has been reversed compared to Fig. 9, i.e., the parameter combinations resulting in the dispersionless case are located on the diagonal from the lower left corner to the upper right corner, and dispersion is of normal type above that diagonal and of anomalous type under it. The physical interpretation of amplitude losses is given in the subsection 'Examples and discussion'.

At a glance it can be noted that in general amplitude losses increase with increasing γ_A^2 as well as with the distance from the dispersionless case. Maximum amplitude losses are 66% for the nonlinear FSE and HE right propagating pulses at high values of γ_A^2 and γ_1^2.

For the FSE (Tables 7–9) in the nonlinear dispersionless case the amplitude is practically maintained for the pulse propagating to the left (losses up to 1% can be seen), while for the pulse propagating to the right amplitude loss is from 0% ($\gamma_A^2 = 0.05$) up to 29% ($\gamma_A^2 = 0.95$). Examples for the dispersionless case can be found in Figs. 20, 24, 27, 30 and 34 from the lowest value of γ_A^2 to the highest value. Following lines $\Gamma = $ const, parallel to the dispersionless case diagonal, it is clear that amplitude losses increase with increasing γ_A^2. In the linear case no amplitude difference can be detected between waves propagating in opposite directions. Examples for the anomalous dispersion case can be found in Figs. 23, 26, 29, 32 and 33, while examples for the normal dispersion case in Figs. 21, 22, 25, 28 and 31. In the linear case the amplitude losses of the pulses are greater than the amplitude losses of the pulses propagating to the left but lower than these of the pulses propagating to the right in the nonlinear cases (see Tables 7–9).

For the HE (Tables 10–12) the same trends can be drawn as for the FSE in the nonlinear and linear cases. However, minor differences can be noted in details. For the nonlinear HE in the dispersionless case amplitude losses of the pulses propagating to the right (from 0% up to 32%) are greater than these of the pulses propagating to the left (amplitude gain from 0% up to 2%).

Comparison of the HE and FSE solutions

In order to calculate the difference between the solutions of the HE and FSE, we introduced the quantity Δ^S, defined by equation (44). In dispersion analysis [37] the difference between acoustic branches of the dispersion curves at one specific dimensionless wavenumber is calculated, while the quantity Δ^S calculates the average difference between solutions of the FSE and HE at the end of integration.

Results of dispersion analysis [37] can be compared to the results obtained here (Figs. 35 and 36). In dispersion analysis up to 5% difference between acoustic branches of the dispersion curves at a specific dimensionless wavenumber is considered 'good', while in the present case the average difference between solutions of the FSE and HE at the end of integration $\Delta^S < 10^{-2}$ is considered 'good'. It must be admitted that both of those numbers are relatively arbitrary. From results (Figs. 35 and 36) one can note that the domain which is good in dispersion analysis sense is a subdomain in the domain which is good in the sense of Δ^S, excluding a small region.

Concurrency of solution is good ($\Delta^S < 10^{-2}$), in case of normal dispersion even if we are outside the domain predicted by dispersion analysis. Moreover, Δ^S has the smallest values in the region $\gamma_A^2 \leq 0.15$, which is not predicted by dispersion analysis. In this region lines $\Delta^S = $ const are nearly vertical, i.e., they practically do not depend on the value of Γ and the dispersion type. In general, the quantity Δ^S increases if γ_A^2 and γ_1^2 increase simultaneously. The linear case has negligibly lower or equal values of Δ^S compared to the nonlinear case.

For a more detailed comparison of the quantity Δ^S between the linear and nonlinear cases several sections of the $\gamma_A^2 - \gamma_1^2$ plane are presented. In Fig. 9 these sections are marked by dotted lines for fixed γ_A^2 and γ_1^2 values, by dash-dotted lines for the anomalous and normal dispersion type sections, and a dashed line marks the dispersionless case. Sections are provided at $\gamma_A^2 = 0.05$ (Fig. 37), $\gamma_A^2 = 0.5$ (Fig. 38), $\gamma_A^2 = 0.95$ (Fig. 39), $\gamma_1^2 = 0.05$ (Fig. 40), $\gamma_1^2 = 0.5$ (Fig. 41), $\gamma_1^2 = 0.95$ (Fig. 42) and for three fixed values of the Γ at $\Gamma = -0.2$ (Fig. 43) for the anomalous dispersion case, $\Gamma = +0.2$ (Fig. 44) for the normal dispersion case and $\Gamma = 0$ (Fig. 45) for the dispersionless case.

In the $\gamma_A^2 = 0.05$ section in Fig. 37 the quantity Δ^S has lower values for the linear case, however, the difference between linear and nonlinear cases is negligible (note the logarithmic scale) and the concurrency of solutions is good. In the nonlinear case the concurrency gets better in the domain around the line $\Gamma = 0$ (dispersionless case), while in the linear case the concurrency of the solutions is relatively constant and better than in the nonlinear case over the whole section. Three examples are provided along this section in Figs. 20–22. Note the 'peakon'-type waveprofile for the nonlinear FSE and HE in Fig. 20 at $\gamma_1^2 = 0.95$ in the dispersionless case, while no peakon emerges in the linear case.

In the $\gamma_A^2 = 0.5$ section in Fig. 38 the difference between the linear and nonlinear cases is negligible and differences between solutions are small enough to be considered good. Local minima exist around the dispersionless case ($\gamma_1^2 = 0.5$) in the interval of $0.25 \leq \gamma_1^2 \leq 0.75$. Three examples are provided for this section in Figs. 26–28. It can be noted that in the nonlinear dispersionless case one of the waveprofiles has morphed into a peakon by the end of integration.

44

In the $\gamma_A^2 = 0.95$ section in Fig. 39 the concurrency of solutions can be considered good ($\Delta^S < 10^{-2}$) around the dispersionless case $\gamma_1^2 \leq 0.4$. This observation is confirmed by three examples provided in Figs. 32–34. The differences between solutions are small (especially in the nonlinear case for the waveprofiles that has morphed into peakon), in the dispersionless case example in Fig. 34 although it must be admitted that solutions of the HE and FSE do have different amplitudes. The same can be stated for the second example located at $\gamma_1^2 = 0.25$ (Fig. 33). However, in the example located at $\gamma_1^2 = 0.95$ (Fig. 32) the concurrency between solutions of the HE and FSE has visibly deteriorated, with a better agreement between linear and nonlinear cases (comparing the nonlinear FSE to the linear FSE) than between solutions of the HE and FSE (comparing the nonlinear HE to the nonlinear FSE).

Next three sections are presented along horizontal lines at fixed values of γ_1^2 (Figs. 40–42). All three figures demonstrate quite clearly that the concurrency of solutions between the FSE and HE deteriorates in the direction of increasing γ_A^2. The difference between linear and nonlinear cases is negligible. At the value of $\gamma_1^2 = 0.05$ in Fig. 40 the concurrency of solutions remains good at all values of γ_A^2. At higher values of γ_1^2, however, the concurrency can no longer be considered good at all values of γ_A^2. In Fig. 41 the concurrency is good at $\gamma_A^2 \leq 0.85$ and in Fig. 42 at $\gamma_A^2 \leq 0.7$.

The last three sections are considered at fixed values of the quantity Γ: a anomalous dispersion case, a dispersionless case and a normal dispersion case. The anomalous dispersion case $\Gamma = -0.2$ section in Fig. 43 and the normal dispersion case $\Gamma = +0.2$ section in Fig. 44 are remarkably similar (note that Fig. 43 covers the interval from $\gamma_A^2 = 0.25$ up to $\gamma_A^2 = 0.95$, while Fig. 44 covers from $\gamma_A^2 = 0.05$ up to $\gamma_A^2 = 0.75$) other than the direction of tails if looking also at examples. The concurrency of the solutions of the FSE and HE is good in all three cases. In the dispersionless case in Fig. 45 the concurrency of solutions is marginally better (≈ 0.05) at the same values of γ_A^2 than in the anomalous and normal dispersion cases that have values closer together.

In the domain of parameters, where according to dispersion analysis the difference of dispersion curves of the HE and FSE is less than 5%, the agreement between solutions of the HE and FSE is good. It must be noted that as long as the dispersion is weak enough and integration interval considered is short enough ($T \leq 100$), the concurrency between solutions of the FSE and HE is good. Overall differences between solutions are small at low values of γ_A^2 and γ_1^2 and increase with the mentioned parameters. The shape of the 'good' agreement domain is similar to the one predicted by dispersion analysis, although there exists an additional domain at low γ_A^2 values (however, it must be noted that good agreement there is logical, as microstructure-related terms are weaker at low values of γ_A^2). In general, the linear case has slightly smaller differences between solutions of the FSE and HE than the nonlinear case, although the difference is small enough to be called negligible.

Specifically: (i) good agreement between solutions of the FSE and HE exists in the considered domain of parameters except at high values of γ_A^2 and γ_1^2; (ii) the differences between solutions of the FSE and HE increase if γ_A^2 and γ_1^2 increase simultaneously; (iii) at low values of γ_A^2 there exists a region where the difference between solutions is very small and which was not predicted by dispersion analysis.

Examples and discussion

Examples in Figs. 20–34 in Appendix B are provided in the sets of three in the direction of increasing γ_A^2 and decreasing γ_1^2. The structure of the figures is described at the beginning of Appendix B. The main focus is on the area, where according to dispersion analysis, the concurrency of the solutions of the HE and FSE should be good, however, two examples are provided also in the corners of the parameter domain as 'far' as possible from the expected domain of good concurrency.

The first three examples in Figs. 20–22 show remarkable stability of the solutions at combinations of material parameters resulting in low values of the combined parameter γ_A^2. Regardless of remarkable stability, it is obvious that there is a fundamental difference between linear and nonlinear cases. In the linear case propagating waves are symmetric with respect to $X = 6\pi$ (coordinate of the peak of the initial pulse), while in the nonlinear cases waves propagating in opposite directions evolve differently (different amplitudes, for example) over the considered integration interval. Even the 'strongest' (in the sense of the quantity Γ (19)) considered normal dispersion case in Fig. 22 has only very small differences compared to the dispersionless case.

The next three examples in Figs. 23–25 show that with increasing γ_A^2 the tails appear in the normal and anomalous dispersion cases and that difference between the amplitudes of waveprofiles propagating in opposite directions increases. In the dispersionless case the pulse propagating to the right has a peakon profile, while the pulse propagating to the left has gained width. In the normal and anomalous dispersion cases close-ups of the bottom sections demonstrate small tails. In the case of normal dispersion a tail appears in the opposite direction of the propagation of the pulse, and vice versa in the case of anomalous dispersion. At the top right panel of the figure, showing minima and maxima against time, it is possible to see that in the case of normal and anomalous dispersions the maximum of the lower pulse starts dropping after the first interaction. Tails are too small to be visible on the contour plots (the lowest amplitude registered in the contour plot is 0.01).

Three examples at $\gamma_A^2 = 0.5$ (Figs. 26–28) could be described as the most expressive of the behaviour of the solutions of the HE and FSE. All interesting effects are strong enough to be visible but not strong enough to overwhelm the main pulses. The pulses are far enough from each other and the tails small enough to be fully separated at the end of integration. Figures 26 and 28 show anomalous and normal dispersion cases, respectively, while the dispersionless case can be seen in Fig. 27. The tails associated

with the propagating pulses appear relatively fast even before the first interactions in anomalous and normal dispersion cases. Differences between solutions of the FSE and HE are easily detectable in the close-up sections of the figures with nonlinear HE pulses having higher amplitudes than the nonlinear FSE pulses by the end of integration.

The penultimate set of examples at $\gamma_A^2 = 0.75$ in Figs. 29–31 does not bring any new effects on the table compared to the examples observed so far. The tails of the waveprofiles are stronger and amplitude losses higher for the main pulses in the case of anomalous and normal dispersion cases.

However, the last set of examples at $\gamma_A^2 = 0.95$ in Figs. 32–34 is more interesting than to the previous examples as it starts with the strongest anomalous dispersion case considered. As noted earlier, the concurrency of the solutions of the HE and FSE worsens with increasing γ_A^2. In Fig. 32 the situation is as 'bad' as it can get within the considered set of parameters. From the provided example it is indeed immediately apparent that the concurrency of the solutions of the FSE and HE is not good. However, the last two examples ($\gamma_1^2 = 0.25$ and $\gamma_A^1 = 0.05$) demonstrate that even at high values of γ_A^2 good concurrency between solutions can be achieved if dispersion is weak ($|\Gamma| \leq 0.3$). One more thing to note is the small oscillations in Fig. 34. It should be mentioned that those exist only in the case of the FSE and not in the HE. The amplitude of those oscillations is between 10^{-3} (high values of γ_A^2) and 10^{-5} (low values of γ_A^2) under the used material parameters (Figs. 27 and 30). Compared to the amplitude of the main pulses in the solutions, the oscillations can be considered negligible. It has been pointed out (for example in [38]) that the FSE has both optical and acoustic dispersion branches, while the HE has only the acoustic branch that might be related to this phenomenon.

Considering the examples on average speeds presented in Tables 1–6, we should mention that what we are actually measuring is the speed of the peak of the waveprofile main pulse. Depending on the dispersion type, waveprofiles are deformed, shifting the peak in the direction of the tail associated with the waveprofile. In the normal dispersion case the tail appears behind the pulse and in the anomalous dispersion case in front of the pulse. So one could argue that 'true' speed of the wave structure can be calculated in the dispersionless case. However, normal and anomalous dispersion cases have one significant qualitative difference when compared to the dispersionless case for the nonlinear FSE and HE. In the dispersionless case waves propagating in opposite directions have equal average speeds regardless of their amplitude, while in the anomalous and normal dispersion cases average speeds of the pulses tend to have some correlation with the amplitude of the pulse. It is also worth keeping in mind that the parameters in use are, in fact, combined by collecting material and geometrical parameters. So the behaviour of solutions can, in turn, be more complex than easily observed in the domain of the three combined parameters, as is, for example, the existence of two subdomains (Figs. 18 and 19) in the nonlinear cases where the

wave propagating to the right is faster than the wave propagating to the left.

On the basis of the examples on amplitude losses presented in Tables 7–12 it should be pointed out that when main pulses lose amplitude, the tails associated with the waveprofiles are stronger. It stands to reason that in the normal and anomalous dispersion cases the main cause of amplitude losses is dispersion. No tails occur in the dispersionless case, however waveprofiles morph during the evolution. The pulse propagating to the right morphs into a peakon (thinner, lower amplitude, sharp peak), while the pulse propagating to the left maintains the amplitude exceptionally well and morphs into a profile that is wider than the initial $sech^2$-type profile. In the cases where dispersion is either normal or anomalous, the pulse propagating to the right has a lower amplitude but the tail associated with it has a higher amplitude than the tail associated with the pulse propagating to the left. In the linear case no such morphing happens and propagating waveprofiles are symmetric with respect to $X = 6\pi$. In this sense the FSE and HE behave in the same way in the linear and nonlinear cases.

The examples demonstrate that the quantity Δ^S is good for describing the average difference between solutions of the HE and FSE, but it does overlook some details, for example, asymmetry between solitary waves propagating in opposite directions (emerging under most parameter combinations in the nonlinear cases) and the presence of additional oscillations in the FSE but not in the HE. It is also worth pointing out that differences (in waveprofiles) between the linear and nonlinear cases are relatively large for some parameter combinations. This is not reflected in Figs. 35–45, showing that the quantity Δ^S (difference between solutions of the HE and FSE) has values of the same order of magnitude in the linear and nonlinear cases.

Soliton-like behaviour can be observed at low values of parameter γ_A^2 as well as when the dispersion related parameter Γ is small. The solitonic behaviour is easiest to spot in the provided figures in the top right panel where two the highest maxima and two lowest minima are shown. At the lowest values of $\gamma_A^2 \leq 0.15$ one can see maxima of interacting waveprofiles restored consistently even after several interactions. At higher values of γ_A^2 the amplitudes are not restored everywhere in the considered parameter domain but only when parameter Γ is low. There is a rough rule of thumb: the lower the value of $\gamma_A^2 \cdot |\Gamma|$, the closer the behaviour of the solutions to the solitonic behaviour. However, even when the quantity $\gamma_A^2 \cdot |\Gamma|$ has low values, some changes can be noticed in the waveprofiles as interactions between waveprofiles are not fully elastic but only almost elastic. The solitonic behaviour is very similar to the one observed in Section 4.1. where the HE in deformation terms (15) was investigated. Although the interactions are not fully elastic, for all practical purposes, when dealing with a low enough number of interactions, it is possible to consider the waves at low values of parameter γ_A^2 or weak enough dispersion to be solitons.

Overall it is clear that nonlinearity or lack of it has a quite significant effect on the behaviour of the solutions of the HE and FSE. For example, the emergence of peakon-type waves in the nonlinear dispersionless cases is an interesting phenomenon (observed, for example, in Publication V).

In general, the speed of the wave mainly depends on parameter γ_A^2, with smaller corrections introduced by parameter γ_1^2 (17). This is in agreement with the physical interpretation of the parameters where γ_1 is interpreted as dimensionless speed of short waves and $\sqrt{1 - \gamma_A^2}$ as the dimensionless speed of long waves. The location of the tails related to the main pulse clearly depends on the dispersion type. This phenomenon is easily explained considering the meaning of the dispersion-related parameter Γ in the present context. For example, in the case of anomalous dispersion the harmonics with a shorter wavelength propagate at a higher phase speed than these of longer waves, causing the tail to appear in the direction of propagation.

Concluding remarks

In the present subsection the main focus was on the solutions of the FSE and confirming that those behave in the same way as the solutions of the HE. The confirmation of the similarity between solutions of the FSE and HE is essential, as for the HE the inverse problem has been solved in [28], opening a door towards practical applications.

To sum up, we can say that the model equations give in most cases similar results and the HE (14) is good a approximation of the FSE (13). The best concurrency between solutions of the HE and FSE were found at low values of parameter γ_A^2. Several interesting effects were observed — in the nonlinear cases waves propagating in opposite directions evolve differently, while no such effect was noticed in the linear case. Moreover, nonlinearity introduces additional effects that are not present in the linear cases like, for example, the emergence of peakon-type waveprofiles in the nonlinear dispersionless cases. More specifically — in the nonlinear dispersionless cases the pulses propagating to the left maintain the amplitude exceptionally well and morph into a profile that is wider than the initial sech^2-type profile, while the pulses propagating to the right morph into a peakon-like shape (thinner, lower amplitude, sharp peak). From the speeds of the pulses it is clear that the speed of the main pulse decreases with increasing γ_A^2 and has minor corrections from parameter γ_1^2. In addition, it was noted that the speed of the main pulse was higher than or equal to the characteristic speed of the system c_0 (42) in the normal dispersion case and smaller than or equal to it in the anomalous dispersion case. An interesting phenomenon can be highlighted regarding the amplitudes of the pulses — the higher the main pulse, the lower the amplitude of the associated tail and vice versa. One could say that tails form a more significant part of the wave structure by the end of the integration interval with increasing γ_A^2. Amplitude loss depends on the values of quantities γ_A^2 and Γ. For a fixed value of γ_A^2, the greater the $|\Gamma|$ the greater the amplitude loss. The next ob-

servations related to the amplitude and wave shape show that the smaller the quantity $\gamma_A^2 \cdot |\Gamma|$, the closer the behaviour of the solutions of the HE (14) and FSE (13) to the solitonic behaviour. In conclusion, we may say that predictions from linear dispersion analysis (in the domain where acoustic branches of dispersion curves of the FSE and HE differ less than 5% solutions of the FSE and HE have good concurrency, and solutions behave differently in the normal and anomalous dispersion cases) hold also for the nonlinear cases. However, nonlinearity introduces additional effects (asymmetry between pulses propagating in opposite directions, formation of peakons, etc.) not taken into account by (linear) dispersion analysis. In addition, numerical results for the FSE (13) and HE (14), considered in the present subsection, confirm previous analytical [28, 29] and numerical (Publications I–III) results for the HE (15). Key results from the present subsection are presented in Conclusions in a more structured way.

5. Conclusions

The central aim of the present thesis was investigation of wave propagation and interaction in Mindlin-type microstructured solids. For this reason numerical solutions of three model equations were analysed — the FSE (13) and HE (14) in the displacement terms as well as the HE (15) in terms of deformations.

The results have been published in six papers that can be grouped as follows: (i) Publications I–III are dedicated to the propagation and interaction of deformation waves covered by the HE (15); (ii) publications IV–VI deal with the propagation and interaction of displacement waves covered by the FSE (13) and HE (14).

Combined parameters γ_A^2 and γ_1^2 (17) define the speed of long and short waves, respectively (see Subsection 2.3.). The greater parameter γ_A^2, the smaller the speed of long waves and the greater parameter γ_1^2, the greater the speed of short waves. On the other hand, the values of parameters A, D, ρ and I are fixed (see Subsection 4.2.2.), and the smaller the value of B, the greater the value of γ_A^2 and the greater the value of C, the greater the value of γ_1^2.

A note about asymmetry between waves propagating in opposite directions should be highlighted. This effect is present in all studied nonlinear cases, however, strength of the observed effect does not depend only on the nonlinear parameters but also on ratios between free energy parameters. Under some parameter combinations (like the ones used to study the HE (15), for example) microstructure nonlinearity is the driving force of such effect, while under some other parameter combinations (like the ones used to study the FSE (13) and HE (14)) macroscale nonlinearity can be the main driving force.

More specifically it is possible to highlight the following results:

- The hierarchical equation (15).

  1. Numerical simulations show that the initial symmetric bell-like pulse (26) is altered to that of asymmetric shape during propagation in the case of $\lambda > 0$. In the case of $\lambda = 0$ the initial pulse (26) propagates at a constant speed and shape until the first interaction. However, it is apparent that interactions are not fully elastic as even in the case of $\lambda = 0$ the initial symmetric bell-like pulse is morphed into ansymmetric one during interactions. Some radiation is generated during interactions in both cases.

  2. The asymmetry of the pulse is reflected by the altering of the shape of the compression region of the pulse as well as in the emergence of the depression zone beside that of compression.

  3. In the case of $\lambda = 0$ and $A_1^0 = A_2^0$ the asymmetry is very weak after the very first interactions. However, the higher the number of interactions,

the more distinctive the asymmetry. In the case of $A_1^0 \neq A_2^0$ the shape of the higher wave has only minor distortions, while the shape of the lower-amplitude wave is subject to stronger distortions.

4. Phase shifts, characteristic of soliton-type interactions, can be easily traced in the case of $A_0^1 \neq A_0^2$. In the case of $A_0^1 = A_0^2$ even the cumulative phase shift over long time intervals is small compared to the considered space interval and/or the distance travelled by interacting waves.

5. If $\lambda = 0$ and $A_0^1 = A_0^2$, then the phase shifts during interactions are equal for both solitary waves. If $\lambda \neq 0$ or $A_0^1 \neq A_0^2$, then the phase shifts during interactions are different.

6. Parameter λ has stronger influence on the character of the solutions in the cases where $A_0^1 = A_0^2$.

7. Over short time intervals and a small number of interactions the behaviour of the solution is very close to the solitonic behaviour in all considered cases. The higher the number of interactions and the longer the time interval, the greater the difference between the initial and restored waveprofiles.

- The hierarchical equation (14) and full system of equations (13).

1. The model equations give in most cases similar results and therefore the HE (14) is a good approximation of the FSE (13) (see Section 4.2.).

2. The best concurrency between solutions of the HE and FSE can be found at low values of parameter $\gamma_A^2 \leq 0.15$ In the parameter domain $\gamma_A^2 \leq 0.15$ the effect of parameter γ_1^2 can be considered negligble.

3. There are small oscillations in front of the propagating wave structure for the higher values of parameter γ_A^2 in the case of the FSE. According to Publication IV, the reason for this effect may be the existence of the optical branch of the dispersion curve (besides the usual acoustic one) in the case of the FSE.

4. The speed of the main pulse decreases with increasing γ_A^2 and has minor corrections from parameter γ_1^2.

5. The speed of the main pulse is higher than or equal to the characteristic speed c_0 (42) of the system in the normal dispersion case and smaller than or equal to it in the anomalous dispersion case.

6. The higher the amplitude loss of the main pulse, the higher the amplitude of the associated tail and vice versa.

7. The direction of the asymmetry of waveprofiles is dependent on the dispersion type and nonlinearity accelerates the emergence of asymmetry.

8. In the nonlinear cases waves propagating in opposite directions evolve differently, while in the linear cases such effect cannot be observed. The linear cases are symmetric with respect to $X = 6\pi$ (the length of the space period is 12π).

9. In the nonlinear dispersionless cases the pulse propagating to the left maintains the amplitude exceptionally well and is wider than the initial sech^2-type profile. The pulse propagating to the right morphs into a peakon-like shape (thinner, lower amplitude, sharp peak).

10. The tails emerge faster and form a more significant part of the wave structure by the end of the integration interval with increasing γ_A^2.

11. The smaller the quantity $\gamma_A^2 \cdot |\Gamma|$, the closer the behaviour of the solutions of the HE (14) and FSE (13) to the solitonic behaviour.

12. Predictions from linear dispersion analysis (solutions of the FSE and HE have good concurrency in the domain where acoustic branches of dispersion curves of the FSE and HE differ less than 5% and behave differently in the normal and anomalous dispersion cases) hold also for the nonlinear cases. However, nonlinearity introduces additional effects (asymmetry between pulses propagating in opposite directions, formation of peakons, etc.) not taken into account by (linear) dispersion analysis.

Prospective studies

Several effects that need further investigation must be pointed out. First, asymmetry between waveprofiles propagating in opposite directions can be observed in the nonlinear cases for all considered model equations. However, the physical background of this phenomenon needs additional analysis. Another interesting effect is the appearance of additional low-amplitude oscillations in the solutions of the FSE that are not present in case of the HE. Several other aspects would also deserve more attention: (i) proper evaluation of wave profile speed (measuring the 'centre' of the waveprofile and tracking its speed); (ii) phase shifts during interactions (there is negligible phase shift if waves have equal amplitudes but in the nonlinear cases they do not have equal amplitudes, so small phase shifts are present); (iii) tracking the speed of harmonics and comparing results with linear dispersion analysis in order to determine the effect of nonlinearity on dispersion; (iv) as in case of the FSE (13) and HE (14) interactions between solitary waves propagating in opposite directions are not entirely elastic, the effect of interactions on the evolution of those waves needs detailed analysis, as done in Publication III for the solitary waves that correspond to the HE (15); (v) discrete spectral analysis [43] should be applied to more detailed analysis of the time-space behaviour of solutions (including possible recurrence of the initial state); etc. Certainly, the long-term objective is to carry out physical experiments according to the results of numerical experiments and to apply the considered models in nondestructive evaluation of materials.

Abstract

The focus of the thesis is on wave propagation in Mindlin-type nonlinear microstructured materials in one-dimensional setting. Model equations are two-wave equations derived by Engelbrecht and Pastrone [13]. Three versions of the model equations are studied: (a) the full system of equations (13) in terms of displacement, (b) the hierarchical model equation (14) in terms of displacement and (c) the hierarchical model equation (15) in terms of deformation. Equations (14) and (15) are of the Boussinesq type. The full system of equations (13) is derived from Euler–Largange equations by determining the suitable free energy function, while equations (14) and (15) are approximations of equation (13) derived by application of the slaving principle [12].

Model equations, nonlinear partial differential equations with mixed derivatives, are solved numerically with pseudospectral method. The initial condition used is a bell-shaped waveprofile. In the case of hierarchical equations a change of variables is employed to enable the application of the pseudospectral method.

The key results of the thesis are: (i) the hierarchical equation (14) is a good approximation to the full system of equations, (ii) if there exists nonlinearity in microstructure, then propagating waveprofiles evolve to be asymmetric and waves propagating in opposite directions evolve differently in time, (iii) interactions between propagating solitary waves are not fully elastic, however, over short time intervals and over a low number of interactions the behaviour of waves is soliton-like, (iv) concurrency of the solutions of the full system of equations (13) and hierarchical equation (14) degrades if parameters γ_A^2 (linked to the speed of the long waves in the system) and γ_1^2 (linked to the speed of the short waves in the system) increase simultaneously, (v) in the nonlinear dispersionless case a 'peakon'-type waveprofile can emerge.

The results of the thesis have been presented in seven international conferences and published in six scientific papers, five of them in journals indexed by ISI Web of Science.

Kokkuvõte

Käesolevas töös uuritakse ühedimensionaalset lainelevi Mindlini-tüüpi mittelineaarsetes mikrostruktuursetes materjalides. Mudelvõrrandid on kahe-laine võrrandid, mis on tuletatud Engelbrechti ja Pastrone poolt [13]. Mudelvõrranditest on uuritud kolme erinevat versiooni: (a) nõndanimetatud täielik võrrandisüsteem (13) (siiretes), (b) hierarhiline võrrand (14) (siiretes), (c) hierarhiline võrrand (15) (deformatsioonides). Võrrandid (14) ja (15) on Boussinesq tüüpi. Võrrandisüsteem (13) on saadud Euleri–Lagrange võrranditest ja hierarhilised võrrandid (14) ja (15) on võrrandi (13) aproksimatsioonid, mis on tuletatud allutusprintsiibi [12] abil.

Mudelvõrrandid (segaosatuletistega mittelineaarsed diferentsiaalvõrrandid) on lahendatud numbriliselt lokaliseeritud algtingimuste ning perioodiliste rajatingimustega. Algtingimusena kasutatakse sech^2-tüüpi lainerofiili. Numbriliseks integreerimiseks on kasutatud pseudospektraalmeetodit kusjuures hierarhiliste võrrandite korral on kasutatud muutujavahetust, mis muudab võimalikuks pseudospektraalmeetodi rakendamise.

Töös on leitud, et: (i) hierarhiline võrrand (14) on täieliku võrrandisüsteemi (13) kvaliteetne lähend, (ii) juhul kui mikrotaseme mittelineaarsust on arvesse võetud (vastav parameeter on mudelvõrrandites nullist erinev), siis muutuvad lained kujult ebasümmeetriliseks ning lisaks omandavad erinevates suundades levivad lained erineva kuju, (iii) interaktsioonid üksiklainete vahel on nõrgalt mitteelastsed, kuid suhteliselt lühikeste ajavahemike ja väikeste interaktsioonide arvu korral käituvad formeerunud üksiklained väga sarnaselt solitonidele, (iv) kokkulangevus täieliku võrrandisüsteemi (13) ja aproksimatsiooni (14) vahel halveneb parameetrite γ_A^2 (seotud pikkade lainete kiirusega süsteemis) ja γ_1^2 (seotud lühikeste lainete kiirusega süsteemis) samaegsel kasvamisel, (v) juhul kui süsteemis dispersioon puudub, kuid mittelineaarsus eksisteerib on võimalik 'peakon'-tüüpi laineprofiilide teke.

Käesoleva töö tulemused on esitatud seitsmel rahvusvahelisel konverentsil ja avaldatud kuues teadusartiklis rahvusvaheliselt tunnustatud erialaajakirjades ja konverentsikogumikes, millest viis on indekseeritud ISI Web of Knowledge poolt.

References

[1] T. B. Benjamin, J. L. Bona, and J. J. Mahony. Model equations for long waves in nonlinear dispersive systems. *Philosophical Transactions of the Royal Society A: Mathematical, Physical and Engineering Sciences*, 272(1220):47–78, 1972.

[2] L. Brillouin. *Wave propagation in periodic structures*. Dover Publications Inc., New York, 1953.

[3] R. Camassa and D. Holm. An integrable shallow water equation with peaked solitons. *Physical Review Letters*, 71(11):1661–1664, 1993.

[4] Y. Chen, J. D. Lee, and A. Eskandarian. Atomistic viewpoint of the applicability of microcontinuum theories. *International Journal of Solids and Structures*, 41(8):2085–2097, 2004.

[5] C. Christov, G. Maugin, and A. Porubov. On Boussinesq's paradigm in nonlinear wave propagation. *Comptes Rendus Mécanique*, 335(9–10):521–535, 2007.

[6] C. Christov, G. Maugin, and M. Velarde. Well-posed Boussinesq paradigm with purely spatial higher-order derivatives. *Physical Review E, Statistical Physics, Plasmas, Fluids, and Related Interdisciplinary Topics*, 54(4):3621–3638, 1996.

[7] C. I. Christov and M. Velarde. Dissipative solitons. *Physica D: Nonlinear Phenomena*, 86(1–2):323–347, 1995.

[8] E. Cosserat and F. Cosserat. *Théorie des corps déformables*. Hermann & Fils, Paris, 1909.

[9] T. Dauxois and M. Peyrard. *Physics of solitons*. Cambridge Univercity Press, New York, 2006.

[10] R. Dodd, J. Eilbeck, J. Gibbon, and H. Morris. *Solitons and nonlinear wave equations*. Academic Press Inc. LTD., London, 1982.

[11] J. Engelbrecht. Beautiful dynamics. *Proceedings of the Estonian Academy of Sciences. Physics/Mathematics*, 1(44):108–119, 1995.

[12] J. Engelbrecht, A. Berezovski, F. Pastrone, and M. Braun. Waves in microstructured materials and dispersion. *Philosophical Magazine*, 85(33–35):4127–4141, 2005.

[13] J. Engelbrecht and F. Pastrone. Waves in microstructured solids with nonlinearities in microscale. *Proceedings of the Estonian Academy of Sciences, Physics, Mathematics*, 52(1):12–21, 2003.

[14] J. Engelbrecht, F. Pastrone, M. Braun, and A. Berezovski. Hierarchies of waves in nonclassical materials. In P. Delsanto, editor, *Universality of Nonclassical Nonlinearity*, pages 29–47, New York, 2006. Springer.

[15] A. Eringen. Linear theory of micropolar elasticity. *Journal of Mathematics and Mechanics*, 15:909–923, 1966.

[16] A. Eringen. *Microcontinuum Field Theories I: Foundations and Solids*. Springer, 1999.

[17] V. Erofeev. *Wave processes in solids with microstructure*. World Scientific, Singapore, 2003.

[18] B. Fornberg. *A practical guide to pseudospectral methods*. Cambridge Univercity Press, Cambridge, 1998.

[19] B. Fornberg and D. Sloan. A review of pseudospectral methods for solving partial differential equations. *Acta Numerica*, 3:203–267, 1994.

[20] B. Fornberg and G. Whitham. A numerical and theoretical study of certain nonlinear wave phenomena. *Philosophical Transactions of the Royal Society of London. Series A, Mathematical and Physical Sciences*, 289(1361):373–404, 1978.

[21] M. Frigo and S. Johnson. The design and implementation of FFTW 3. *Proceedings of the IEEE*, 93(2):216–231, 2005.

[22] J. Guo and T. R. Taha. Parallel implementation of the split-step and the pseudospectral methods for solving higher KdV equation. *Mathematics and Computers in Simulation*, 62(1–2):41–51, 2003.

[23] G. Herrmann and J. D. Achenbach. Application of theories of generalized Cosserat continua to the dynamics of composite materials. In E. Kröner, editor, *Mechanics of Generalized Continua*, pages 69–79, Berlin, 1968. Springer.

[24] A. Hindmarsh. *ODEPACK, a Systematized Collection of ODE Solvers*, volume 1. North-Holland, Amsterdam, 1983.

[25] L. Ilison and A. Salupere. Propagation of $sech^2$-type solitary waves in hierarchical KdV-type systems. *Mathematics and Computers in Simulation*, 79(11):3314–3327, 2009.

[26] L. Ilison, A. Salupere, and P. Peterson. On the propagation of localized perturbations in media with microstructure. *Proceedings of the Estonian Academy of Sciences, Physics, Mathematics*, 56(2):84–92, 2007.

[27] O. Ilison and A. Salupere. On the propagation of solitary pulses in microstructured materials. *Chaos, Solitons & Fractals*, 29(1):202–214, 2006.

[28] J. Janno and J. Engelbrecht. An inverse solitary wave problem related to microstructured materials. *Inverse Problems*, 21:2019–2034, 2005.

[29] J. Janno and J. Engelbrecht. Solitary waves in nonlinear microstructured materials. *Journal of Physics A: Mathematical and General*, 38:5159–5172, 2005.

[30] E. Jones, T. Oliphant, and P. Peterson. SciPy: open source scientific tools for Python, 2007.

[31] H. Kalisch and J. Lenells. Numerical study of traveling-wave solutions for the Camassa-Holm equation. *Chaos, Solitons & Fractals*, 25(2):287–298, 2005.

[32] H. Kreiss and J. Oliger. Comparison of accurate methods for the integration of hyperbolic equations. *Tellus*, 30:341–357, 1972.

[33] G. Maugin. *Material inhomogeneities in elasticity*. Chapman & Hall, London, 1993.

[34] G. Maugin. *Nonlinear waves in elastic crystals*. Oxford Univercity Press, Oxford, 1999.

[35] A. Metrikine and H. Askes. One-dimensional dynamically consistent gradient elasticity models derived from a discrete microstructure. Part 1: Generic formulation. *European Journal of Mechanics. A. Solids*, (21):555–572, 2002.

[36] R. Mindlin. Micro-structure in linear elasticity. *Archive for Rational Mechanics and Analysis*, 16(1):51–78, 1964.

[37] T. Peets, M. Randrüüt, and J. Engelbrecht. On modelling dispersion in microstructured solids. *Wave Motion*, 45(4):471–480, 2008.

[38] T. Peets and K. Tamm. Dispersion analysis of wave motion in microstructured solids. In T.-T. Wu and C.-C. Ma, editors, *IUTAM Symposium on Recent Advances of Acoustic Waves in Solids: Proceedings, Taipei, Taiwan, May 25–28, 2009*, volume 26 of *IUTAM Bookseries*, pages 349–354, Dordrecht, 2010. Springer.

[39] P. Peterson. F2PY: Fortran to Python interface generator, 2005.

[40] A. Porubov, G. Maugin, V. Gursky, and V. Krzhizhanovskaya. On some localized waves described by the extended KdV equation. *Comptes Rendus Mécanique*, 333(7):528–533, 2005.

[41] A. V. Porubov. *Amplification of nonlinear strain waves in solids*. World Scientific, Hong Kong, 2003.

[42] A. Salupere. On the application of pseudospectral methods for solving nonlinear evolution equations and discrete spectral analysis. In *Proceedings of 10th Nordic Seminar on Computational Mechanics.*, Tallinn, 1997. Tallinn Technical Universty,.

[43] A. Salupere. The pseudospectral method and discrete spectral analysis. In E. Quak and T. Soomere, editors, *Applied Wave Mathematics*, pages 301–334, Berlin, 2009. Springer.

[44] A. Salupere, J. Engelbrecht, and P. Peterson. On the long-time behaviour of soliton ensembles. *Mathematics and Computers in Simulation*, 62:137–147, 2003.

[45] A. Salupere, L. Ilison, J. Engelbrecht, and O. Ilison. On solitons in microstructured solids and granular materials. *Mathematics and Computers in Simulation*, 69:502–513, 2005.

[46] A. Salupere, L. Ilison, and K. Tamm. On numerical simulation of propagation of solitons in microstructured media. In M. Todorov, editor, *Proceedings of the 34th Conference on Applications of Mathematics in Engineering and Economics*, pages 155–165, Melville, NY, 2008. vol. 1067 of AIP Conference Proceedings.

[47] A. Salupere, K. Tamm, and J. Engelbrecht. Numerical simulation of interaction of solitary deformation waves in microstructured solids. *International Journal of Non-Linear Mechanics*, 43(3):201–208, 2008.

[48] A. Salupere, K. Tamm, J. Engelbrecht, and P. Peterson. On the interaction of deformation waves in microstructured solids. *Proceedings of the Estonian Academy of Sciences, Physics, Mathematics*, 56(2):93–99, 2007.

[49] K. Tamm and A. Salupere. On the propagation of solitary waves in Mindlin-type microstructured solids. *Proceedings of the Estonian Academy of Sciences*, 59(2):118–125, 2010.

[50] K. Tamm and A. Salupere. On the propagation of 1D solitary waves in Mindlin-type microstructured solids. *Mathematics and Computers in Simulation*, (in press, doi: 10.1016/j.matcom.2010.06.022), 2011.

[51] G. Whitham. *Linear and nonlinear waves*. Wiley-Interscience, 1974.

Appendix A: Accuracy

One of the simplest approaches to determining the adequate number of grid points is to compare solitary waves at the end of integration and find the number of grid points where no longer significant changes occur in the shape. Direct comparison of solitary waves has higher sensitivity to the number of grid points used than spectral characteristics or conservation laws that tend to stabilize at a lower number of grid points than waveprofiles, as will be observed in the present case. Spectral characteristics and conservation laws are mentioned in the present appendix in the text without figures.

Under a wide domain of parameters for equations (13), (14) and (15) it is reasonable to examine solutions in several points in the parameter domain. For cheking of the numerical accuracy first two equations (13) and (14) are used. We will consider three points in the middle of our parameter domain for normal dispersion, anomalous dispersion and for the dispersionless case. As the PSM is used, even a relatively low number of grid points is adequate. However, as the goal is to compare solutions directly, it is important to have a sufficiently high number of grid points to see all the needed details, with keeping the number of grid points as low as possible to keep the processor time consumption reasonable. The particular ODE solver used from the ODEPACK library [24] is 'lsoda'. Allowed error margins for the numerical integration are $rtol = 10^{-7}$, $atol = 10^{-9}$, $nsteps = 5 \times 10^6$, for the relative error, absolute error and maximum number of sub-steps allowed per time step ($\Delta T = 0.2$), respectively.

To choose the dispersion type in the points parameter C is used. All other parameters are the same for all the points: material and geometrical parameters $A = 12$, $B = 4.167$, $D = 5.0$, $N = 1.0$, $M = 0.290$, $\rho = 10.0$, $I = 8.0$, $l_o = 1.0$, $L_o = 50.0$, $U_o = 1.0$, $\varepsilon = 0.02$, $\delta = 0.02$.

Waves at the end of integration were examined with grid points numbering from $n = 32$ (2^5) up to $n = 8192$ (2^{13}). In addition to direct comparison of waveprofiles, spectral characteristics (spectral density and cumulative spectrum) [43] and energy conservation were checked. Figures 11 to 16 are presented only for the comparison of waveprofiles as other characteristics settle into stable values at a lower number of grid points. Panels in Figs. 11 to 16 are: close-up views of the left pulse peak (panel (A)), right pulse peak (panel (B)), left pulse bottom section (panel (C)) and right pulse bottom section (panel (D)). Close-up areas of the bottom sections are marked by a box in the bottom panel, while for peaks boxes are omitted to keep the main figure in the bottom readable.

The normal dispersion case point ($\gamma_A^2 = 0.5$, $\gamma_1^2 = 0.3$, $\gamma_N = 0.5$) with parameter $C = 2.88$. In the normal dispersion case the lowest number of grid points that gives satisfactory accuracy for the solitary wave is 512 for the FSE (Fig. 11) and 256
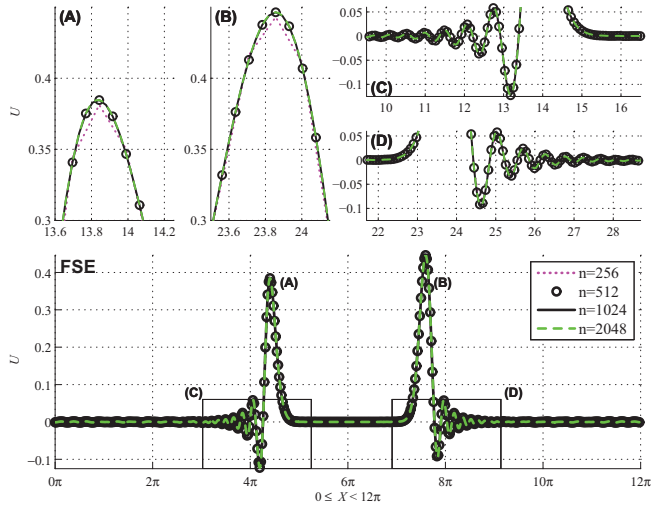
Figure 11: The FSE solitary wave comparison in the normal dispersion case at $T = 100$ and $n = 2^8 \ldots 2^{11}$.
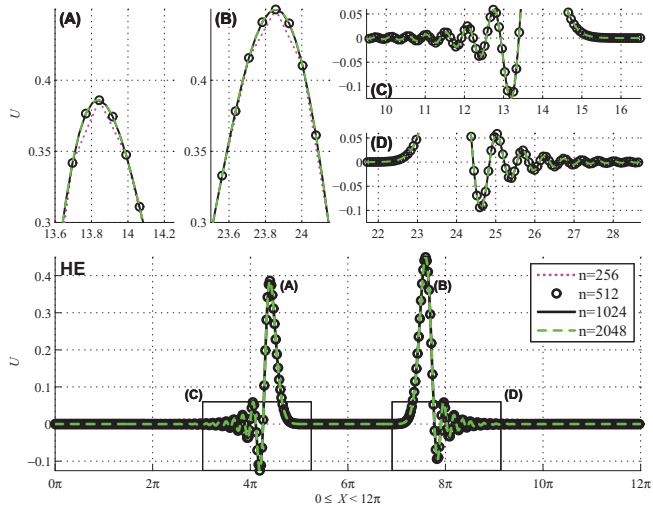
Figure 12: The HE solitary wave comparison in the normal dispersion case at $T = 100$ and $n = 2^8 \ldots 2^{11}$.
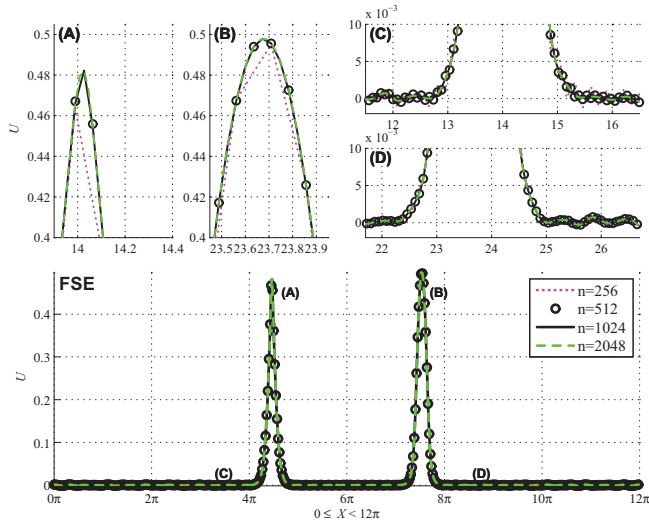
Figure 13: The FSE solitary wave comparison in the dispersionless case at $T = 100$ and $n = 2^8 \ldots 2^{11}$.
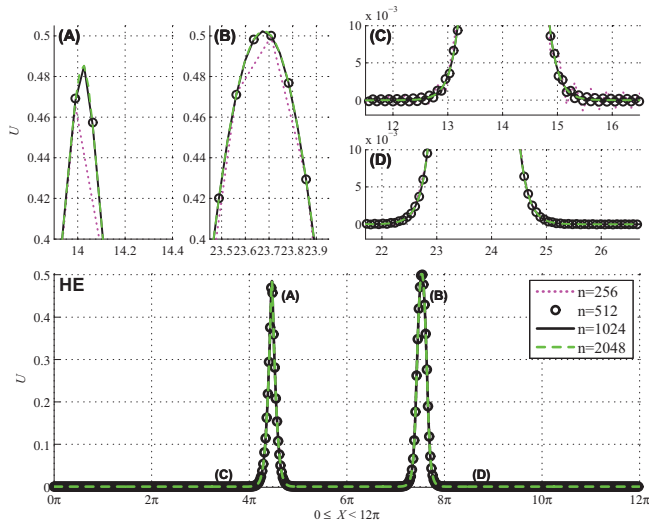
Figure 14: The HE solitary wave comparison in the dispersionless case at $T = 100$ and $n = 2^8 \ldots 2^{11}$.

62
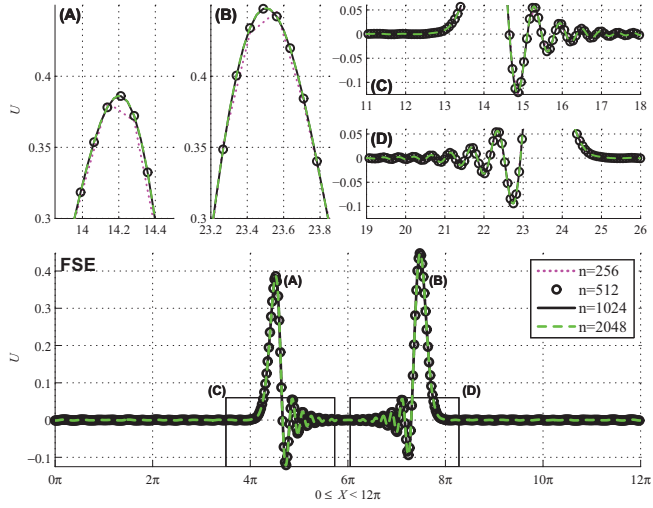
Figure 15: The FSE solitary wave comparison in the anomalous dispersion case at $T = 100$ and $n = 2^8 \ldots 2^{11}$.
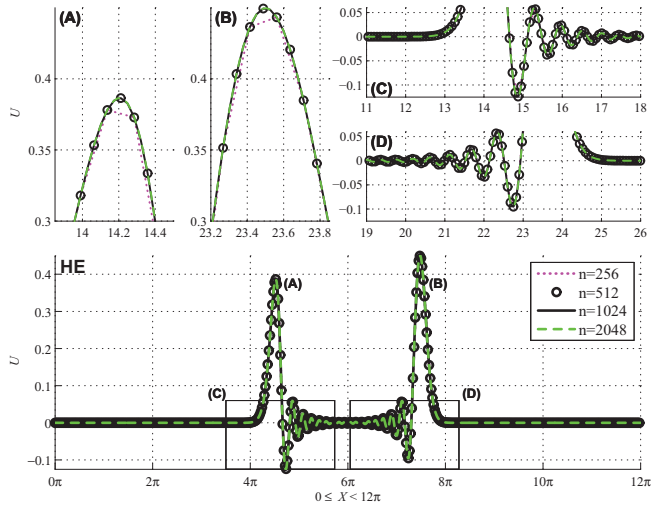
Figure 16: The HE solitary wave comparison in the anomalous dispersion case at $T = 100$ and $n = 2^8 \ldots 2^{11}$.

63
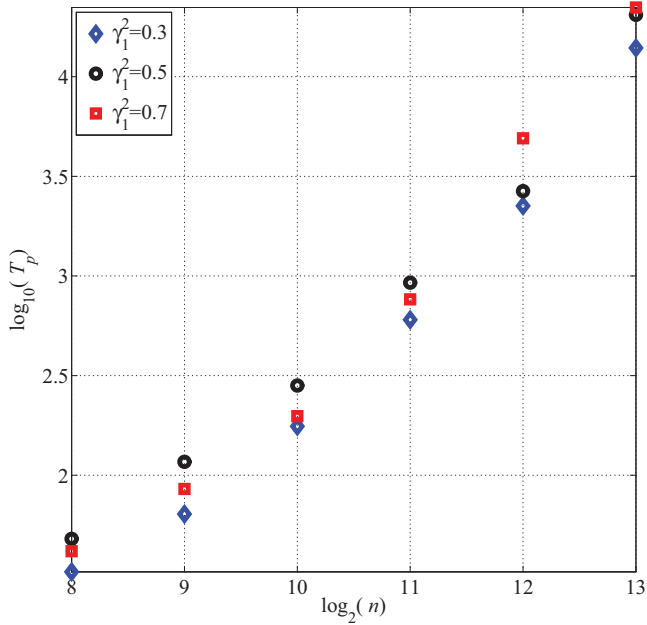
Figure 17: Processor time T_p against the number of grid points n in the logarithmic scale.

for the HE (Fig. 12). For the tail part of the wave profile 512 grid points would be adequate for both equations.

It must be noted that in the sense of spectral densities a considerably lower number of grid points is capable of giving satisfactory accuracy. No significant differences can be spotted in the first 9 spectral components when we have more than 64 grid points. the number of spectral components in the Fourier series is $n/2$, i.e., if $n = 32$, one has 16 spectral components, if $n = 64$, one has 32 spectral components, and so on.

Kinetic and free (potential) energy expressions in dimensionless form can be found in Subsection 4.2.3. (see equation (38)). Total energy is the sum of potential and kinetic energy $E = K + W$. From the standpoint of energy conservation, it is possible to say that $n = 128$ would be an adequate number of grid points.

As for the density of total energy (see equation (39) in Subsection 4.2.3.) only $n = 32$ gives a different result than a higher number of grid points. However, looking at free energy W and kinetic energy K it is possible to find differences between $n = 32$, $n = 64$ and $n = 128$, while $n \geq 256$ has no significant changes compared to $n = 128$. The same can be observed in the dispersionless and anomalous dispersion cases.

64

The dispersionless case point ($\gamma_A^2 = 0.5$, $\gamma_1^2 = 0.5$, $\gamma_N = 0.5$) with parameter $C = 4.8$. In the dispersionless case one can observe that for the FSE (Fig. 13) and the HE (Fig. 14) the lowest number of grid points that gives satisfactory accuracy for the peak of the solitary wave is 1024 points. While in the dispersionless case there is no tail (amplitude of oscillations[1] that can be seen in Fig. 13 is $\approx 10^{-3}$), it must be noted that to get an accurate representation of the oscillations in the FSE, one needs 1024 grid points or more.

The anomalous dispersion case point ($\gamma_A^2 = 0.5$, $\gamma_1^2 = 0.7$, $\gamma_N = 0.5$) with parameter $C = 6.72$. In the anomalous dispersion case the lowest number of grid points that gives satisfactory accuracy for the peak of the solitary wave and the tail part is 512 points for the FSE (Fig. 15) and HE (Fig. 16).

Processor time T_p measured is for obtaining solutions to the HE and FSE in the presented points. Time is measured in seconds and presented in the logarithmic scale in Fig. 17. As one can observe in Fig. 17 processor time consumption increases at the rate that is expected for the PSM with the increasing number of grid points [18, 19, 20], i.e., roughly exponential growth (note the logarithmic scale on the vertical axis). Considering all the points observed, it is reasonable to pick $2^{10} = 1024$ grid points to guarantee acceptable accuracy for the numerical analysis of solutions. With the use of 1024 grid points the numerical experiment consumed roughly 33 days of processor time. Full coverage of the parameter domain used in the thesis with 2048 grid points would have taken roughly 108 days of processor time (estimate is based on test runs in several parts of the parameter domain in addition to points presented here, even a higher number of grid points was examined only in the presented three points).

---

[1]The origin of these oscillations is discussed in Subsection 4.2.4.

Appendix B: Tables and figures

The behaviour of the solutions of the FSE (13) and HE (14) is characterised with the help of 12 tables and 28 figures.

Tables 1–6 show average speeds (42) of the main pulses for the solutions of the FSE and HE in the nonlinear and linear cases. Tables 7–12 show amplitude losses (43) by the end of integration for the main pulses of the solutions of the FSE and HE in the nonlinear and linear cases.

Tables are followed by two figures (Figs. 18 and 19) showing two subdomains where the waves propagating to the right are faster than the waves propagating to the left for the nonlinear FSE and HE.

Fifteen example points shown in Fig. 9 are used to give an overview of the behaviour of the solutions over the γ_A^2–γ_1^2 domain in the nonlinear and linear cases. In order to present detailed description of the behaviour of the solutions, Figs. 20–34 are divided into seven panels. In the top left panel there is the contour plot of the solution of the nonlinear FSE which characterizes the time-space behaviour of the solution. In the top right panel the two highest maxima and two lowest minima of waveprofiles are plotted against time (the nonlinear FSE). It should be noted that in most of the nonlinear cases waves propagating in opposite directions end up with different maxima and minima. In the bottom panel waveprofiles at the end of integration are presented for three cases: a nonlinear FSE, a linear FSE and the nonlinear HE. Waveprofiles that correspond to the linear HE are not provided, as they behave qualitatively in the same way as these corresponding to the linear FSE and skipping them makes figures easier to read. The middle four panels contain close-up views of the left pulse peak (panel (A)), right pulse peak (panel (B)), left pulse bottom section (panel (C)) and right pulse bottom section (panel (D)). Close-up areas of the bottom sections are marked by a box in the bottom panel, while for peaks boxes are omitted to keep the main figure in the bottom readable.

Differences between solutions of the FSE (13) and HE (14) are highlighted in Figs. 35–45. In Figs. 18–19 the quantity Δ^S (44) is plotted against γ_A^2 and γ_1^2 for the linear and nonlinear cases, respectively. In Figs. 37–45 the quantity Δ^S is plotted against γ_1^2, γ_A^2 and Γ along different straight lines in the $\gamma_A^2 - \gamma_1^2$ plane (see Fig. 9).

Table 1: Average speed of the left propagating pulse for the nonlinear FSE.

$\gamma_1^2 \setminus \gamma_2^2$	0.05	0.1	0.15	0.2	0.25	0.3	0.35	0.4	0.45	0.5	0.55	0.6	0.65	0.7	0.75	0.8	0.85	0.9	0.95
0.05	0.9746	0.9484	0.9213	0.8933	0.8646	0.8349	0.8041	0.7720	0.7389	0.7042	0.6679	0.6294	0.5881	0.5442	0.4952	0.4426	0.3819	0.3118	0.2236
0.1	0.9746	0.9484	0.9213	0.8934	0.8646	0.8350	0.8042	0.7722	0.7390	0.7044	0.6680	0.6296	0.5884	0.5446	0.4961	0.4436	0.3839	0.3161	0.2291
0.15	0.9746	0.9484	0.9213	0.8934	0.8647	0.8351	0.8044	0.7723	0.7392	0.7046	0.6682	0.6299	0.5887	0.5450	0.4968	0.4450	0.3872	0.3203	0.2321
0.2	0.9746	0.9484	0.9214	0.8935	0.8648	0.8351	0.8045	0.7725	0.7394	0.7048	0.6685	0.6301	0.5892	0.5456	0.4982	0.4472	0.3907	0.3230	0.2343
0.25	0.9746	0.9484	0.9214	0.8936	0.8649	0.8353	0.8046	0.7726	0.7396	0.7050	0.6688	0.6305	0.5897	0.5464	0.5000	0.4495	0.3931	0.3251	0.2361
0.3	0.9746	0.9485	0.9215	0.8936	0.8650	0.8354	0.8047	0.7728	0.7398	0.7053	0.6691	0.6310	0.5905	0.5477	0.5019	0.4507	0.3945	0.3266	0.2376
0.35	0.9746	0.9485	0.9215	0.8937	0.8651	0.8355	0.8049	0.7730	0.7400	0.7056	0.6695	0.6316	0.5916	0.5490	0.5031	0.4517	0.3954	0.3275	0.2390
0.4	0.9746	0.9485	0.9216	0.8938	0.8652	0.8356	0.8051	0.7733	0.7403	0.7060	0.6701	0.6324	0.5927	0.5499	0.5039	0.4524	0.3968	0.3281	0.2402
0.45	0.9746	0.9485	0.9216	0.8939	0.8653	0.8358	0.8052	0.7735	0.7407	0.7065	0.6708	0.6333	0.5934	0.5505	0.5047	0.4533	0.3981	0.3289	0.2412
0.5	0.9746	0.9485	0.9217	0.8940	0.8654	0.8359	0.8055	0.7739	0.7412	0.7071	0.6715	0.6340	0.5940	0.5509	0.5054	0.4536	0.3988	0.3299	0.2422
0.55	0.9747	0.9486	0.9217	0.8940	0.8655	0.8361	0.8057	0.7742	0.7416	0.7077	0.6721	0.6344	0.5945	0.5513	0.5058	0.4541	0.3991	0.3309	0.2430
0.6	0.9747	0.9486	0.9218	0.8941	0.8657	0.8363	0.8060	0.7746	0.7421	0.7082	0.6725	0.6348	0.5948	0.5517	0.5061	0.4546	0.3996	0.3320	0.2436
0.65	0.9747	0.9486	0.9218	0.8942	0.8658	0.8365	0.8062	0.7749	0.7425	0.7086	0.6729	0.6351	0.5951	0.5519	0.5064	0.4551	0.4006	0.3329	0.2443
0.7	0.9747	0.9486	0.9218	0.8943	0.8659	0.8367	0.8065	0.7753	0.7429	0.7089	0.6731	0.6354	0.5954	0.5522	0.5070	0.4554	0.4017	0.3335	0.2448
0.75	0.9747	0.9486	0.9219	0.8944	0.8660	0.8368	0.8067	0.7756	0.7432	0.7092	0.6734	0.6356	0.5957	0.5525	0.5075	0.4554	0.4023	0.3339	0.2453
0.8	0.9747	0.9487	0.9219	0.8944	0.8661	0.8370	0.8070	0.7759	0.7434	0.7094	0.6736	0.6358	0.5958	0.5526	0.5076	0.4560	0.4025	0.3341	0.2458
0.85	0.9747	0.9487	0.9220	0.8945	0.8663	0.8372	0.8072	0.7761	0.7436	0.7096	0.6738	0.6359	0.5960	0.5529	0.5079	0.4565	0.4025	0.3344	0.2463
0.9	0.9747	0.9487	0.9220	0.8946	0.8664	0.8374	0.8074	0.7763	0.7439	0.7098	0.6740	0.6361	0.5960	0.5530	0.5082	0.4566	0.4028	0.3347	0.2468
0.95	0.9747	0.9487	0.9220	0.8946	0.8665	0.8376	0.8076	0.7765	0.7440	0.7100	0.6741	0.6363	0.5963	0.5534	0.5082	0.4571	0.4035	0.3351	0.2473
c_0	0.9747	0.9487	0.9220	0.8944	0.8660	0.8367	0.8062	0.7746	0.7416	0.7071	0.6708	0.6325	0.5916	0.5477	0.5000	0.4472	0.3873	0.3162	0.2236

Table 2: Average speed of the right propagating pulse for the nonlinear FSE.

$\gamma_1^2 \backslash \gamma_2^2$	0.05	0.1	0.15	0.2	0.25	0.3	0.35	0.4	0.45	0.5	0.55	0.6	0.65	0.7	0.75	0.8	0.85	0.9	0.95
0.05	0.9744	0.9480	0.9210	0.8932	0.8645	0.8348	0.8041	0.7720	0.7390	0.7043	0.6680	0.6295	0.5882	0.5443	0.4952	0.4426	0.3815	0.3113	0.2234
0.1	0.9744	0.9481	0.9210	0.8932	0.8645	0.8349	0.8042	0.7722	0.7391	0.7045	0.6681	0.6297	0.5885	0.5446	0.4961	0.4435	0.3832	0.3161	0.2295
0.15	0.9744	0.9481	0.9211	0.8932	0.8646	0.8350	0.8043	0.7723	0.7392	0.7046	0.6683	0.6299	0.5888	0.5450	0.4967	0.4447	0.3872	0.3208	0.2321
0.2	0.9744	0.9481	0.9211	0.8933	0.8646	0.8350	0.8044	0.7724	0.7394	0.7048	0.6685	0.6301	0.5891	0.5455	0.4978	0.4472	0.3912	0.3232	0.2340
0.25	0.9744	0.9481	0.9211	0.8934	0.8647	0.8351	0.8045	0.7726	0.7395	0.7050	0.6688	0.6304	0.5896	0.5461	0.5000	0.4498	0.3933	0.3251	0.2357
0.3	0.9744	0.9482	0.9212	0.8934	0.8648	0.8352	0.8046	0.7727	0.7397	0.7052	0.6690	0.6308	0.5902	0.5477	0.5023	0.4509	0.3946	0.3264	0.2372
0.35	0.9744	0.9482	0.9212	0.8935	0.8649	0.8353	0.8047	0.7729	0.7399	0.7055	0.6693	0.6313	0.5916	0.5493	0.5033	0.4517	0.3955	0.3273	0.2385
0.4	0.9745	0.9482	0.9213	0.8935	0.8649	0.8354	0.8049	0.7731	0.7401	0.7058	0.6698	0.6325	0.5930	0.5500	0.5040	0.4523	0.3967	0.3279	0.2396
0.45	0.9745	0.9482	0.9213	0.8936	0.8650	0.8355	0.8050	0.7733	0.7404	0.7062	0.6708	0.6336	0.5936	0.5504	0.5047	0.4532	0.3980	0.3286	0.2407
0.5	0.9745	0.9483	0.9213	0.8937	0.8651	0.8357	0.8052	0.7736	0.7408	0.7071	0.6718	0.6341	0.5941	0.5508	0.5053	0.4534	0.3986	0.3296	0.2416
0.55	0.9745	0.9483	0.9214	0.8937	0.8652	0.8358	0.8054	0.7739	0.7416	0.7080	0.6723	0.6344	0.5945	0.5512	0.5057	0.4539	0.3989	0.3306	0.2424
0.6	0.9745	0.9483	0.9214	0.8938	0.8653	0.8360	0.8057	0.7746	0.7424	0.7084	0.6726	0.6348	0.5947	0.5515	0.5060	0.4544	0.3994	0.3317	0.2430
0.65	0.9745	0.9484	0.9215	0.8939	0.8655	0.8362	0.8062	0.7753	0.7428	0.7087	0.6729	0.6350	0.5950	0.5517	0.5063	0.4548	0.4004	0.3325	0.2436
0.7	0.9745	0.9484	0.9216	0.8940	0.8656	0.8367	0.8068	0.7756	0.7431	0.7090	0.6731	0.6353	0.5953	0.5520	0.5068	0.4552	0.4014	0.3331	0.2442
0.75	0.9746	0.9484	0.9216	0.8941	0.8660	0.8371	0.8071	0.7759	0.7433	0.7092	0.6733	0.6354	0.5956	0.5523	0.5073	0.4551	0.4020	0.3335	0.2447
0.8	0.9746	0.9485	0.9217	0.8944	0.8664	0.8373	0.8073	0.7761	0.7435	0.7094	0.6736	0.6357	0.5956	0.5523	0.5074	0.4557	0.4022	0.3337	0.2451
0.85	0.9746	0.9486	0.9220	0.8947	0.8666	0.8375	0.8074	0.7763	0.7437	0.7096	0.6737	0.6358	0.5958	0.5527	0.5076	0.4562	0.4022	0.3339	0.2456
0.9	0.9747	0.9487	0.9222	0.8949	0.8667	0.8377	0.8076	0.7765	0.7439	0.7098	0.6739	0.6360	0.5958	0.5528	0.5080	0.4563	0.4025	0.3342	0.2461
0.95	0.9747	0.9488	0.9223	0.8950	0.8668	0.8378	0.8077	0.7766	0.7440	0.7099	0.6740	0.6361	0.5961	0.5531	0.5080	0.4568	0.4032	0.3347	0.2466
c_0	0.9747	0.9487	0.9220	0.8944	0.8660	0.8367	0.8062	0.7746	0.7416	0.7071	0.6708	0.6325	0.5916	0.5477	0.5000	0.4472	0.3873	0.3162	0.2236

Table 3: Average speed of the pulse for the linear FSE.

$\gamma_1^2 \setminus \gamma_2^2$	0.05	0.1	0.15	0.2	0.25	0.3	0.35	0.4	0.45	0.5	0.55	0.6	0.65	0.7	0.75	0.8	0.85	0.9	0.95
0.05	0.9745	0.9482	0.9211	0.8932	0.8645	0.8348	0.8041	0.7720	0.7389	0.7434	0.6679	0.6294	0.5881	0.5442	0.4952	0.4426	0.3817	0.3115	0.2235
0.1	0.9745	0.9482	0.9211	0.8933	0.8645	0.8349	0.8042	0.7722	0.7390	0.7436	0.6681	0.6296	0.5885	0.5446	0.4961	0.4435	0.3835	0.3161	0.2294
0.15	0.9745	0.9482	0.9212	0.8933	0.8646	0.8350	0.8043	0.7723	0.7392	0.7437	0.6682	0.6299	0.5887	0.5449	0.4967	0.4448	0.3872	0.3206	0.2322
0.2	0.9745	0.9482	0.9212	0.8934	0.8647	0.8351	0.8044	0.7724	0.7394	0.7439	0.6685	0.6301	0.5891	0.5455	0.4979	0.4472	0.3910	0.3231	0.2342
0.25	0.9746	0.9483	0.9212	0.8934	0.8648	0.8351	0.8045	0.7726	0.7395	0.7441	0.6687	0.6304	0.5896	0.5462	0.5000	0.4497	0.3932	0.3251	0.2359
0.3	0.9746	0.9483	0.9213	0.8935	0.8648	0.8353	0.8046	0.7727	0.7397	0.7444	0.6690	0.6308	0.5903	0.5477	0.5021	0.4509	0.3946	0.3265	0.2374
0.35	0.9746	0.9483	0.9213	0.8935	0.8649	0.8354	0.8048	0.7729	0.7399	0.7447	0.6694	0.6314	0.5916	0.5492	0.5033	0.4518	0.3955	0.3274	0.2387
0.4	0.9746	0.9484	0.9214	0.8936	0.8650	0.8355	0.8049	0.7731	0.7402	0.7451	0.6699	0.6324	0.5929	0.5500	0.5040	0.4524	0.3968	0.3280	0.2399
0.45	0.9746	0.9484	0.9214	0.8937	0.8651	0.8356	0.8051	0.7734	0.7405	0.7455	0.6708	0.6335	0.5936	0.5505	0.5047	0.4533	0.3980	0.3288	0.2410
0.5	0.9746	0.9484	0.9215	0.8938	0.8652	0.8357	0.8053	0.7737	0.7409	0.7464	0.6717	0.6341	0.5941	0.5509	0.5054	0.4535	0.3988	0.3297	0.2419
0.55	0.9746	0.9484	0.9215	0.8938	0.8653	0.8359	0.8055	0.7740	0.7416	0.7472	0.6722	0.6345	0.5945	0.5512	0.5058	0.4540	0.3990	0.3308	0.2427
0.6	0.9746	0.9485	0.9216	0.8939	0.8655	0.8361	0.8058	0.7746	0.7423	0.7477	0.6726	0.6348	0.5948	0.5516	0.5061	0.4545	0.3995	0.3318	0.2434
0.65	0.9746	0.9485	0.9216	0.8940	0.8656	0.8363	0.8062	0.7752	0.7427	0.7481	0.6729	0.6351	0.5951	0.5519	0.5064	0.4550	0.4006	0.3327	0.2440
0.7	0.9746	0.9485	0.9217	0.8941	0.8658	0.8367	0.8067	0.7755	0.7430	0.7484	0.6732	0.6354	0.5953	0.5521	0.5069	0.4553	0.4016	0.3333	0.2445
0.75	0.9746	0.9486	0.9218	0.8943	0.8660	0.8370	0.8072	0.7758	0.7433	0.7487	0.6734	0.6355	0.5957	0.5524	0.5074	0.4553	0.4022	0.3337	0.2450
0.8	0.9747	0.9486	0.9219	0.8944	0.8663	0.8372	0.8074	0.7761	0.7435	0.7489	0.6736	0.6358	0.5957	0.5525	0.5075	0.4559	0.4023	0.3339	0.2455
0.85	0.9747	0.9486	0.9220	0.8946	0.8664	0.8374	0.8075	0.7763	0.7437	0.7491	0.6737	0.6359	0.5959	0.5528	0.5078	0.4564	0.4024	0.3341	0.2460
0.9	0.9747	0.9487	0.9220	0.8947	0.8666	0.8376	0.7004	0.7764	0.7439	0.7493	0.6740	0.6361	0.5959	0.5529	0.5081	0.4564	0.4027	0.3344	0.2465
0.95	0.9747	0.9487	0.9221	0.8948	0.8667	0.8377	0.8077	0.7766	0.7441	0.7494	0.6741	0.6362	0.5962	0.5533	0.5081	0.4570	0.4033	0.3349	0.2469
c_0	0.9747	0.9487	0.9220	0.8944	0.8660	0.8367	0.8062	0.7746	0.7416	0.7071	0.6708	0.6325	0.5916	0.5477	0.5000	0.4472	0.3873	0.3162	0.2236

Table 4: Average speed of the left propagating pulse for the nonlinear HE.

$\gamma_1^2 \setminus \gamma_2^2$	0.05	0.1	0.15	0.2	0.25	0.3	0.35	0.4	0.45	0.5	0.55	0.6	0.65	0.7	0.75	0.8	0.85	0.9	0.95
0.05	0.9746	0.9484	0.9213	0.8933	0.8646	0.8349	0.8041	0.7721	0.7389	0.7042	0.6678	0.6294	0.5881	0.5441	0.4953	0.4426	0.3816	0.3119	0.2237
0.1	0.9746	0.9484	0.9213	0.8934	0.8646	0.8350	0.8042	0.7722	0.7390	0.7044	0.6680	0.6295	0.5884	0.5445	0.4960	0.4436	0.3838	0.3163	0.2295
0.15	0.9746	0.9484	0.9213	0.8935	0.8647	0.8351	0.8044	0.7723	0.7392	0.7046	0.6682	0.6298	0.5887	0.5450	0.4969	0.4449	0.3873	0.3206	0.2325
0.2	0.9746	0.9484	0.9214	0.8935	0.8648	0.8351	0.8045	0.7725	0.7394	0.7048	0.6685	0.6301	0.5892	0.5455	0.4981	0.4472	0.3908	0.3231	0.2347
0.25	0.9746	0.9484	0.9214	0.8936	0.8649	0.8353	0.8046	0.7727	0.7396	0.7050	0.6688	0.6305	0.5897	0.5464	0.5000	0.4495	0.3930	0.3249	0.2363
0.3	0.9746	0.9485	0.9215	0.8937	0.8650	0.8354	0.8047	0.7728	0.7398	0.7053	0.6691	0.6309	0.5905	0.5477	0.5019	0.4509	0.3946	0.3263	0.2377
0.35	0.9746	0.9485	0.9215	0.8937	0.8651	0.8355	0.8049	0.7730	0.7400	0.7056	0.6695	0.6316	0.5916	0.5491	0.5032	0.4518	0.3959	0.3275	0.2389
0.4	0.9746	0.9485	0.9216	0.8938	0.8652	0.8356	0.8051	0.7733	0.7403	0.7060	0.6701	0.6325	0.5927	0.5499	0.5040	0.4526	0.3969	0.3286	0.2399
0.45	0.9746	0.9485	0.9216	0.8939	0.8653	0.8358	0.8052	0.7735	0.7407	0.7065	0.6708	0.6333	0.5935	0.5505	0.5047	0.4532	0.3979	0.3295	0.2409
0.5	0.9746	0.9485	0.9217	0.8940	0.8654	0.8359	0.8055	0.7739	0.7412	0.7071	0.6715	0.6340	0.5940	0.5510	0.5053	0.4537	0.3987	0.3303	0.2418
0.55	0.9747	0.9486	0.9217	0.8940	0.8655	0.8361	0.8057	0.7742	0.7416	0.7077	0.6721	0.6344	0.5945	0.5513	0.5058	0.4542	0.3994	0.3311	0.2426
0.6	0.9747	0.9486	0.9218	0.8941	0.8657	0.8363	0.8060	0.7746	0.7421	0.7082	0.6725	0.6348	0.5948	0.5517	0.5062	0.4546	0.4001	0.3318	0.2434
0.65	0.9747	0.9486	0.9218	0.8942	0.8658	0.8365	0.8062	0.7750	0.7425	0.7086	0.6729	0.6351	0.5952	0.5520	0.5066	0.4550	0.4008	0.3325	0.2441
0.7	0.9747	0.9486	0.9218	0.8943	0.8659	0.8367	0.8065	0.7753	0.7429	0.7089	0.6732	0.6354	0.5954	0.5522	0.5070	0.4554	0.4014	0.3331	0.2448
0.75	0.9747	0.9486	0.9219	0.8944	0.8660	0.8368	0.8067	0.7757	0.7432	0.7092	0.6734	0.6356	0.5958	0.5525	0.5073	0.4557	0.4019	0.3337	0.2454
0.8	0.9747	0.9487	0.9219	0.8944	0.8661	0.8370	0.8070	0.7759	0.7435	0.7094	0.6736	0.6358	0.5958	0.5526	0.5077	0.4561	0.4025	0.3342	0.2460
0.85	0.9747	0.9487	0.9220	0.8945	0.8663	0.8372	0.8072	0.7762	0.7437	0.7096	0.6738	0.6360	0.5958	0.5527	0.5080	0.4564	0.4030	0.3347	0.2466
0.9	0.9747	0.9487	0.9220	0.8946	0.8664	0.8374	0.8074	0.7764	0.7439	0.7098	0.6740	0.6362	0.5960	0.5529	0.5082	0.4566	0.4034	0.3352	0.2471
0.95	0.9747	0.9487	0.9220	0.8946	0.8665	0.8376	0.8076	0.7765	0.7440	0.7100	0.6742	0.6363	0.5966	0.5530	0.5085	0.4569	0.4039	0.3357	0.2477
c_0	0.9747	0.9487	0.9220	0.8944	0.8660	0.8367	0.8062	0.7746	0.7416	0.7071	0.6708	0.6325	0.5916	0.5477	0.5000	0.4472	0.3873	0.3162	0.2236

Table 5: Average speed of the right propagating pulse for the nonlinear HE.

$\gamma_1^2 \setminus \gamma_2^2$	0.05	0.1	0.15	0.2	0.25	0.3	0.35	0.4	0.45	0.5	0.55	0.6	0.65	0.7	0.75	0.8	0.85	0.9	0.95
0.05	0.9744	0.9480	0.9210	0.8932	0.8645	0.8348	0.8041	0.7721	0.7389	0.7043	0.6679	0.6295	0.5882	0.5443	0.4953	0.4426	0.3813	0.3113	0.2235
0.1	0.9744	0.9481	0.9210	0.8932	0.8645	0.8349	0.8042	0.7722	0.7391	0.7045	0.6681	0.6296	0.5885	0.5446	0.4959	0.4435	0.3832	0.3162	0.2298
0.15	0.9744	0.9481	0.9211	0.8932	0.8646	0.8350	0.8043	0.7723	0.7392	0.7046	0.6683	0.6299	0.5888	0.5450	0.4967	0.4446	0.3873	0.3211	0.2324
0.2	0.9744	0.9481	0.9211	0.8933	0.8646	0.8350	0.8044	0.7724	0.7394	0.7048	0.6685	0.6301	0.5892	0.5455	0.4977	0.4472	0.3913	0.3233	0.2343
0.25	0.9744	0.9481	0.9211	0.8933	0.8647	0.8351	0.8045	0.7726	0.7395	0.7050	0.6687	0.6304	0.5896	0.5461	0.5000	0.4498	0.3933	0.3249	0.2359
0.3	0.9744	0.9482	0.9212	0.8934	0.8648	0.8352	0.8046	0.7727	0.7397	0.7052	0.6690	0.6308	0.5902	0.5477	0.5023	0.4509	0.3947	0.3262	0.2372
0.35	0.9744	0.9482	0.9212	0.8935	0.8648	0.8353	0.8047	0.7729	0.7399	0.7055	0.6693	0.6313	0.5916	0.5493	0.5033	0.4518	0.3959	0.3273	0.2383
0.4	0.9745	0.9482	0.9213	0.8935	0.8649	0.8354	0.8049	0.7731	0.7401	0.7058	0.6698	0.6325	0.5930	0.5500	0.5041	0.4524	0.3968	0.3283	0.2394
0.45	0.9745	0.9482	0.9213	0.8936	0.8650	0.8355	0.8050	0.7733	0.7404	0.7062	0.6708	0.6336	0.5936	0.5505	0.5047	0.4530	0.3977	0.3292	0.2403
0.5	0.9745	0.9483	0.9213	0.8936	0.8651	0.8357	0.8052	0.7735	0.7408	0.7071	0.6718	0.6341	0.5941	0.5509	0.5052	0.4535	0.3985	0.3300	0.2412
0.55	0.9745	0.9483	0.9214	0.8937	0.8652	0.8358	0.8054	0.7739	0.7416	0.7080	0.6723	0.6345	0.5944	0.5512	0.5057	0.4540	0.3992	0.3307	0.2420
0.6	0.9745	0.9483	0.9214	0.8938	0.8653	0.8360	0.8057	0.7746	0.7424	0.7084	0.6726	0.6348	0.5947	0.5515	0.5061	0.4544	0.3999	0.3314	0.2427
0.65	0.9745	0.9484	0.9215	0.8939	0.8655	0.8362	0.8062	0.7753	0.7428	0.7087	0.6729	0.6350	0.5950	0.5518	0.5065	0.4548	0.4005	0.3321	0.2434
0.7	0.9745	0.9484	0.9216	0.8940	0.8656	0.8367	0.8068	0.7757	0.7431	0.7090	0.6731	0.6353	0.5953	0.5520	0.5068	0.4551	0.4011	0.3327	0.2441
0.75	0.9746	0.9484	0.9216	0.8941	0.8660	0.8371	0.8071	0.7759	0.7433	0.7092	0.6733	0.6355	0.5956	0.5523	0.5071	0.4554	0.4016	0.3332	0.2447
0.8	0.9746	0.9485	0.9217	0.8944	0.8664	0.8374	0.8073	0.7761	0.7435	0.7094	0.6735	0.6357	0.5956	0.5524	0.5074	0.4557	0.4022	0.3338	0.2453
0.85	0.9746	0.9486	0.9220	0.8947	0.8666	0.8375	0.8074	0.7763	0.7437	0.7096	0.6737	0.6358	0.5956	0.5525	0.5077	0.4560	0.4026	0.3343	0.2459
0.9	0.9747	0.9487	0.9222	0.8949	0.8667	0.8377	0.8076	0.7765	0.7439	0.7098	0.6739	0.6360	0.5958	0.5527	0.5080	0.4563	0.4031	0.3348	0.2465
0.95	0.9747	0.9488	0.9223	0.8950	0.8668	0.8378	0.8077	0.7766	0.7440	0.7099	0.6740	0.6361	0.5964	0.5528	0.5082	0.4566	0.4035	0.3353	0.2470
c_0	0.9747	0.9487	0.9220	0.8944	0.8660	0.8367	0.8062	0.7746	0.7416	0.7071	0.6708	0.6325	0.5916	0.5477	0.5000	0.4472	0.3873	0.3162	0.2236

Table 6: Average speed of the pulse for the linear HE.

$\gamma_1^2 \setminus \gamma_2^2$	0.05	0.1	0.15	0.2	0.25	0.3	0.35	0.4	0.45	0.5	0.55	0.6	0.65	0.7	0.75	0.8	0.85	0.9	0.95
0.05	0.9745	0.9482	0.9211	0.8932	0.8645	0.8348	0.8041	0.7720	0.7389	0.7042	0.6679	0.6294	0.5881	0.5442	0.4953	0.4425	0.3814	0.3115	0.2236
0.1	0.9745	0.9482	0.9211	0.8933	0.8645	0.8349	0.8042	0.7722	0.7390	0.7044	0.6680	0.6296	0.5884	0.5445	0.4959	0.4435	0.3835	0.3162	0.2298
0.15	0.9745	0.9482	0.9212	0.8933	0.8646	0.8350	0.8043	0.7723	0.7392	0.7046	0.6682	0.6298	0.5887	0.5449	0.4967	0.4447	0.3873	0.3209	0.2326
0.2	0.9745	0.9482	0.9212	0.8934	0.8647	0.8351	0.8044	0.7724	0.7393	0.7048	0.6685	0.6301	0.5891	0.5455	0.4978	0.4472	0.3911	0.3233	0.2346
0.25	0.9746	0.9483	0.9212	0.8934	0.8648	0.8351	0.8045	0.7726	0.7395	0.7050	0.6687	0.6304	0.5896	0.5462	0.5000	0.4497	0.3932	0.3250	0.2361
0.3	0.9746	0.9483	0.9213	0.8935	0.8648	0.8352	0.8046	0.7727	0.7397	0.7052	0.6690	0.6308	0.5903	0.5477	0.5022	0.4510	0.3947	0.3263	0.2375
0.35	0.9746	0.9483	0.9213	0.8935	0.8649	0.8354	0.8048	0.7729	0.7399	0.7055	0.6694	0.6314	0.5916	0.5493	0.5033	0.4518	0.3959	0.3275	0.2387
0.4	0.9746	0.9484	0.9214	0.8936	0.8650	0.8355	0.8049	0.7731	0.7402	0.7058	0.6699	0.6325	0.5929	0.5500	0.5041	0.4525	0.3969	0.3285	0.2397
0.45	0.9746	0.9484	0.9214	0.8937	0.8651	0.8356	0.8051	0.7734	0.7405	0.7063	0.6708	0.6335	0.5936	0.5505	0.5047	0.4531	0.3978	0.3294	0.2407
0.5	0.9746	0.9484	0.9215	0.8938	0.8652	0.8357	0.8053	0.7737	0.7409	0.7071	0.6718	0.6341	0.5941	0.5509	0.5053	0.4536	0.3986	0.3302	0.2415
0.55	0.9746	0.9484	0.9215	0.8938	0.8653	0.8359	0.8055	0.7740	0.7416	0.7079	0.6723	0.6345	0.5945	0.5513	0.5058	0.4541	0.3994	0.3309	0.2423
0.6	0.9746	0.9485	0.9216	0.8939	0.8655	0.8361	0.8058	0.7746	0.7423	0.7084	0.6726	0.6348	0.5948	0.5516	0.5062	0.4545	0.4000	0.3316	0.2431
0.65	0.9746	0.9485	0.9216	0.8940	0.8656	0.8363	0.8062	0.7752	0.7427	0.7087	0.6729	0.6351	0.5951	0.5519	0.5066	0.4549	0.4007	0.3323	0.2438
0.7	0.9746	0.9485	0.9217	0.8941	0.8658	0.8361	0.8067	0.7755	0.7430	0.7090	0.6732	0.6353	0.5954	0.5522	0.5069	0.4553	0.4012	0.3329	0.2445
0.75	0.9746	0.9486	0.9218	0.8943	0.8660	0.8370	0.8070	0.7758	0.7433	0.7093	0.6734	0.6356	0.5957	0.5524	0.5072	0.4556	0.4018	0.3335	0.2451
0.8	0.9747	0.9486	0.9219	0.8944	0.8663	0.8372	0.8072	0.7761	0.7435	0.7095	0.6736	0.6358	0.5957	0.5525	0.5076	0.4559	0.4023	0.3340	0.2457
0.85	0.9747	0.9486	0.9220	0.8946	0.8664	0.8374	0.8074	0.7763	0.7437	0.7096	0.6738	0.6359	0.5957	0.5526	0.5078	0.4562	0.4028	0.3345	0.2463
0.9	0.9747	0.9487	0.9220	0.8947	0.8666	0.8376	0.8075	0.7765	0.7439	0.7098	0.6740	0.6361	0.5960	0.5531	0.5081	0.4565	0.4033	0.3350	0.2468
0.95	0.9747	0.9487	0.9221	0.8948	0.8667	0.8377	0.8077	0.7766	0.7441	0.7100	0.6741	0.6363	0.5965	0.5528	0.5084	0.4568	0.4037	0.3355	0.2474
c_0	0.9747	0.9487	0.9220	0.8944	0.8660	0.8367	0.8062	0.7746	0.7416	0.7071	0.6708	0.6325	0.5916	0.5477	0.5000	0.4472	0.3873	0.3162	0.2236

Table 7: Amplitude loss (in %) of the left propagating pulse for the nonlinear FSE.

$\gamma_r^2 \backslash \gamma_l^2$	0.05	0.1	0.15	0.2	0.25	0.3	0.35	0.4	0.45	0.5	0.55	0.6	0.65	0.7	0.75	0.8	0.85	0.9	0.95
0.05	0	0	2	5	8	11	14	18	20	22	23	25	26	26	26	24	21	13	0
0.1	0	0	2	4	7	11	13	16	18	20	21	22	23	22	21	18	11	1	16
0.15	0	0	1	4	7	9	12	15	17	18	19	20	19	18	15	8	1	13	30
0.2	0	0	1	3	6	9	11	13	15	16	17	16	15	12	6	1	10	24	37
0.25	0	0	1	3	5	7	10	11	13	14	13	13	10	5	0	8	22	31	43
0.3	0	0	1	2	4	6	8	10	11	11	10	8	4	1	6	17	28	37	46
0.35	0	0	0	2	4	5	7	8	8	8	6	2	1	5	15	24	33	41	50
0.4	0	0	0	1	3	4	5	6	6	4	2	0	4	12	20	29	36	44	52
0.45	0	0	0	1	2	3	4	4	3	1	0	3	10	18	25	32	39	47	54
0.5	0	0	0	1	1	2	2	2	1	0	2	8	15	22	29	36	41	49	55
0.55	0	0	0	0	1	1	1	0	0	1	6	12	19	26	32	38	44	51	57
0.6	0	0	0	0	0	0	0	0	1	4	10	16	22	29	35	40	46	52	58
0.65	0	0	0	0	0	0	0	0	3	8	13	19	26	32	37	43	48	54	59
0.7	0	0	0	0	0	0	0	2	5	11	16	22	28	33	37	44	49	55	60
0.75	0	0	0	0	0	0	1	4	8	13	19	24	30	36	39	46	50	57	61
0.8	0	0	0	0	0	0	2	6	9	16	21	26	32	37	42	47	52	58	61
0.85	0	0	0	0	0	1	4	8	13	18	23	29	34	39	44	48	53	59	61
0.9	0	0	0	0	0	2	5	9	14	20	25	30	35	41	45	49	54	60	62
0.95	0	0	0	0	1	3	6	11	16	22	26	32	37	42	47	50	54	61	62

Table 8: Amplitude loss (in %) of the right propagating pulse for the nonlinear FSE.

$\gamma_1^2 \setminus \gamma_2^2$	0.05	0.1	0.15	0.2	0.25	0.3	0.35	0.4	0.45	0.5	0.55	0.6	0.65	0.7	0.75	0.8	0.85	0.9	0.95
0.05	3	7	11	15	19	22	25	28	30	32	33	35	36	37	38	38	38	36	29
0.1	3	6	11	14	18	21	24	26	29	30	32	33	34	34	35	34	32	18	44
0.15	2	6	10	14	17	20	23	25	27	29	30	31	32	31	30	27	13	36	49
0.2	2	6	10	13	17	20	22	24	26	27	28	29	29	27	24	10	32	42	53
0.25	2	6	9	13	16	18	21	23	24	25	26	26	24	21	8	27	37	45	55
0.3	2	5	9	12	15	17	20	21	22	23	23	22	19	7	23	33	42	49	57
0.35	2	5	8	11	14	16	18	19	20	20	19	16	6	21	30	38	45	51	59
0.4	2	5	8	11	13	15	17	18	18	17	14	5	19	27	34	41	47	53	61
0.45	2	5	7	10	12	14	15	15	15	12	4	17	24	31	37	43	48	55	61
0.5	2	4	7	9	11	12	13	13	11	3	14	22	28	34	40	45	50	57	62
0.55	1	4	6	8	10	11	10	9	3	12	19	26	31	37	42	47	52	58	63
0.6	1	3	6	7	8	9	7	2	11	17	23	28	34	39	44	49	53	59	63
0.65	1	3	5	6	7	6	2	9	15	20	26	31	36	41	46	50	54	60	64
0.7	1	3	4	5	4	1	7	12	17	23	28	33	38	42	46	51	55	61	65
0.75	1	2	3	3	1	6	10	15	19	25	30	35	39	44	47	52	56	62	65
0.8	1	2	2	1	4	8	13	17	22	27	32	36	40	45	49	53	57	63	65
0.85	0	1	1	3	7	10	15	19	24	29	33	38	42	45	50	54	58	64	66
0.9	0	0	2	5	8	12	16	21	26	30	35	39	43	47	51	55	59	66	66
0.95	0	1	3	6	10	14	18	22	27	31	36	40	44	49	53	55	59	66	66

Table 9: Amplitude loss (in %) for the linear FSE.

$\gamma_1^2 \backslash \gamma_2^2$	0.05	0.1	0.15	0.2	0.25	0.3	0.35	0.4	0.45	0.5	0.55	0.6	0.65	0.7	0.75	0.8	0.85	0.9	0.95
0.05	0	2	6	9	13	16	19	22	25	27	28	30	31	32	32	31	29	24	2
0.1	0	2	5	9	12	16	18	21	23	25	26	28	28	28	28	25	19	3	29
0.15	0	2	5	8	11	14	17	20	22	23	25	25	25	24	22	17	2	24	40
0.2	0	2	4	8	11	14	16	18	20	21	22	22	22	19	14	2	19	33	45
0.25	0	1	4	7	10	12	15	17	18	19	19	19	16	12	2	17	28	39	50
0.3	0	1	4	6	9	11	14	15	16	17	16	14	10	2	13	25	34	43	52
0.35	0	1	3	6	8	10	12	13	14	13	12	8	1	12	22	31	38	47	54
0.4	0	1	3	5	7	9	10	11	11	10	6	1	10	19	27	35	41	49	56
0.45	0	1	2	4	6	7	8	9	8	5	1	8	16	24	31	38	44	50	58
0.5	0	1	2	4	5	6	6	6	4	1	7	14	21	28	34	41	46	52	59
0.55	0	0	2	3	4	5	4	3	1	5	12	19	25	31	37	42	48	53	60
0.6	0	0	1	2	3	3	2	1	4	10	16	22	28	34	39	45	50	53	61
0.65	0	0	1	2	2	1	0	3	8	13	19	25	31	36	41	46	51	53	61
0.7	0	0	1	1	1	0	2	6	11	16	22	27	33	38	43	48	52	54	61
0.75	0	0	0	0	0	1	4	8	14	19	24	29	34	40	44	49	53	55	62
0.8	0	0	0	0	1	3	6	11	16	21	26	31	36	42	45	50	55	56	62
0.85	0	0	0	0	2	4	8	13	18	23	28	33	38	43	47	51	55	56	62
0.9	0	0	0	1	3	6	10	15	20	25	30	34	39	44	48	52	56	56	63
0.95	0	0	0	1	4	7	12	16	21	26	31	36	40	45	49	53	57	57	63

75

Table 10: Amplitude loss (in %) of the left propagating pulse for the nonlinear HE.

$\gamma_t^2 \backslash \gamma_l^2$	0.05	0.1	0.15	0.2	0.25	0.3	0.35	0.4	0.45	0.5	0.55	0.6	0.65	0.7	0.75	0.8	0.85	0.9	0.95
0.05	0	0	2	4	8	11	14	17	19	21	23	24	24	25	25	23	15	11	-2
0.1	0	0	1	4	7	10	13	16	18	20	21	22	22	22	20	16	9	-2	15
0.15	0	0	1	3	6	9	12	15	16	18	19	19	18	17	14	7	-2	11	29
0.2	0	0	1	3	6	8	11	12	14	15	16	16	14	11	5	-1	9	23	37
0.25	0	0	1	3	5	7	9	11	12	13	13	12	9	4	-1	7	20	31	42
0.3	0	0	1	2	4	6	8	10	10	10	9	7	2	-1	5	16	27	37	46
0.35	0	0	0	2	3	5	6	9	8	7	5	2	-1	4	14	23	32	41	49
0.4	0	0	0	1	3	4	5	5	5	3	1	-1	2	11	20	28	36	44	52
0.45	0	0	0	1	2	3	3	3	2	0	-1	2	9	17	25	32	39	47	54
0.5	0	0	0	0	1	2	2	1	0	0	1	7	14	22	29	35	42	49	55
0.55	0	0	0	0	1	1	0	0	0	0	5	12	18	29	32	38	44	51	56
0.6	0	0	0	0	0	0	0	0	0	4	9	16	22	29	34	40	46	53	57
0.65	0	0	0	0	0	0	0	0	2	7	13	19	25	31	35	42	47	55	59
0.7	0	0	0	0	0	0	0	1	5	10	16	22	28	33	39	44	49	56	60
0.75	0	0	0	0	0	0	0	3	8	13	19	24	30	36	41	46	50	57	61
0.8	0	0	0	0	0	0	2	5	10	15	21	26	32	37	42	47	51	58	61
0.85	0	0	0	0	0	1	3	7	12	17	23	28	34	39	44	48	52	58	61
0.9	0	0	0	0	0	2	5	9	14	19	25	30	35	41	45	49	53	59	62
0.95	0	0	0	0	1	3	6	11	16	21	27	32	37	42	46	50	55	60	62

Table 11: Amplitude loss (in %) of the right propagating pulse for the nonlinear HE.

$\gamma_1^2 \setminus \gamma_2^2$	0.05	0.1	0.15	0.2	0.25	0.3	0.35	0.4	0.45	0.5	0.55	0.6	0.65	0.7	0.75	0.8	0.85	0.9	0.95
0.05	3	7	11	15	18	22	25	28	30	32	33	35	36	37	37	38	38	36	32
0.1	3	6	10	14	18	21	24	26	28	30	32	33	34	34	34	33	32	18	44
0.15	2	6	10	14	17	20	23	26	27	29	30	31	31	31	30	27	13	36	49
0.2	2	6	10	13	16	19	22	24	26	27	28	28	28	27	24	10	32	42	53
0.25	2	6	9	13	16	18	21	23	24	25	26	25	24	21	8	27	38	46	55
0.3	2	5	9	12	15	17	19	21	22	23	23	22	18	6	24	33	42	49	57
0.35	2	5	8	11	14	16	18	19	20	20	19	16	5	21	30	37	45	52	59
0.4	2	5	8	11	13	15	16	17	18	17	14	4	18	28	34	41	47	54	61
0.45	2	4	7	10	12	14	15	15	15	12	3	16	24	31	37	43	49	56	61
0.5	2	4	7	9	11	12	13	12	10	3	14	21	28	35	40	45	51	57	62
0.55	1	4	6	8	10	10	10	9	2	12	19	25	31	36	42	47	52	59	62
0.6	1	3	5	7	8	8	7	2	10	17	23	28	34	39	44	48	53	60	63
0.65	1	3	5	6	6	6	2	9	15	20	25	31	36	41	46	50	54	61	64
0.7	1	3	4	5	4	1	7	12	18	23	28	33	38	43	47	51	56	62	64
0.75	1	2	3	3	1	6	10	15	20	25	30	35	39	44	48	52	56	63	65
0.8	1	2	2	1	4	8	13	17	22	27	32	36	41	45	49	53	57	63	65
0.85	0	1	0	3	6	10	15	19	24	28	33	38	42	47	50	54	57	64	66
0.9	0	0	2	5	8	12	16	21	26	30	35	39	43	48	51	55	55	65	66
0.95	0	0	3	6	9	14	18	22	27	32	36	40	44	49	52	55	59	65	66

Table 12: Amplitude loss (in %) for the linear HE.

$\gamma_1^2 \setminus \gamma_4^2$	0.05	0.1	0.15	0.2	0.25	0.3	0.35	0.4	0.45	0.5	0.55	0.6	0.65	0.7	0.75	0.8	0.85	0.9	0.95
0.05	0	2	5	9	13	16	19	22	24	26	28	29	31	31	31	30	29	23	0
0.1	0	2	5	8	12	15	18	21	23	25	26	27	28	28	27	25	19	0	29
0.15	0	2	5	8	11	14	17	19	21	23	24	25	25	24	21	16	0	23	39
0.2	0	1	4	7	10	13	16	18	20	21	22	22	21	19	13	0	19	33	45
0.25	0	1	4	7	10	12	15	16	18	19	19	18	16	11	0	16	28	39	49
0.3	0	1	3	6	9	11	13	15	16	16	15	14	9	0	13	24	34	43	52
0.35	0	1	3	5	8	10	12	13	13	13	11	7	0	11	21	30	38	46	54
0.4	0	1	3	5	7	9	10	11	11	9	6	0	9	19	27	34	41	49	56
0.45	0	1	2	4	6	7	8	8	7	5	0	7	16	24	31	38	44	51	58
0.5	0	1	2	3	5	6	6	5	3	0	6	13	21	28	34	40	46	52	59
0.55	0	0	2	3	4	4	4	2	0	5	11	18	25	31	37	43	48	53	59
0.6	0	0	1	2	3	3	2	0	3	9	15	22	28	34	39	44	50	53	60
0.65	0	0	1	1	2	1	0	2	7	13	19	25	30	36	41	46	51	53	61
0.7	0	0	1	1	1	0	2	5	11	16	22	27	33	38	43	47	52	54	61
0.75	0	0	0	0	0	1	4	8	13	19	24	29	34	40	45	49	53	55	61
0.8	0	0	0	0	1	3	6	11	15	21	26	31	36	41	46	50	54	55	61
0.85	0	0	0	0	2	4	8	13	19	23	28	33	38	43	47	51	55	56	62
0.9	0	0	0	1	3	6	10	15	20	25	30	34	39	44	48	52	56	56	63
0.95	0	0	0	1	4	7	12	16	21	26	31	36	40	45	49	53	57	57	63
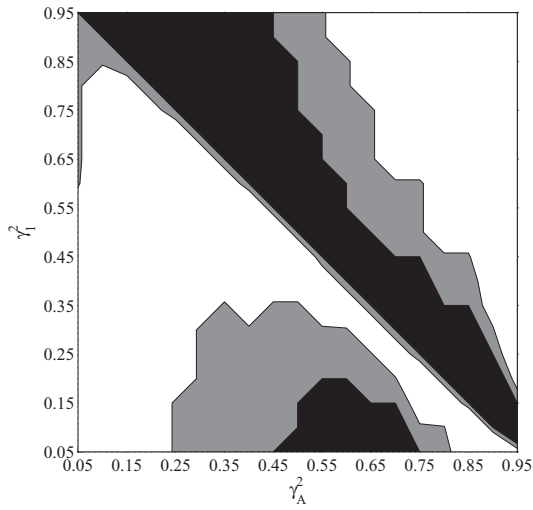
Figure 18: Speed differences between pulses propagating to the left and right for the FSE in the nonlinear case. Black — the pulse propagating to the right is faster; white — the pulse propagating to the left is faster; grey — equal speeds.
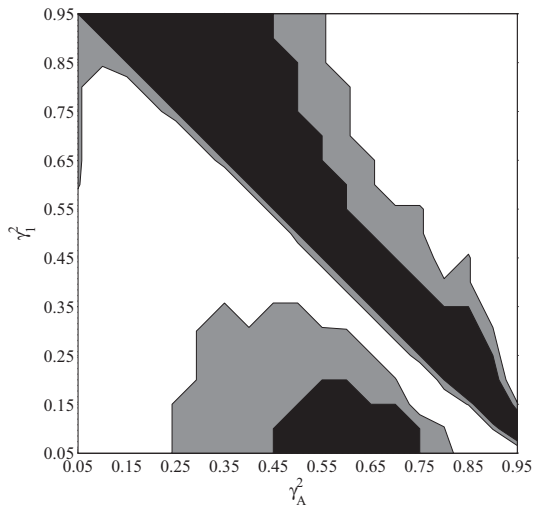
Figure 19: Speed differences between pulses propagating to the left and right for the HE in the nonlinear case. Black — the pulse propagating to the right is faster; white — the pulse propagating to the left is faster; grey — equal speeds.
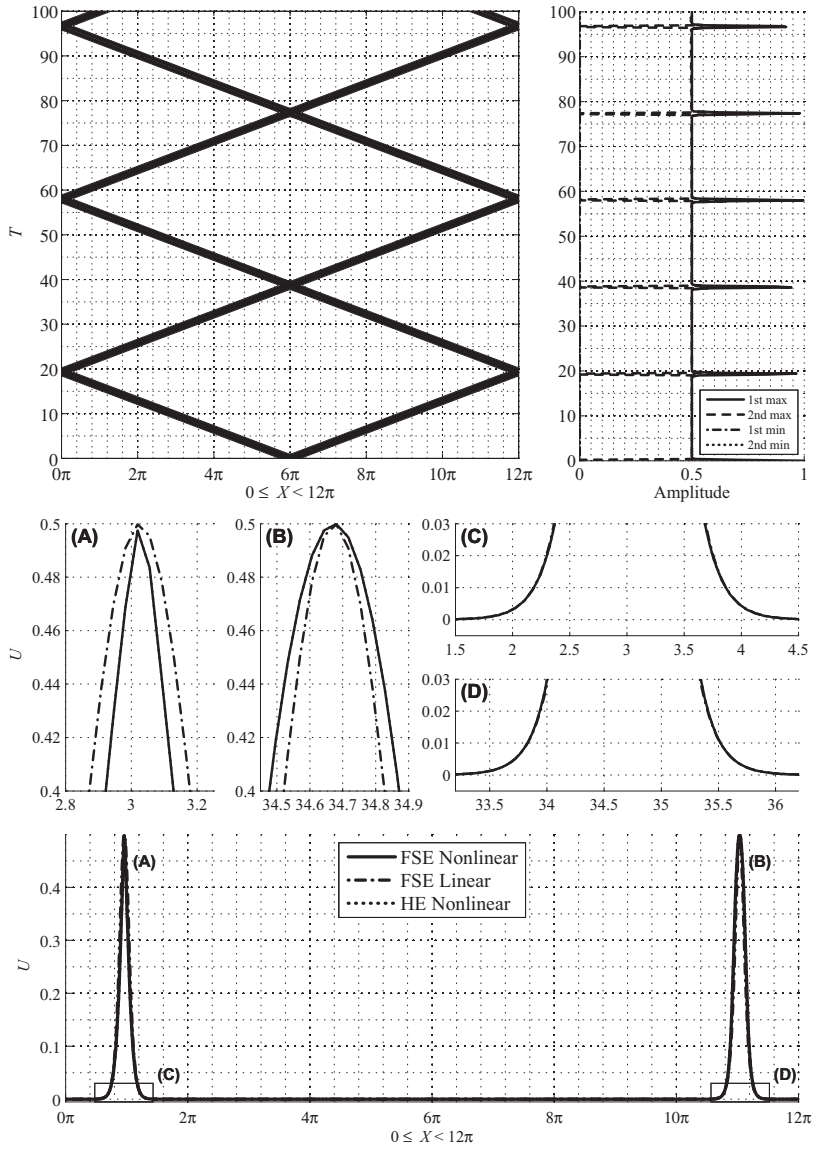
Figure 20: Solutions of the FSE and HE for $\gamma_A^2 = 0.05$, $\gamma_1^2 = 0.95$. See page 66 for the structure of the figure.

80
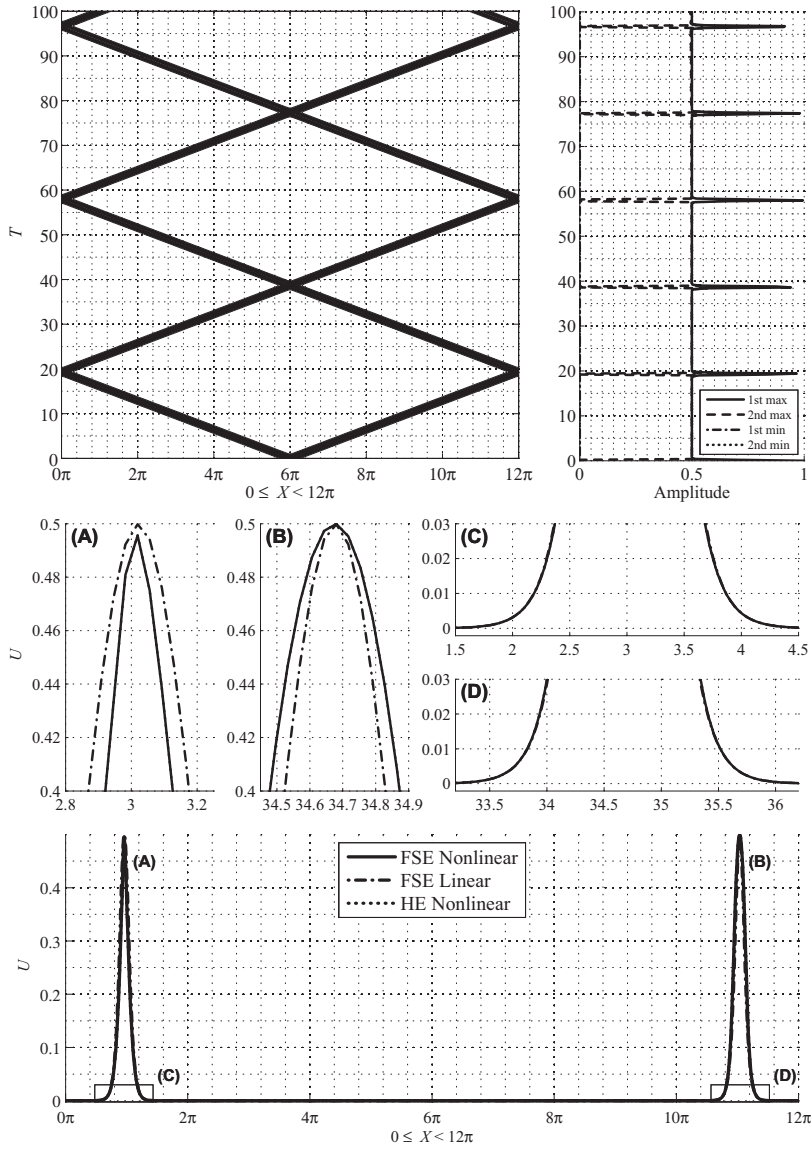
Figure 21: Solutions of the FSE and HE for $\gamma_A^2 = 0.05$, $\gamma_1^2 = 0.75$. See page 66 for the structure of the figure.
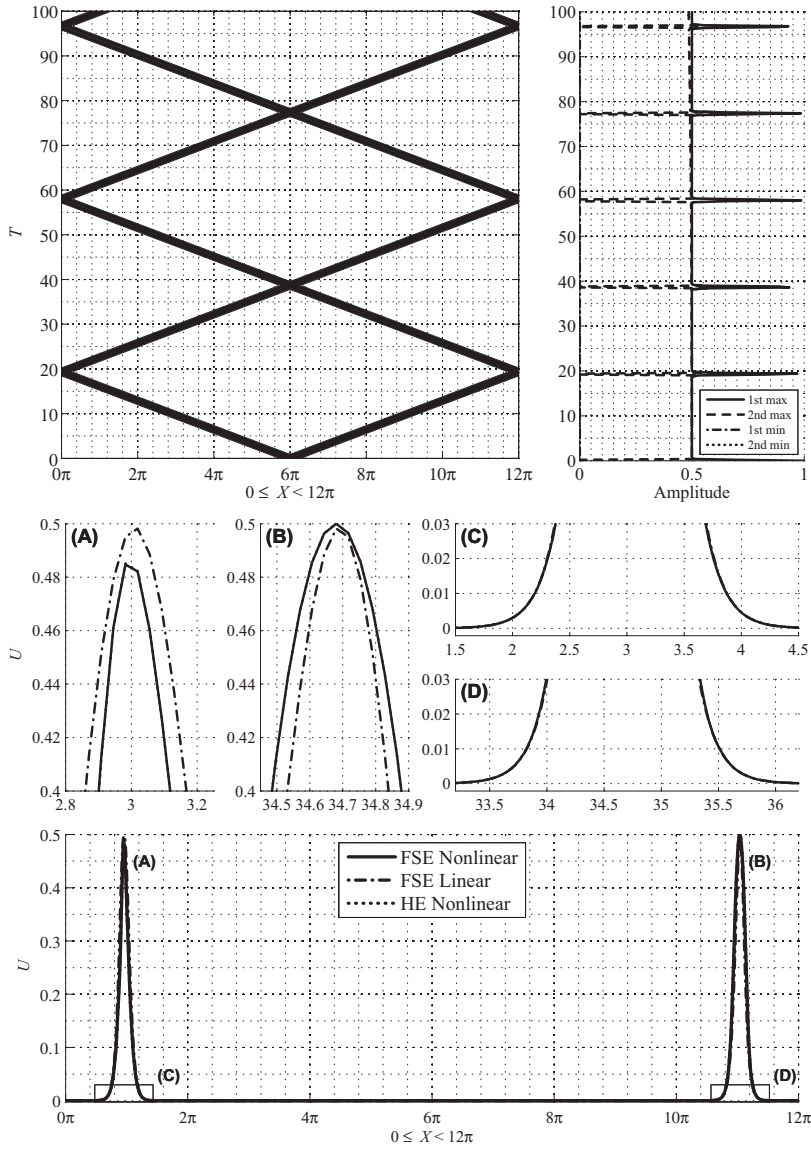
Figure 22: Solutions of the FSE and HE for $\gamma_A^2 = 0.05$, $\gamma_1^2 = 0.05$. See page 66 for the structure of the figure.
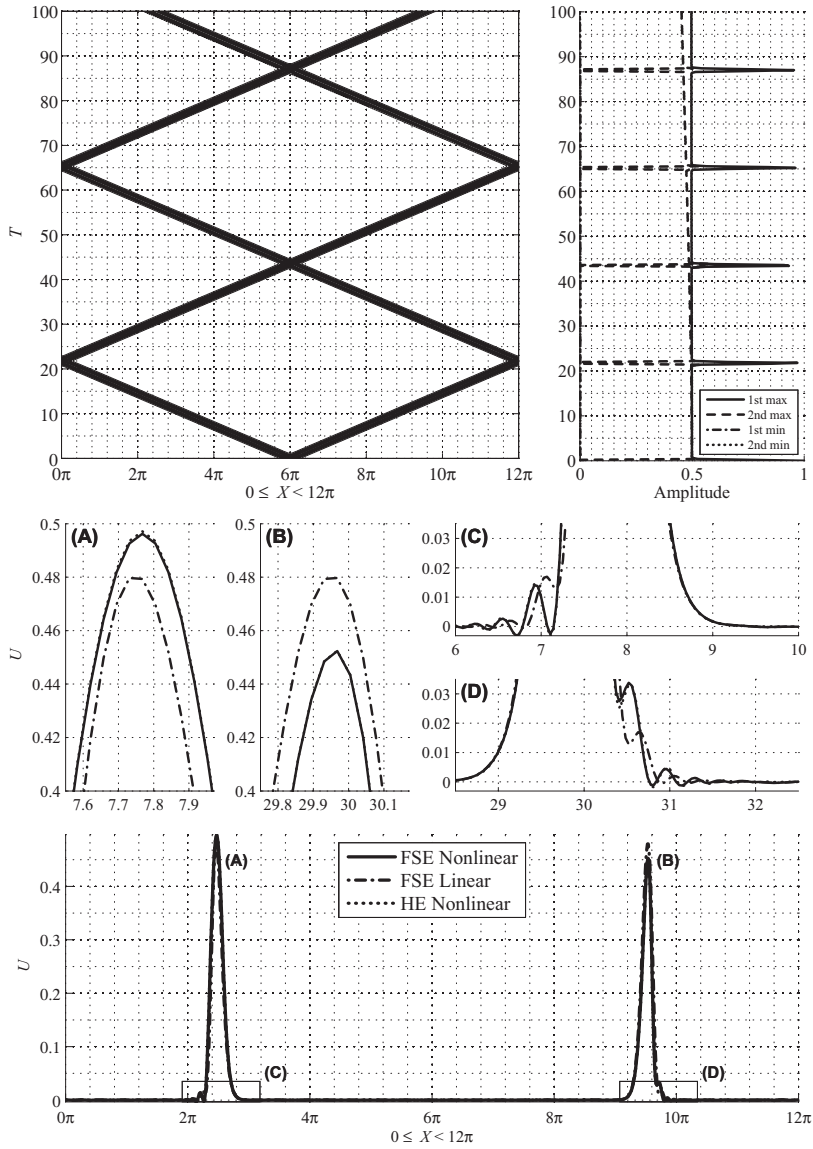
Figure 23: Solutions of the FSE and HE for $\gamma_A^2 = 0.25$, $\gamma_1^2 = 0.95$. See page 66 for the structure of the figure.
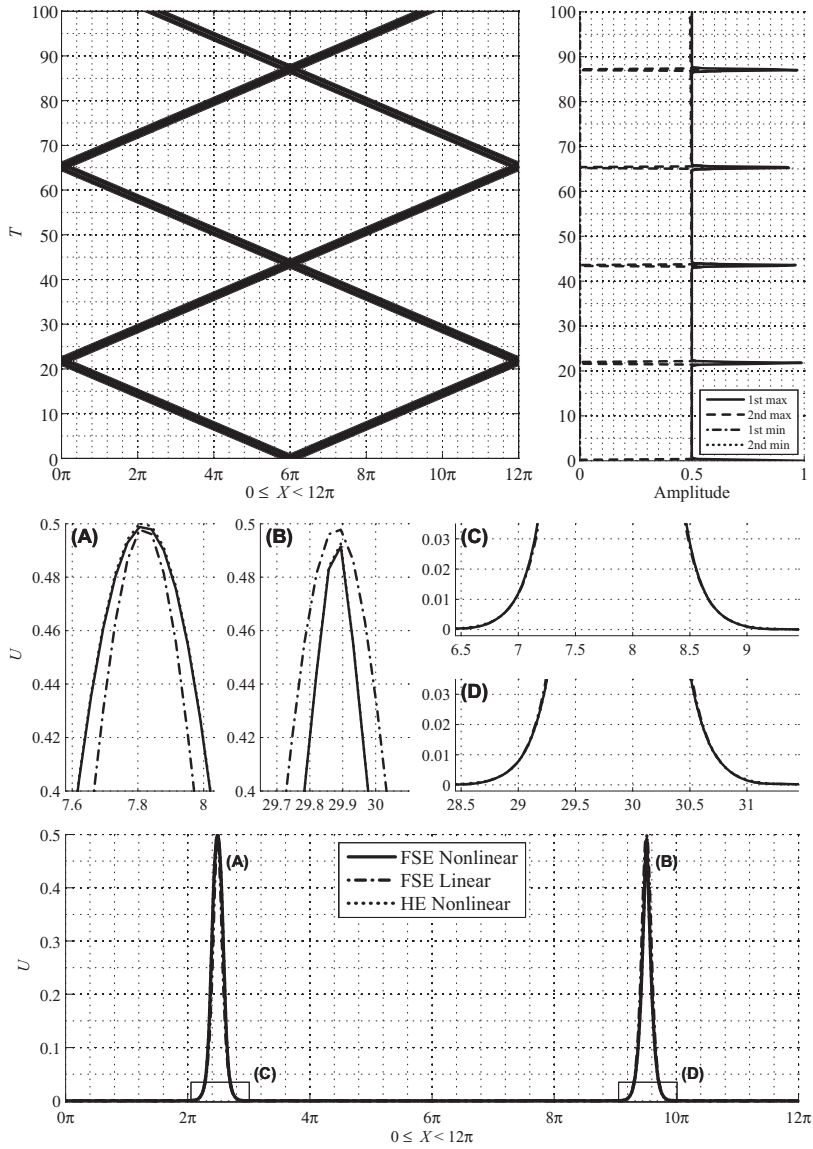
Figure 24: Solutions of the FSE and HE for $\gamma_A^2 = 0.25$, $\gamma_1^2 = 0.75$. See page 66 for the structure of the figure.

84
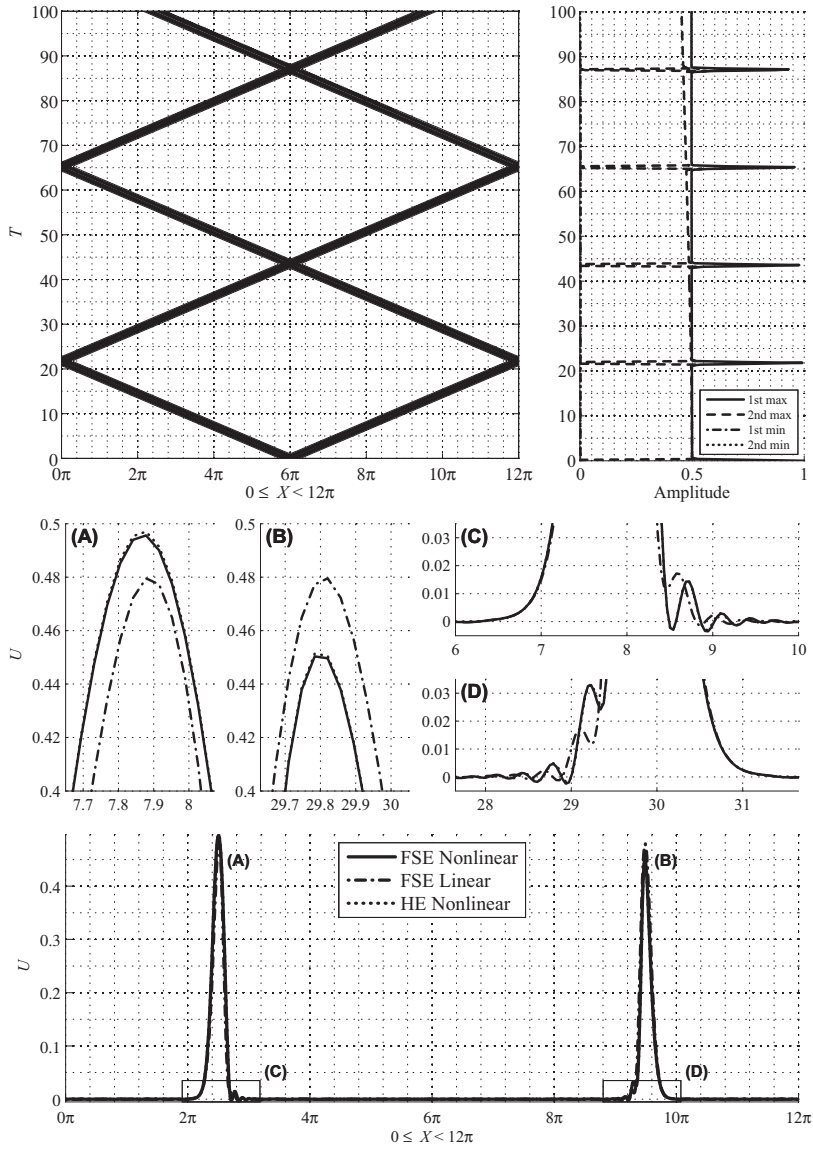
Figure 25: Solutions of the FSE and HE for $\gamma_A^2 = 0.25$, $\gamma_1^2 = 0.55$. See page 66 for the structure of the figure.
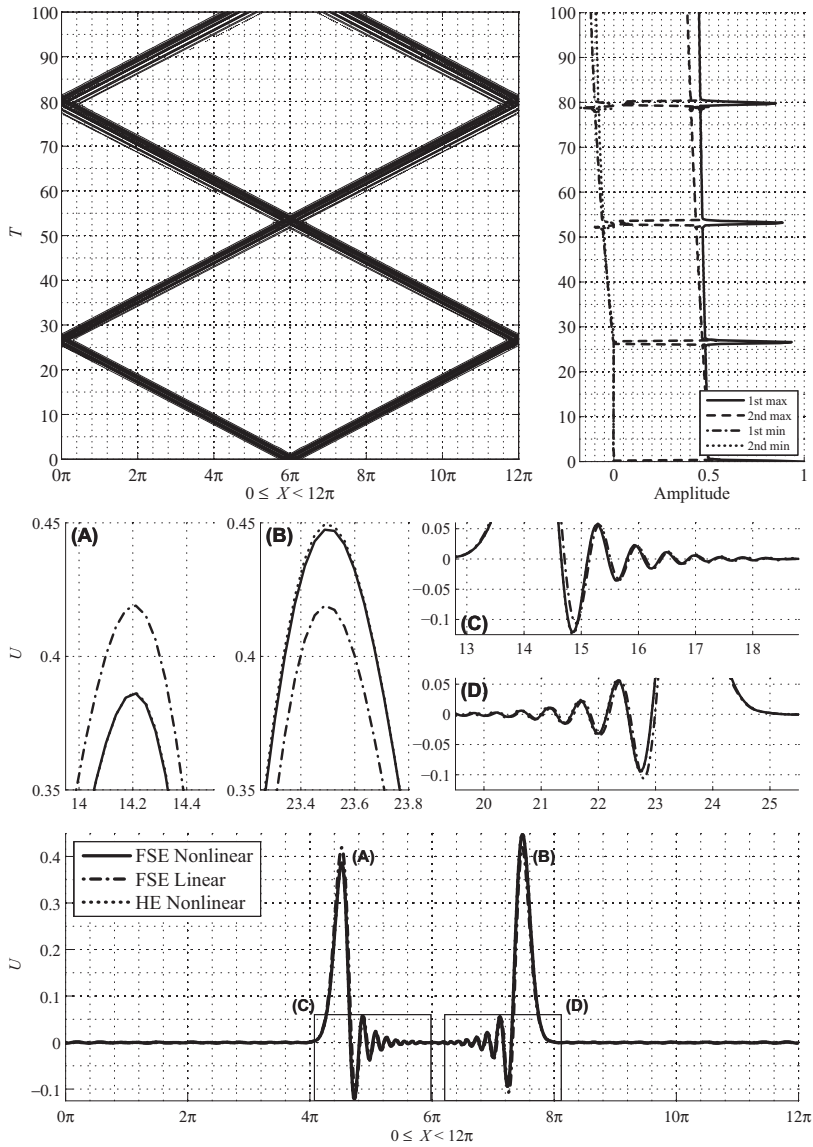
Figure 26: Solutions of the FSE and HE for $\gamma_A^2 = 0.5$, $\gamma_1^2 = 0.7$. See page 66 for the structure of the figure.
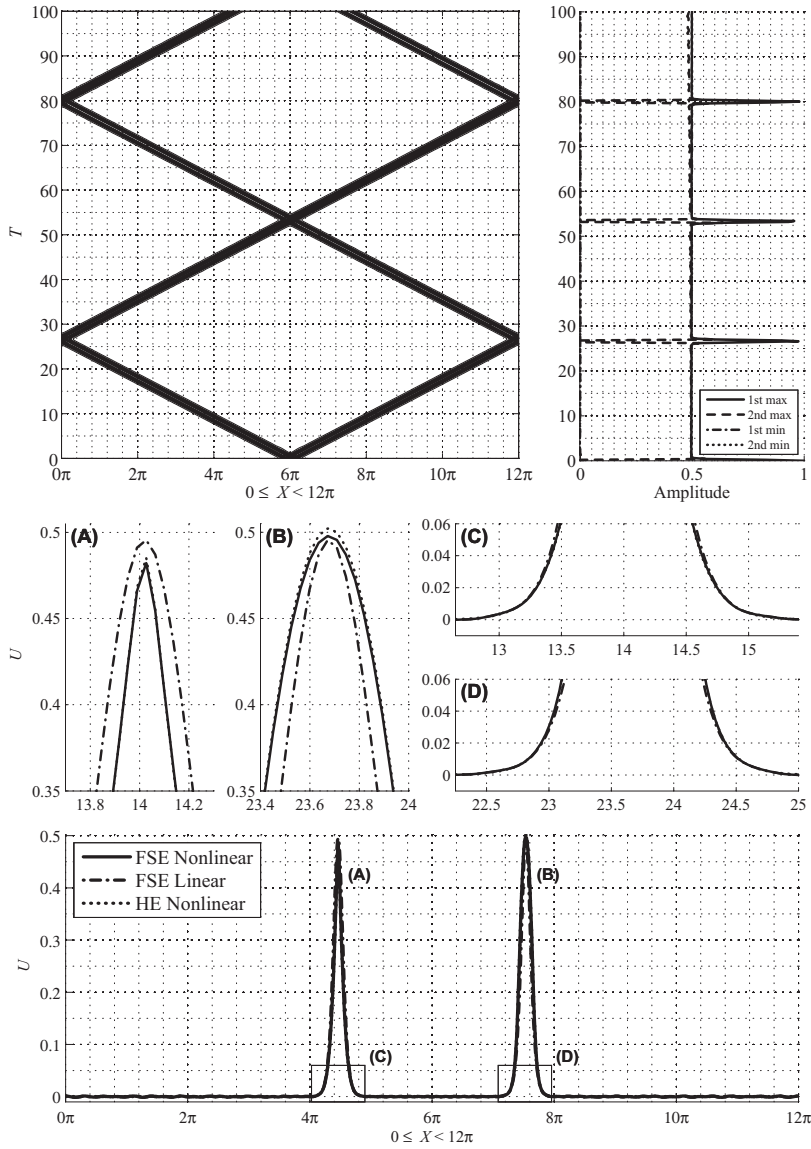
Figure 27: Solutions of the FSE and HE for $\gamma_A^2 = 0.5$, $\gamma_1^2 = 0.5$. See page 66 for the structure of the figure.
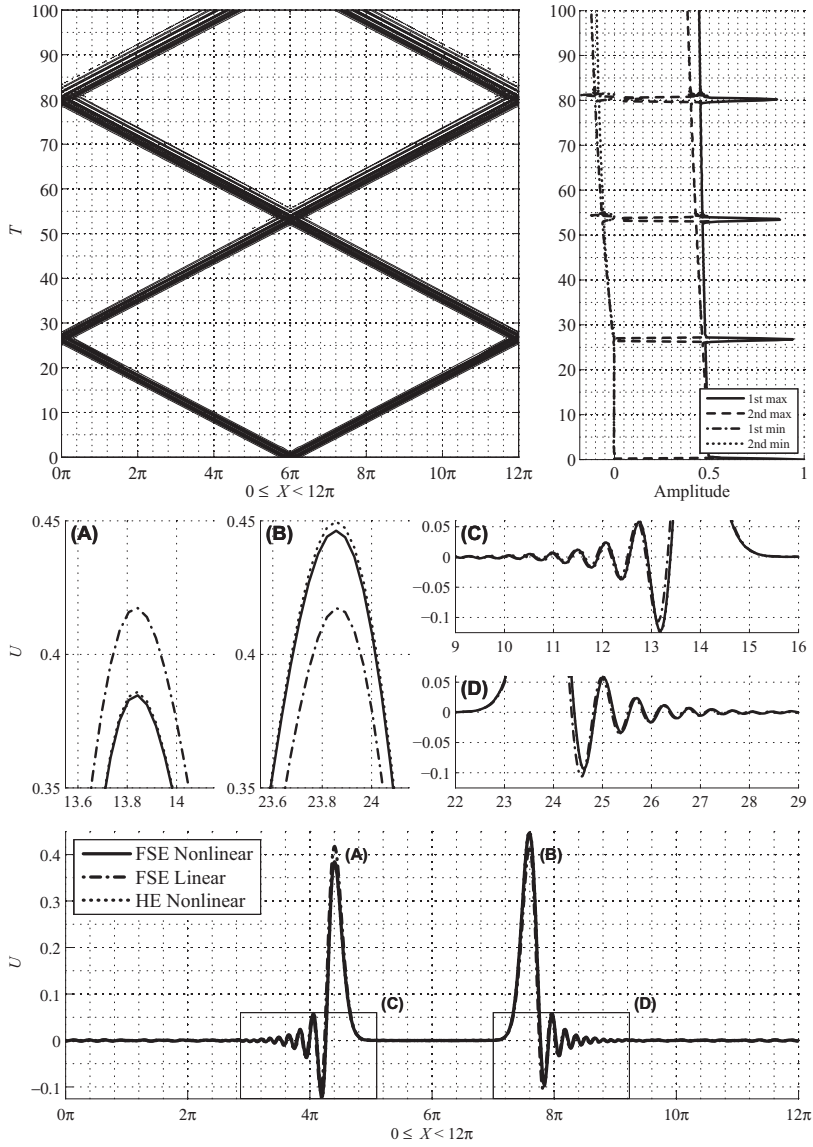
Figure 28: Solutions of the FSE and HE for $\gamma_A^2 = 0.5$, $\gamma_1^2 = 0.3$. See page 66 for the structure of the figure.
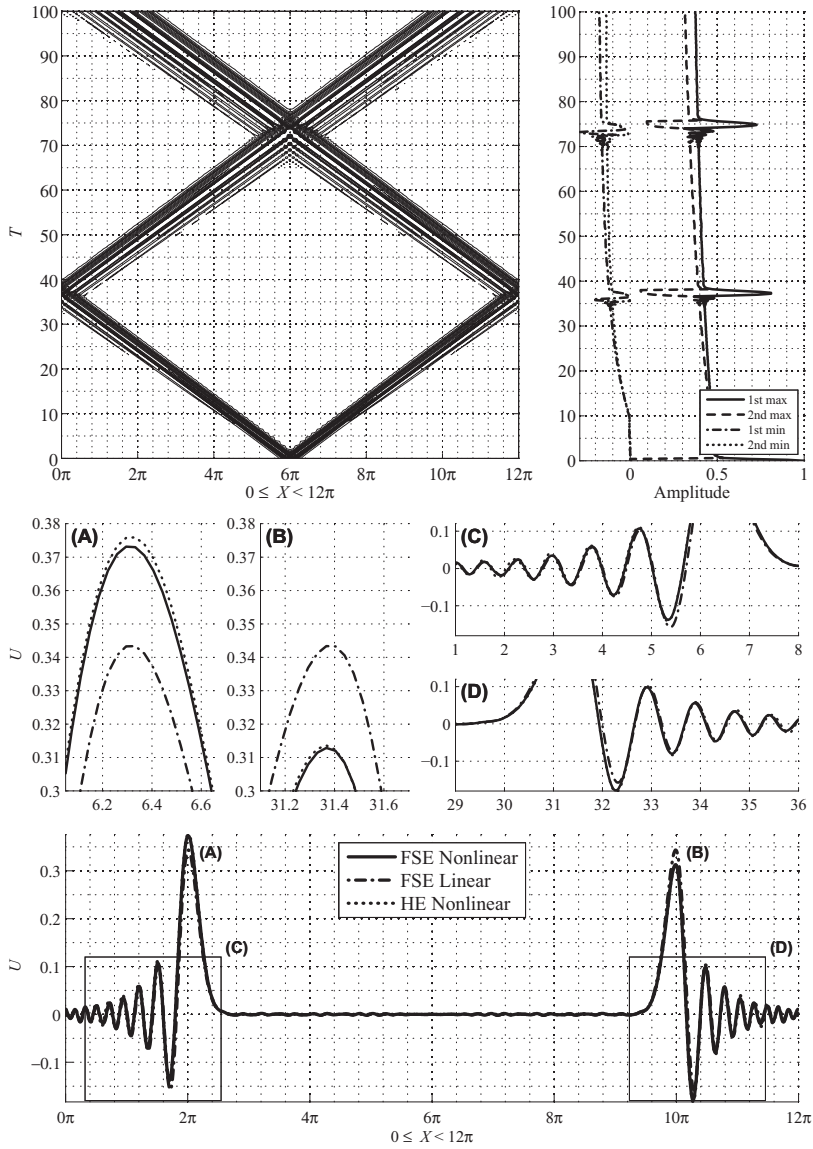
Figure 29: Solutions of the FSE and HE for $\gamma_A^2 = 0.75$, $\gamma_1^2 = 0.45$. See page 66 for the structure of the figure.
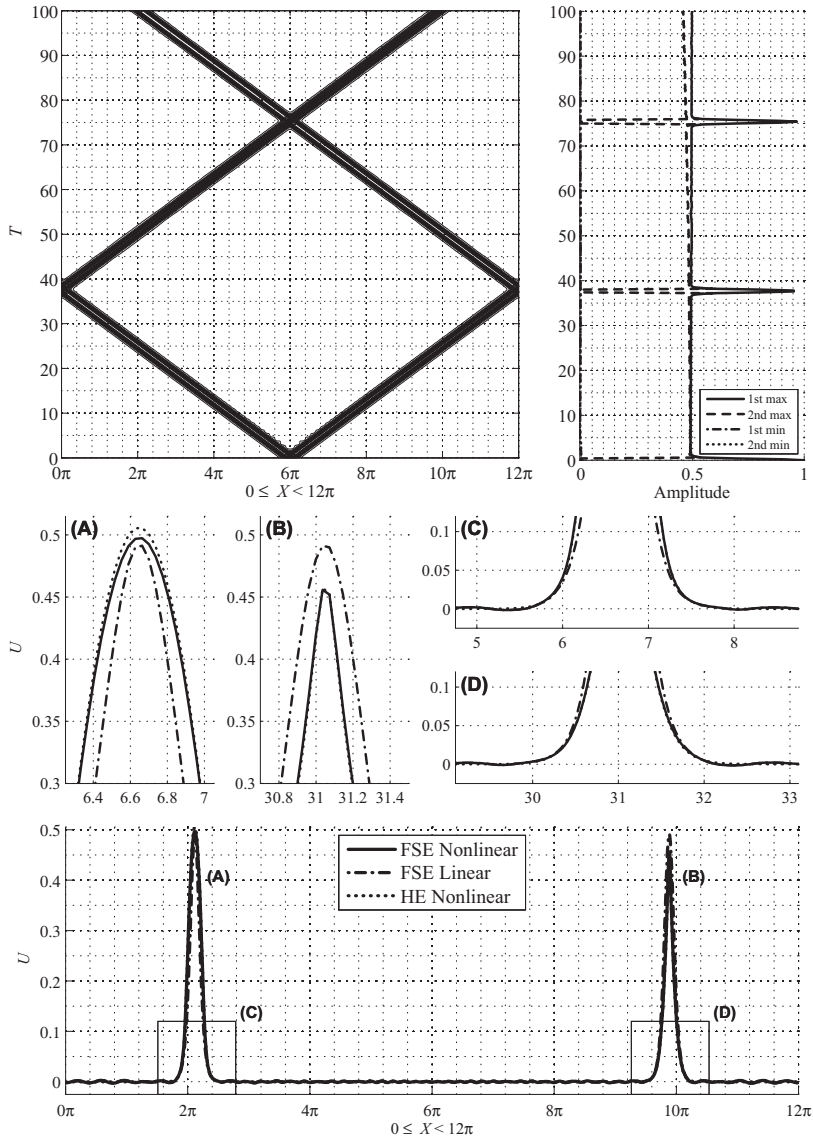
Figure 30: Solutions of the FSE and HE for $\gamma_A^2 = 0.75$, $\gamma_1^2 = 0.25$. See page 66 for the structure of the figure.

90
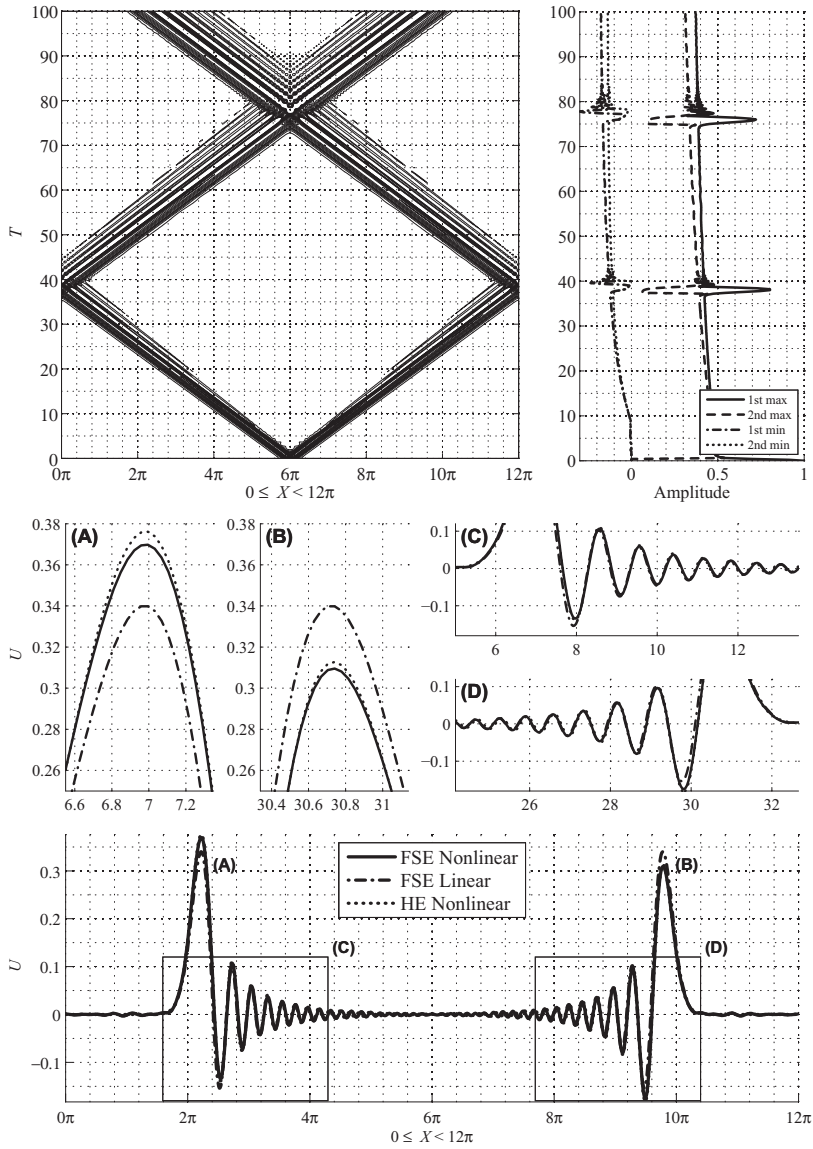
Figure 31: Solutions of the FSE and HE for $\gamma_A^2 = 0.75$, $\gamma_1^2 = 0.05$. See page 66 for the structure of the figure.
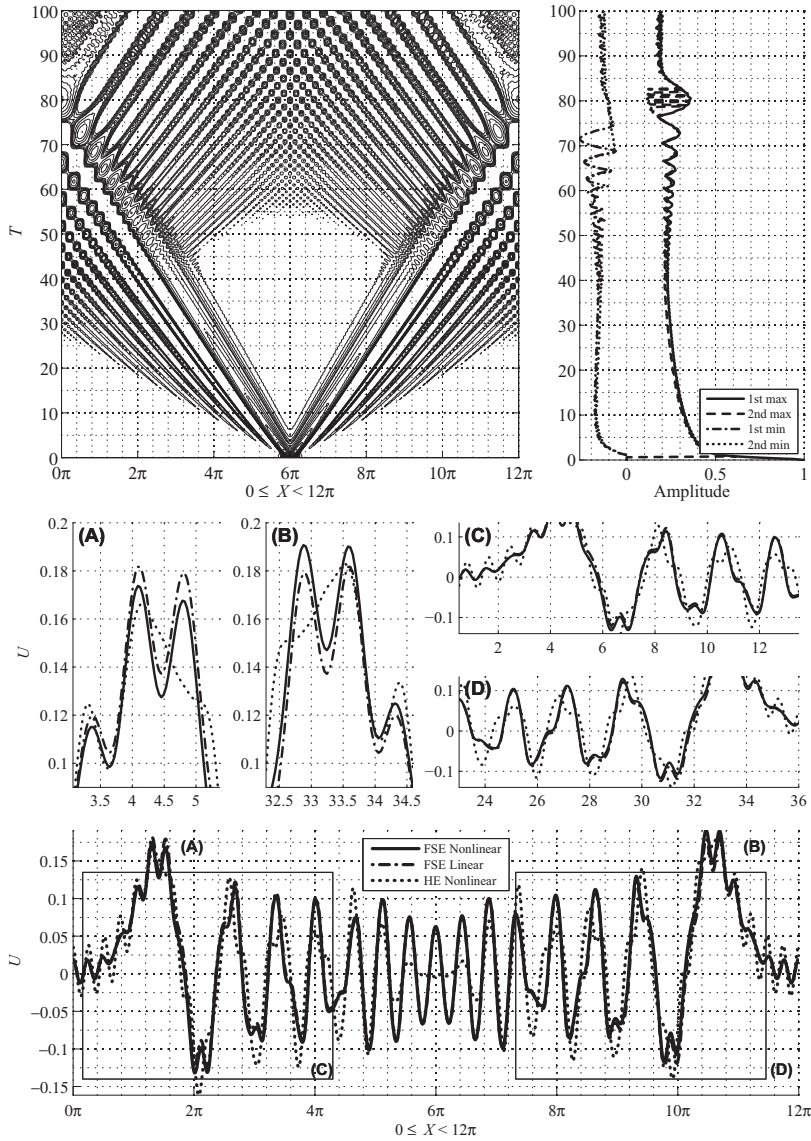
Figure 32: Solutions of the FSE and HE for $\gamma_A^2 = 0.95$, $\gamma_1^2 = 0.95$. See page 66 for the structure of the figure.
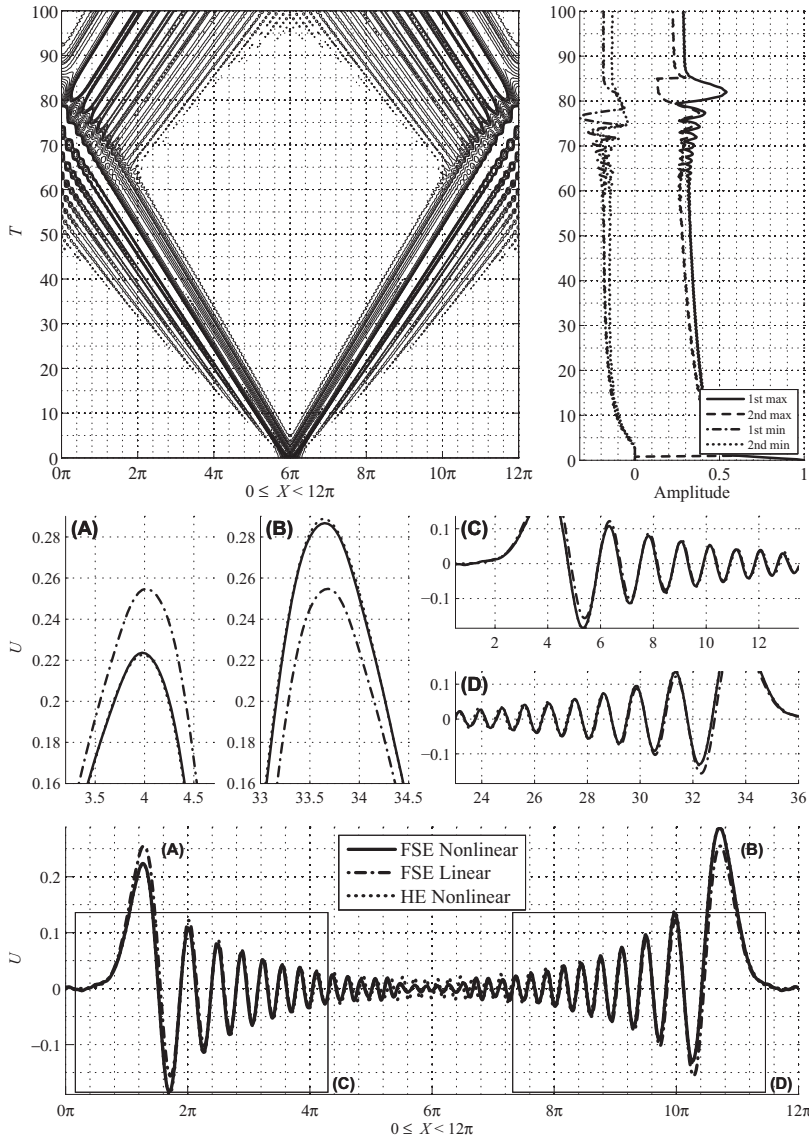
Figure 33: Solutions of the FSE and HE for $\gamma_A^2 = 0.95$, $\gamma_1^2 = 0.25$. See page 66 for the structure of the figure.
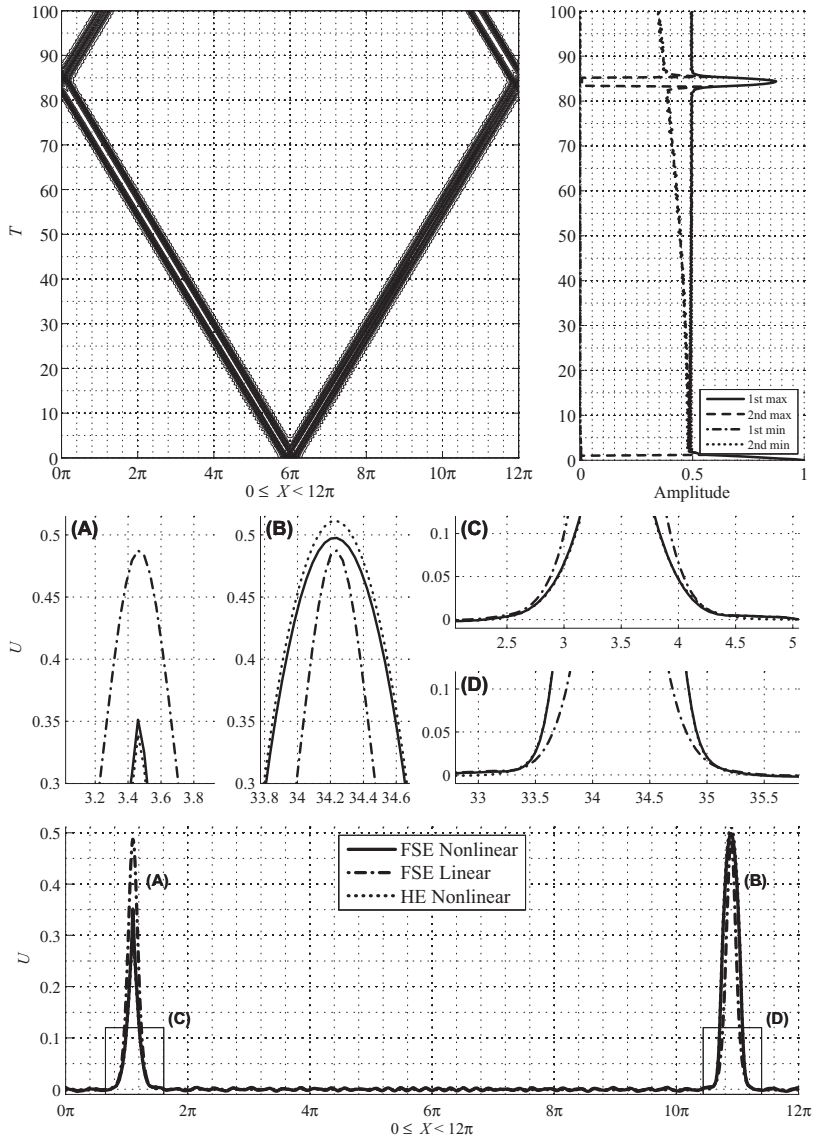
Figure 34: Solutions of the FSE and HE for $\gamma_A^2 = 0.95$, $\gamma_1^2 = 0.05$. See page 66 for the structure of the figure.

94
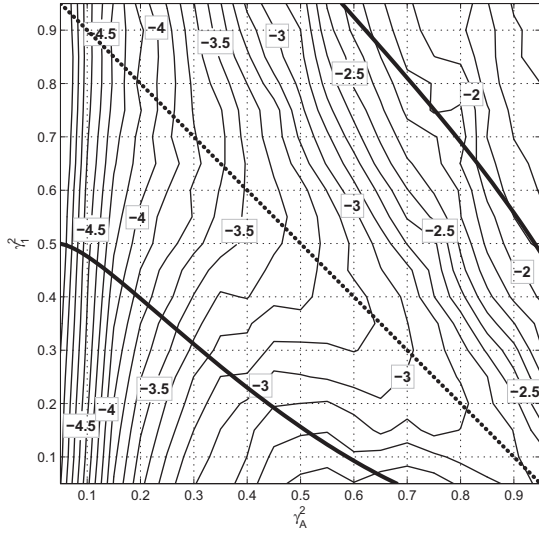
Figure 35: Quantity $\log_{10}\left(\Delta^S\right)$ against γ_1^2 and γ_A^2 in the linear case.
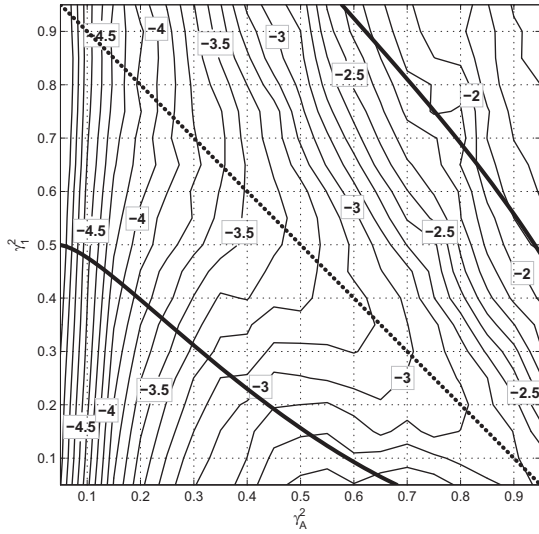
Figure 36: Quantity $\log_{10}\left(\Delta^S\right)$ against γ_1^2 and γ_A^2 in the nonlinear case.
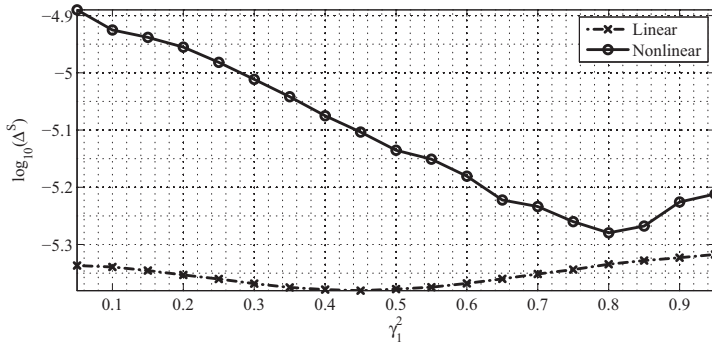
Figure 37: Quantity $\log_{10}\Delta^S$ against γ_1^2 at $\gamma_A^2 = 0.05$.
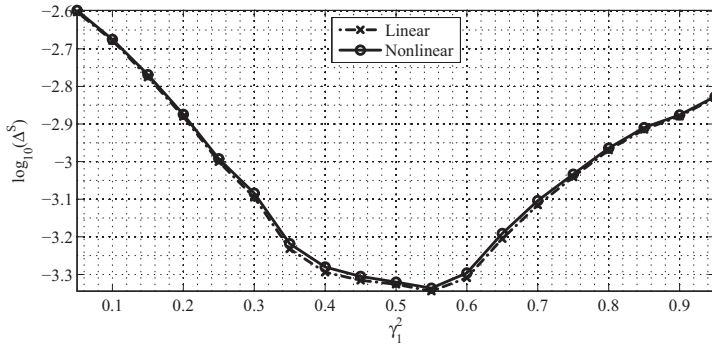
Figure 38: Quantity $\log_{10}\Delta^S$ against γ_1^2 at $\gamma_A^2 = 0.5$.
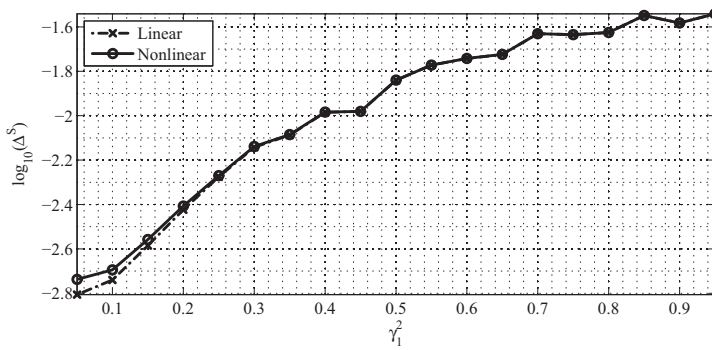
Figure 39: Quantity $\log_{10}\Delta^S$ against γ_1^2 at $\gamma_A^2 = 0.95$.

96
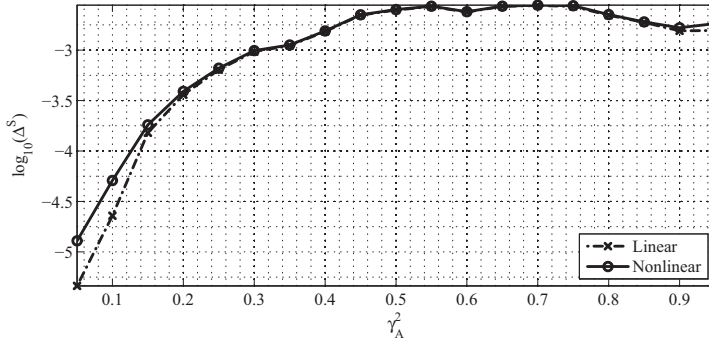
Figure 40: Quantity $\log_{10} \Delta^S$ against γ_A^2 at $\gamma_1^2 = 0.05$.
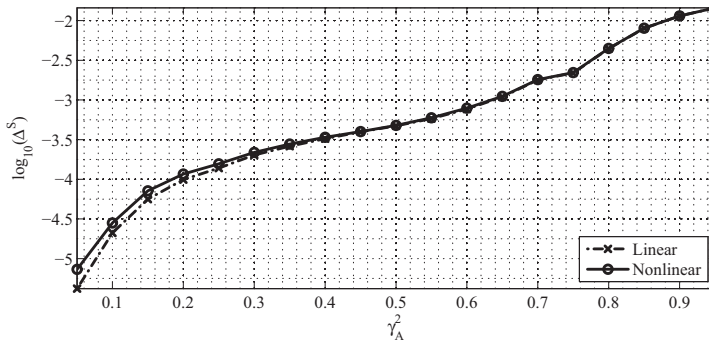
Figure 41: Quantity $\log_{10} \Delta^S$ against γ_A^2 at $\gamma_1^2 = 0.5$.
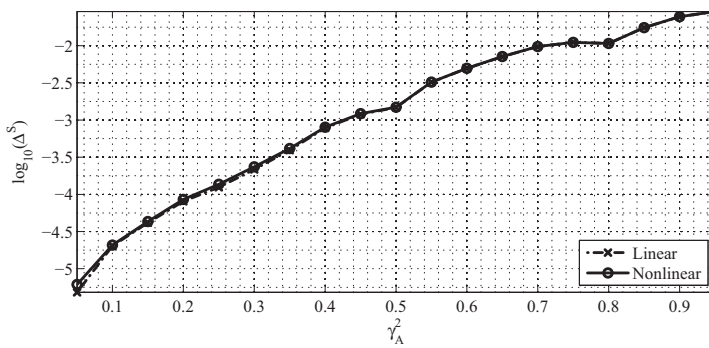
Figure 42: Quantity $\log_{10} \Delta^S$ against γ_A^2 at $\gamma_1^2 = 0.95$.
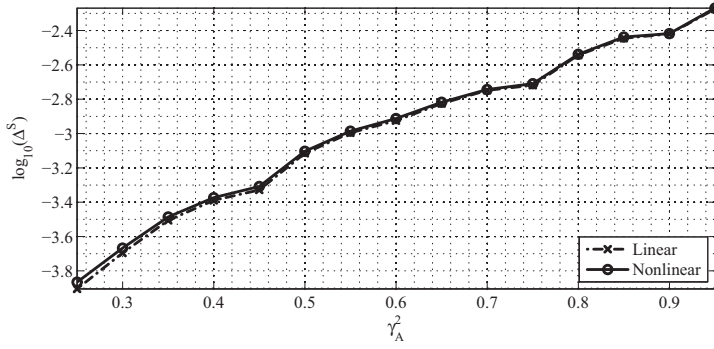
Figure 43: Quantity $\log_{10}\Delta^S$ against γ_A^2 at $\Gamma = -0.2$ (anomalous dispersion).
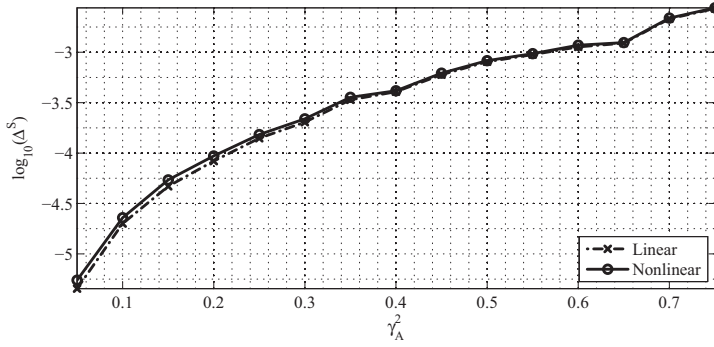
Figure 44: Quantity $\log_{10}\Delta^S$ against γ_A^2 at $\Gamma = +0.2$ (normal dispersion).
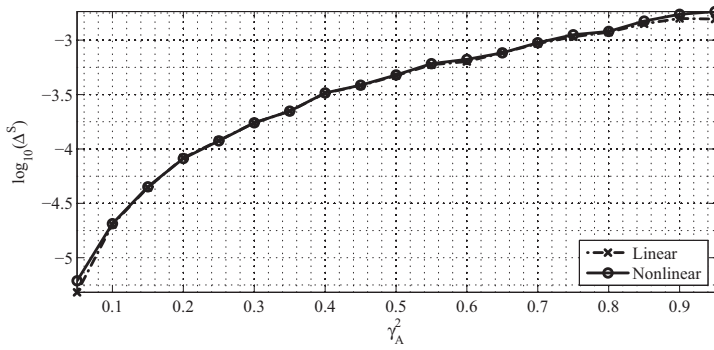
Figure 45: Quantity $\log_{10}\Delta^S$ against γ_A^2 at $\Gamma = 0$ (dispersionless case).

Appendix C: CV

General information

Name: Kert Tamm
Date and place of birth: 20 March 1979, Tallinn
Nationality: Estonian
Home address: Olevi 5, 10920 Tallinn
Phone: +372 52 83 521
E-mail: kert@cens.ioc.ee

Education

2006–2011 Tallinn University of Technology, Engineering Physics, PhD.
2004–2006 Tallinn University of Technology, Engineering Physics, MSc.
2000–2004 Tallinn University of Technology, Engineering Physics, BSc.
1994–1999 Tallinn Polytechnic School, Telecommunication, Radio technician.

Career

2005–2006 Engineering Bureau 'Printsiip'
2004– ... Institute of Cybernetics at TUT
2004–2005 Engineering Bureau 'Peipman'
1999–2000 Estonian Defense Forces, Communication Battalion
1998–1999 Estonian Public Broadcasting

Academic activity

2006 **MSc thesis**: 'Deformation waves in microstructured solids'. The main subject is the propagation and interaction of deformation waves in microstructured solids. The hierarchical model equation (derived by J. Engelbrecht and F. Pastrone) is used.

2004 **BSc thesis**: 'Soliton formation in the Boussinesq model' (in Estonain). The main subject is the formation and interaction of solitons. Numerical methods are used to solve the Boussinesq equation under localized and harmonic initial conditions and periodic boundary conditions.

Conferences:

A. Salupere (speaker), J. Engelbrecht, L. Ilison and K. Tamm, 'On solitary waves and solitons in hierarchical systems', IMACS 2005, The Fourth International Conference on Nonlinear Evolution Equations and Wave Phenomena: Computation and Theory, The University of Georgia, April 10–14, 2005, Athens, USA.

A. Salupere (speaker), K. Tamm and Jüri Engelbrecht, 'Interaction of deformation waves in microstructured solids', EUROMECH Colloquium 478, Non-equilibrium Dynamical Phenomena in Inhomogeneous Solids, June 13–16, 2006, Tallinn.

A. Salupere (speaker), K. Tamm and J. Engelbrecht, 'Propagation of solitary pulses in microstructured solids', 6th European Solid Mechanics Conference, 28 August–1 September, 2006, Budapest, Hungary.

A. Salupere (speaker), K. Tamm and J. Engelbrecht, 'Interaction of solitary deformation waves in microstructured solids', The Fifth IMACS International Conference on Nonlinear Evolution Equations and Wave Phenomena: Computation and Theory, The University of Georgia, April 16–19, 2007, Athens, USA.

A. Salupere (speaker), K. Tamm and J. Engelbrecht, 'Emergence and interaction of solitary waves in microstructured solids', XII International Workshop on Nonlinear Elasticity in Materials, Ajaccio, June 3–9, 2007, Corsica, France.

A. Salupere (speaker), K. Tamm and J. Engelbrecht, 'Numerical simulation of propagation of solitary deformation waves in microstructured solids', The Ninth U.S. National Congress on Computational Mechanics (USNCCM IX), July 23–26, 2007, San Francisco, USA.

A. Salupere (speaker), M. Randrüüt and K. Tamm, 'Emergence of soliton trains in microstructured materials', XXII International Congress of Theoretical and Applied Mechanics ICTAM 2008, August 24–29, 2008, Adelaide, Australia.

K. Tamm (speaker), 'Deformatsioonilained Mindlini tüüpi mikrostruktuuriga materjalides' ('Deformation waves in Mindlin-type microstructured materials'), XIII Estonian Days of Mechanics, Sept 15–16, 2008, Tallinn, Estonia.

K. Tamm (speaker) and A. Salupere, 'On propagation of 1D solitary waves in Mindlin-type microstructured solids', The Sixth IMACS International Conference on Nonlinear Evolution Equations and Wave Phenomena: Computation and Theory, The University of Georgia, March 23–26, 2009, Athens, USA.

T. Peets (speaker) and K. Tamm, 'Dispersion analysis on wave motion in microstructured solids', Symposium on Recent Advances of Acoustic Waves in Solids, May 25–28, 2009, Taiwan.

K. Tamm (speaker) and A. Salupere, 'Emergence of solitary waves in Mindlin-type microstructured solids', International Conference on Complexity of Nonlinear Waves, Institute of Cybernetics, Tallinn University of Technology, October 5–7, 2009, Tallinn, Estonia.

Publications

A. Salupere, J. Engelbrecht, L. Ilison and K. Tamm, 'On solitary waves and solitons in hierarchical systems'. In: T. R. Taha (ed), Book of Abstracts, The Fourth International Conference on Nonlinear Evolution Equations and Wave Phenomena: Computation and Theory, Athens, Georgia, USA, April 10–14, 2005, The University of Georgia, 2005, p. 158.

A. Salupere, K. Tamm and J. Engelbrecht, 'Interaction of deformation waves in microstructured solids'. In: Book of Abstracts, EUROMECH Colloquium 478, Non-equilibrium Dynamical Phenomena in Inhomogeneous Solids, Tallinn, Estonia, 2006, p. 32.

A. Salupere, K. Tamm, J. Engelbrecht and P. Peterson, 'On the interaction of deformation waves in microstructured solids'. Proceedings of the Estonian Academy of Sciences, Physics, Mathematics, 56 (2007), pp. 93–99.

A. Salupere, L. Ilison and K. Tamm, 'On numerical simulation of propagation of solitons in microstructured media'. In: M.D. Todorov (ed), Applications of Mathematics in Engineering and Economics, vol. 1067 of AIP Conference Proceedings (2008), pp. 155–165.

A. Salupere, K. Tamm and J. Engelbrecht, 'Numerical simulation of interaction of solitary deformation waves in microstructured solids'. International Journal of Non-Linear Mechanics, 43 (2008), pp. 201–208.

A. Salupere, M. Randrüüt and K. Tamm, 'Emergence of soliton trains in microstructured materials'. In: J. Denier, M. Finn and T. Mattner (eds), XXII International Congress of Theoretical and Applied Mechanics ICTAM 2008, Abstracts book, The University of Adelaide, Adelaide, 2008, p. 260.

K. Tamm and A. Salupere, 'On propagation of 1D solitary waves in Mindlin-type microstructured solids'. In: T. R. Taha (ed), Book of Abstracts, The Sixth IMACS International Conference on Nonlinear Evolution Equations and Wave Phenomena: Computation and Theory, The University of Georgia, Athens, Georgia, USA, 2009, p. 86.

K. Tamm and A. Salupere, 'Emergence of solitary deformation waves in Mindlin-type microstructured solids'. In: A. Berezovski, T. Soomere (eds), International Conference on Complexity of Nonlinear Waves: Book of Abstracts, October 5–7, 2009, Tallinn, Estonia, p. 33.

T. Peets and K. Tamm, 'Dispersion Analysis of Wave Motion in Microstructured Solids'. In: Tsung–Tsong Wu, Chien–Ching Ma (eds), IUTAM Symposium on Recent Advances of Acoustic Waves in Solids: Proceedings, Taipei, Taiwan, May 25–28, 2009, volume 26 of IUTAM Bookseries, Springer, Dordrecht, 2010, pp. 349–354.

K. Tamm and A. Salupere, 'On the propagation of solitary waves in Mindlin-type microstructured solids'. Proceedings of the Estonian Academy of Sciences, 59 (2010), pp. 118–125.

K. Tamm and A. Salupere, 'On the propagation of 1D solitary waves in Mindlin-type microstructured solids'. Mathematics and Computers in Simulation, (2011), *in press*.

J. Engelbrecht, A. Salupere and K. Tamm, 'Waves in microstructured solids and the Boussinesq paradigm'. Wave Motion, (2011), *submitted*.

Command of languages:

Estonian (native), English (good), Finnish (satisfactory), Russian (poor)

Computer languages:

Fortran, Python

Experienced in the use of:

Windows, Linux, AutoCAD, MatCAD, LaTeX, Mathematica, Maple, MATLAB, Maxima

Elulookirjeldus

Isikuandmed

Nimi: Kert Tamm
Sünniaeg ja koht: 20 märts 1979 Tallinn
Kodakondsus: Eesti
Kodune aadress: Olevi 5, Tallinn, 10920
Telefon: +372 52 83 521
E-post: kert@cens.ioc.ee

Haridus

2006–2011 Tallinna Tehnikaülikool, Tehniline füüsika, PhD.
2004–2006 Tallinna Tehnikaülikool, Tehniline füüsika, MSc.
2000–2004 Tallinna Tehnikaülikool, Tehniline füüsika, BSc.
1994–1999 Tallinna Polütehnikum, Telekommunikatsioon, Raadiotehnik.

Karjäär

2005–2006 Inseneribüroo Printsiip OÜ
2004–...   Küberneetika Instituut, CENS
2004–2005 Inseneribüroo Peipman OÜ
1999–2000 Eesti kaitsevägi, Sidepataljon
1998–1999 Eesti Raadio

Akadeemiline tegevus
Esitatud inglise keelses elulookirjelduses.

Keeled:
eesti (emakeel), inglise (hea), soome (rahuldav), vene (nõrk).

Arvutikeeled:
Fortran, Python.

Valdan kasutamist:
Windows, Linux, AutoCAD, LaTeX, Mathematica, Maple, MatCAD, MATLAB, Maxima.

Appendix D: Publications

Publication I: A. Salupere, K. Tamm, J. Engelbrecht, and P. Peterson. On the interaction of deformation waves in microstructured solids. *Proceedings of the Estonian Academy of Sciences, Physics, Mathematics*, 56(2):93–99, 2007

Publication II: A. Salupere, L. Ilison, and K. Tamm. On numerical simulation of propagation of solitons in microstructured media. In M. Todorov, editor, *Proceedings of the 34th Conference on Applications of Mathematics in Engineering and Economics*, pages 155–165, Melville, NY, 2008. vol. 1067 of AIP Conference Proceedings

Publication III: A. Salupere, K. Tamm, and J. Engelbrecht. Numerical simulation of interaction of solitary deformation waves in microstructured solids. *International Journal of Non-Linear Mechanics*, 43(3):201–208, 2008

Publication IV: T. Peets and K. Tamm. Dispersion analysis of wave motion in microstructured solids. In T.-T. Wu and C.-C. Ma, editors, *IUTAM Symposium on Recent Advances of Acoustic Waves in Solids: Proceedings, Taipei, Taiwan, May 25–28, 2009*, volume 26 of *IUTAM Bookseries*, pages 349–354, Dordrecht, 2010. Springer

Publication V: K. Tamm and A. Salupere. On the propagation of solitary waves in Mindlin-type microstructured solids. *Proceedings of the Estonian Academy of Sciences*, 59(2):118–125, 2010

Publication VI: K. Tamm and A. Salupere. On the propagation of 1D solitary waves in Mindlin-type microstructured solids. *Mathematics and Computers in Simulation*, (in press, doi: 10.1016/j.matcom.2010.06.022), 2011

Publication I

A. Salupere, **K. Tamm**, J. Engelbrecht and P. Peterson
On the interaction of deformation waves in microstructured solids.

On the interaction of deformation waves in microstructured solids

Andrus Salupere[a,b], Kert Tamm[a,b], Jüri Engelbrecht[a], and Pearu Peterson[a]

[a] Centre for Nonlinear Studies, Institute of Cybernetics at Tallinn University of Technology, Akadeemia tee 21, 12618 Tallinn, Estonia; salupere@ioc.ee, je@ioc.ee
[b] Department of Mechanics, Tallinn University of Technology, Ehitajate tee 5, 19086 Tallinn, Estonia

Abstract. The modelling of wave propagation in microstructured materials should be able to account for various scales of microstructure. In the present paper governing equations for 1D waves in microstructured material are presented, based on the Mindlin model and the hierarchical approach. The governing equation under consideration has an analytical solution only in limit cases, therefore numerical analysis is carried out. Numerical solutions are found in the case of localized initial conditions by employing the pseudospectral method. Special attention is paid to the solitonic character of the solution.

Key words: microstructured solids, Mindlin model, solitary waves, solitons.

1. INTRODUCTION AND MODEL EQUATIONS

The modelling of wave propagation in microstructured materials (alloys, crystallites, ceramics, functionally graded materials, etc.) should be able to account for various scales of microstructure [1−3]. The scale-dependence involves dispersive as well as nonlinear effects. It is widely known that the balance between these two effects may result in the emergence of solitary waves and solitons.

Propagation of solitary waves in microstructured solids is analysed by making use of different models (see [3−5] and references therein). However, the crucial point related to the derivation of governing equations is the distinction between nonlinearities on macro- and microlevel, together with proper modelling of dispersive effects. In [6−8] the Mindlin model [9] and hierarchical approach by

Engelbrecht and Pastrone [3] is used in order to derive governing equations. Basic model equations for 1D waves in microstructured material are

$$\rho u_{tt} = \sigma_x, \quad I\psi_{tt} = \eta_x - \tau. \tag{1}$$

Here u denotes the macrodisplacement, ψ the microdeformation, ρ the macrodensity, I the microinertia, σ the macrostress, η the microstress, τ the interactive force, x space coordinate, and t time. The free energy function is considered in the following form:

$$W = \frac{1}{2}au_x^2 + \frac{1}{2}B\psi^2 + \frac{1}{2}C\psi_x^2 + D\psi u_x + \frac{1}{6}Nu_x^3 + \frac{1}{6}M\psi_x^3, \tag{2}$$

where a, B, C, D, M, and N are constants. Then, using the formulae

$$\sigma = \frac{\partial W}{\partial u_x}, \qquad \eta = \frac{\partial W}{\partial \psi_x}, \qquad \tau = \frac{\partial W}{\partial \psi}, \tag{3}$$

Eqs (1) are expressed in terms of variables u and ψ:

$$\rho u_{tt} = au_{xx} + Nu_x u_{xx} + D\psi_x, \quad I\psi_{tt} = C\psi_{xx} + M\psi_x\psi_{xx} - Du_x - B\psi. \tag{4}$$

After introducing dimensionless variables $X = x/L$, $T = tc_0/L$, $U = u/U_0$, the scale parameter $\delta = l^2/L^2$ (L and U_0 can be amplitude and wavelength of the initial excitation, respectively; $c_0^2 = a/\rho$ and l is the scale of the microstructure) and making use of the slaving principle [3], the following hierarchical model equation is obtained from Eqs (4):

$$U_{TT} - bU_{XX} - \frac{\mu}{2}\left(U_X^2\right)_X - \delta\left(\beta U_{TT} - \gamma U_{XX} - \delta^{1/2}\frac{\lambda}{2}U_{XX}^2\right)_{XX} = 0, \tag{5}$$

where b, μ, β, γ, and λ are constants (see [7,8] for details). If the scale parameter δ is small, then the wave process is governed by properties of the macrostructure, and vice-versa, if δ is large, then properties of the microstructure govern the process. For future analysis Eq. (5) is expressed in terms of deformation $v = U_X$ and lower-case letters x and t are used for dimensionless coordinate and time:

$$v_{tt} = bv_{xx} + \frac{\mu}{2}\left(v^2\right)_{xx} + \delta\left(\beta v_{tt} - \gamma v_{xx}\right)_{xx} - \delta^{3/2}\frac{\lambda}{2}\left[\left(v_x\right)^2\right]_{xxx}. \tag{6}$$

Equation (6) admits the analytic solitary wave solution

$$v(x - ct) = A \operatorname{sech}^2\frac{\varkappa(x - ct)}{2}, \quad A = \frac{3(c^2 - b)}{\mu}, \quad \varkappa = \sqrt{\frac{c^2 - b}{\delta(\beta c^2 - \gamma)}} \tag{7}$$

only if $\lambda = 0$ [7,8]. If $\lambda \neq 0$, one can find a travelling wave solution $v(x - ct)$ for Eq. (6) in the form of an asymmetric solitary wave by numerical integration

94

under asymptotic boundary conditions. The analytic conditions for the existence of solitary waves modelled by Eq. (6) are given by Janno and Engelbrecht in [7,8]:

$$\mu \neq 0, \ \ \beta c^2 - \gamma \neq 0, \ \ c^2 - b \neq 0, \ \ \frac{c^2 - b}{\beta c^2 - \gamma} > 0, \ \ \left(\frac{\beta c^2 - \gamma}{c^2 - b}\right)^3 > \frac{4\lambda^2}{\mu^2}. \quad (8)$$

In the present paper the interaction of sech^2-shaped waves (7) is analysed numerically.

2. STATEMENT OF THE PROBLEM AND NUMERICAL TECHNIQUE

The main goals of the present paper are (i) to simulate numerically the interactions between solitary waves (7); (ii) to estimate the influence of the microlevel nonlinear parameter λ on the solution, and (iii) to examine the solitonic character of the solution. For this reason Eq. (6) is integrated numerically under the initial conditions

$$v(x,0) = \sum_{i=1}^{2} A_i \, \mathrm{sech}^2 \, \frac{\varkappa_i (x - \xi_i)}{2}, \qquad 0 \leq x < 2k\pi. \quad (9)$$

Here amplitudes A_i and the widths $\varkappa_i$ ($i = 1, 2$) correspond to different initial speeds $c_1 \neq c_2$ and ξ_i are initial phase shifts. It is clear that if $c_1 c_2 < 0$, head-on collision and if $c_1 c_2 > 0$, the overtaking interaction takes place, and the lower the value of $\varkappa_i$, the wider the initial solitary wave.

For numerical integration the pseudospectral method (PsM) based on the discrete Fourier transform (DFT) [10,11] is used and therefore periodic boundary conditions

$$v(x,t) = v(x + 2k\pi, t) \quad (10)$$

are applied. The idea of the PsM is to approximate space derivatives making use of the DFT and then to use standard ODE solvers for integration with respect to time. Due to the mixed partial derivative term $\delta\beta v_{ttxx}$, the model Eq. (6) cannot be directly integrated by the PsM. Therefore we introduce a new variable Φ and apply properties of the DFT:

$$\Phi = v - \delta\beta v_{xx} = F^{-1}[(1 + \delta\beta\omega^2)F(v)],$$

$$v = F^{-1}\left[\frac{F(\Phi)}{1 + \delta\beta\omega^2}\right], \quad \frac{\partial^n v}{\partial x^n} = F^{-1}\left[\frac{(i\omega)^n F(\Phi)}{1 + \delta\beta\omega^2}\right]. \quad (11)$$

Here $\omega = 0, \pm 1, \pm 2, \ldots, \pm (N/2 - 1), -N/2$, i is the imaginary unit, N denotes the number of space-grid points, F the DFT, and F^{-1} the inverse DFT. Finally the equation

$$\Phi_{tt} = \left[bv + \frac{\mu}{2}v^2 - \delta\gamma v_{xx} - \delta^{3/2}\frac{\lambda}{2}(v_x^2)_x\right]_{xx} \quad (12)$$

is solved numerically by the PsM under initial and boundary conditions (9) and (10), respectively. Calculations are carried out using the SciPy package [12]: for the DFT the FFTW [13] library and for the ODE solver the F2PY [14] generated Python interface to the ODEPACK Fortran code [15] are used.

3. RESULTS AND DISCUSSION

Three different interaction cases are considered in the present section. Travelling wave solutions in the form of an asymmetric solitary wave can exist for all considered sets of parameters, i.e., parameters for Eq. (6) and initial condition (9) are chosen according to conditions (8).

In order to analyse *head-on collision of solitary waves with equal amplitudes*, the case where parameters for Eq. (6) are $b = 0.7683$, $\mu = 0.125$, $\delta = 9$, $\beta = 7.6452$, $\gamma = 6.1817$, $\lambda = 0$, solitary wave speeds $c_1 = 0.9$ and $c_2 = -0.9$, the corresponding amplitudes $A_1 = A_2 = 1.0$ and widths $\varkappa_1 = \varkappa_2 = 0.65$ is considered. Numerical integration is carried out for $0 \leq t \leq 500$ and the length of the space period is 24π. The amplitudes of the waves increase during interactions and initial amplitudes are restored after interactions (Fig. 1a) like in the case of Boussinesq models [16]. The amplitude of the wave profile attains a value close to the double initial amplitude at every "peak" of the interaction in the considered time interval. However, the behaviour of the amplitude curve between interactions varies essentially – the more interactions have taken place, the more distinctive the changes are. Analysis of trajectories of single waves demonstrates that unlike Boussinesq models, solitary waves are not phase shifted during interactions in the present case. This phenomenon is reflected in Fig. 1b – after eleven interactions two solitary waves are still in the same phase. However, the shape of initial waves (9) is altered during interactions and it is clear that, instead of initial symmetric bell-like waves, asymmetric solitary waves are formed, shown at $t = 460.8$. Therefore the
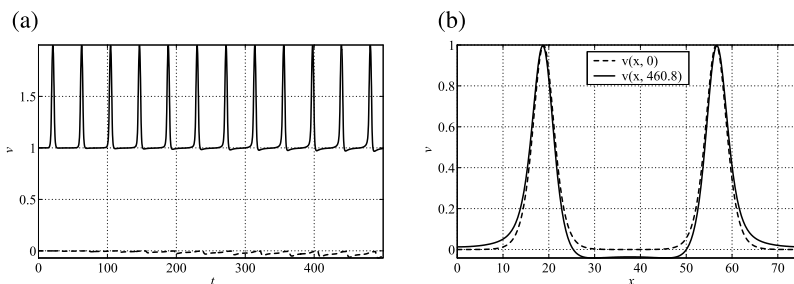
Fig. 1. Head-on collision of solitary waves with equal amplitudes. (a) Waveprofile minima and maxima against time. (b) The initial waveprofile and the waveprofile after eleven interactions at $t = 460.8$.

96

interaction process is near elastic (i.e. the height of waves is restored but the initial shape is slightly altered after interactions) in the present case.

In order to examine *head-on collision of solitary waves with nonequal amplitudes*, the case where parameters for Eq. (6) are $b = 0.7683$, $\mu = 0.125$, $\delta = 9$, $\beta = 7.6452$, $\gamma = 6.1817$, $\lambda = 0$, solitary wave speeds $c_1 = 0.9$ and $c_2 = -0.9115$, the corresponding amplitudes $A_1 = 1.0$, $A_2 = 1.0$ and widths $\varkappa_1 = 0.65$, $\varkappa_2 = 0.202$ is considered. Numerical integration is carried out for $0 \leq t \leq 500$ and the length of the space period is 96π. In the present case the behaviour of the waveprofile maxima and minima is similar to the case considered above, i.e., during the interaction the amplitude attains the value close to $A_1 + A_2$, between interactions both solitary waves restore initial values, and the behaviour of the amplitude curves between interactions varies depending on the number of passed interactions (Fig. 2a). The analysis of trajectories of solitary waves demonstrates that in the present case solitary waves are phase shifted during interactions and in Fig. 2b one can see that after three interactions at $t = 335.2$ the distance between solitary waves is changed compared to that at $t = 0$. Like in the previous case, both solitary waves are asymmetric after several interactions (more distinctive asymmetry can be detected for the lower one). Nevertheless, one can conclude that the interaction process is near elastic in the present case.

During *overtaking interaction* both solitary waves are phase shifted but do not restore their shape after the interaction. This case is not analysed in the present paper.

Numerical experiments with $\lambda \neq 0$ were carried out in order to estimate the *influence of microlevel nonlinearity*. Analysis of solutions for $\lambda = 0$ and $\lambda = 0.005$ demonstrates that in the case of head-on interaction, both solutions practically coincide – maximal differences between corresponding waveprofiles, i.e. $\max_{t,x}(v(t,x)|_{\lambda=0} - v(t,x)|_{\lambda=0.005})$, are of order 0.01. For $\lambda = 0.5$ the microlevel nonlinear effects are stronger and they are able to change the character of interactions. In Fig. 3 the waveprofile maxima and minima reflect head-on collision, which is less elastic than for $\lambda = 0$.
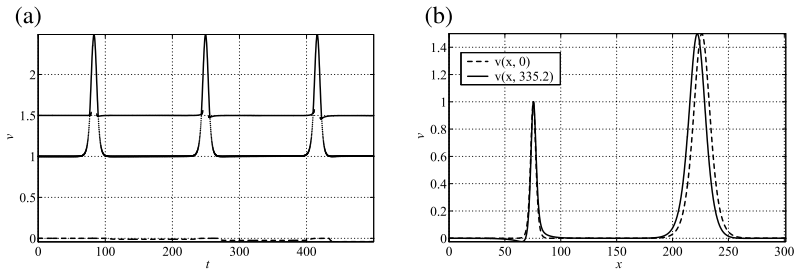
Fig. 2. Head-on collision of solitary waves with nonequal amplitudes. (a) Waveprofile minima and maxima against time. (b) The initial waveprofile and the waveprofile after two interactions at $t = 335.2$.
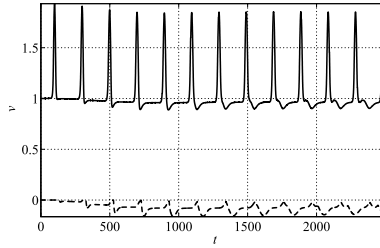
Fig. 3. Head-on collision of solitary waves with equal amplitudes. Waveprofile minima and maxima against time for $\lambda = 0.5$.

4. CONCLUSIONS

The characteristic feature of the governing equation (6) is that, unlike the well-known evolution equations, it describes two waves instead of one. A similar situation occurs for waves in rods [5]. This gives us an opportunity to analyse also head-on collisions of waves.

In the case of $\lambda = 0$, bell-like solitary waves (9) can propagate with constant speed and shape, but during head-on collisions the initial symmetric shape changes to asymmetric. In the case of $\lambda \neq 0$, the initial symmetric shape is altered even before the first interaction. Analysis of the results of our numerical experiments demonstrates that for $\lambda = 0$ and for relatively small values of λ interactions between solitary waves are near elastic. Consequently, the behaviour of solitary waves is very close to solitonic behaviour. If initial waves have speeds $c_1 = -c_2$, then solitons do not become phase-shifted during interactions. The higher the value of λ, the less elastic the head-on collision and therefore the less solitonic the behaviour of interacting waves. The overtaking interaction is not elastic either for $\lambda = 0$ or for $\lambda \neq 0$.

Numerical experiments in order to analyse the long-time behaviour of solutions over a wide range of material parameters and initial conditions are in progress. Clearly, the two-wave governing equation, possessing solitary wave type solutions, needs more attention in the future.

ACKNOWLEDGEMENT

98

REFERENCES

1. Eringen, A. C. *Microcontinuum Field Theories. I Foundations and Solids*. Springer, New York, 1999.
2. Phillips, R. *Crystals, Defects and Microstructures. Modelling Across Scales*. Cambridge University Press, Cambridge, 2001.
3. Engelbrecht, J. and Pastrone, F. Waves in microstructured solids with strong nonlinearities in microscale. *Proc. Estonian Acad. Sci. Phys. Math.*, 2003, **52**, 12–20.
4. Erofeev, V. I. *Wave Processes in Solids with Microstructure*. World Scientific, Singapore, 2003.
5. Porubov, A. V. *Amplification of Nonlinear Strain Waves in Solids*. World Scientific, Singapore, 2003.
6. Engelbrecht, J., Berezovski, A., Pastrone, F. and Braun, M. Waves in microstructured materials and dispersion. *Phil. Mag.*, 2005, **85**, 4127–4141.
7. Janno, J. and Engelbrecht, J. Solitary waves in nonlinear microstructured materials. *J. Phys. A: Math. Gen.*, 2005, **38**, 5159–5172.
8. Janno, J. and Engelbrecht, J. An inverse solitary wave problem related to microstructured materials. *Inverse Probl.*, 2005, **21**, 2019–2034.
9. Mindlin, R. D. Micro-structure in linear elasticity. *Arch. Rat. Mech. Anal.*, 1964, **16**, 51–78.
10. Fornberg, B. *A Practical Guide to Pseudospectral Methods*. Cambridge University Press, Cambridge, 1998.
11. Salupere, A., Engelbrecht, J. and Peterson, P. On the long-time behaviour of soliton ensembles. *Math. Comput. Simul.*, 2003, **62**, 137–147.
12. Jones, E., Oliphant, T., Peterson, P. et al. *SciPy: Open Source Scientific Tools for Python*. 2001, available at http://www.scipy.org
13. Frigo, M. and Johnson, S. G. The design and implementation of FFTW3. *Proc. IEEE*, 2005, **93**, 216–231.
14. Peterson, P. *Fortran to Python Interface Generator*. 2005, available at http://cens.ioc.ee/projects/f2py2e/
15. Hindmarsh, A. C. Odepack, a systematized collection of ODE solvers. In *Scientific Computing* (Stepleman, R. S. et al., eds). North-Holland, Amsterdam, 1983, 55–64.
16. Christov, C. I. and Maugin, G. A. An implicit difference scheme for the long-time evolution of localized solutions of a generalized Boussinesq system. *J. Comput. Phys.*, 1995, **116**, 39–51.

Deformatsioonilainete interaktsioonist mikrostruktuursetes tahkistes

Andrus Salupere, Kert Tamm, Jüri Engelbrecht ja Pearu Peterson

Mikrostruktuursetes tahkistes toimuva lainelevi modelleerimisel tuleb arvesse võtta erinevaid mikrostruktuuri mastaape. Põhivõrrandite tuletamisel on eriti oluline mikro- ja makrotaseme mittelineaarsete efektide eristamine ning dispersiivsete efektide adekvaatne modelleerimine. Artiklis vaatluse all olevate ühedimensiooniliste lainete levi kirjeldavate võrrandite tuletamisel on kasutatud Mindlini mikrostruktuurse materjali mudelit ja lainehierarhiate teooriat. Kuna kasutatavatele võrranditele eksisteerivad analüütilised lahendid vaid teatavatel piirjuhtudel, siis on lahendite leidmisel ja tulemuste analüüsimisel kasutatud numbrilisi meetodeid. Põhitähelepanu on pööratud lahendi solitonilise iseloomu selgitamisele.

Publication II

A. Salupere, L. Ilison and **K. Tamm**
On numerical simulation of propagation of solitons in microstructured media.
In M. Todorov, editor, *Proceedings of the 34th Conference on Applications of Mathematics in Engineering and Economics*, pages 155–165, Melville, NY, 2008. vol. 1067 of AIP Conference Proceedings

On Numerical Simulation of Propagation of Solitons in Microstructured Media

A. Salupere, L. Ilison and K. Tamm

Center for Nonlinear Studies, Institute of Cybernetics at Tallinn University of Technology,
Dept. of Mechanics, Tallinn University of Technology,
Akadeemia tee 21, 12618, Tallinn, Estonia

Abstract. Wave propagation in microstructured media is simulated numerically making use of two different models. In the first case a Korteweg–de Vries type equation is used for modeling 1D wave motion in granular materials. In the second case a Boussinesq type equation is applied for modeling 1D wave motion in Mindlin type microstructured solids. Both equations are integrated numerically under localized initial conditions by employing the discrete Fourier transform (DFT) based pseudospectral method. Emergence of trains of solitons is demonstrated in both cases.

Keywords: Solitons, Korteweg-de Vries type equation, Boussinesq type equation, pseudospectral method, granular materials, microstructured solids.
PACS: 05.45.Yv, 02.60.Cb

INTRODUCTION

Microstructured materials (alloys, ceramics, functionally graded materials, etc) are characterised by various scales of microstructure. This circumstance should be taken into account when wave propagation in such materials is modeled [1, 2, 3]. The scale-dependence involves dispersive as well as nonlinear effects and it is widely known, that the balance between these two effects may result in emerging of solitary waves and solitons.

Two examples of microstructured materials are considered in the present paper. In the first case one-dimensional wave propagation in dilatant granular materials is studied. Corresponding model equation

$$u_t + uu_x + \alpha_1 u_{xxx} + \beta \left(u_t + uu_x + \alpha_2 u_{xxx} \right)_{xx} = 0 \tag{1}$$

is derived by Giovine and Oliveri [4]. Here variable u is bulk density, x — space coordinate, t — time; α_1 and α_2 are macro- and microlevel dispersion parameters, respectively, and β is a parameter involving the ratio of the grain size and the wavelength. Equation (1) consists of two Korteweg–de Vries (KdV) operators: the first describes the motion in the macrostructure and the second (in the brackets) — the motion in the microstructure. Equation (1) is clearly hierarchical in the Whitham's sense — the parameter β controls the influence of the microstructure [5]. Due to that kind of hierarchy the equation (1) could by called hierarchical Korteweg–de Vries (HKdV) equation.

In the second case a Boussinesq-type [6] equation

$$v_{tt} - bv_{xx} - \frac{\mu}{2} \left(v^2 \right)_{xx} - \delta \left(\beta v_{tt} + \gamma v_{xx} \right)_{xx} + \delta^{3/2} \frac{\lambda}{2} \left(v_x^2 \right)_{xxx} = 0 \tag{2}$$

is used in order to model one-dimensional wave propagation in microstructured solids. Here v is deformation, x — space coordinate, t — time, b, μ, δ, β, and γ are material parameters (see [7, 8] for details). In order to derive equation (2) the Mindlin model [9] of continua with microstructure and hierarchical approach by Engelbrecht and Pastrone [1] is applied. This equation is referred below as the MEP equation.

The main goal of the present paper is to simulate numerically the emergence of trains of solitons by means of two different material models. For this reason model equations (1) and (2) are integrated numerically under localised initial conditions. Results are analysed in terms of solitonics, i.e., the goal is to understand whether or no solitary waves that emerge from initial $sech^2$-type pulse propagate at constant speed and amplitude and interact elastically. Interaction of solitary waves is called elastic, if they restore their speed and amplitude after interactions. During elastic interaction solitons may experience phase shift. In turn, if interactions between solitary waves are elastic they are called solitons.

NUMERICAL TECHNIQUE

In the present paper the discrete Fourier transform (DFT) based pseudospectral method (PsM) [10, 11] is used for numerical integration of model equations, i.e., for numerical simulation of wave propagation. Let us introduce the DFT and the inverse DFT (IDFT) as follows:

$$U(k,t) = \mathrm{F}u = \sum_{j=0}^{N-1} u(j\Delta x, t) \exp\left(-\frac{2\pi i j k}{N}\right),\tag{3}$$

$$u(j\Delta x, t) = \mathrm{F}^{-1}U = \frac{1}{N}\sum_k U(k,t)\exp\left(-\frac{2\pi i j k}{N}\right).\tag{4}$$

Here $u(x,t)$ is a periodic function (with space period 2π, i.e., $0 \le x \le 2\pi$), N – the number of space grid points, $\Delta x = 2\pi/N$ – the space step, i – the imaginary unit, $k = 0, \pm 1, \pm 2, \ldots, \pm(N/2 - 1), -N/2$ are wavenumbers, F denotes the DFT and F^{-1} the IDFT. Space derivatives of function $u(x,t)$ can now be calculated making use of properties of the DFT [12, 13]:

$$\frac{\partial^n u(x,t)}{\partial x^n} = \mathrm{F}^{-1}\left[(ik)^n \mathrm{F}u\right].\tag{5}$$

If the length of the space period for $u(x,t)$ is not 2π, but $2m\pi$, then one must use quantity k/m instead of k in last formulae:

$$\frac{\partial^n u(x,t)}{\partial x^n} = \mathrm{F}^{-1}\left[\left(\frac{ik}{m}\right)^n \mathrm{F}u\right].\tag{6}$$

In a nutshell the idea of the PsM is very simple. If a PDE is given in a general form

$$u_t = \Phi\left(u, u_x, u_{xx}, \ldots\right)\tag{7}$$

then one can formally reduce the latter to ODE

$$u_t = \Psi(u) \tag{8}$$

making use of formulae (6), which can be considered as numerical differential operators. The ODE (8) can now be integrated with respect to time variable t by standard ODE solvers. The method is called pseudospectral because integration with respect to time is carried out in physical space and the Fourier transform related quantities are used only for calculation of space derivatives.

The HKdV equation (1) includes mixed partial derivative term βu_{xxt}. Therefore the usual PsM algorithm cannot be applied directly and one has to introduce suitable change of variables. At first the HKdV equation is rewritten in the form

$$(u + \beta u_{xx})_t + (u + 3\beta u_{xx}) u_x + (\alpha_1 + \beta u) u_{xxx} + \beta \alpha_2 u_{xxxxx} = 0 \tag{9}$$

and a variable

$$\phi = u + \beta u_{xx} \tag{10}$$

is introduced. Making use of the DFT and its properties the last expression can be rewritten in form

$$\phi = F^{-1}(Fu) + \beta F^{-1}\left(-k^2 Fu\right) = F^{-1}\left[\left(1 - \beta k^2\right) Fu\right]. \tag{11}$$

In turn, the variable u and its space derivatives can be expressed from (11) in terms of variable ϕ:

$$u = F^{-1}\left[\frac{F\phi}{1 - \beta k^2}\right], \qquad \frac{\partial^n u}{\partial x^n} = F^{-1}\left[\frac{(ik)^n F\phi}{1 - \beta k^2}\right]. \tag{12}$$

It is clear, that in order to avoid division by zero, one can consider only such values for parameter β which result in $1 - \beta k^2 \neq 0$. Finally equation (9) is rewritten in the form

$$\phi_t = -(u + 3\beta u_{xx})u_x - (\alpha_1 + \beta u) u_{xxx} - \alpha_2 \beta u_{xxxxx}. \tag{13}$$

where the variable u and its space derivatives could be expressed in terms of ϕ according to formulae (12). Therefore equation (13) can be considered as an ODE with respect to variable ϕ and could be integrated numerically making use of standard ODE solvers.

The MEP equation (2) includes a mixed partial derivative term $\delta \beta v_{xxtt}$ and therefore it is rewritten in the form

$$(v - \delta \beta v_{xx})_{tt} - b v_{xx} - \frac{\mu}{2}\left(v^2\right)_{xx} + \delta \gamma v_{xxxx} + \delta^{3/2}\frac{\lambda}{2}\left(v_x^2\right)_{xxx} = 0 \tag{14}$$

and new variable

$$\phi = v - \delta \beta v_{xx} = F^{-1}(Fv) - \delta \beta F^{-1}\left(-k^2 Fv\right) = F^{-1}[(1 + \delta \beta k^2)Fv] \tag{15}$$

is introduced. From the latter variable v and its space derivatives can be expressed in terms of variable ϕ:

$$v = F^{-1}\left[\frac{F\phi}{1 + \delta \beta k^2}\right], \qquad \frac{\partial^n v}{\partial x^n} = F^{-1}\left[\frac{(ik)^n F\phi}{1 + \delta \beta k^2}\right]. \tag{16}$$

Finally we can rewrite equation (14) in the form

$$\phi_{tt} = \left[bv + \frac{\mu}{2} v^2 - \delta \gamma v_{xx} - \delta^{3/2} \frac{\lambda}{2} \left(v_x^2 \right)_x \right]_{xx} \qquad (17)$$

where variable v and its space derivatives are expressed through new variable ϕ making use of expressions (16).

RESULTS AND DISCUSSION

Emergence of trains of solitons from localised initial excitation will be discussed in the present section in case of the HKdV as well as in case of the MEP equations. For this reason both equations are integrated numerically by PsM under sech^2-type initial conditions and periodic boundary conditions.

The HKdV Equation

The HKdV (1) is integrated under initial condition

$$u(x,0) = A \operatorname{sech}^2 \frac{x - x_0}{\delta}, \qquad \delta = \sqrt{\frac{12 \alpha_1}{A}}, \qquad 0 \le x \le 16\pi, \qquad x_0 = 8\pi, \qquad (18)$$

where A is the amplitude and δ the width of the initial pulse. It is clear that the latter is the analytical solution of KdV equation that corresponds to the first KdV operator in equation (1).

Numerical experiments are carried out for $0 < \alpha_1 < 1$, $0 < \alpha_2 < 1$ and $\beta = 111.11, 11.111, 1.111, 0.111, 0.0111$. These particular values of β are selected in order to to avoid division by zero in expressions (12). The number of space grid points is $n = 1024$ and the length of the time interval is $t_f = 100$. Ilison and Salupere [14, 15, 16] have demonstrated that depending on values of material parameters α_1, α_2 and β solutions of different types can emerge from initial sech^2-shape wave. Here we demonstrate a case where the solution type is a train of KdV solitons. This solution type appears for $\alpha_2 < \alpha_1$ in cases of $\beta = 111.11$ and $\beta = 11.111$, i.e., in cases when the influence of the microstructure is relatively strong but microlevel dispersion parameter is smaller than that of the macrolevel.

In the present paper the following values of material parameters are considered: $\alpha_1 = 0.4$, $\alpha_2 = 0.01$ and $\beta = 111.11$. Amplitude of the initial pulse is $A = 4$. Time-slice plot (Figure 1) and pseudocolor plot (Figure 2) demonstrate the formation of train of solitons in the beginning of integration interval and subsequent interactions between emerged solitons. In Figure 3 the initial wave profile at $t = 0$ and waveprofile at $t = 18.7$ (just before emerged solitons start to interact) is plotted against space coordinate x. In this figure eight solitons can be clearly detected. However, the formation of soliton train is not finished at $t \approx 18.7$ — Figure 2 demonstrates that trajectory of the ninth soliton appears only for $t > 35$. Analysis of numerical results demonstrate that the amplitude of
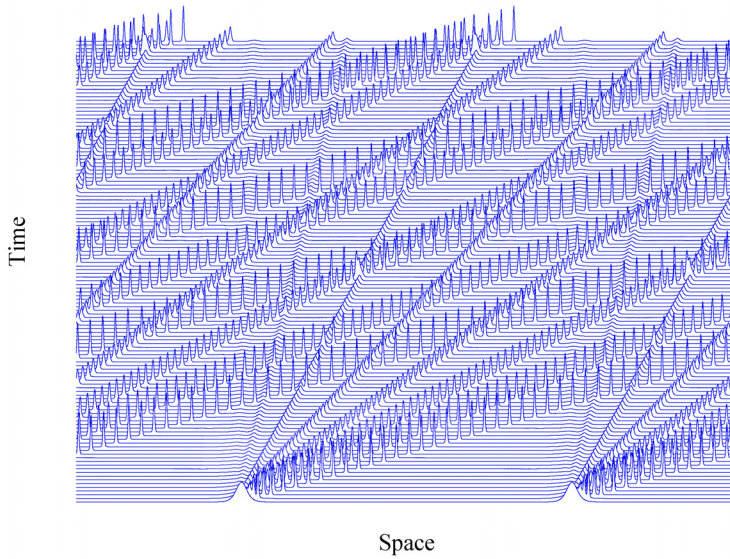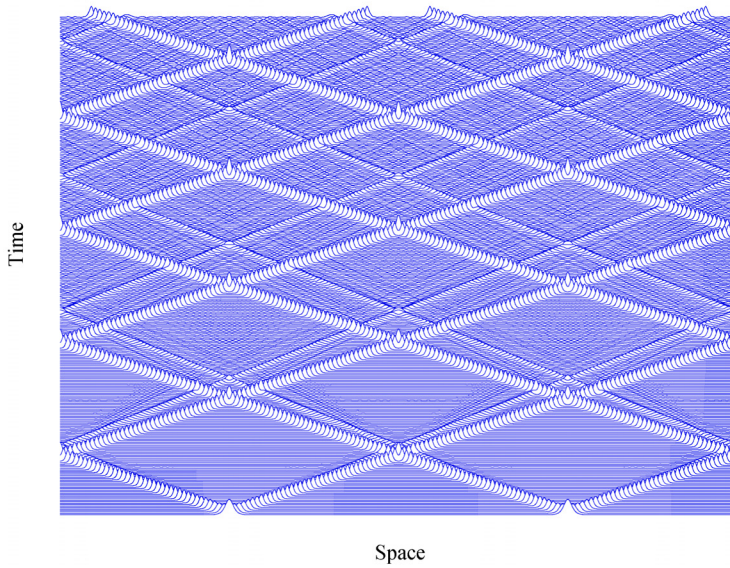
FIGURE 1. Emergence of train of KdV solitons in case of the HKdV model — time-slice plot over two space periods
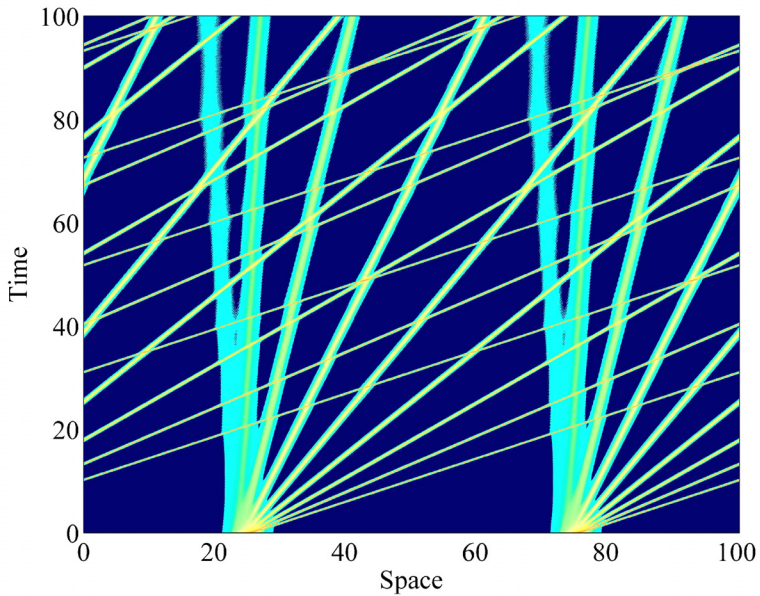
**FIGURE 2.** Emergence of train of KdV solitons in case of the HKdV model — pseudocolor plot over two space periods
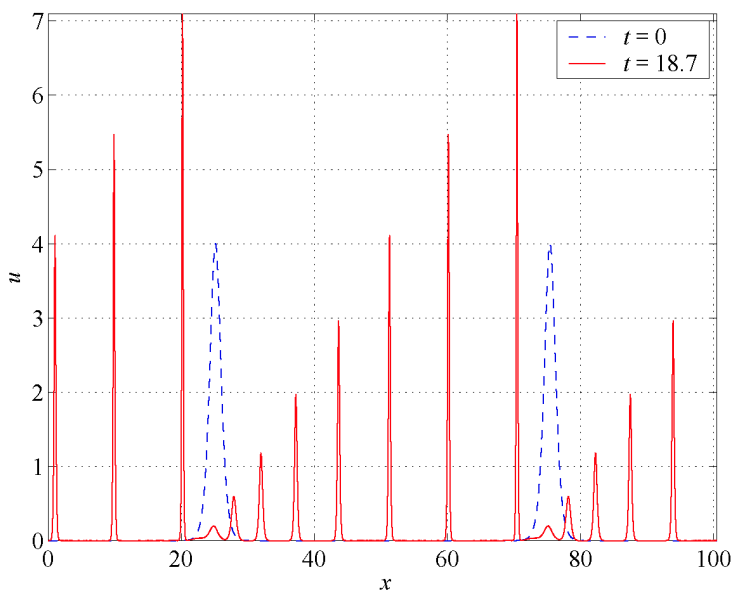
FIGURE 3. Initial wave and train of KdV solitons at $t = 18.7$ over two space periods in case of the HKdV model
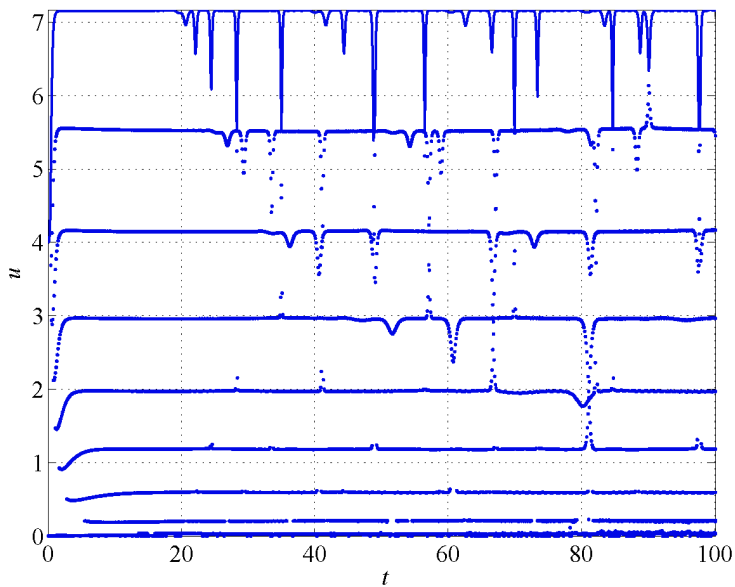
FIGURE 4. Wave profile maxima against time in case of the HKdV model

the ninth soliton is of order of 0.025 and therefore it is hard to distinguish it in time-slice plot in Figure 1 or in amplitude curves in Figure 4. Furthermore, a very small amplitude tail can be detected besides the soliton train. The behaviour of the emerged solitons is practically identical to these emerged in case of KdV equation (see Figures 1–4): (i) the higher solitons in the train (three higher solitons in the present case) are higher than the initial pulse, (ii) the higher the soliton the higher its speed, (iii) if two solitons interact then the amplitude (height) of the higher soliton decreases during interactions, (iv) after interactions solitons restore their initial amplitude and speed. For these reasons the considered type of solution is called train of KdV solitons.

For other sets of material parameters (from the same domain, i.e., $\alpha_2 < \alpha_1$ and $\beta = 111.11$ or $\beta = 11.111$) the tail that forms besides the train of solitons can be more distinctive, but it does not influence the behavior of emerged solitons essentially — it only causes small amplitude oscillations of amplitudes of solitons. Nevertheless, the character of the interactions remains practically elastic because of the amplitudes oscillate with respect to the initial level and speeds of solitons are not altered.

The MEP Equation

In [17] we studied head on collisions of solitary waves over long time intervals. Notwithstanding that interactions were not completely elastic we concluded that the behavior of the solution was very close to solitonic. Here the MEP equation is integrated under initial conditions

$$v(x,0) = A \operatorname{sech}^2 B(x - x_0), \qquad 0 \le x \le 200\pi, \qquad x_0 = 100\pi. \qquad (19)$$

In the numerical experiment, discussed below, values $A = 1$ and $B = 0.05$ are the pulse amplitude and width respectively, $c = 0$ is the initial phase velocity and $b = 0.719$, $\mu = 2.083$, $\delta = 0.25$ $\beta = 45.040$, $\gamma = 9.375$, $\lambda = 2.083$ are the equation parameters. The time-space behavior of the solution can be observed in Figures 5–9. The MEP equation is of Boussinesq type and therefore contrary to the HKdV equation, waves going to the left as well as to the right can emerge. Figures 5 and 6 demonstrate that two solitons that propagate to the right and two solitons that propagate to the left form in the present case. Because of the fact that the phase velocity of the initial wave is zero, solitons going to the right and solitons going to the left have equal amplitudes and equal speeds. In Figures 7 and 8 some typical wave profiles are plotted against space coordinate x. Time moment $t = 418$ corresponds to the beginning of the integration interval before interactions, at $t = 1128$ and $t = 4525$ interactions between the two highest solitons take place, at $t = 1845$ interaction between the higher and the lower solitons and at $t = 2704$ between the two lower solitons take place. In Figure 9 amplitudes of solitons are plotted against the time. It is clear, that interactions between emerged solitons are not completely elastic — Figures 5–8 demonstrate that each interaction produces small amplitude radiation. The more interactions have taken place the more distinctive the radiation is (see Figures 7 and 8). During interactions the amplitudes of waves increase and after interactions they are almost restored on the initial level. However, amplitudes of waves are not constant between interactions but oscillate with respect to the initial level.

FIGURE 5. Emergence of trains of solitons in case of the MEP model — time-slice plot over two space periods
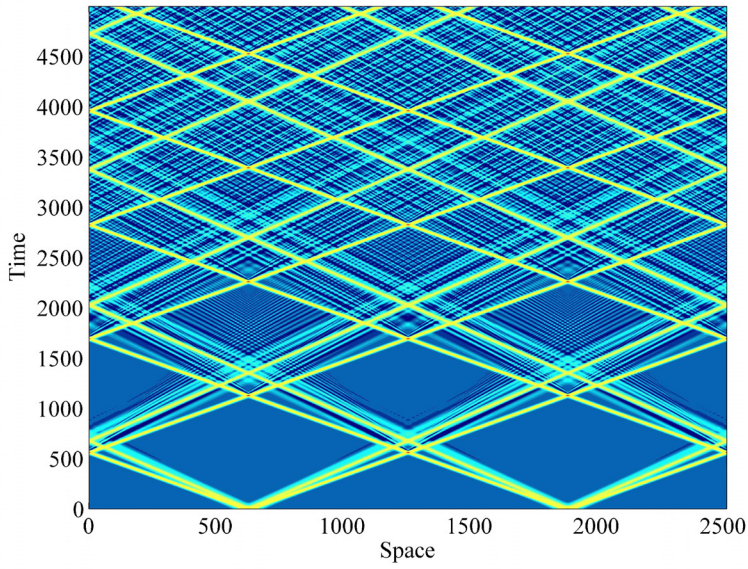
FIGURE 6. Emergence of trains of solitons in case of the MEP model — pseudocolor plot over two space periods

162
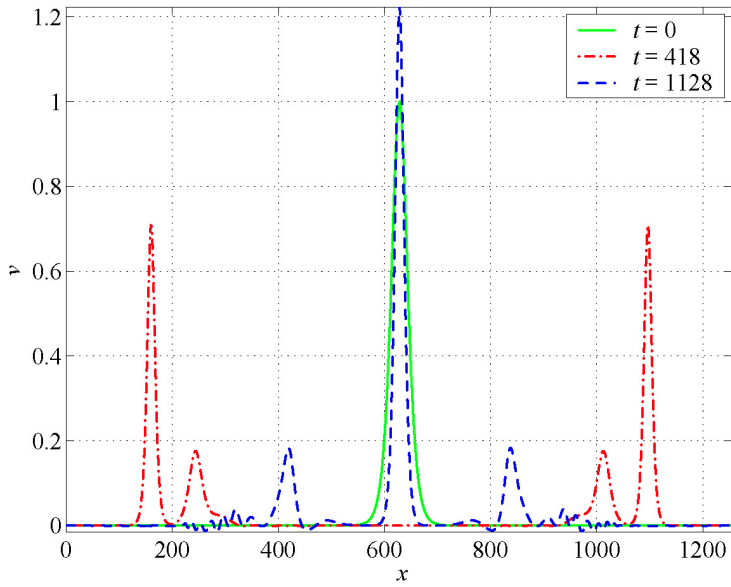
FIGURE 7. Single wave profiles in case of the MEP model
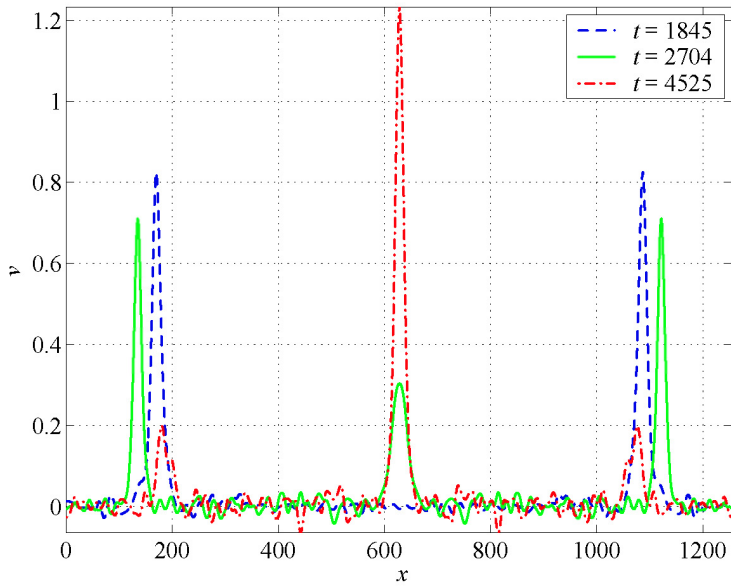
FIGURE 8. Single wave profiles in case of the MEP model

163
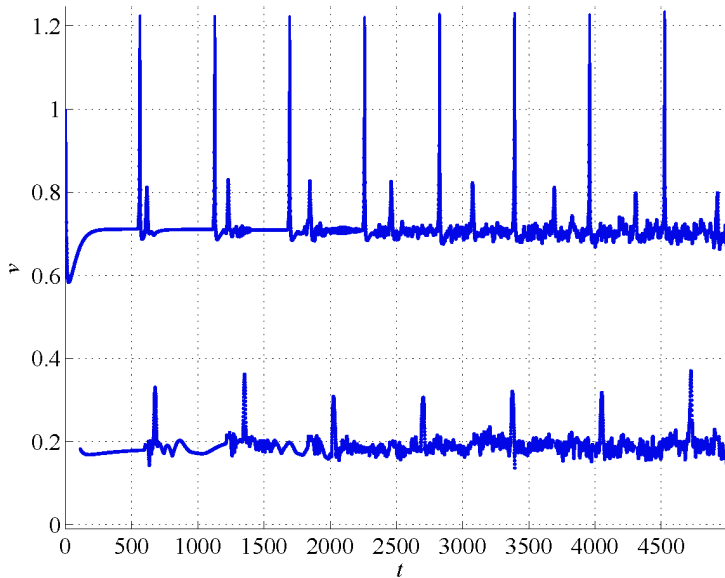
FIGURE 9. Amplitudes of solitons against time in case of the MEP model

These oscillations are caused by the radiation produced during interactions. Therefore the more interactions have taken place the more distinctive are the oscillations of soliton amplitudes (see Figure 9). The speed of waves is not altered during interactions. To sum up, one can say that interactions between emerged localized waves are almost elastic and thereof we call them solitons.

Of course, for different values of parameters of the MEP equation and of the initial pulse the number of emerged solitons can be higher than two. If other parameters (except the width B_0) are fixed, then the smaller the parameter B_0 (the wider the initial pulse) the larger the number of solitons in the train.

CONCLUSIONS

In the present paper propagation and interaction of solitons is studied in case of the HKdV as well as in case of the MEP model. Corresponding equations are integrated numerically under $sech^2$-type initial conditions making use of the PsM. Analysis of numerical results demonstrates that emerged solitary waves practically restore their amplitudes and speeds throughout interactions. Therefore the interactions are practically elastic and the emerged solitary waves can be called solitons in both considered cases.

ACKNOWLEDGMENTS

REFERENCES

1. J. Engelbrecht and F. Pastrone, *Proc. Estonian Acad. Sci. Phys. Math.* **52**, 12–20 (2003).
2. V. I. Erofeev, *Wave Processes in Solids with Microstructure*, World Scientific, Singapore, 2003.
3. A. V. Porubov, *Amplification of Nonlinear Strain Waves in Solids*, World Scientific, Singapore, 2003.
4. P. Giovine and F. Oliveri, *Meccanica* **30**, 341–357 (1995).
5. G. Whitham, *Linear and Nonlinear Waves*, John Wiley & Sons, New York, 1974.
6. C. Christov, G. Maugin, and A. Porubov, *Comptes Rendus Mécanique* **335**, 521–535 (2007).
7. J. Janno and J. Engelbrecht, *J. Phys. A: Math. Gen.* **38**, 5159–5172. (2005).
8. J. Janno and J. Engelbrecht, *Inverse Probl.* **21**, 2019–2034 (2005).
9. R. D. Mindlin, *Arch. Rat. Mech. Anal.* **16**, 51–78 (1964).
10. H.-O. Kreiss and J. Oligeri, *Tellus* **24**, 199–215 (1972).
11. B. Fornberg, *A Practical Guide to Pseudospectral Methods*, Cambridge University Press, Cambridge, 1998.
12. E. Oran Brigham, *The Fast Fourier Transform and Its Applications*, Prentice Hall Int., London, 1988.
13. R. N. Bracewell, *The Fast Fourier Transform and Its Applications*, McGraw-Hill, New York, 1978.
14. L. Ilison and A. Salupere, Propagation of localised perturbations in granular materials, Research Report Mech 287/07, Institute of Cybernetics at Tallinn University of Technology (2007).
15. L. Ilison, A. Salupere, and P. Peterson, *Proc. Estonian Acad. Sci. Phys. Math.* **56**, 84–92 (2007).
16. L. Ilison and A. Salupere, *Math. Comput. Simulat.* (2008), (submitted).
17. A. Salupere, K. Tamm, and J. Engelbrecht, *Int. J. Non-linear Mech.* **43**, 201–208 (2008).

Publication III

Numerical simulation of interaction of solitary deformation waves in microstructured solids

A. Salupere [a,b,*], K. Tamm [a,b], J. Engelbrecht [a]

[a] *Centre for Nonlinear Studies, Institute of Cybernetics at Tallinn University of Technology, Akadeemia tee 21, 12618 Tallinn, Estonia*
[b] *Department of Mechanics, Tallinn University of Technology, Ehitajate tee 5, 19086 Tallinn, Estonia*

Abstract

In the present paper 1D wave propagation in microstructured solids is modelled based on the Mindlin theory and hierarchical approach. The governing equation under consideration is non-integrable therefore it is analysed numerically. Propagation and interaction of localised initial pulses is simulated numerically over long time intervals by employing the pseudospectral method. Special attention is paid to the solitonic character of the solution.
© 2007 Elsevier Ltd. All rights reserved.

PACS: 05.45.Yv; 46.40.Cd

Keywords: Microstructured solids; Mindlin model; Solitary waves; Solitons

1. Introduction and model equations

Wide application of microstructured materials (like alloys, crystallites, ceramics, functionally graded materials, etc.) in technology needs also proper testing methods in order to evaluate the properties of such materials. This need is especially acute because microstructural properties affect considerably the macrobehaviour of a compound material or a structure. In most general terms, microstructure means the existence of grains, inclusions, layers, block walls, etc., and the influence of anisotropy. There are powerful methods in continuum mechanics in order to describe the influence of such irregularities of media starting from early works of Cosserats and Voigt up to contemporary formulations. Corresponding models should be able to account for various scales of microstructure (see [1–4] and references therein). The scale-dependence involves

dispersive as well as different non-linear effects and if they are balanced then solitary waves and/or solitons may emerge.

Solitary waves in microstructured solids are analysed using different models (see [4–6] and references therein). However, the crucial point related to the derivation of governing equations is to distinguish between non-linearities on macro- and microlevel together with proper modelling of dispersive effects. In [7–9] the Mindlin model [10] and hierarchical approach by Engelbrecht and Pastrone [4] is used in order to derive governing equations. By Mindlin [10], microstructured material is interpreted as an elastic continuum including microstructure that could be "a molecule of a polymer, a crystallite of a polycrystal or a grain of a granular material". This microstructure is modelled by microelements within the macrostructure. According to Eringen and Mindlin [1,10] fundamental balance laws should be formulated for macro- and microlevel separately. For 1D model this approach results in equations of motion in the following form:

$$\rho u_{tt} = \sigma_x,$$
$$I\psi_{tt} = \eta_x - \tau. \qquad (1)$$

Here u is the macrodisplacement, ψ the microdeformation, ρ the macrodensity, I the microinertia, σ the macrostress, η the

---

* Corresponding author at: Centre for Nonlinear Studies, Institute of Cybernetics at Tallinn University of Technology, Akadeemia tee 21, 12618 Tallinn, Estonia.

E-mail addresses: salupere@ioc.ee (A. Salupere), kert@cens.ioc.ee (K. Tamm), je@ioc.ee (J. Engelbrecht).

microstress and τ the interactive force. The free energy function is considered in the following form:

$$W = W_2 + W_3,$$

$$W_2 = \frac{1}{2}au_x^2 + \frac{1}{2}B\psi^2 + \frac{1}{2}C\psi_x^2 + D\psi u_x,$$

$$W_3 = \frac{1}{6}Nu_x^3 + \frac{1}{6}M\psi_x^3, \tag{2}$$

where a, B, C, D, M, N are constants. Here the quadratic term W_2 gives rise to the linear stress and the cubic W_3—to the non-linear part of stress. Then using the formulae

$$\sigma = \frac{\partial W}{\partial u_x}, \quad \eta = \frac{\partial W}{\partial \psi_x}, \quad \tau = \frac{\partial W}{\partial \psi} \tag{3}$$

Eqs. (1) are expressed in terms of variables u and ψ

$$\rho u_{tt} = au_{xx} + Nu_x u_{xx} + D\psi_x,$$

$$I\psi_{tt} = C\psi_{xx} + M\psi_x \psi_{xx} - Du_x - B\psi. \tag{4}$$

Next, slaving principle [4,7] is applied (in order to eliminate the microdeformation ψ from latter equations) and in terms of dimensionless variables $X = x/L$, $T = tc_0/L$, $U = u/U_0$, scale parameter $\delta = l^2/L^2$ (L and U_0 are amplitude and wavelength of the initial excitation, respectively; $c_0^2 = a/\rho$ and l is the scale of the microstructure) Eqs. (4) result in the hierarchical model equation

$$L_1 - \delta L_2 = 0,$$

$$L_1 = U_{TT} - bU_{XX} - \frac{\mu}{2}(U_X^2)_X,$$

$$L_2 = \left(\beta U_{TT} - \gamma U_{XX} - \delta^{1/2}\frac{\lambda}{2}U_{XX}^2\right)_{XX}, \tag{5}$$

where L_1 is macrostructure wave operator and L_2 microstructure wave operator. New dimensionless material constants b, μ, β, γ and λ are introduced during change of variables and they are directly related to constants a, B, C, D, M, N in free energy expression (2) (see [8,9] for details). If the scale parameter δ is small then the wave process is governed by properties of the macrostructure and vice versa, if δ is large, then properties of the microstructure govern the process.

For future analysis Eq. (5) is expressed in terms of deformation $v = U_X$ and lower-case letters x and t are used for dimensionless coordinate and time.

$$v_{tt} - bv_{xx} - \frac{\mu}{2}(v^2)_{xx}$$

$$- \delta(\beta v_{tt} - \gamma v_{xx})_{xx} + \delta^{3/2}\frac{\lambda}{2}[(v_x)^2]_{xxx} = 0. \tag{6}$$

The full derivation of governing equation (6) can be found in [7,8].

Eq. (6) is non-integrable but it is possible to find its travelling wave solution $v(x - ct)$ in the form of an asymmetric solitary wave using numerical integration under asymptotic boundary conditions (i.e. $u, u_x, u_{xx}, \ldots \to 0$, if $x \to \pm\infty$). The analytic conditions for the existence of solitary waves modelled by

Eq. (6) are given by Janno and Engelbrecht in [8,9]:

$$\frac{c^2 - b}{\beta c^2 - \gamma} > 0, \quad \left(\frac{\beta c^2 - \gamma}{c^2 - b}\right)^3 > \frac{4\lambda^2}{\mu^2},$$

$$\mu \neq 0, \quad \beta c^2 - \gamma \neq 0, \quad c^2 - b \neq 0. \tag{7}$$

In the case of $\lambda = 0$ the non-linearity in the microscale is neglected and Eq. (6) admits bell-like solitary wave solution [6,9]

$$v(x - ct) = A \operatorname{sech}^2 \frac{\varkappa(x - ct)}{2},$$

$$A = \frac{3(c^2 - b)}{\mu}, \quad \varkappa = \sqrt{\frac{c^2 - b}{\delta(\beta c^2 - \gamma)}}. \tag{8}$$

From the viewpoint of soliton dynamics, three problems are of importance: the existence of solitary waves, the emergence of solitary waves and the interaction of solitary waves. The latter is important in order to prove the solitonic character of solitary waves, i.e. to understand whether solitary waves are able to propagate at constant speed and shape and to restore these quantities after interactions. If yes, these solitary waves are called solitons. Here in this paper the basic model is a two-wave equation with complicated dispersive and non-linear terms. The existence of solitary waves is proved by Janno and Engelbrecht [8,9], the preliminary analysis of emergence of trains of solitary waves is presented in our earlier study [11] and here we present the preliminary results on interaction of solitary waves. The notion of solitary waves is used because the elastic interaction should prove whether these waves are solitons or not. As it is shown below, the problem is complicated and needs further analysis.

2. Statement of the problem and numerical technique

In the present paper the propagation and the interaction of localised initial pulses in microstructured materials (governed by Eq. (6)) is simulated numerically over long time intervals. Two goals are stated (i) to examine the solitonic character of the solution and (ii) to estimate the influence of the microlevel non-linear parameter λ on the solution.

For this reason Eq. (6) is integrated numerically under localised initial conditions

$$v(x, 0) = \sum_{i=1}^{2} A_i^0 \operatorname{sech}^2 \frac{\varkappa_i(x - \xi_i)}{2}, \quad 0 \leqslant x < 2k\pi. \tag{9}$$

Initial amplitudes A_i^0 and the widths $\varkappa_i$ ($i = 1, 2$) correspond to different initial speeds $c_1 \neq c_2$, ξ_i are initial phase shifts and k is integer. It is clear that in case $c_1 c_2 < 0$ head-on collision and in case of $c_1 c_2 > 0$ overtaking interaction takes place (if periodic boundary conditions are applied then this is true as in case $c_1 > c_2$ as well as in case $c_1 < c_2$).

For numerical integration discrete Fourier transform (DFT) based pseudospectral method (PsM) [12,13] is used and

therefore periodic boundary conditions

$$v(x, t) = v(x + 2k\pi, t) \qquad (10)$$

are applied.

In a nutshell, the idea of the PsM is to approximate space derivatives making use of DFT and then to use standard ODE solvers for integration with respect to the time. Due to the mixed partial derivative term $\delta\beta v_{ttxx}$ the model Eq. (6) cannot be directly integrated by PsM. Therefore we introduce new variable

$$\Phi = v - \delta\beta v_{xx}. \qquad (11)$$

In terms of DFT the latter can be presented in the form

$$\Phi = F^{-1}[(1 + \delta\beta\omega^2)F(v)], \qquad (12)$$

where F denotes the DFT, F^{-1} the inverse DFT and $\omega = \pm 1, \pm 2, \ldots, \pm(N/2 - 1), -N/2$. Then variable v and its spatial derivatives are expressed in terms of the variable Φ

$$v = F^{-1}\left[\frac{F(\Phi)}{1 + \delta\beta\omega^2}\right],$$

$$\frac{\partial^n v}{\partial x^n} = F^{-1}\left[\frac{(i\omega)^n F(\Phi)}{1 + \delta\beta\omega^2}\right]. \qquad (13)$$

Finally, Eq. (6) can be rewritten in terms of variable Φ

$$\Phi_{tt} = \left[bv + \frac{\mu}{2}v^2 - \delta\gamma v_{xx} - \delta^{3/2}\frac{\lambda}{2}(v_x^2)_x\right]_{xx} \qquad (14)$$

(v and its space derivatives are calculated making use of expressions (12) and (13)). In order to simulate the propagation and the interaction of localised pulses, Eq. (14) is solved numerically by PsM under initial and boundary conditions (9) and (10), respectively.

Calculations are carried out using SciPy package [14]: for DFT the FFTW [15] library and for ODE solver the F2PY [16] generated Python interface to ODEPACK Fortran code [17] is used.

3. Results and discussion

In the present section two different head-on interaction cases are considered. In the first case solitary waves of equal amplitude propagate at equal initial speed in opposite directions ($c_1 = -c_2 = 0.9$) and in the second case solitary waves of different amplitude propagate at initial speeds $c_1 = 0.9$ and $c_2 = -0.9115$. Five parameters for Eq. (6) are fixed: $b = 0.7683$, $\mu = 0.125$, $\delta = 9$, $\beta = 7.6452$, $\gamma = 6.1825$, but λ has three different values 0, 0.0025 and 0.005. For $|c_i| = 0.9115$ and $|c_i| = 0.9$ conditions (7) are satisfied for all considered values of parameter λ. We stress here that if conditions (7) are satisfied, then travelling wave solutions in the form of single asymmetric solitary wave can exist for Eq. (6) [8,9]. Numerical integration is carried out for $0 \leqslant t \leqslant 6000$, wave profiles are saved at every

$\Delta t = 0.5$, the length of the space period is 60π and the number of space-grid points is $n = 1024$. According to expression (8)$_2$ amplitude $A = 1.00$ corresponds to the speed $|c_i| = 0.9$ and amplitude $A = 1.50$ to the speed $|c_i| = 0.9115$. In all considered cases amplitudes of solitary waves increase during interactions and decrease after interactions. If initial amplitudes, shapes and velocities are restored after interactions—like in case of Boussinesq models—then such solitary waves can be called solitons.

In [18] the same interaction types were studied for remarkably shorter time intervals ($0 \leqslant t \leqslant 500$). For the equal initial amplitude case the length of the space interval was 24π and in the case of non-equal amplitudes 96π. It was found that for $\lambda = 0$ and for relatively small values of parameters the behaviour of solitary waves was very close to that of solitons for the considered time and space intervals. Interaction between equal amplitude solitary waves was found to take place without phase shifts, but if interacting waves have different amplitude, then both were phase-shifted.

3.1. Head-on collision of solitary waves with equal amplitudes

In the present subsection the interaction between two solitary waves having initial velocities are $c_1 = -c_2 = 0.9$ and equal initial amplitudes $A_0 = 1.00$ is studied. In Fig. 1, wave-profile maxima (heights) are plotted against time for two different values of parameter λ. In the beginning of the integration interval ($t < 500$) height at "peaks" of interaction A^i ("peaks" of interaction correspond to local maxima of amplitude curves in Fig. 1) is close to double initial amplitude of interacting solitary waves. However for $t > 500$ the amplitude A^i increases apparently, cf. Fig. 2 where the amplitude A^i is plotted against time for different values of λ. For $t < 1000$ all three curves practically coincide, but for higher values of t they diverge essentially—the higher the value of λ the lower the values of A^i. At $t = 3000$ the value of A^i is more than 6% higher than double initial amplitude of interacting solitary waves for all three values of λ.

The length of time intervals between "peaks" of interaction does not depend on λ and is between values 104.63 and 104.71. It is clear from Fig. 1 that for $t < 500$ interacting solitary waves more or less restore their initial heights for certain time intervals. However, for higher values of t such a phenomenon does not take place. Furthermore, for $\lambda > 0$ right- and left-propagating solitary waves have different heights A_R and A_L between interactions. In Fig. 3 averaged amplitudes A_R^a and A_L^a are plotted against the number of interactions. Values of A_R^a and A_L^a after kth interaction are obtained by averaging amplitudes of right- and left-propagating solitary waves over time intervals where both amplitudes have near constant values between kth and $(k + 1)$th interactions (cf. Fig. 1). Analysis of single wave profiles and data in Fig. 3 demonstrate that for $\lambda > 0$ amplitude $A_R^a > A_L^a$ until 15th interaction and vice versa $A_R^a < A_L^a$ after 15th interaction. The higher the value of λ the higher the amplitude A_L and the lower the amplitude A_R at $t = 3000$. This phenomenon depicts the behaviour at the given set of parameters and the critical value can be
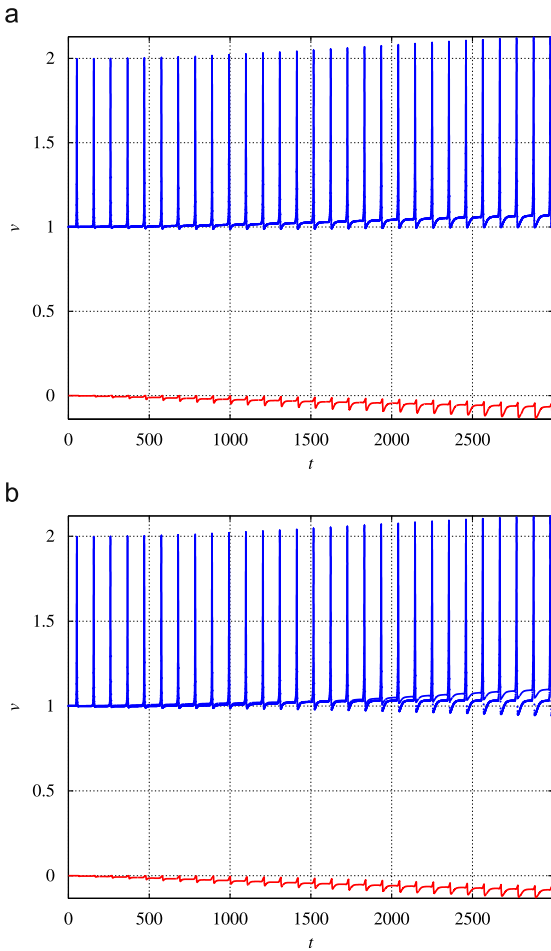
a

b

Fig. 1. Wave-profile maxima and minimum against time in case of $c_1 = -c_2 = 0.9$: (a) $\lambda = 0$; (b) $\lambda = 0.005$.
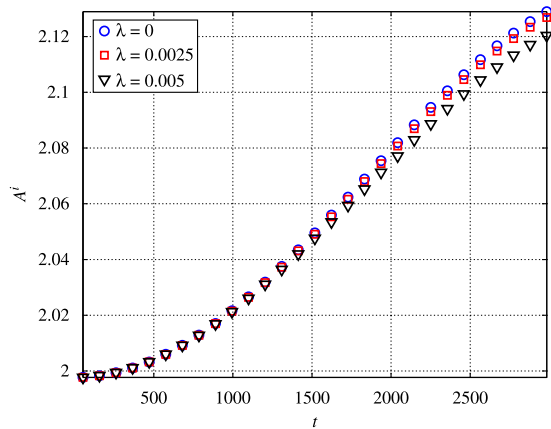

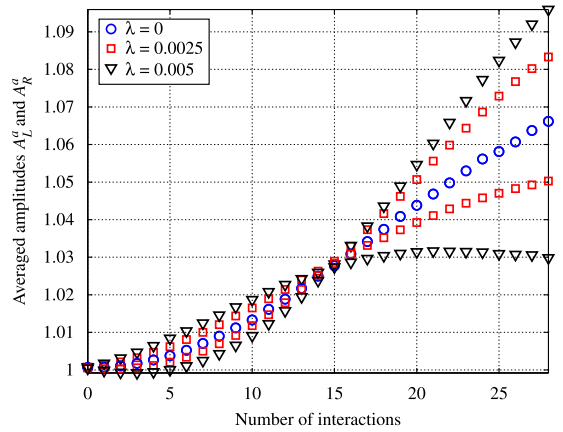Fig. 2. Amplitude at "peaks" of interactions A^i against time in case of $c_1 = -c_2 = 0.9$.

Fig. 3. Averaged amplitudes between interactions A_R^a and A_L^a against the number of interactions in case of $c_1 = -c_2 = 0.9$.

changed at other sets. It is evident that the averaged amplitudes tend to certain limits at larger number of interactions. The fact that amplitudes are not restored after interactions indicates that interactions between solitary waves are not elastic, i.e., a certain exchange of energy takes place between solitary waves during interaction. One can see below that the initial symmetric shape of solitary waves is also altered during interactions.

Between interactions both solitary waves propagate practically at initial speed. In order to estimate phase shifts during interactions the actual trajectories of solitary waves are compared with straight lines $x_i = \xi_i \pm 0.9t$, i.e., with phase-shift free trajectories (ξ_i are initial phase shifts, cf. (9)). In Fig. 4 cumulative phase shift in space is plotted against the number of interactions. The cumulative phase shift is calculated as average deviation between two considered trajectories over time interval $t_k + 25 \leqslant t \leqslant t_{k+1} - 25$ (time moments t_k and t_{k+1} correspond to kth and $(k + 1)$th interactions, respectively). For the case $\lambda = 0$ both waves are shifted by the same extent and the cumulative phase shift after 28th interaction is about 0.81 which is 0.43% of the length of the space period. For $\lambda > 0$ phase shifts for right- and left-propagating solitary waves are different—right-propagating solitary wave is less phase-shifted than that of the left-propagating. However, compared to the length of the space period the cumulative phase shift is less than 1% in all considered cases.

Janno and Engelbrecht have shown in [8,9] that for Eq. (6) exists symmetric bell-shaped travelling wave solution for $\lambda = 0$ and asymmetric travelling wave solution—for $\lambda > 0$. In our numerical experiments single solitary wave (8) propagates at constant amplitude and speed in case of $\lambda = 0$. In case of $\lambda > 0$ the initial symmetric solitary wave is deformed to that of asymmetric. Numerical analysis of interactions of solitary waves (8) demonstrate that due to interactions initial symmetric solitary waves are deformed to that of asymmetric even in case $\lambda = 0$. This phenomenon can be observed in Fig. 5 where maximally separated wave profiles are plotted besides wave profiles at

a

b

c
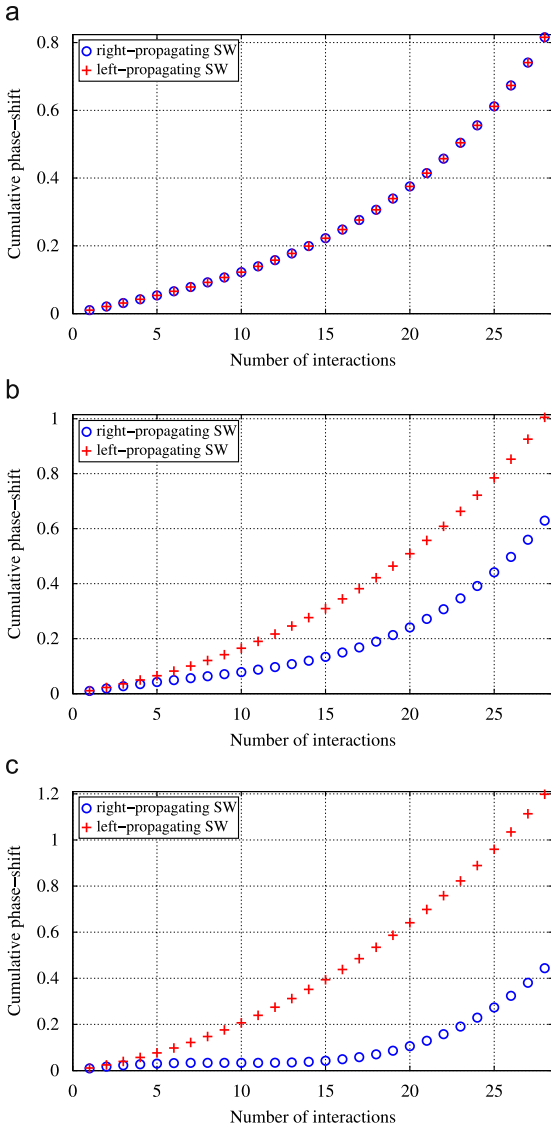
Fig. 4. Cumulative phase shift of left- and right-propagating solitary waves against the number of interactions in case of $c_1 = -c_2 = 0.9$: (a) $\lambda = 0$; (b) $\lambda = 0.0025$; (c) $\lambda = 0.005$.
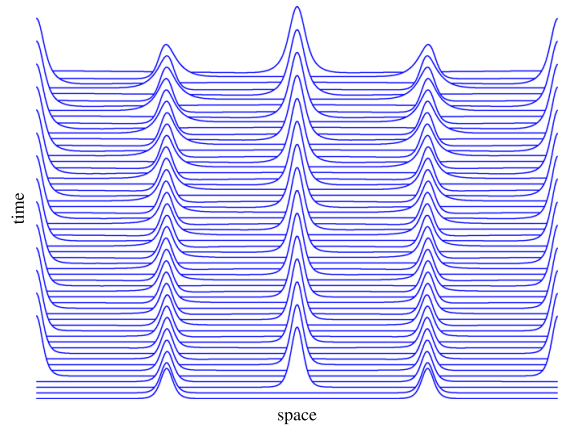

Fig. 5. Timeslices of wave profiles at $t = 0$, at interaction "peaks" and at time moments when two solitary waves are maximally separated in case of $c_1 = -c_2 = 0.9$ and $\lambda = 0$.
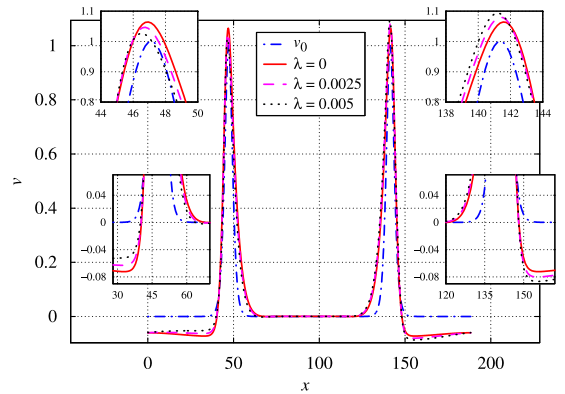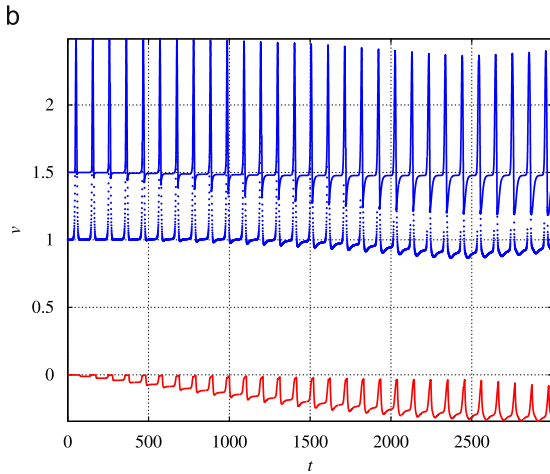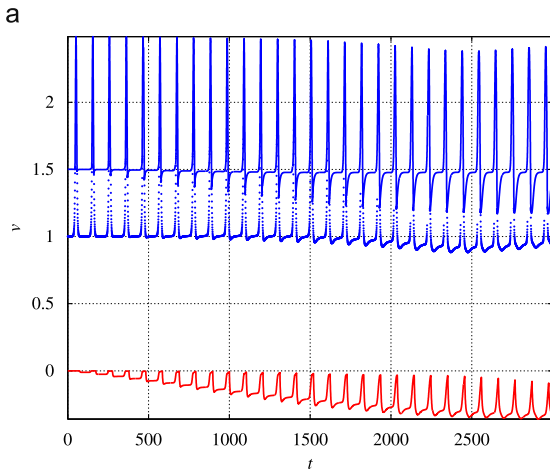

Fig. 6. Initial wave profile and maximally separated wave profiles after 28th interaction in case of $c_1 = -c_2 = 0.9$.

interactions have taken place the stronger it is (cf. wave-profile minimum curve in Fig. 1).

3.2. Head-on collision of solitary waves with non-equal amplitudes

In the present subsection we discuss interactions between two solitary waves having initial amplitudes $A_1^0 = 1.00$ and $A_2^0 = 1.50$ and initial velocities $c_1 = 0.9$ and $c_2 = -0.9115$. In Fig. 7 amplitude curves are plotted for $\lambda = 0$ and $\lambda = 0.005$. In the beginning of the integration interval the amplitude of waves at "peak" of interactions A^i is close to the sum of initial amplitudes like in the previous case. However, unlike the previous case the amplitude A^i is decreasing during the integration time interval. In Fig. 8 amplitudes A^i are plotted against time for three different values of parameter λ. The higher the value of λ the larger the decrease of the amplitude A^i. The length of time

interaction "peaks". The asymmetry of solitary waves is clearly visible in Fig. 6 where solitary waves are plotted at $t = 0$ and at time moment when they are maximally separated after 28th interaction (the left solitary wave is propagating to the right and the right one to the left). It is clear that the higher the value of λ, the more asymmetric is the corresponding wave. Due to the asymmetry both waves are partly located below zero. Physically such a phenomenon can be interpreted as region of depression ($v > 0$ correspond to compression). The depression region is always located behind the propagating wave and the more

a

b

Fig. 7. Wave-profile maxima and minimum against time in case of $c_1 = 0.9$ and $c_2 = -0.9115$: (a) $\lambda = 0$; (b) $\lambda = 0.005$.
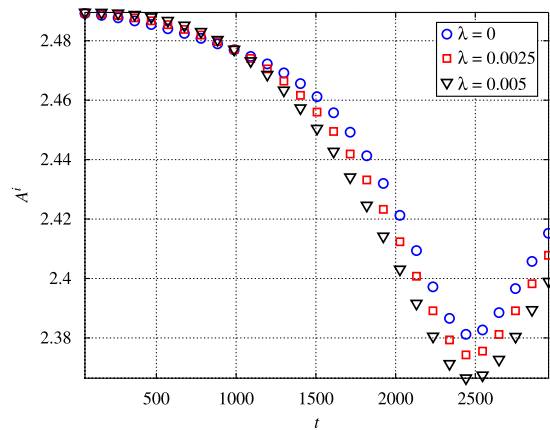
Fig. 8. Amplitudes at "peaks" of interactions in case of $c_1 = 0.9$ and $c_2 = -0.9115$.
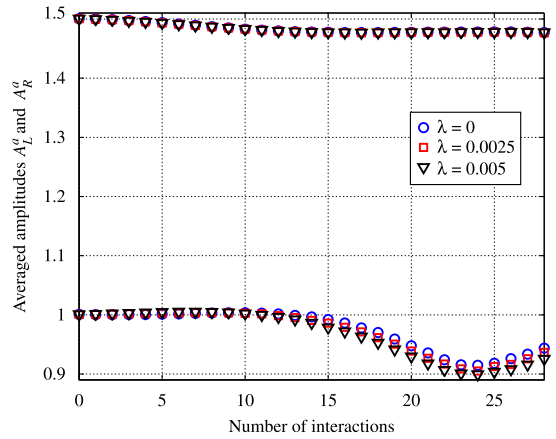
Fig. 9. Average amplitude between interactions in case of $c_1 = 0.9$ and $c_2 = -0.9115$.

intervals between "peaks" of interaction does not depend on λ (like in the previous case) and is now between values 103.35 and 104.00.

The behaviour of the higher (left-propagating) solitary wave between interactions is practically independent on the value of the parameter λ—after the first interaction the initial amplitude is practically restored, but then the average amplitude $A_{\mathrm{L}}^{\mathrm{a}}$ decreases and after the 15th interaction near $t = 1500$ retains constant value (see Figs. 7 and 9). The amplitude of the lower (right-propagating) solitary wave behaves between interactions just the other way round—the amplitude $A_{\mathrm{R}}^{\mathrm{a}}$ is practically constant in the beginning of the interaction interval and starts to decrease after the 12th interaction near $t = 1200$. Furthermore, up to the 12th interaction the right-propagating solitary wave practically restores its initial height.

Both solitary waves propagate between interaction at initial speed and we calculate the cumulative phase shift in the same way like in the previous case. Results are presented in Fig. 10 for three values of parameter λ. In the present case the maximal value of the cumulative phase shift is near 9 (in previous case it was up to 1.2). Up to the 21st interaction the left-propagating, i.e., the higher solitary wave is more phase-shifted than that of the right-propagating for all three values of λ. After that the cumulative phase shift for the right-propagating, i.e., the lower solitary wave increases rapidly from the value near 2.5 up to the value near 9 without reference to the value of the parameter λ.

The larger the number of interactions the more asymmetric is the lower solitary wave. Due to the asymmetry, the part of the wave profile behind it is located below zero like in the previous case. For higher values of t wave-profile minimum has values close to zero only for very short time intervals near "peaks" of interactions (Fig. 7). In Fig. 11 solitary waves are plotted at $t = 0$ and at time moment when they are maximally separated after 28th interaction (the left solitary wave is propagating to the right and the right one to the left) for three values of λ. In the present case parameter λ has very weak influence on the

a

b

c
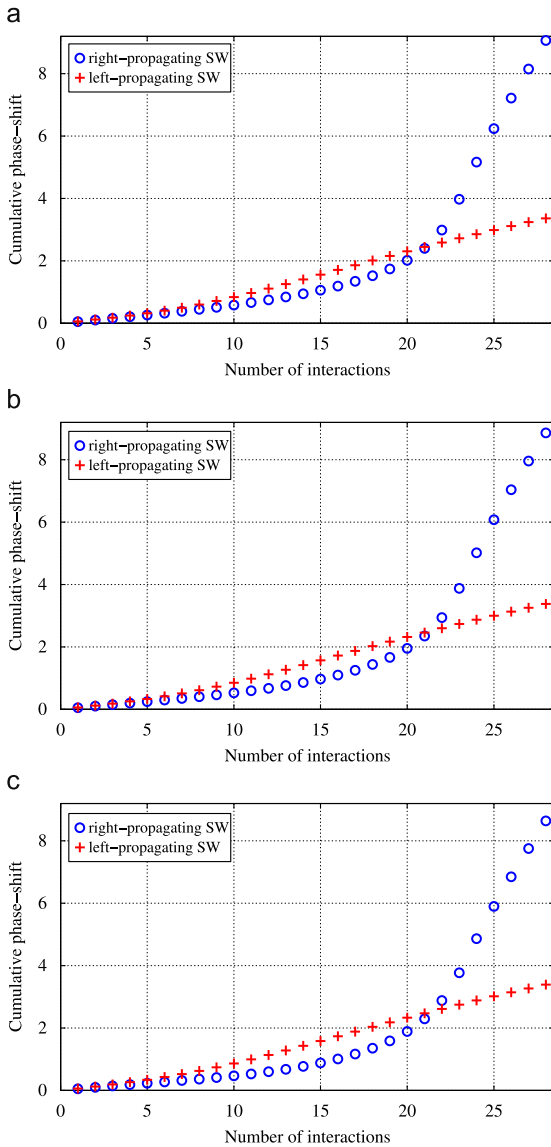
Fig. 10. Phase shifts of left and right going solitary waves in case of $c_1 = 0.9$ and $c_2 = -0.9115$: (a) $\lambda = 0$; (b) $\lambda = 0.0025$; (c) $\lambda = 0.005$.

shape of the wave profile—amplitude of the lower solitary wave decreases slightly when λ increases, but one cannot distinct three profiles in case of the higher solitary wave.

4. Conclusions

Well known and widely used evolution equations (Korteweg–de Vries equation and its modifications for example) are one-wave equations (the order of time derivative is 1), i.e., they are able to govern only overtaking interactions of solitary waves.
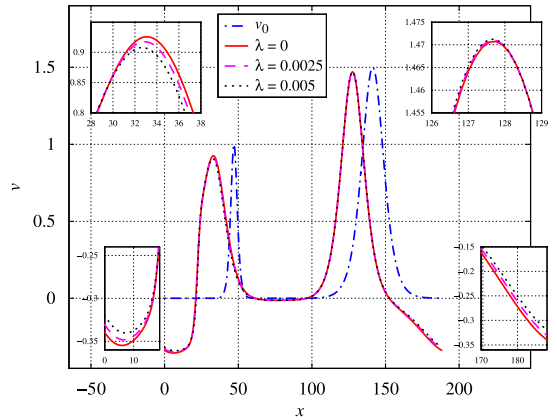
Fig. 11. Initial wave profile and maximally separated wave profiles after 28th interaction in case of $c_1 = 0.9$ and $c_2 = -0.9115$.

Eq. (6) (used in the present paper) is a two-wave equation (the order of time derivative is 2) and therefore gives us possibility to analyse also head-on collisions of waves.

In case of $\lambda = 0$ single symmetric bell-like solitary wave (8) is an analytical solution of Eq. (6) and it propagates with a constant speed and shape. Our numerical simulations have demonstrated that in case of $\lambda > 0$ the symmetric shape of initial single bell-like solitary wave (8) is altered to asymmetric shape during propagation. In the present paper the head-on collision of two sech^2-shape localised initial pulses is studied in case of $\lambda = 0$ as well as $\lambda > 0$. Material parameters for Eq. (6) and initial conditions (9) were chosen according to conditions (7), i.e., for all considered sets of parameters travelling wave solutions in the form of single asymmetric solitary wave can exist for Eq. (6).

Main results are the following:

- Interactions between solitary waves are not completely elastic even in case of $\lambda = 0$—during interactions the symmetric shape of initial waves is altered to that of asymmetric. In case of $\lambda = 0$ and $A_1^0 = A_2^0$ the asymmetry is very weak after very first interactions. However, the higher the number of interactions, the more distinctive the asymmetry without reference to the values of parameter λ and initial velocities. In case of $A_1^0 \neq A_2^0$ the shape of the higher solitary wave is altered only slightly, but that of the lower one significantly.
- The asymmetry of the pulse is reflected in the altering of the shape of compression region of the pulse ($v > 0$) as well as in the emergence of depression zone ($v < 0$) beside that of compression. This phenomenon is more distinctive in case of $A_1^0 \neq A_2^0$.
- Phase shifts, characteristic for soliton type interactions, can be easily traced in case of $A_1^0 \neq A_2^0$. In case of $A_1^0 = A_2^0$ even the cumulative phase shift over long time intervals is small compared to the considered space interval and/or distance travelled by interacting waves.

- In the beginning of the integration interval the height (amplitude) of interacting waves is practically restored between interactions. For higher values of t the height can be altered remarkably. In case of $A_1^0 = A_2^0$ heights of right- and left-propagating waves are restored on unequal levels.
- The non-linearity of the microstructure (parameter λ) has stronger influence on the character of solution in the case of equal initial amplitudes $A_1^0 = A_2^0$ (cf. set of Figs. 1–4, 6 with Figs. 7–11).
- Over short time intervals and small number of interactions the behaviour of the solution is very close to the solitonic behaviour in all considered cases. The higher the number of interactions and the longer the time interval the more the initial and the restored wave profiles differ.

In order to explain phenomena described in this paper in more detail, a further analysis based on energy distribution and spectral changes is needed. Clearly, two-wave interactions differ from one-wave interactions. The special analysis of one-wave interactions is presented in [19,20], the same should be done for this model.

Acknowledgement

References

[1] A. Eringen, Microcontinuum Field Theories. I: Foundations and Solids, Springer, New York, 1999.

[2] R. Phillips, Crystals, Defects and Microstructures. Modelling Across Scales, Cambridge University Press, Cambridge, 2001.

[3] G. Maugin, Nonlinear Waves in Elastic Crystals, Oxford University Press, Oxford, 1999.

[4] J. Engelbrecht, F. Pastrone, Waves in microstructured solids with nonlinearities in microscale, Proc. Est. Acad. Sci. Phys. Math. 52 (1) (2003) 12–20.

[5] V.I. Erofeev, Wave Processes in Solids with Microstructure, World Scientific, Singapore, 2003.

[6] A.V. Porubov, Amplification of Nonlinear Strain Waves in Solids, World Scientific, Singapore, 2003.

[7] J. Engelbrecht, A. Berezovski, F. Pastrone, M. Braun, Waves in microstructured materials and dispersion, Philos. Mag. 85 (2005) 4127–4141.

[8] J. Janno, J. Engelbrecht, Solitary waves in nonlinear microstructured materials, J. Phys. A: Math. Gen. 38 (2005) 5159–5172.

[9] J. Janno, J. Engelbrecht, An inverse solitary wave problem related to microstructured materials, Inverse Probl. 21 (2005) 2019–2034.

[10] R.D. Mindlin, Micro-structure in linear elasticity, Arch. Ration. Mech. Anal. 16 (1964) 51–78.

[11] J. Engelbrecht, A. Berezovski, A. Salupere, Nonlinear deformation waves in solids and dispersion, Wave Motion 44 (6) (2007) 493–500.

[12] B. Fornberg, A Practical Guide to Pseudospectral Methods, Cambridge University Press, Cambridge, 1998.

[13] A. Salupere, J. Engelbrecht, P. Peterson, On the long-time behaviour of soliton ensembles, Math. Comput. Simulation 62 (2003) 137–147.

[14] E. Jones, T. Oliphant, P. Peterson, et al., SciPy: open source scientific tools for Python ⟨http://www.scipy.org⟩, 2001.

[15] M. Frigo, S.G. Johnson, The design and implementation of FFTW3, Proc. IEEE 93 (2) (2005) 216–231.

[16] P. Peterson, F2PY: fortran to python interface generator ⟨http://cens.ioc.ee/projects/f2py2e/⟩, 2005.

[17] A.C. Hindmarsh, Odepack, a systematized collection of ODE solvers, in: R.S. Stepleman et al. (Eds.), Scientific Computing, North-Holland, Amsterdam, 1983, pp. 55–64.

[18] A. Salupere, K. Tamm, J. Engelbrecht, P. Peterson, On interaction of deformation waves in microstructured solids, Proc. Est. Acad. Sci. Phys. Math. 56 (2) (2007) 93–99.

[19] A. Salupere, J. Engelbrecht, P. Peterson, Long-time behaviour of soliton ensembles, Part I—emergence of ensembles, Chaos Solitons Fractals 14 (2002) 1413–1424.

[20] A. Salupere, J. Engelbrecht, P. Peterson, Long-time behaviour of soliton ensembles, Part II—periodical patterns of trajectories, Chaos Solitons Fractals 15 (2003) 29–40.

Publication IV

T. Peets and **K. Tamm**
Dispersion analysis of wave motion in microstructured solids.
In T.-T. Wu and C.-C. Ma, editors, *IUTAM Symposium on Recent Advances of Acoustic Waves in Solids: Proceedings, Taipei, Taiwan, May 25–28, 2009*, volume 26 of IUTAM Bookseries, pages 349–354, Dordrecht, 2010. Springer

Dispersion Analysis of Wave Motion in Microstructured Solids

Tanel Peets and Kert Tamm

Centre for Nonlinear Studies, Institute of Cybernetics at Tallinn University of Technology, Akadeemia tee 21, 12618 Tallinn, Estonia

tanelp@cens.ioc.ee

Abstract. The Mindlin-type model is used for describing longitudinal waves in microstructured solids. This model involves explicitly the internal parameters and therefore tends to be rather complicated. An hierarchical approximation is derived, which is able to grasp the main effects of dispersion with wide variety of parameters. Attention is paid to the internal degrees of freedom of the microstructure and their influence on the dispersion effects. It is shown how the internal degrees of freedom can change the effects of dispersion.

1. Introduction

It is well recognized by modern science, that matter is not continuous but has an internal structure. Clearly this microstructure plays a significant role when modelling wave propagation – waves that have a wavelength shorter than a certain threshold value, "feel" the microstructure.

There are two approaches in modelling the microstructure - one group of models are based on lattice theory [1-3], another on continuum theory [4-6].

In the discrete approach the volume elements of the matter are treated as point masses with a defined distribution and some interaction between the discrete masses. The governing equations are then deduced following the Newton's law.

In the microcontinuum theory, the macro- and microstructure of the continua are separated. Then the conservation laws for both structures should either be separately formulated [4,5], or the microstructural quantities (cells) are separately taken into account in one set of conservation laws. Engelbrecht *et al.* [6] have derived the one-dimensional model for longitudinal waves in microstructured materials based on Mindlin model [5]. This model will be the basis of our analysis. These governing equations of wave motion tend to be rather complicated and therefore there is a need for simplification. A slaving principle is used in order to derive a hierarchical asymptotic Whitham-type model.

An important effect caused by microstructure is dispersion. A wave packet can be viewed as a collection of harmonic waves. If such a wave travels through a microstructured material, then different harmonics "feel" the microstructure according to their wavelength and travel with different speeds. The variation of phase velocity with wavenumber is the hallmark of dispersion [7,8].

Generally if there is N particles per unit cell in discrete model, then N dispersion curves appear (3N in case of 3D model). The lower curve is called an acoustic branch, the upper curves are called optical branches and they only appear when there are at least 2 particles per unit cell. Optical branches are said to reflect the internal degrees of freedom [1,9].

Because of the inclusion of the microstructure, the dispersion curves derived from the 1D microcontinuum model, also give two distinct curves [4,6,9]. As in discrete model these curves are acoustical and optical modes where an optical modes are interpreted as internal degrees of freedom or "internal modes"[5,9]. The dispersion curve derived from the Whitham-type approximate model has only an acoustical branch. It means that the approximate model does not account directly for internal degrees of freedom. The authors have shown that this approximation is acceptable with wide variety of parameters. However the question that remains is when the internal modes can be ignored.

2. The Basic Model

The basic model is that of Mindlin [5] and we follow the presentation of its ideas in [6]. The main idea is to distinguish between macro- and microdisplacements $u_i(x_i, t)$ and $u_j'(x_i', t)$, respectively. Assuming that microdisplacement is defined in coordinates x_k', moving with a microvolume (cell), we define $u_j' = x_k' \varphi_{kj}(x_i, t)$, where φ_{kj} is an arbitrary function. It is clear that actually it is the microdeformation while $\partial u_j^n / \partial u_i^n = \partial_i^n u_j^n = \varphi_{ij}$. Further we consider the simplest 1D case and drop the indices i and j.

Now the fundamental balance laws can be formulated separately for macroscopic and microscopic scales. Introducing the Lagrangian $L = K - W$, formed from the kinetic and potential energies

$$K = \frac{1}{2}\rho u_t^2 + \frac{1}{2}I\varphi_t^2, \quad W = W(u_x, \varphi, \varphi_x), \tag{2.1}$$

where ρ and I denote the macroscopic density and the microinertia, respectively, we can use the corresponding Euler-Lagrange equations:

$$\left(\frac{\partial L}{\partial u_t}\right)_t + \left(\frac{\partial L}{\partial u_x}\right)_x - \left(\frac{\partial L}{\partial u}\right) = 0, \quad \left(\frac{\partial L}{\partial \varphi_t}\right)_t + \left(\frac{\partial L}{\partial \varphi_x}\right)_x - \left(\frac{\partial L}{\partial \varphi}\right) = 0. \tag{2.2}$$

Here and further, the indices x and t denote differentiation.

The partial derivatives

$$\sigma = \partial W / \partial u_x, \quad \eta = \partial W / \partial \varphi_x, \quad F = \partial W / \partial \varphi, \tag{2.3}$$

are recognized as the macrostress, the microstress and the interactive force, respectively.

The simplest potential energy function describing the influence of a microstructure is a quadratic function

$$W = \frac{1}{2} a u_x^2 + A \varphi u_x + \frac{1}{2} B \varphi^2 + \frac{1}{2} C \varphi_x^2, \tag{2.4}$$

where a,A,B,C denote material constants. Introducing Eq. (2.4) into Eq. (2.3) we get finally

$$\rho u_{tt} = a u_{xx} + A \varphi_x, \quad I \varphi_{tt} = C \varphi_{xx} - A u_x - B \varphi. \tag{2.5}$$

This is the governing system of two second-order equations that can also be represented in the form of one fourth-order equation

$$u_{tt} = \left(c_0^2 - c_A^2\right) u_{xx} - p^2 \left(u_{tt} - c_0^2 u_{xx}\right)_{tt} + p^2 c_1^2 \left(u_{tt} - c_0^2 u_{xx}\right)_{xx}, \tag{2.6}$$

where material parameters $c_0^2 = a / \rho$, $c_1^2 = C / I$, $c_A^2 = A^2 / \rho B$, $p^2 = I / B$, are introduced. The parameters c_0, c_1, c_A are velocities while p is a time parameter. This is the basic linear equation governing 1D longitudinal waves in microstructured solids. It has been shown by Sun *et al.* that Mindlin type model can also be used for modeling wave dispersion in layered media [10].

An approximation of Eq. (2.6) can be obtained by using the slaving principle. It is supposed that the inherent length-scale l is small compared with the wavelength L of the excitation. The following dimensionless variables and parameters are introduced $U=u/U_0$, $X=x/L$, $T=c_0 t/L$, $\delta=(l/L)^2$, $\varepsilon=U_0/L$, where U_0 is the amplitude of the excitation. In addition it is assumed that $I=\rho l^2 I^*$ and $C=l^2 C^*$, where I^* is dimensionless and C^* has the dimensions of stress.

Next the system (2.5) is rewritten in its dimensionless form and the slaving principle [11] is applied. Then we get finally

$$U_{TT} = \left(1 - \frac{c_A^2}{c_0^2}\right) U_{XX} + \frac{c_A^2}{c_B^2} \left(U_{TT} - \frac{c_1^2}{c_0^2} U_{XX}\right)_{XX}, \tag{2.7}$$

where $c_B^2 = L^2/p^2 = BL^2/I$. Note that c_B involves the scales L and l and c_A includes the interaction effects through parameter A. Restoring dimensions, Eq. (2.7) yields

$$u_{tt} = \left(c_0^2 - c_A^2\right) u_{xx} + p^2 c_A^2 \left(u_{tt} - c_1^2 u_{xx}\right)_{xx}. \tag{2.8}$$

This is an example of the Whitham-type hierarchical equation.

3. Dispersion Analysis

The dispersion relations for Eqs. (2.6) and (2.8) are

$$
\begin{aligned}
\omega^2 &= \left(c_0^2 - c_A^2\right)k^2 + p^2\left(\omega^2 - c_0^2 k^2\right)\left(\omega^2 - c_1^2 k^2\right), \\
\omega^2 &= \left(c_0^2 - c_A^2\right)k^2 - p^2 c_A^2\left(\omega^2 - c_1^2 k^2\right)k^2.
\end{aligned}
\tag{3.1}
$$

In order to reduce the number of independent variables, the wave number, the frequency and the propagation speeds are normalized defining $\xi = pc_0 k$, $\eta = p\omega$, $\gamma_A = c_A/c_0$, $\gamma_1 = c_1/c_0$. Using these new quantities the dispersion relations (3.1) assume the forms

$$
\begin{aligned}
\eta^2 &= \left(1 - \gamma_A^2\right)\xi^2 + \left(\eta^2 - \xi^2\right)\left(\eta^2 - \gamma_1^2 \xi^2\right), \\
\eta^2 &= \left(1 - \gamma_A^2\right)\xi^2 - \gamma_A^2\left(\eta^2 - \gamma_1^2 \xi^2\right)\xi^2,
\end{aligned}
\tag{3.2}
$$

where the parameters γ_A and γ_1 have the values $0 < \gamma_A < 1$ and $0 < \gamma_1 < 1$ respectively.

The characteristic dispersion curves are shown in Fig. 3.1. The full dispersion relation (3.2a), which is represented by the continuous line, represents two distinct branches – acoustical and optical. The acoustical branch is analogous to the case of elastic vibrations where all the cells move in unison. These are external modes. The optical branch reflects the role of the internal modes, which involve the distortion of the cells [5,9].

The optical branch is always concave, the acoustical branch can be either concave or convex or linear, which represents anomalous, normal or no dispersion respectively. This concavity and convexity of the acoustic dispersion curve shows explicitly the influence of basic material properties [12].

The full model (2.6) and approximate model (2.7) can be compared using numerical analysis. The initial value problem in dimensionless form under periodic boundary conditions is solved using the pseudospectral method [13]. The initial profile is chosen $U(X,0) = sech^2(\kappa X/2)$, where κ is the width of the profile.

Figures 3.2 and 3.3 show the results of the numerical analysis. Figure 3.2 represents the case when acoustical branch is concave (anomalous dispersion). It is clear from the numerical experiment that although there are small differences between the full model (2.6) and approximation (2.7), the approximation is able to display the main effects of dispersion i.e. the type of the dispersion.

Figure 3.3 shows a numerical experiment in case when there is no dispersion in approximate dispersion relation (3.2b) and in the acoustic branch of the full dispersion relation (3.2a). The approximate model indeed shows no dispersion effects – the initial

profile moves with constant speed and shape. The full model (2.6) however displays a small effect of dispersion, which is due to the optical bra nch or internal modes. The dispersion effects do not appear immediately, but may take some time to appear.
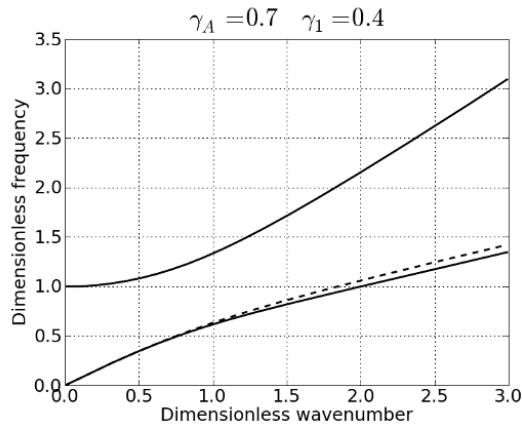
Fig. 3.1 The characteristic dispersion curves. Solid lines represent full dispersion relation, dashed line represents approximate dispersion relation.
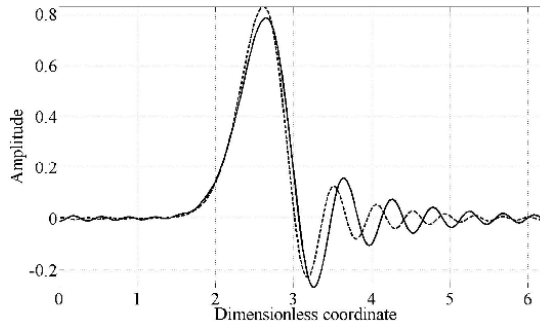

Fig. 3.2 The solutions of full model (solid line) and approximation (dashed line), in case of γ_A=0.9 and γ_1=0.7.
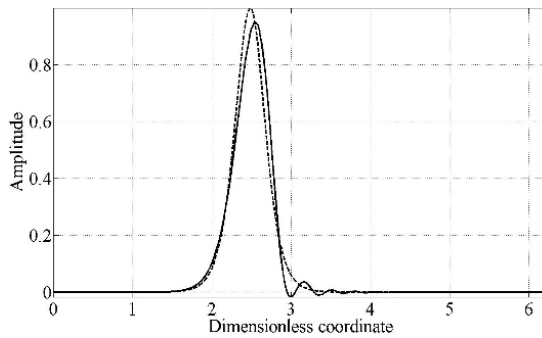
Fig. 3.3 The solutions of full model (solid line) and approximation (dashed line), in case of γ_A=0.9 and γ_1=0.7.

4. Final Remarks

The numerical analysis demonstrates that the full and approximate models give in most cases similar results. There are however conditions when approximate dispersion curve (3.2b) coincides well with the acoustic branch of the full dispersion curve (3.2a), but the numerical experiment gives different types of dispersion for the full model (2.6) and for the approximation (2.7). This is likely to be present when acoustic curve displays normal dispersion.

These effects need further investigations and will be presented in further publications.

References

[1]   Brillouin, L.: *Wave Propagation in Periodic Structures. Dover Publications*, INC, NY (1953).
[2]   Metrikine, A.V., Askes, H.: One-dimensional dynamically consistent gradient elasticity models derived from a discrete microstructure. Part 1: Generic formulation. *Eur. J. Mech. A. Solids* **21** (2002) 555-572.
[3]   Maugin, G.A.: *Nonlinear Waves in Elastic Crystals.* Oxford University Press (1999).
[4]   Eringen, A.C.: Linear theory of micropolar elasticity. *J. Math. Mech.* **15** 909-923 (1966).
[5]   Mindlin, R.D.: Microstructure in linear elasticity. *Arch. Rat. Mech. Anal.* **16** 51-78 (1964).
[6]   Engelbrecht, J., Berezovski, A., Pastrone, F., Braun, M.: Waves in microstructured materials and dispersion. *Philos. Mag.* **85**(33-35) 4127-4141(2005).
[7]   Nettel, S.: *Wave physics. Oscillations - Solitons - Chaos.* New York: Springer (1995).
[8]   Main, I.G.: *Vibrations and Waves in Physics.* Cambridge University Press (1984).
[9]   Chen, Y., Lee, J.D.: Analysis of photon dispersion relations from atomic model to continuum theory. *Nanotech* **1** 396-399 (2002).
[10]   Sun, C.-T., Achenbach, J.D., Herrmann, G.: Continuum theory for a laminated medium. *J. Appl. Mech. Trans. ASME* **35**(3) 467-475 (1968).
[11]   Christiansen, P.L., Muto, V., Rionero, S.: Solitary wave solution to a system of Boussinesq-like equations. *Chaos Solitons Fractals* **2** 45-50 (1992).
[12]   Peets, T., Randrüüt, M., Engelbrecht, J.: On modelling dispersion in microstructured solids. *Wave Motion* **45** 471-480 (2008).
[13]   Salupere, A., Tamm, K., Engelbrecht, J.: Numerical simulation of interaction of solitary deformation waves in microstructured solids. *Int. J. Non Linear Mech.* **43** 201-208 (2008).

Publication V

K. Tamm and A. Salupere
On the propagation of solitary waves in Mindlin-type microstructured solids.
Proceedings of the Estonian Academy of Sciences, 59(2):118–125, 2010

MECHANICS

On the propagation of solitary waves in Mindlin-type microstructured solids

Kert Tamm[a,b] and Andrus Salupere[a,b*]

[a] Centre for Nonlinear Studies, Institute of Cybernetics at Tallinn University of Technology, Akadeemia tee 21, 12618 Tallinn, Estonia
[b] Department of Mechanics, Tallinn University of Technology, Ehitajate tee 5, 19086 Tallinn, Estonia; kert@cens.ioc.ee

Abstract. The Mindlin–Engelbrecht–Pastrone model is applied to simulating 1D wave propagation in microstructured solids. The model takes into account the nonlinearity in micro- and macroscale. Numerical solutions are found for the full system of equations (FSE) and the hierarchical equation (HE). The latter is derived from the FSE by making use of the slaving principle. Analysis of results demonstrates good agreement between the solutions of the FSE and HE in the considered domain of parameters. For numerical integration the pseudospectral method is used.

Key words: nonlinearity, microstructured solids, solitons, dispersion, pseudospectral methods.

1. INTRODUCTION

Microstructured materials are characterized by the existence of intrinsic space-scales in matter, like the lattice period, the size of a grain or a crystallite, or the distance between the microcracks, etc., which introduce the scale-dependence into the governing equations (see, e.g., [3,5,15,22,23] and references therein). The scale-dependence involves dispersive as well as nonlinear effects. If these two effects are balanced, solitons and solitary waves can exist in such media.

For numerical simulation of wave propagation in nonlinear dispersive media with the microstructure a model derived by Engelbrecht and Pastrone [2,11,12] is employed in the present paper. The model is based on Mindlin's and Eringen's earlier works [4,17]. In this approach the microelement is taken as a deformable cell and balance laws are formulated separately for macro- and microscale. At first the Lagrangian

$$L = K - W, \quad K = \frac{1}{2}\rho u_t^2 + \frac{1}{2}I\varphi_t^2, \quad W = W(u_x, \varphi, \varphi_x), \tag{1}$$

is introduced. Here K is the kinetic energy, W is the free energy, I is the microinertia, φ is the microdeformation, u is the macrodisplacement, ρ is the macroscale density, and partial derivatives are denoted by subscripts. In order to take into account the nonlinearity in micro- and macroscale, the free energy W can be written as follows:

$$W = \frac{A}{2}u_x^2 + \frac{B}{2}\varphi^2 + \frac{C}{2}\varphi_x^2 + D\varphi u_x + \frac{N}{6}u_x^3 + \frac{M}{6}\varphi_x^3. \tag{2}$$

---

* Corresponding author, salupere@ioc.ee

Here A, B, C, D are material parameters responsible for the linear part of the model and N, M are responsible for the nonlinearity in macro- and microscale, respectively [11,12]. Making use of the free energy function (2) and Euler–Lagrange equations, we obtain the equations of motion

$$\rho u_{tt} = D\varphi_x + Au_{xx} + Nu_x u_{xx}, \quad I\varphi_{tt} = C\varphi_{xx} + M\varphi_x\varphi_{xx} - B\varphi - Du_x. \tag{3}$$

For further analysis dimensionless variables $X = x/L_o$, $T = (\sqrt{A}t)/(\sqrt{\rho}L_o)$, $U = u/U_o$, $\delta = l_o^2/L_o^2$, $\varepsilon = U_o/L_o$ are introduced [11,12]. Here U_o and L_o are the amplitude and the wavelength of the initial excitation, and l_o is the characteristic scale of the microstructure. All together we have eleven different parameters – eight of them are material (six free energy parameters, macroscale density, and microinertia) and three are geometrical (the amplitude and wavelength of the initial excitation and the scale of the microstructure). The change of variables results in the dimensionless equations of motion

$$U_{TT} = \frac{DL_o}{AU_o}\varphi_X + \frac{NU_o}{AL_o}U_X U_{XX} + U_{XX}, \quad \varphi_{TT} = \frac{C\rho}{AI}\varphi_{XX} - \frac{B\rho L_o^2}{AI}\varphi - \frac{D\rho U_o L_o}{AI}U_X + \frac{M\rho}{AIL_o}\varphi_X\varphi_{XX}. \tag{4}$$

Equations (4) are referred to as the full system of equations (FSE for short) below. By applying the slaving principle [3,21], a single equation can be derived in terms of the macrodisplacement U from the FSE:

$$U_{TT} - bU_{XX} - \frac{\mu}{2}\left(U_X^2\right)_X = \delta\left(\beta U_{TT} - \gamma U_{XX} + \frac{\lambda\sqrt{\delta}}{2}U_{XX}^2\right)_{XX}. \tag{5}$$

Equation (5) is written in the form that makes its hierarchical nature (in Whitham's sense) clearly visible. In terms of material and geometrical parameters, constants in (5) are: $b = 1 - (D^2/AB)$, $\mu = (NU_o)/(AL_o)$; $\beta = (ID^2)/(\rho l_o^2 B^2)$, $\gamma = (CD^2)/(AB^2 l_o^2)$, $\lambda = (D^3 MU_o)/(AB^3 l_o^3 L_o)$. Equation (5) can be considered as an approximation of FSE (4) and is referred to as the hierarchical equation (HE) below. On the other hand, HE (5) is of Boussinesq type [1].

In papers [26–28] we studied the interaction and solitonic character of emerging solitary waves in case of the HE. The main aim of this paper is to compare the propagation of sech^2-type solitary waves in the Mindlin-type microstructured solid for the HE and FSE in the range of parameters where both the macro- and microstructure are to be taken into account. The existence of the solution of the inverse solitary wave problem for the HE is proved in [11]. Therefore it is important to estimate the accuracy of the approximation (the HE) in the domain of parameters where dispersion curves for the HE and FSE differ less than 5%.

The paper is organized as follows. In Section 2 the problem is stated and the numerical technique is described. Results are presented in Section 3 and conclusions are drawn in Section 4.

2. STATEMENT OF THE PROBLEM AND NUMERICAL TECHNIQUE

In order to simulate numerically the propagation of solitary waves in Mindlin-type microstructured solids, HE (5) and FSE (4) are numerically integrated under sech^2-type localized initial conditions and periodic boundary conditions

$$U(X,0) = U_o \operatorname{sech}^2 \kappa X, \quad U(X,T) = U(X + 2m\pi, T), \quad m = 1, 2, 3, \ldots. \tag{6}$$

For the amplitude and width of the initial pulse we use the values $U_o = 1$ and $\kappa = \pi/2$. For numerical integration the pseudospectral method based on the discrete Fourier transform (DFT) is used. Periodic boundary conditions have period of 12π, i.e., $m = 6$ in (6). Initial phase speed is taken to be zero, which can be interpreted as starting from the peak of the interaction of two waves propagating in opposite directions. For the FSE two more initial conditions are needed for the microdeformation. We assume that at $T = 0$ the microdeformation and the corresponding velocity are zero, i.e. $\varphi(X,0) = 0$ and $\varphi_T(X,0) = 0$.

The goals of the present paper are: (i) to solve HE (5) and FSE (4) under localized initial conditions for the weak normal dispersion case; (ii) to compare solutions of the HE and FSE for the linear and the nonlinear case; (iii) to compare solutions of the HE and FSE along a weak normal dispersion line (see Section 3 for details).

The DFT-based pseudospectral method (PSM) [6,14,24,25] is applied in numerical integration in the present paper. In a nutshell, the idea of the PSM is to approximate space derivatives making use of the DFT and then to use standard ODE solvers for integration with respect to time. However, the regular PSM algorithm is derived for $u_t = \Phi(u, u_x, u_{2x}, \ldots, u_{mx})$ type equations, but we have also a mixed partial derivative term $\delta\beta U_{TTXX}$ in HE (5) and therefore the standard PSM has to be modified [9,10,24,26,28]. Therefore we rewrite HE (5) so that all partial derivatives with respect to time are in the LHS of the HE, and introduce a new variable $\Phi = U - \delta\beta U_{XX}$. After that, making use of properties of the DFT, we can express the variable U and its spatial derivatives in terms of the new variable Φ:

$$U = \mathrm{F}^{-1}\left[\frac{\mathrm{F}(\Phi)}{1 + \delta\beta k^2}\right], \quad \frac{\partial^m U}{\partial x^m} = \mathrm{F}^{-1}\left[\frac{(ik)^m \mathrm{F}(\Phi)}{1 + \delta\beta k^2}\right]. \tag{7}$$

Here F denotes the DFT, F^{-1} the inverse DFT, $k = \pm 1, \pm 2, \ldots \pm (n/2 - 1), -n/2$, and n is the number of space-grid points. Finally, equation (5) can be rewritten in terms of the variable Φ:

$$\Phi_{TT} = bU_{XX} + \frac{\mu}{2}\left(U_X^2\right)_X - \delta\left(\gamma U_{XX} - \frac{\lambda\sqrt{\delta}}{2}U_{XX}^2\right)_{XX}. \tag{8}$$

In equation (8) all partial derivatives of U with respect to X are calculated in terms of Φ by making use of the expression (7). Therefore one can apply the PSM for numerical integration of equation (8). Full system of equations (4) is reduced to the system of first-order differential equations which are solved by the standard PSM without any further modifications.

In the present paper calculations are carried out with the Python package SciPy [13], using the FFTW library [7] for the DFT and the F2PY [20] generated Python interface to the ODEPACK Fortran code [8] for the ODE solver.

3. RESULTS

The dispersion type for the HE can be determined by the sign of the quantity $\Gamma = 1 - \gamma_1^2 - \gamma_A^2$, where $\gamma_A^2 = (D^2)/(AB)$, $\gamma_1^2 = (\rho C)/(AI)$; see [3] for details. One can interpret γ_1 as the dimensionless speed of short waves and $\sqrt{1 - \gamma_A^2}$ as the dimensionless speed of long waves. If Γ is positive, we have the normal dispersion case, if Γ is negative, we have the anomalous dispersion case, and if Γ is equal to zero, we have the dispersionless case.

According to the dispersion analysis carried out in [19], acoustic branches of the HE and FSE are close to each other in the area between solid curves in Fig. 1, which corresponds to 5% difference between acoustic branches for the dimensionless wavenumber $\xi = 1.5$ ($\xi = k\sqrt{(AI)/(B\rho)}$, where k is the wavenumber). The FSE also has a second, so-called 'optical' branch. The dotted line corresponds to parameter combinations that result in the dispersionless case for acoustic branches. We have solved the stated problem for values of material and geometrical parameters that result in $\gamma_A^2 - \gamma_1^2$ plane points along the line $\Gamma = 0.05$ (Fig. 1). Here we discuss three cases in detail: points P1, P9, and P18 in Fig. 1. For the nonlinear case we define an additional parameter $\gamma_N = \lambda/\mu = (D^3 M)/(B^3 N l_o^3)$, describing the relation between nonlinearity in macro- and microscale. According to equation (5), λ is responsible for the microscale nonlinearity and μ for the macroscale nonlinearity. In the nonlinear case material parameters M and N are chosen so that $\gamma_N = 0.5$.
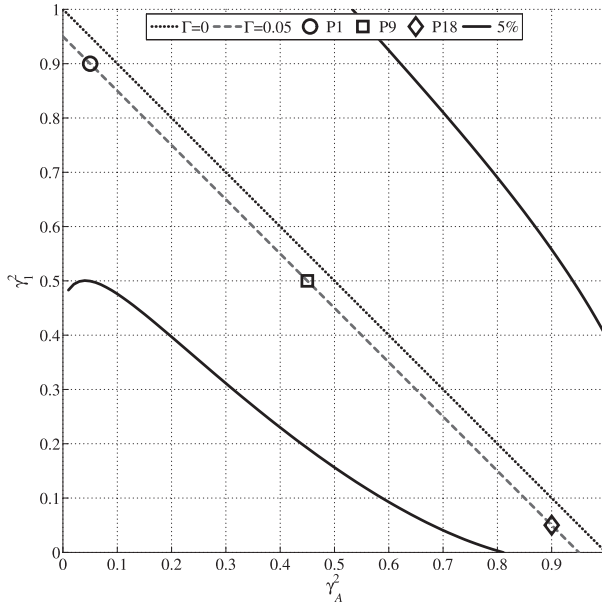
Fig. 1. Domain in the γ_A^2–γ_1^2 plane where the difference between acoustic branches of dispersion curves for the HE and FSE is less than 5%.

Nondimensional material parameters $\widehat{A} = 12$, $\widehat{C} = 9$, $\widehat{D} = 5$, $\widehat{N} = 1$, $\widehat{\rho} = 10$, and geometrical parameters $\widehat{l}_o = 1$, $\widehat{L}_o = 50$, $\widehat{U}_o = 1$ for all cases. The parameters $\widehat{I}$, $\widehat{B}$, $\widehat{M}$ vary, giving the following values for γ_A^2 and γ_1^2:

$$
\begin{aligned}
&\text{P1}: \gamma_A^2 = 0.05; \quad \gamma_1^2 = 0.90; \quad \widehat{B} = 125/3; \quad \widehat{I} = 25/3; \quad \widehat{M} = 15625/54; \\
&\text{P9}: \gamma_A^2 = 0.45; \quad \gamma_1^2 = 0.50; \quad \widehat{B} = 125/27; \quad \widehat{I} = 15; \quad \widehat{M} = 15625/39966; \\
&\text{P18}: \gamma_A^2 = 0.90; \quad \gamma_1^2 = 0.05; \quad \widehat{B} = 125/54; \quad \widehat{I} = 150; \quad \widehat{M} = 15625/314928.
\end{aligned}
\tag{9}
$$

The parameter $\gamma_N = 0.5$ in the nonlinear case and has no value in the linear case (in the linear case N and M are zero). The integration interval is from zero to $T_f = 100$. In all considered cases two solitary waves that propagate in opposite directions emerge from the initial pulse (6). For point P1 five interactions between the emerged solitary waves take place in the time interval $0 < T \leq 100$. For points P9 and P18 the number of interactions in the time interval $0 < T \leq 100$ is three and one, respectively.

3.1. Numerical results

Dispersion analysis carried out in [19] shows good agreement between acoustic branches of the HE and FSE at the chosen datapoints. However, it does not take into account the optical branch of the FSE and nonlinear effects. At P1 we can see that agreement between solutions of the HE and FSE is almost perfect even after five interactions of the two emerged solitary waves (Fig. 2). The left pulse in Fig. 2 is propagating to the right and the right pulse to the left. Analysis of the results demonstrates that in the linear case (lighter curves) the right and the left propagating waves are practically identical. However, in nonlinear cases (darker curves) the solitary waves propagating to the right are sharper, narrower, and slightly lower than the right propagating solitary waves in linear cases. Vice versa, the pulses propagating to the left are wider in nonlinear cases. The waveprofiles that correspond to the HE and the waveprofiles that correspond to the FSE practically coincide
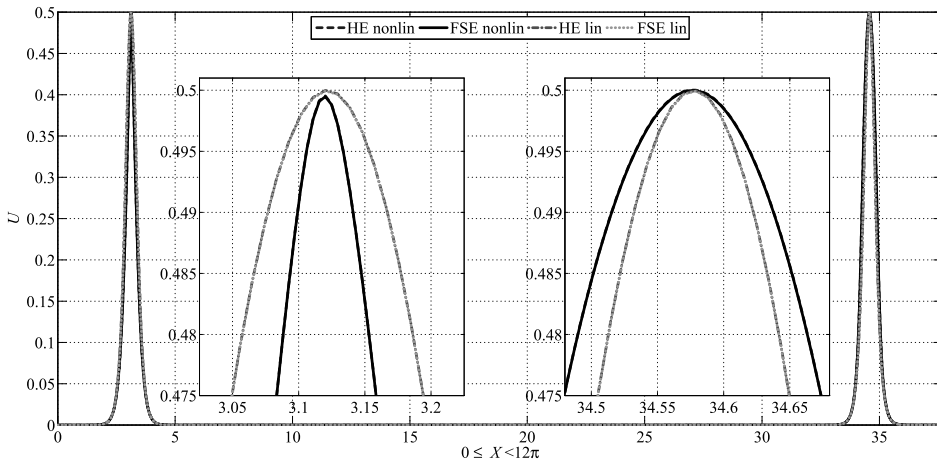
Fig. 2. Waveprofiles at the end of the integration interval for $\gamma_A^2 = 0.05$ and $\gamma_1^2 = 0.9$ (point P1 in Fig. 1).

in linear as well as in nonlinear cases. In order to measure the difference between solutions of the HE and FSE, we introduce the quantity

$$\Delta^S = \sum_{i=1}^{n} \frac{\Delta_i}{n}, \quad \text{where} \quad \Delta_i = \left| U^{\text{HE}}(X_i, T_f) - U^{\text{FSE}}(X_i, T_f) \right|, \tag{10}$$

and n is the number of gridpoints. In the linear case $\Delta^S = 4.98 \times 10^{-6}$ and in the nonlinear case $\Delta^S = 5.15 \times 10^{-6}$ at point P1.

At point P9 the agreement between the solutions of the HE and FSE is good. In Fig. 3 waveprofiles are plotted at the end of the integration interval (when three interactions between the emerged solitary waves have taken place). All waveprofiles are asymmetric. Like at point P1 the left pulse in Fig. 3 is propagating to the right and the right pulse is propagating to the left. One can see that in the nonlinear case again the right
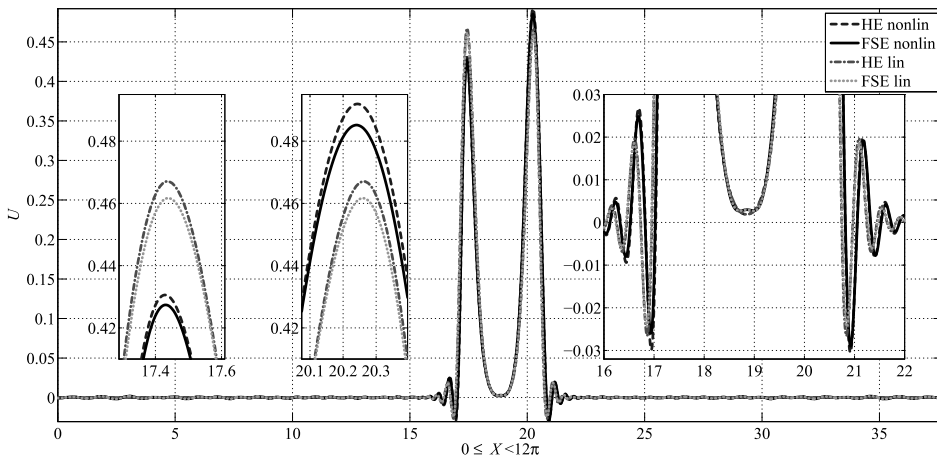
Fig. 3. Waveprofiles at the end of integration for $\gamma_A^2 = 0.45$ and $\gamma_1^2 = 0.5$ (point P9 in Fig. 1).
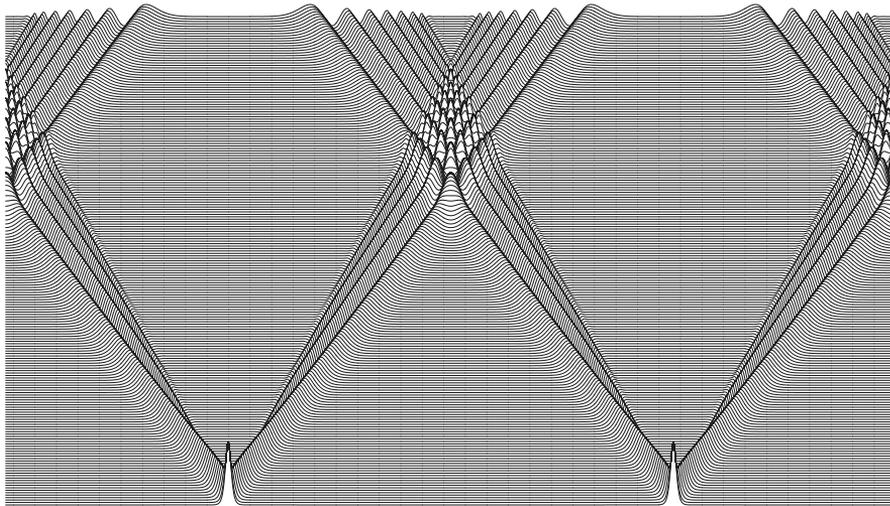
Fig. 4. Time-slice plot of the solution of the linear HE for $\gamma_A^2 = 0.9$ and $\gamma_1^2 = 0.05$ (point P18 in Fig. 1).

propagating wave is sharper and lower than the left propagating wave. However, now waves that correspond to the FSE are visibly lower than these of the HE. In the linear case both the right and left propagating waves have the same amplitude, and symmetry $U(x - 6\pi, t) = U(6\pi - x, t)$. In all cases a small tail is formed behind the solitary wave. In nonlinear cases the tails have higher amplitudes than in the linear case. In the linear case $\Delta^S = 8.02 \times 10^{-4}$ and in the nonlinear case $\Delta^S = 8.17 \times 10^{-4}$ at P9.

In order to characterize the time-space behaviour of the solution at point P18, the time-slice plot over two space periods is presented in Fig. 4. In the present case the initial solitary wave is deformed to the wave having the shape similar to the Airy function $\text{Ai}(X)$. Single waveprofiles in Fig. 5 demonstrate that after one interaction of the two emerging wave structures the agreement between the solutions of the HE and
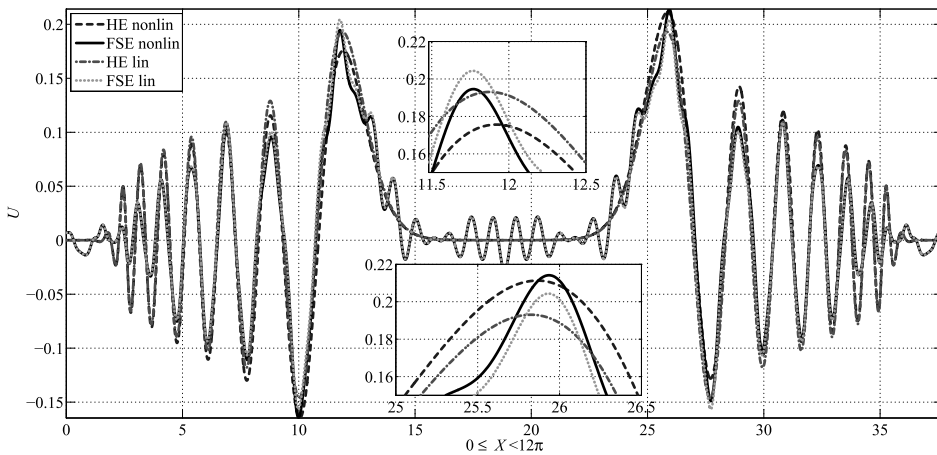
Fig. 5. Waveprofiles at the end of integration for $\gamma_A^2 = 0.9$ and $\gamma_1^2 = 0.05$ (point P18 in Fig. 1).

FSE is good at P18. Like at points P1 and P9 the waves propagating to the left and to the right have equal amplitudes in linear cases. However, now the amplitude is higher in case of the FSE. In the nonlinear case the situation is similar to that of at points P1 and P9 – waves that propagate to the right are lower than those propagating to the left. Unlike in previous cases, additional oscillations that propagate in front of the main wave-structure are generated for the FSE. These oscillations are practically identical in linear and nonlinear cases (see Fig. 5). In the linear case $\Delta^S = 0.0185$ and in the nonlinear case $\Delta^S = 0.0190$ at P18.

4. DISCUSSION AND CONCLUSIONS

Moving along the weak normal dispersion line $\Gamma = 0.05$ (Fig. 1) to the right (γ_A^2 increases), the differences between the solutions of the HE and FSE increase (Fig. 6).
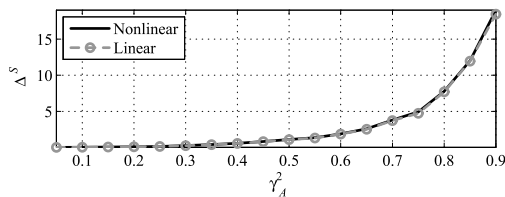
Fig. 6. Quantity Δ^S against γ_A^2 at $T = 100$.

As noted above, there are significant oscillations in front of the propagating wave-structure for higher values of γ_A^2 in case of the FSE (Fig. 5). In case of the HE one cannot detect such oscillations (Figs 4 and 5). This might be due to the fact that according to the dispersion analysis carried out in [18], the FSE has besides the acoustic dispersion curve, a second higher frequency curve. This so-called optical branch reflects internal degrees of freedom according to the hypothesis in [16] and can have a visible effect on the solutions of the FSE, similar to the results shown, for example, in [18]. However, the emergence and origin of those oscillations need futher analysis.

Overall, we may conclude that if we stay in the domain of parameters, where according to the dispersion analysis the difference between dispersion curves of the HE and FSE is less than 5%, we have, indeed, a good agreement between solutions of the HE and FSE. Specifically: (i) predictions from the dispersion analysis hold also for the nonlinear cases, however, the nonlinearity introduces additional effects not taken into account by the linear dispersion analysis; (ii) following the weak normal dispersion line, the agreement between the solutions of the HE and FSE weakens if γ_A^2 increases; (iii) the nonlinearity amplifies the asymmetry between the waveprofiles propagating in opposite directions.

As the interactions between waveprofiles propagating in opposite directions are not entirely elastic, the effect of interactions on the evolution of those waveprofiles needs detailed analysis as done in [28] for the solitary waves that correspond to the HE.

REFERENCES

1. Christov, C. I., Maugin, G. A., and Porubov, A. V. On Boussinesq's paradigm in nonlinear wave propagation. *C. R. Mecanique*, 2007, **335**, 521–535.

2. Engelbrecht, J. and Pastrone, F. Waves in microstructured solids with nonlinearities in microscale. *Proc. Estonian Acad. Sci. Phys. Math.*, 2003, **52**, 12–20.

3. Engelbrecht, J., Berezovski, A., Pastrone, F., and Braun, M. Waves in microstructured materials and dispersion. *Phil. Mag.*, 2005, **85**, 4127–4141.

4. Eringen, A. C. *Microcontinuum Field Theories I: Foundations and Solids*. Springer, Berlin, 1999.

5. Erofeev, V. I. *Wave Processes in Solids with Microstructure*. World Scientific, Singapore, 2003.

6. Fornberg, B. *A Practical Guide to Pseudospectral Methods*. Cambridge University Press, Cambridge, 1998.

7. Frigo, M. and Johnson, S. G. The design and implementation of FFTW3. *Proc. IEEE*, 2005, **93**, 216–231.

8. Hindmarsh, A. C. Odepack, a systematized collection of ODE solvers. In *Scientific Computing* (Stepleman, R. S. et al., eds). North-Holland, Amsterdam, 1983, 55–64.

9. Ilison, L. and Salupere, A. Propagation of sech^2-type solitary waves in hierarchical KdV-type systems. *Math. Comput. Simulat.*, 2009, **79**, 3314–3327.

10. Ilison, L., Salupere, A., and Peterson, P. On the propagation of localized perturbations in media with microstructure. *Proc. Estonian Acad. Sci. Phys. Math.*, 2007, **56**, 84–92.

11. Janno, J. and Engelbrecht, J. An inverse solitary wave problem related to microstructured materials. *Inverse Problems*, 2005, **21**, 2019–2034.

12. Janno, J. and Engelbrecht, J. Solitary waves in nonlinear microstructured materials. *J. Phys. A: Math. Gen.*, 2005, **38**, 5159–5172.

13. Jones, E., Oliphant, T., Peterson, P. et al. SciPy: Open source scientific tools for Python, http://www.scipy.org, 2007.

14. Kreiss, H.-O. and Oliger, J. Comparison of accurate methods for the integration of hyperbolic equations. *Tellus*, 1972, **30**, 341–357.

15. Maugin, G. *Nonlinear Waves in Elastic Crystals*. Oxford University Press, Oxford, 1999.

16. Metrikine, A. V. On causality of the gradient elasticity models. *J. Sound Vib.*, 2006, **297**, 727–742.

17. Mindlin, R. D. Micro-structure in linear elasticity. *Arch. Rat. Mech. Anal.*, 1964, **16**, 51–78.

18. Peets, T. and Tamm, K. Dispersion analysis of wave motion in microstructured solids. In *IUTAM Symposium on Recent Advances of Acoustic Waves in Solids* (Tsung-Tsong Wu and Chien-Ching Ma, eds). Springer, Berlin, 2009 (accepted).

19. Peets, T., Randrüüt, M., and Engelbrecht, J. On modelling dispersion in microstructured solids. *Wave Motion*, 2008, **45**, 471–480.

20. Peterson, P. F2PY: Fortran to Python interface generator, http://cens.ioc.ee/projects/f2py2e/ (2005).

21. Porubov, A. V. *Amplification of Nonlinear Strain Waves in Solids*. World Scientific, Hong Kong, 2003.

22. Randrüüt, M. and Braun, M. On one-dimensional solitary waves in microstructured solids. *Wave Motion*, 2010, **47**, 217–230.

23. Randrüüt, M., Salupere, A., and Engelbrecht, J. On modelling wave motion in microstructured solids. *Proc. Estonian Acad. Sci.*, 2009, **58**, 241–246.

24. Salupere, A. The pseudospectral method and discrete spectral analysis. In *Applied Wave Mathematics* (Quak E. and Soomere, T., eds). Springer, Berlin, 2009, 301–334.

25. Salupere, A., Engelbrecht, J., and Peterson, P. On the long-time behaviour of soliton ensembles. *Math. Comput. Simulat.*, 2003, **62**, 137–147.

26. Salupere, A., Tamm, K., Engelbrecht, J., and Peterson, P. On the interaction of deformation waves in microstructured solids. *Proc. Estonian Acad. Sci. Phys. Math.*, 2007, **56**, 93–99.

27. Salupere, A., Ilison, L., and Tamm, K. On numerical simulation of propagation of solitons in microstructured media. In *Proceedings of the 34th Conference on Applications of Mathematics in Engineering and Economics (AMEE '08), Volume 1067 of AIP Conference Proceedings* (Todorov, M. D., ed.). American Institute of Physics, 2008, 155–165.

28. Salupere, A., Tamm, K., and Engelbrecht, J. Numerical simulation of interaction of solitary deformation waves in microstructured solids. *Int. J. Non-Linear Mech.*, 2008, **43**, 201–208.

Üksiklainete formeerumine Mindlini-tüüpi mikrostruktuursetes tahkistes

Kert Tamm ja Andrus Salupere

Lainelevi modelleerimiseks Mindlini-tüüpi mikrostruktuursetes tahkistes on kasutatud Jüri Engelbrechti ja Franco Pastrone tuletatud mudelit. Vaadeldav mudel kirjeldab mikrostruktuuriga füüsikaliselt mitte-lineaarset materjali, kus mittelineaarsus esineb nii mikro- kui makrotasandil. Numbrilised lahendid on leitud nn täielikule võrrandisüsteemile (4) ja sellest allutusprintsiibi abil tuletatud hierarhilisele võrrandile (5). Saadud lahendeid on võrreldud nii lineaarsel kui mittelineaarsel juhul. On näidatud, et vaadeldud parameetrite piirkonnas on lahendite kokkulangevus hea.

Publication VI

K. Tamm and A. Salupere
On the propagation of 1D solitary waves in Mindlin-type microstructured solids.

Accepted Manuscript

Title: On the propagation of 1D solitary waves in Mindlin-type microstructured solids

Authors: Kert Tamm, Andrus Salupere

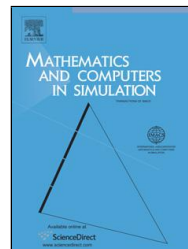Please cite this article as: K. Tamm, A. Salupere, On the propagation of 1D solitary waves in Mindlin-type microstructured solids, *Mathematics and Computers in Simulation* (2008), doi:10.1016/j.matcom.2010.06.022

On the propagation of 1D solitary waves in Mindlin-type microstructured solids.

Kert Tamm [a,b], Andrus Salupere [a,b,*]

[a] *Centre for Nonlinear Studies, Institute of Cybernetics at Tallinn University of Technology, Akadeemia tee 21, 12618, Tallinn, Estonia*

[b] *Department of Mechanics, Tallinn University of Technology, Ehitajate tee 5, 19086, Tallinn, Estonia*

Abstract

The Mindlin model and hierarchical approach by Engelbrecht and Pastrone are used for modelling 1D wave propagation in microstructured solids. After introducing the free energy function, one gets from Euler–Lagrange equations a system of equations of motion. Making use of the slaving principle, a nonlinear hierarchical wave equation can be derived. Equations are solved numerically under localized initial conditions. For numerical integration the pseudospectral method based on the Fourier transform is used. The influence of free energy parameters on the character of dispersion and wave propagation is studied. Numerical results of hierarchical approximation and the full equation system will be compared and the quality of the approximation will be discussed.

Key words: Nonlinearity, Microstructured solids, Solitons, Dispersion, Granular materials, Pseudospectral methods

1 Introduction

In applications of microstructured materials adequate testing methods are needed in order to evaluate the properties of such materials. Studies involving nonlinear wave propagation in continuous media with microstructure have considerably increased in the recent years (see e.g. [3,6,17,23,24] and references

---

* Corresponding author.
  Email addresses: `kert@cens.ioc.ee` (Kert Tamm), `salupere@ioc.ee` (Andrus Salupere).

therein). Microstructured materials are characterized by the existence of intrinsic space-scales in matter like the size of a grain or a crystallite, lattice period, distance between the microcracks, etc., that introduce some scale-dependence into the governing equations [3]. The scale-dependence involves dispersive as well as nonlinear effects, and if these two effects are balanced, solitary waves and solitons can exist in such media.

The basic model derived by Engelbrecht and Pastrone [4] is based on Mindlin's and Eringen's earlier works. In this approach the microelement is taken as a deformable cell (with rigid cells one would get the Cosserat model). The displacement u of a material particle in terms of macrostructure is defined by its components $u_i \equiv x_i - X_i$. At each material point there is attached a microstructure described kinematically by a microdisplacement u' defined by its components $u'_i \equiv x'_i - X'_i$. If the displacement gradient is small, one can assume that the origin of the coordinates x'_i and X'_i moves with the macroscale displacement u. This is one of Mindlin's basic assumptions, which allows one to express microdeformation in terms of macrodisplacement. The fundamental balance laws for microstructured materials can be formulated separately for macro- and microscale [5]. In the 1D case the balance laws can be derived from the Lagrangian

$$L = K - W, \tag{1}$$

formed from the kinetic and potential energies

$$K = \frac{1}{2}\rho u_t^2 + \frac{1}{2}I\varphi_t^2, \quad W = W(u_x, \varphi, \varphi_x). \tag{2}$$

Here ρ denotes the macroscopic density, I the microinertia, u the macrodisplacement and φ the microdeformation. The subscript x denotes the spatial partial derivative and the subscript t the partial derivative with respect to time. Using Euler–Lagrange equations, one will arrive at the equations of motion

$$\rho u_{tt} - \left(\frac{\partial W}{\partial u_x}\right)_x = 0, \quad I\varphi_{tt} - \left(\frac{\partial W}{\partial \varphi_x}\right)_x + \frac{\partial W}{\partial \varphi} = 0. \tag{3}$$

The partial derivatives

$$\sigma = \frac{\partial W}{\partial u_x}, \quad \eta = \frac{\partial W}{\partial \varphi_x}, \quad \tau = \frac{\partial W}{\partial \varphi}, \tag{4}$$

are known as the macrostress, microstress and interactive force, respectively [3]. With the use of (4), equations of motion (3) take a familiar form

$$\rho u_{tt} = \sigma, \quad I\varphi_{tt} = \eta_x - \tau. \tag{5}$$

2

In the 1D nonlinear case the free (potential) energy W can be written as

$$W = \frac{A}{2}u_x^2 + \frac{B}{2}\varphi^2 + \frac{C}{2}\varphi_x^2 + D\varphi u_x + \frac{N}{6}u_x^3 + \frac{M}{6}\varphi_x^3, \qquad (6)$$

where parameters A, B, C, D are responsible for the linear part of the model and N, M are responsible for the nonlinearity in macro- and microscale, respectively [12]. Inserting energy function (6) into equations (4) and (5) results in the equations of motion

$$\rho u_{tt} = D\varphi_x + Au_{xx} + Nu_x u_{xx},$$
$$I\varphi_{tt} = C\varphi_{xx} + M\varphi_x\varphi_{xx} - B\varphi - Du_x. \qquad (7)$$

For further analysis dimensionless variables are introduced [12]:

$$X = \frac{x}{L_o}, \quad T = \sqrt{\frac{A}{\rho}}\frac{t}{L_o}, \quad U = \frac{u}{A_o}, \quad \delta = \frac{l_o^2}{L_o^2}, \quad \varepsilon = \frac{A_o}{L_o}. \qquad (8)$$

Here A_o is the amplitude of the initial excitation, L_o is the wavelength of the initial excitation and l_o is the characteristic scale of the microstructure. Making use of expressions (8), the dimensionless equations of motion are obtained:

$$U_{TT} = \frac{DL_o}{AA_o}\varphi_X + \frac{NA_o}{AL_o}U_X U_{XX} + U_{XX},$$
$$\varphi_{TT} = \frac{C\rho}{AI}\varphi_{XX} - \frac{B\rho L_o^2}{AI}\varphi - \frac{D\rho A_o L_o}{AI}U_X + \frac{M\rho}{AIL_o}\varphi_X\varphi_{XX}. \qquad (9)$$

Equations (9) are referred to as the 'Full Equation System' (FES for short) below. Applying the slaving principle [3,22], a single equation in terms of the macrodisplacement U can be derived from the FES:

$$U_{TT} - bU_{XX} + 0.5\mu(U_X^2)_X = \delta(\beta U_{TT} - \gamma U_{XX} - 0.5\sqrt{\delta}\lambda U_{XX}^2)_{XX}, \qquad (10)$$

where

$$b = 1 - \frac{D^2}{AB}, \quad \mu = \frac{NA_o}{AL_o}, \quad \beta = \frac{ID^2}{\rho l_o^2 B^2}, \quad \gamma = \frac{CD^2}{AB^2 l_o^2}, \quad \lambda = \frac{D^3 MA_o}{AB^3 l_o^3 L_o}. \qquad (11)$$

Equation (10) is hierarchical in Whitham's sense and can be considered as an approximation of FES (9). Equation (10) is referred to as 'the hierarchical equation' (HE) below. On the other hand, the HE is of Boussinesq type [2]. In a nutshell, the slaving principle is a technique that allows elimination of the microdeformation φ from FES (9). The corresponding procedure is described in detail in papers [3,20]. It is clear that the macrodisplacement u is easier to measure than the microdeformation φ. Therefore the macrodisplacement u can be used in applications. Furthermore, Janno and Engelbrecht have proved the existence of the solution of the inverse solitary wave problem for the HE, i.e., they have shown that material parameters in equation (10) can be determined

3

from wave propagation parameters (wave speed, amplitude changes or phase shifts) [12].

The main aim of this paper is to compare the propagation of sech^2-type solitary waves in the Mindlin-type microstructured solid for the HE and FES in the range of parameters where both macro- and microstructure are taken into account. The paper is organized as follows. In Section 2 the problem is stated. In Section 3 the numerical technique is described. Different dispersion cases are introduced and discussed in Section 4, followed by relevant discussion and conclusions.

2   Statement of the problem

In order to simulate numerically the propagation of solitary waves in Mindlin-type microstructured solid, equations HE (10) and FES (9) are numerically integrated under the sech^2-type localized initial conditions and periodic boundary conditions

$$U(X,0) = A_o \, \text{sech}^2(\frac{B_o X}{2}), \quad U(X,T) = U(X+2k\pi, T), \quad \text{k} = 1,2,\ldots, \quad (12)$$

where $A_o = 1$ is the amplitude of the initial pulse and $B_o = \pi$ is the width parameter. For numerical integration the pseudospectral method (PSM) based on the discrete Fourier transform (DFT) is used. Periodic boundary conditions have period of 2π. For speed we use the initial condition

$$U(X,0)_T = -c \cdot U(X,0)_X, \quad \text{with} \quad U(X,T) = U(\xi), \quad \xi = X - cT, \quad (13)$$

where c is the phase speed of the initial wave. If the nonlinearity is sufficiently weak one can use

$$c = \sqrt{1 - \frac{D^2}{AB}}, \quad (14)$$

as the initial phase speed estimate that corresponds to the phase speed of the classical wave equation. For the FES two more initial conditions are needed for microstructure;

$$\varphi(X,0) = 0, \qquad \varphi(X,0)_T = 0. \quad (15)$$

The goals of the present paper are:

(1) To solve HE (10) and FES (9) under localized initial conditions for three different cases:

- dispersionless case,
- normal dispersion case,
- anomalous dispersion case.

(2) To compare solutions of the HE and FES for the linear and nonlinear case.

3 Numerical technique

As stated in Section 2, the DFT-based PSM [7,16,25,27] is applied in numerical integration in the present study. We use the following version of the DFT:

$$
\widehat{U}(k,t) = \mathrm{F}U = \sum_{j=0}^{n-1} U(j\Delta x, t) \exp\left(-\frac{2\pi i j k}{n}\right), \tag{16}
$$

where n is the number of space-grid points, $\Delta x = 2\pi/n$ – the space step, i – the imaginary unit, $k = 0, \pm 1, \pm 2, \ldots, \pm(n/2 - 1), -n/2$ and F denotes the DFT. Now partial derivatives of U with respect to the space coordinate X

$$
\frac{\partial^n U}{\partial X^n} = \mathrm{F}^{-1}\left[(ik)^n \mathrm{F}(U)\right], \tag{17}
$$

where F^{-1} denotes the inverse DFT. According to the idea of the PSM, the partial derivatives with respect to the space coordinate are approximated by making use of formula (17), thereby reducing a PDE to an ODE and allowing for straightforward integration with an ODE solver.

The regular PSM algorithm is derived for $u_t = \Phi(u, u_x, u_{2x}, \ldots, u_{nx})$ type equations. However, in our case HE (10) includes a mixed partial derivative and therefore the standard PSM has to be modified [10,11,26,28]. We start by writing HE (10) so that all partial derivatives with respect to time are in the LHS. In order to apply the PSM, we have to introduce a new variable

$$
\Phi = U - \frac{ID^2}{B^2 L_o^2 \rho} U_{XX}. \tag{18}
$$

Expression (18) can be rewritten as

$$
\Phi = \mathrm{F}^{-1}\left[\left(1 + \frac{ID^2}{B^2 L_o^2 \rho} k^2\right) \mathrm{F}(U)\right]. \tag{19}
$$

From equation (19), in turn, the dimensionless macrodisplacement U can be expressed as

$$
U = \mathrm{F}^{-1}\left[\frac{\mathrm{F}(\Phi)}{1 + \frac{ID^2}{B^2 L_o^2 \rho} k^2}\right]. \tag{20}
$$

5

Taking (20) into account, partial derivatives of U can be expressed as

$$\frac{\partial^n U}{\partial X^n} = F^{-1} \left[\frac{(ik)^n F(\Phi)}{1 + \frac{ID^2}{B^2 L_o^2 \rho} k^2} \right], \tag{21}$$

which allow us to express the HE in the form suitable for the application of the PSM

$$\begin{aligned}
\Phi_{TT} = {} & \left(1 - \frac{D^2}{AB} \right) U_{XX} - \frac{CD^2}{AB^2 L_o^2} U_{XXXX} \\
& + \frac{N}{\varepsilon A} U_X U_{XX} + \frac{M \varepsilon D^3 \sqrt{\delta}}{AB^3 l_o L_o^2} \left(U_{XX} U_{XXXX} + U_{XXX}^2 \right).
\end{aligned} \tag{22}$$

In other words, in equation (22) all partial derivatives of U with respect to X are calculated in terms of Φ by making use of expression (21).

In the present paper calculations are carried out with the package SciPy [14] using: the FFTW library [8] for the DFT and the F2PY [21] generated Python interface to the ODEPACK Fortran code [9] for the ODE solver.

4 Results and discussion

According to papers [3,13], the dispersion type can be determined by the sign of quantity

$$\Gamma = 1 - \gamma_1^2 - \gamma_A^2, \quad \text{where} \quad \gamma_A^2 = \frac{D^2}{AB}, \quad \gamma_1^2 = \frac{\rho C}{AI}. \tag{23}$$

Here γ_1 can be interpreted as the dimensionless speed of short (high-frequency) waves and $\sqrt{1 - \gamma_A^2}$ as the dimensionless speed of long (low-frequency) waves. If Γ is positive, we have the normal dispersion case (the phase speed is higher than the group speed), if negative, the anomalous dispersion case (the group speed is higher than the phase speed) and if equal to zero, we have the dispersionless case (the phase speed and the group speed are equal).

All together we have 11 different parameters – 8 physical (6 energy parameters, macroscale density and microinertia) and 3 geometrical (amplitude and wavelength of the initial excitation and the scale of the microstructure).

According to the (linear) dispersion analysis carried out in [20], the dispersive properties of the FES and HE are in good agreement in the range of parameters shown in Fig. 1. Solid lines in the figure represent a 5% difference between the acoustical branches of the dispersion curves of the HE and FES and the dashed line represents all parameter combinations resulting in the dispersionless case

6
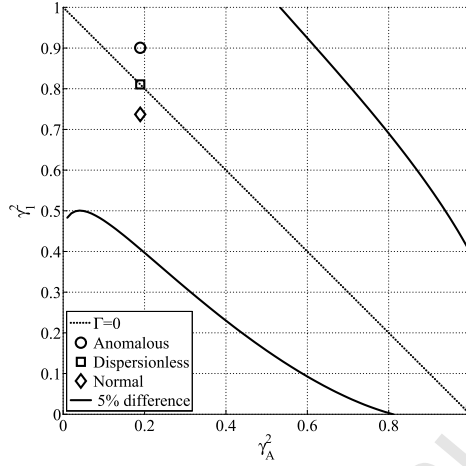
Fig. 1. Domain in the $\gamma_A^2 - \gamma_1^2$ plane where the HE and FES are in good agreement.

i.e., $\Gamma = 0$. In [20] the good agreement between the FES and the HE is defined as smaller than the 5% difference between the acustical branches of the HE and FES at the dimensionless wavenumber $\xi = k\sqrt{(AI)/(B\rho)} = 1.5$, where k is the wavenumber and A, I, B, ρ are the same parameters as in (9) and (11). In Fig. 1 above the dashed line we have the anomalous dispersion type and under the dashed line the normal dispersion type. We say that between those two solid curves we have good agreement between the HE and the FES (in the sense of dispersion).

Three dispersion cases are considered below, with the following values of parameters. (1) For the dispersionless case:

$$
\begin{aligned}
&A = 12, \quad B = 11, \quad C = 7, \quad D = 5, \quad N = 0 \text{ and } 1, \quad M = 0 \text{ and } 0.1; \\
&A_o = 1, \quad l_o = 1, \quad L_o = 15, \quad \rho = 13, \quad I = 9.3551;
\end{aligned} \tag{24}
$$

resulting in $\gamma_A^2 = 0.1894$ and $\gamma_1^2 = 0.8106$, marked with a square in Fig. 1.

(2) For the normal dispersion case:

$$
\begin{aligned}
&A = 12, \quad B = 11, \quad C = 7, \quad D = 5, \quad N = 0 \text{ and } 1, \quad M = 0 \text{ and } 0.1; \\
&A_o = 1, \quad l_o = 1, \quad L_o = 15, \quad \rho = 13, \quad I = 10.2897;
\end{aligned} \tag{25}
$$

resulting in $\gamma_A^2 = 0.1894$ and $\gamma_1^2 = 0.7370$, marked with a diamond in Fig. 1.

(3) For the anomalous dispersion case:

$$
\begin{aligned}
&A = 12, \quad B = 11, \quad C = 7, \quad D = 5, \quad N = 0 \text{ and } 1, \quad M = 0 \text{ and } 0.1; \\
&A_o = 1, \quad l_o = 1, \quad L_o = 15, \quad \rho = 13, \quad I = 8.4206;
\end{aligned} \tag{26}
$$

7

resulting in $\gamma_A^2 = 0.1894$ and $\gamma_1^2 = 0.9006$, marked with a circle in Fig. 1.

The only parameter that is different in sets (24), (25) and (26) is microinertia I. In the linear case we will set free energy parameters N and M to zero and in the nonlinear case to 1 and 0.1, respectively. The integration interval is from $T = 0$ to $T = 50$. However, in the figures below, the waveprofiles and phase diagrams are presented at $T = 49$ when the waveprofiles are located in the middle of the space period. The curves that correspond to the HE are plotted by (red) dashed lines and the curves corresponding to the FES by (black) solid lines. Phaseplots are used to highlight small differences in the waveprofiles and to emphasise the asymmetry of the propagating pulses. For the harmonic wave $U_X - U$ phaseplot results in a circle and in the case of the sech^2-type profile, has the shape of a water drop.
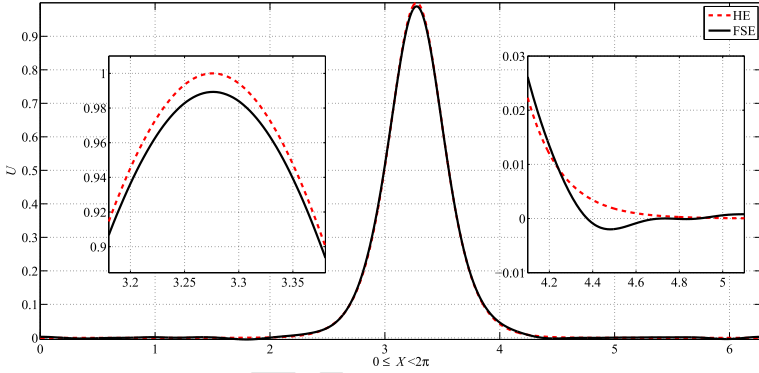
Fig. 2. Waveprofiles at $T = 49$ for the linear dispersionless case.

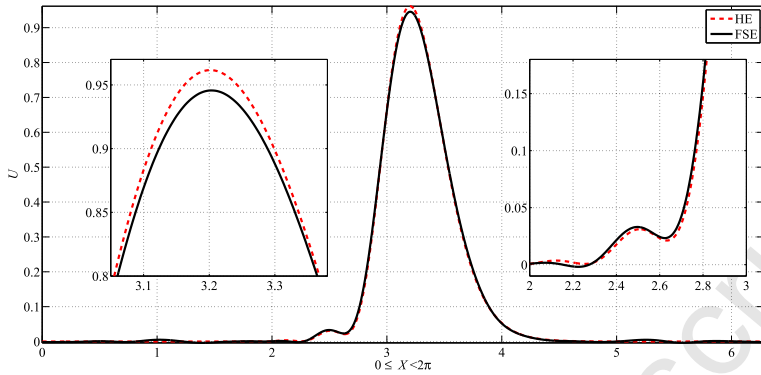Fig. 3. Waveprofiles at $T = 49$ for the nonlinear dispersionless case.

8
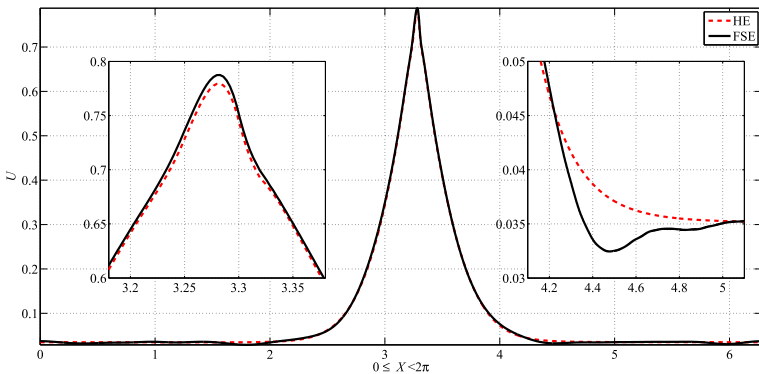
4.1 Dispersionless case

In the dispersionless case (see Figs. 2–7) we have good agreement between the results of the HE and FES as predicted by the dispersion analysis in [20]. In the linear case the waveprofiles practically coincide at the end of the integration interval (see Figs. 2, 4 and 6). Figure 4 demonstrates that in case of the HE as well as the FES the pulse propagates with a constant amplitude and small deviation between the HE and the FES takes place at the very beginning of the integration interval. Small differences in the waveprofiles are easier to spot in the phase diagram in Fig. 6. In the nonlinear dispersionless case the agreement between the waveprofiles is better (Figs. 3, 5 and 7). However, in that case the waveprofile morphs into a peakon-type profile [1,15], as can be seen in Figs. 3 and 7, and the amplitude of the pulse decreases more than 20% during the integration interval (Fig. 5).
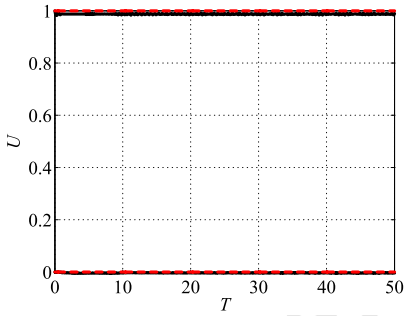
Fig. 4. Waveprofile minima and maxima for the linear dispersionless case.
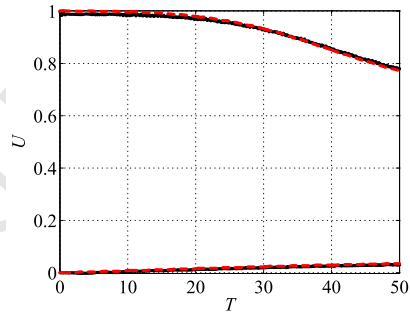
Fig. 5. Waveprofile minima and maxima for the nonlinear dispersionless case.
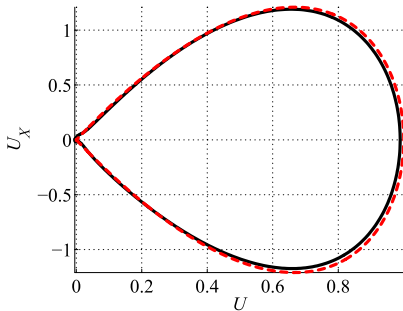
Fig. 6. Phaseplot $U_X - U$ at $T = 49$ for the linear dispersionless case.
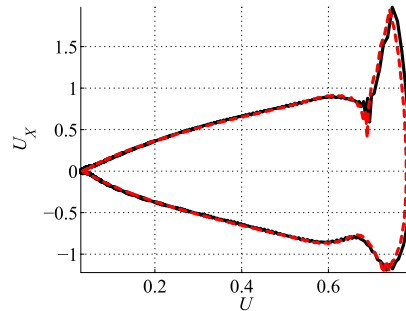
Fig. 7. Phaseplot $U_X - U$ at $T = 49$ for the nonlinear dispersionless case.

9

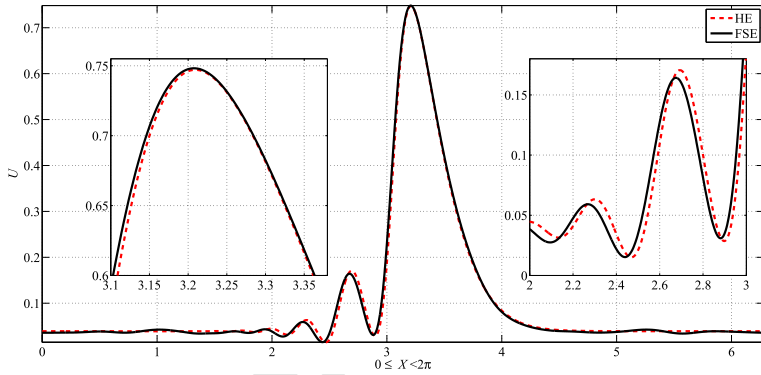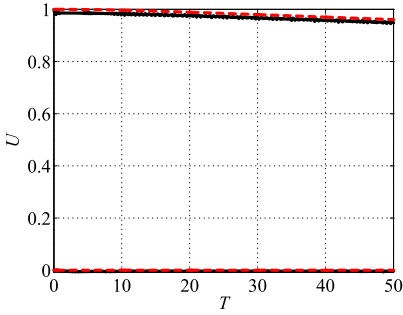Fig. 8. Waveprofiles at $T = 49$ for the linear normal dispersion case.

Fig. 9. Waveprofiles at $T = 49$ for the nonlinear normal dispersion case.

4.2 Normal dispersion case

In the normal dispersion case (see Figs. 8–13) we have good agreement between the results of the HE and FES. In the linear case the waveprofiles almost coincide at the end of the integration interval (Fig. 8) and waveprofile maxima and minima are in good agreement during the whole integration interval (Fig. 10). Good agreement between the waveprofiles is apparent in the phaseplot at $T = 49$ in Fig. 12. In the nonlinear case the 'main part' of the waveprofile has even better agreement than in the linear case (cf. Figs. 9 and 13). However, as can be seen in Figs. 9 and 13, differences in the 'tail part' of the waveprofile are more distinctive for the nonlinear case. In the nonlinear normal dispersion case the amplitude of the pulse decreases more than 25% during the integration interval (Fig. 11).

10

Fig. 10. Waveprofile minima and maxima for the linear normal dispersion case.
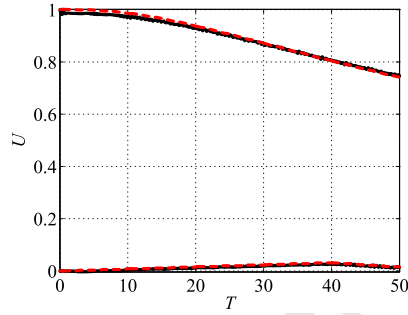

Fig. 11. Waveprofile minima and maxima for the nonlinear normal dispersion case.
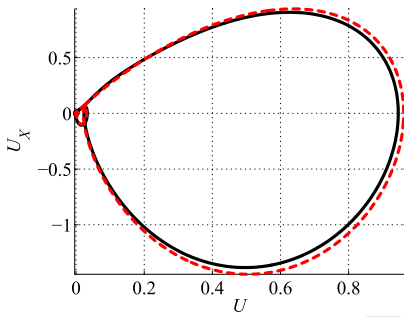

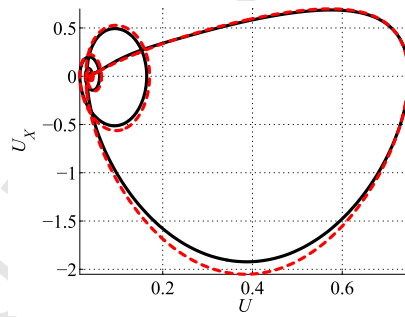Fig. 12. Phaseplot $U_X - U$ at $T = 49$ for the linear normal dispersion case.

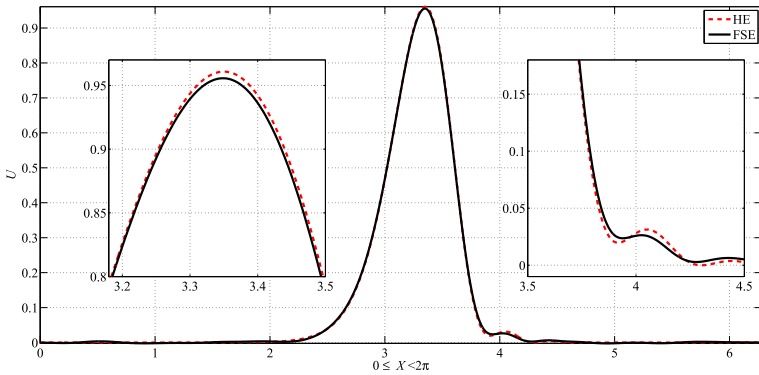Fig. 13. Phaseplot $U_X - U$ at $T = 49$ for the nonlinear normal dispersion case.

Fig. 14. Waveprofiles at $T = 49$ for the linear anomalous dispersion case.

4.3   Anomalous dispersion case

In the anomalous dispersion case(see Figs. 14–19) we have good agreement between the results of the HE and FES regarding time dependencies of wave-
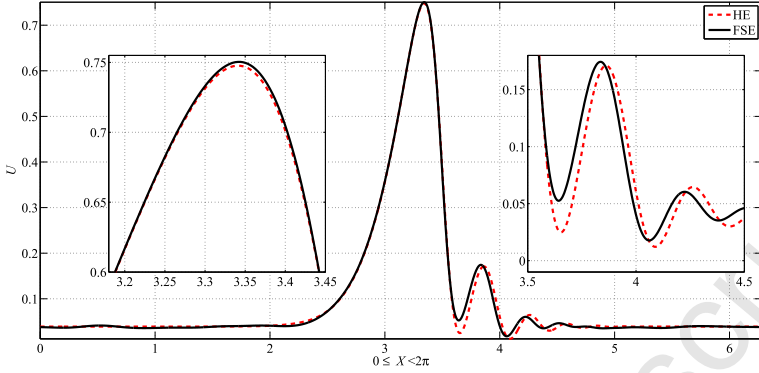
11

Fig. 15. Waveprofiles at $T = 49$ for the nonlinear anomalous dispersion case.
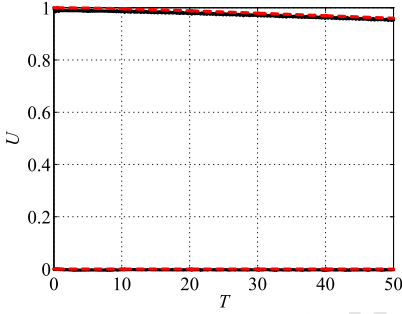

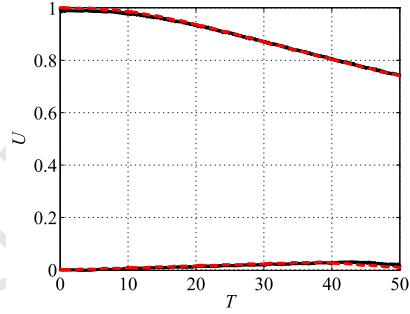Fig. 16. Waveprofile minima and maxima for the linear anomalous dispersion case.

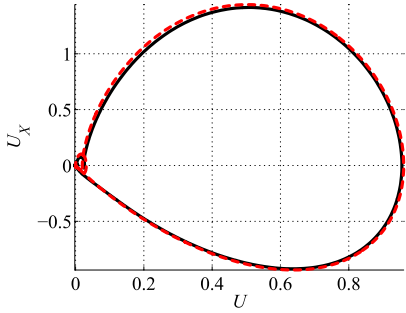Fig. 17. Waveprofile minima and maxima for the nonlinear anomalous dispersion case.

Fig. 18. Phaseplot $U_X - U$ at $T = 49$ for the linear anomalous dispersion case.
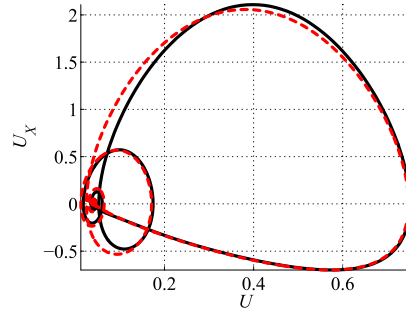

Fig. 19. Phaseplot $U_X - U$ at $T = 49$ for the nonlinear anomalous dispersion case.

profile maxima and minima (Figs. 16 and 17) and the shape of the 'main part' of the waveprofile (Figs. 14, 15, 18 and 19). However, noticeable differ-

ences between the 'tail parts' of the waveprofiles that correspond to the HE or the FES can be detected for the nonlinear case (Figs. 15 and 19). In case of anomalous dispersion the speed of short waves is higher than that of long waves and therefore the tail is formed in front of the pulse.

4.4 Discussion

The difference between solutions of the HE and FES in the 'tail part' of the waveprofile is more distinctive in the nonlinear anomalous case (see Fig. 19) than in the nonlinear dispersionless (see Fig. 7) and nonlinear normal dispersion case (Fig. 13). This might be due to the fact that according to the dispersion analysis carried out in [19], the FES has besides the acoustical dispersion curve, another, higher-frequency curve. This so-called optical branch reflects the influence of internal degrees of freedom according to a hypothesis posed in [19] and has certain influence on the solutions of the FES, similar to the results shown, for example, in [18]. Our analysis has shown that the optical branch in the FES is not strong enough to dominate over the acoustical branch and to give rise to the situation where the HE and FES have different dispersion types. This phenomenon, however, needs further analysis. In the dispersionless case the solution of the FES has very small oscillations with anomalous character (optical branch is of the anomalous dispersion type) but it is not entirely clear whether they are caused by the optical branch or have some other character. For example, application of incorrect initial speed estimate can cause the initial pulse to split into two waves, where one is propagating in the direction defined by the initial phase speed and the other in the opposite direction.

One can to see that the direction of the asymmetry of waveprofiles is dependent on the dispersion type (Figs. 8 and 9 versus Figs. 14 and 15) and that the nonlinearity accelerates the emergence of asymmetry (Figs. 8,12,14 and 18 versus 9,13,15 and 19).

5   Conclusions

We have good agreement between the solutions of the HE and FES if we stay in the domain of parameters where according to the dispersion analysis, the difference of dispersion curves of the HE and FES is less than 5%.

- Dispersionless case
(1) For the dispersionless case we have good agreement between solutions of the HE and FES.

13

(2) In the linear case the waveprofile conserves its shape and maximum amplitude.

(3) In the nonlinear case the waveprofile morphs into a peakon-type profile and loses over 20% of its maximum amplitude over the integration interval.

- Normal dispersion case

(1) For the normal dispersion case we have good agreement between the solutions of the HE and FES.

(2) In the linear case the waveprofiles that correspond to the HE practically coincide with these corresponding to the FES.

(3) In the nonlinear case the 'main pulses' of the HE and FES are in good agreement, but small differences can be detected in the 'tail part'.

(4) The maximum amplitude of the waveprofile decreases more than 5% for the linear case and more than 25% for the nonlinear case.

- Anomalous dispersion case

(1) In the anomalous dispersion case we have good agreement between the solutions of the HE and FES.

(2) In the linear case the solutions of the HE and FES practically coincide.

(3) In the nonlinear case the 'main pulses' of the HE and FES are in good agreement, but noticeable differences can be detected in the 'tail part'.

(4) The maximum amplitude of the waveprofile decreases more than 5% for the linear case and more than 25% for the nonlinear case.

- The direction of the asymmetry of waveprofiles depends on the dispersion type.

- Nonlinearity accelerates the emergence of the asymmetry of waveprofiles.

The interaction of solitary waves that correspond to the FES needs detailed analysis as done in [29] for solitary waves corresponding to the HE.

Acknowledgements

References

[1] R. Camassa, D. D. Holm, An integrable shallow water equation with peaked solitons, Physical Review Letters 71 (1993) 1661–1664.

[2] C. I. Christov, G. A. Maugin, A. V. Porubov, On Boussinesq's paradigm in nonlinear wave propagation, C. R. Mecanique 335 (2007) 521–535.

14

[3] J. Engelbrecht, A. Berezovski, F. Pastrone, M. Braun, Waves in microstructured materials and dispersion, Phil. Mag. 85 (2005) 4127–4141.

[4] J. Engelbrecht, F. Pastrone, Waves in microstructured solids with nonlinearities in microscale, Proc. Estonian Acad. Sci. Phys. Math. 52 (2003) 12–20.

[5] A. C. Eringen, Microcontinuum Field Theories I: Foundations and Solids, Springer, Berlin, 1999.

[6] V. I. Erofeev, Wave Processes in Solids with Microstructure, World Scientific, Singapore, 2003.

[7] B. Fornberg, A Practical Guide to Pseudospectral Methods, Cambridge University Press, Cambridge, 1998.

[8] M. Frigo, S. G. Johnson, The design and implementation of FFTW3, Proc. IEEE 93 (2) (2005) 216–231.

[9] A. C. Hindmarsh, Odepack, a systematized collection of ODE solvers, in: R. S. Stepleman, et al. (eds.), Scientific Computing, North-Holland, Amsterdam, 1983, pp. 55–64.

[10] L. Ilison, A. Salupere, P. Peterson, On the propagation of localised perturbations in media with microstructure, Proc. Estonian Acad. Sci. Phys. Math. 56 (2007) 84–92.

[11] L. Ilison, A. Salupere, Propagation of sech^2-type solitary waves in hierarchical KdV-type systems, Mathematics and Computers in Simulation 79 (2009) 3314–3327.

[12] J. Janno, J. Engelbrecht, An inverse solitary wave problem related to microstructured materials, Inverse Problems 21 (2005) 2019–2034.

[13] J. Janno, J. Engelbrecht, Solitary waves in nonlinear microstructured materials, J. Phys. A: Math. Gen. 38 (2005) 5159–5172.

[14] E. Jones, T. Oliphant, P. Peterson, et al., SciPy: Open source scientific tools for Python, http://www.scipy.org (2007).

[15] H. Kalisch, J. Lenells, Numerical study of traveling-wave solutions for the Camassa–Holm equation, Chaos, Solitons and Fractals 25 (2005) 287–298.

[16] H.-O. Kreiss, J. Oliger, Comparison of accurate methods for the integration of hyperbolic equations, Tellus 30 (1972) 341–357.

[17] G. A. Maugin, Nonlinear Waves in Elastic Crystals, Oxford Univ. Press, Oxford, 1999.

[18] A. V. Metrikine, On causality of the gradient elasticity models, Journal of Sound and Vibration 297 (2006) 727–742.

[19] T. Peets, K. Tamm, Dispersion Analysis of Wave Motion in Microstructured Solids, in: Tsung-Tsong Wu and Chien-Ching Ma (eds), IUTAM Symposium on Recent Advances of Acoustic Waves in Solids, Springer, Berlin, (accepted) .

[20] T. Peets, M. Randrüüt, J. Engelbrecht, On modelling dispersion in microstructured solids, Wave Motion 45 (2008) 471–480.

[21] P. Peterson, F2PY: Fortran to Python interface generator, http://cens.ioc.ee/projects/f2py2e/ (2005).

[22] A. V. Porubov, Amplification of Nonlinear Strain Waves in Solids, World Scientific, Hong Kong, 2003

[23] M. Randrüüt, M. Braun, On One-dimensional Solitary Waves in Microstructured Solids, Wave Motion 47 (2010) 217–230.

[24] M. Randrüüt, A. Salupere, J. Engelbrecht, On modelling wave motion in microstructured solids, Proc. Estonian Acad. Sci. Phys. Math. 58 (2009) 241–246.

[25] A. Salupere, On the application of the pseudospectral method for solving the Korteweg–de Vries equation, Proc. Estonian Acad. Sci. Phys. Math. 44 (1) (1995) 73–87.

[26] A. Salupere, The Pseudospectral Method and Discrete Spectral Analysis, in: Ewald Quak and Tarmo Soomere (eds), Applied Wave Mathematics – Selected Topics in Solids, Fluids and Mathematical Methods, Springer, Berlin, (2009) 301–334.

[27] A. Salupere, J. Engelbrecht, P. Peterson, On the long-time behaviour of soliton ensembles, Math. Comput. Simulation 62 (2003) 137–147.

[28] A. Salupere, L. Ilison, K. Tamm, On Numerical Simulation of Propagation of Solitons in Microstructured Media, in: M.D. Todorov (ed), Proceedings of the 34th Conference on Applications of Mathematics in Engineering and Economics (AMEE '08), volume 1067 of AIP Conference Proceedings, American Institute of Physics, 2008 , pp. 155–165.

[29] A. Salupere, K. Tamm, J. Engelbrecht, Numerical simulation of interaction of solitary deformation waves in microstructured solids, Int. J. of Non-Linear Mech. 43 (2008) 201–208.

16

DISSERTATIONS DEFENDED AT
TALLINN UNIVERSITY OF TECHNOLOGY ON
NATURAL AND EXACT SCIENCES

1. **Olav Kongas.** Nonlinear dynamics in modeling cardiac arrhytmias. 1998.

2. **Kalju Vanatalu.** Optimization of processes of microbial biosynthesis of isotopically labeled biomolecules and their complexes. 1999.

3. **Ahto Buldas.** An algebraic approach to the structure of graphs. 1999.

4. **Monika Drews.** A metabolic study of insect cells in batch and continuous culture: application of chemostat and turbidostat to the production of recombinant proteins. 1999.

5. **Eola Valdre.** Endothelial-specific regulation of vessel formation: role of receptor tyrosine kinases. 2000.

6. **Kalju Lott.** Doping and defect thermodynamic equilibrium in ZnS. 2000.

7. **Reet Koljak.** Novel fatty acid dioxygenases from the corals Plexaura homomalla and Gersemia fruticosa. 2001.

8. **Anne Paju.** Asymmetric oxidation of prochiral and racemic ketones by using sharpless catalyst. 2001.

9. **Marko Vendelin.** Cardiac mechanoenergetics in silico. 2001.

10. **Pearu Peterson.** Multi-soliton interactions and the inverse problem of wave crest. 2001.

11. **Anne Menert.** Microcalorimetry of anaerobic digestion. 2001.

12. **Toomas Tiivel.** The role of the mitochondrial outer membrane in in vivo regulation of respiration in normal heart and skeletal muscle cell. 2002.

13. **Olle Hints.** Ordovician scolecodonts of Estonia and neighbouring areas: taxonomy, distribution, palaeoecology, and application. 2002.

14. **Jaak Nõlvak.** Chitinozoan biostratigrapy in the Ordovician of Baltoscandia. 2002.

15. **Liivi Kluge.** On algebraic structure of pre-operad. 2002.

16. **Jaanus Lass.** Biosignal interpretation: Study of cardiac arrhytmias and electromagnetic field effects on human nervous system. 2002.

17. **Janek Peterson.** Synthesis, structural characterization and modification of PA-MAM dendrimers. 2002.

18. **Merike Vaher.** Room temperature ionic liquids as background electrolyte additives in capillary electrophoresis. 2002.

19. **Valdek Mikli.** Electron microscopy and image analysis study of powdered hardmetal materials and optoelectronic thin films. 2003.

20. **Mart Viljus.** The microstructure and properties of fine-grained cermets. 2003.

21. **Signe Kask.** Identification and characterization of dairy-related Lactobacillus. 2003.

22. **Tiiu-Mai Laht.** Influence of microstructure of the curd on enzymatic and microbiological processes in Swiss-type cheese. 2003.

23. **Anne Kuusksalu.** 2–5A synthetase in the marine sponge Geodia cydonium. 2003.

24. **Sergei Bereznev.** Solar cells based on polycristalline copper-indium chalcogenides and conductive polymers. 2003.

25. **Kadri Kriis.** Asymmetric synthesis of C2-symmetric bimorpholines and their application as chiral ligands in the transfer hydrogenation of aromatic ketones. 2004.

26. **Jekaterina Reut.** Polypyrrole coatings on conducting and insulating substracts. 2004.

27. **Sven Nõmm**. Realization and identification of discrete-time nonlinear systems. 2004.

28. **Olga Kijatkina.** Deposition of copper indium disulphide films by chemical spray pyrolysis. 2004.

29. **Gert Tamberg.** On sampling operators defined by Rogosinski, Hann and Blackman windows. 2004.

30. **Monika Übner.** Interaction of humic substances with metal cations. 2004.

31. **Kaarel Adamberg.** Growth characteristics of non-starter lactic acid bacteria from cheese. 2004.

32. **Imre Vallikivi.** Lipase-catalysed reactions of prostaglandins. 2004.

33. **Merike Peld.** Substituted apatites as sorbents for heavy metals. 2005.

34. **Vitali Syritski.** Study of synthesis and redox switching of polypyrrole and poly(3,4-ethylenedioxythiophene) by using in-situ techniques. 2004.

35. **Lee Põllumaa.** Evaluation of ecotoxicological effects related to oil shale industry. 2004.

36. **Riina Aav.** Synthesis of 9,11-secosterols intermediates. 2005.

37. **Andres Braunbrück.** Wave interaction in weakly inhomogeneous materials. 2005.

38. **Robert Kitt.** Generalised scale-invariance in financial time series. 2005.

39. **Juss Pavelson.** Mesoscale physical processes and the related impact on the summer nutrient fields and phytoplankton blooms in the western Gulf of Finland. 2005.

40. **Olari Ilison.** Solitons and solitary waves in media with higher order dispersive and nonlinear effects. 2005.

41. **Maksim Säkki.** Intermittency and long-range structurization of heart rate. 2005.

42. **Enli Kiipli.** Modelling seawater chemistry of the East Baltic Basin in the late Ordovician–Early Silurian. 2005.

43. **Igor Golovtsov.** Modification of conductive properties and processability of polyparaphenylene, polypyrrole and polyaniline. 2005.

44. **Katrin Laos.** Interaction between furcellaran and the globular proteins (bovine serum albumin ?-lactoglobulin). 2005.

45. **Arvo Mere.** Structural and electrical properties of spray deposited copper indium disulphide films for solar cells. 2006.

46. **Sille Ehala.** Development and application of various on- and off-line analytical methods for the analysis of bioactive compounds. 2006.

47. **Maria Kulp.** Capillary electrophoretic monitoring of biochemical reaction kinetics. 2006.

48. **Anu Aaspõllu.** Proteinases from Vipera lebetina snake venom affecting hemostasis. 2006.

49. **Lyudmila Chekulayeva.** Photosensitized inactivation of tumor cells by porphyrins and chlorins. 2006.

50. **Merle Uudsemaa.** Quantum-chemical modeling of solvated first row transition metal ions. 2006.

51. **Tagli Pitsi.** Nutrition situation of pre-school children in Estonia from 1995 to 2004. 2006.

52. **Angela Ivask.** Luminescent recombinant sensor bacteria for the analysis of bioavailable heavy metals. 2006.

53. **Tiina Lõugas.** Study on physico-chemical properties and some bioactive compounds of sea buckthorn (Hippophae rhamnoides L.). 2006.

54. **Kaja Kasemets.** Effect of changing environmental conditions on the fermentative growth of Saccharomyces cerevisae S288C: auxo-accelerostat study. 2006.

55. **Ildar Nisamedtinov.** Application of 13C and fluorescence labeling in metabolic studies of Saccharomyces spp. 2006.

56. **Alar Leibak.** On additive generalisation of Vorono?'s theory of perfect forms over algebraic number fields. 2006.

57. **Andri Jagomägi.** Photoluminescence of chalcopyrite tellurides. 2006.

58. **Tõnu Martma.** Application of carbon isotopes to the study of the Ordovician and Silurian of the Baltic. 2006.

59. **Marit Kauk.** Chemical composition of CuInSe 2 monograin powders for solar cell application. 2006.

60. **Julia Kois.** Electrochemical deposition of CuInSe2 thin films for photovoltaic applications. 2006.

61. **Ilona Oja Acik.** Sol-gel deposition of titanium dioxide films. 2007.

62. **Tiia Anmann.** Integrated and organized cellular bioenergetic systems in heart and brain. 2007.

63. **Katrin Trummal.** Purification, characterization and specificity studies of metalloproteinases from Vipera lebetina snake venom. 2007.

64. **Gennadi Lessin.** Biochemical definition of coastal zone using numerical modeling and measurement data. 2007.

65. **Enno Pais.** Inverse problems to determine non-homogeneous degenerate memory kernels in heat flow. 2007.

66. **Maria Borissova.** Capillary electrophoresis on alkylimidazolium salts. 2007.

67. **Karin Valmsen.** Prostaglandin synthesis in the coral Plexaura homomalla: control of prostaglandin stereochemistry at carbon 15 by cyclooxygenases. 2007.

68. **Kristjan Piirimäe.** Long-term changes of nutrient fluxes in the drainage basin of the gulf of Finland – application of the PolFlow model. 2007.

69. **Tatjana Dedova.** Chemical spray pyrolysis deposition of zinc sulfide thin films and zinc oxide nanostructured layers. 2007.

70. **Katrin Tomson.** Production of labelled recombinant proteins in fed-batch systems in Escherichia coli. 2007.

71. **Cecilia Sarmiento.** Suppressors of RNA silencing in plants. 2008.

72. **Vilja Mardla.** Inhibition of platelet aggregation with combination of antiplatelet agents. 2008.

73. **Maie Bachmann.** Effect of Modulated microwave radiation on human resting electroencephalographic signal. 2008.

74. **Dan Hüvonen.** Terahertz spectroscopy of low-dimensional spin systems. 2008.

75. **Ly Villo.** Stereoselective chemoenzymatic synthesis of deoxy sugar esters involving Candida antarctica lipase B. 2008.

76. **Johan Anton.** Technology of integrated photoelasticity for residual stress measurement in glass articles of axisymmetric shape. 2008.

77. **Olga Volobujeva.** SEM study of selenization of different thin metallic films. 2008.

78. **Artur Jõgi.** Synthesis of 4'-substituted 2,3'-dideoxynucleoside analogues. 2008.

79. **Mario Kadastik.** Doubly charged Higgs boson decays and implications on neutrino physics. 2008.

80. **Fernando Pérez-Caballero.** Carbon aerogels from 5-methylresorcinol-formaldehyde gels. 2008.

81. **Sirje Vaask.** The comparability, reproducibility and validity of Estonian food consumption surveys. 2008.

82. **Anna Menaker.** Electrosynthesized conducting polymers, polypyrrole and poly(3,4-ethylenedioxythiophene), for molecular imprinting. 2009.

83. **Lauri Ilison.** Solitons and solitary waves in hierarchical Korteweg-de Vries type systems. 2009.

84. **Kaia Ernits.** Study of In2S3 and ZnS thin films deposited by ultrasonic spray pyrolysis and chemical deposition. 2009.

85. **Veljo Sinivee.** Portable spectrometer for ionizing radiation "Gammamapper". 2009.

86. **Jüri Virkepu.** On Lagrange formalism for Lie theory and operadic harmonic oscillator in low dimensions. 2009.

87. **Marko Piirsoo.** Deciphering molecular basis of Schwann cell development. 2009.

88. **Kati Helmja.** Determination of phenolic compounds and their antioxidative capability in plant extracts. 2010.

89. **Merike Sõmera.** Sobemoviruses: genomic organization, potential for recombination and necessity of P1 in systemic infection. 2010.

90. **Kristjan Laes.** Preparation and impedance spectroscopy of hybrid structures based on CuIn3Se5 photoabsorber. 2010.

91. **Kristin Lippur.** Asymmetric synthesis of 2,2'-bimorpholine and its 5,5'-substituted derivatives. 2010.

92. **Merike Luman.** Dialysis dose and nutrition assessment by an optical method. 2010.

93. **Mihhail Berezovski.** Numerical simulation of wave propagation in heterogeneous and microstructured materials. 2010.

94. **Tamara Aid-Pavlidis.** Structure and regulation of BDNF gene. 2010.

95. **Olga Bragina.** The role of Sonic Hedgehog pathway in neuro- and tumorigenesis. 2010.

96. **Merle Randrüüt.** Wave propagation in microstructured solids: solitary and periodic waves. 2010.

97. **Marju Laars.** Asymmetric organocatalytic Michael and aldol reactions mediated by cyclic amines. 2010.

98. **Maarja Grossberg.** Optical properties of multinary semiconductor compounds for photovoltaic applications. 2010.

99. **Alla Maloverjan.** Vertebrate homologues of Drosophila fused kinase and their role in Sonic Hedgehog signalling pathway. 2010.

100. **Priit Pruunsild.** Neuronal Activity-Dependent Transcription Factors and Regulation of Human BDNF Gene. 2010.

101. **Tatjana Knazeva.** New Approaches in Capillary Electrophoresis for Separation and Study of Proteins. 2011.

102. **Atanas Katerski.** Chemical Composition of Sprayed Copper Indium Disulfide Films for Nanostructured Solar Cells. 2011.

103. **Kristi Timmo.** Formation of Properties of CuInSe2 and Cu2ZnSn(S,Se)4 Monograin Powders Synthesized in Molten KI. 2011.